Co-combustion of Fossil Fuels and Waste

Wu, Hao; Glarborg, Peter; Dam-Johansen, Kim; Jappe Frandsen, Flemming

Publication date:
2011

Document Version
Publisher's PDF, also known as Version of record

Co-combustion of Fossil Fuels and Waste

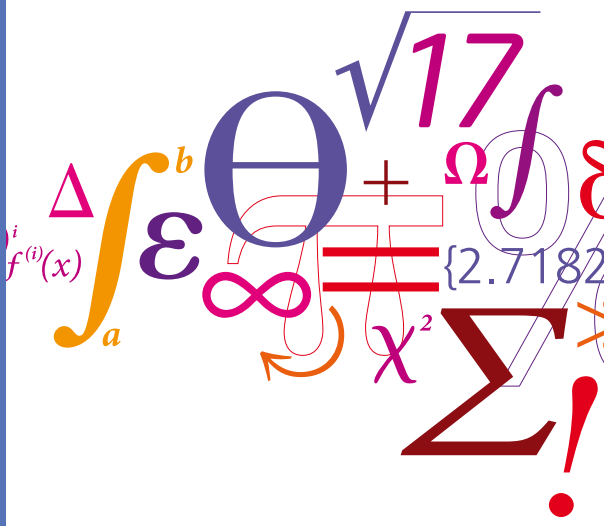

Hao Wu
Ph.D. Thesis
May 2011

DTU Chemical Engineering
Department of Chemical and Biochemical Engineering

Co-combustion of Fossil Fuels and Waste

Ph.D. Thesis

Hao Wu

May 31, 2011

Supervisors:
Peter Glarborg
Kim Dam-Johansen
Flemming Jappe Frandsen

CHEC Research Centre
Department of Chemical and Biochemical Engineering
Technical University of Denmark

DTU Chemical Engineering
Department of Chemical and Biochemical Engineering

Address: Centre on Combustion and Harmful Emission Control (CHEC)
Department of Chemical and
Biochemical Engineering
Technical University of Denmark
Søltofts Plads, Building 229
DK-2800 Kgs. Lyngby
Denmark
Phone: +45 4525 2957
Fax: +45 4525 2258
Web: www.chec.kt.dtu.dk

Print: J&R Frydenberg A/S
København
November 2011

ISBN: 978-87-92481-55-9

Preface

The present dissertation is written to fulfill the partial requirements of obtaining a Ph.D. degree at the Technical University of Denmark. The work has been carried out between November 2007 and May 2011 in the CHEC (Combustion and Harmful Emission Control) research centre at the Department of Chemical and Biochemical Engineering, Technical University of Denmark. The work has been funded by the Technical University of Denmark, Energinet.dk, Nordic Energy Research, and B&W Vølund A/S. The supervisors were Professor Peter Glarborg, Professor Kim Dam-Johansen, and Dr. Techn. Flemming J. Frandsen.

I would like to express my sincere gratitude to my supervisors for their guidance during my study. Peter was always available for fruitful discussions and carefully reading my manuscripts. He has also continuously given me encouragements and constructive suggestions on research. Kim introduced me into the field of combustion research, and was always inspiring and supportive in many aspects. Flemming ensured the financial support of this work and benefited me greatly through his excellent ash course and doctoral thesis as well as a number of conferences he catalyzed me to attend. A special thank goes to Associate Professor Peter Arendt Jensen, who was not my official supervisor but followed my work closely and provided a lot of valuable inputs.

I am grateful to Bo Sander at DONG Energy Power A/S for his significant support to this work. I am thankful to Anne Juul Damø at CHEC for the pleasant cooperation during the full-scale measurements at Esbjergværket. My thanks also go to Martin Røkke and Kasper Lundtorp at B&W Vølund A/S, who have made the bran project possible and provided a lot of insightful comments. M.Sc. student Maria Castro is appreciated for her contribution to the bran project. Edith Thomsen at DONG Energy Power A/S, Laila Leth at DTU Management, and Thomas W. Hansen at DTU CEN are gratefully acknowledged for the high quality chemical and microscopic analyses, which are the important base of this work. The people involved in the Nordic Graduate School in Biofuels Science and Technology – Phase 2 (BiofuelsGS2) are thanked for organizing very good and relevant PhD courses and annual seminars.

I would like to thank the technical staff at CHEC for their assistance in the experimental work, particularly Carsten Nørby and Thomas Wolfe. Moreover, I am grateful to many people at CHEC for creating a very friendly and enjoyable working environment, especially Per A. Sørensen, Jakob M. Christensen, Weigang Lin, Yuanjing Zheng, Ke Qin, Jacob Brix, and Kristen P. Nørgaard who has kindly helped me to translate the Danish resume.

Finally, I wish to dedicate this thesis to my parents, to my grandparents and to my wife Haiyan Wu for their support and understanding through the years.

Hao Wu

Lyngby, May 2011

Summary

The Ph.D. thesis deals with the alternative and high efficiency methods of using waste-derived fuels in heat and power production. The focus is on the following subjects: 1) co-combustion of coal and solid recovered fuel (SRF) under pulverized fuel combustion conditions; 2) dust-firing of straw and the utilization of a waste-derived material as an additive; 3) the combustion of a biomass residue rich in phosphorus.

Co-combustion of coal and SRF was conducted in an entrained flow reactor (EFR). The work revealed that when coal was co-fired with up to 25 wt% SRF, the burnout and the emissions of SO_2 and NO were decreased with increasing share of SRF, probably due to the combustion characteristics of the SRF and/or the interactions between the SRF and the coal in co-combustion. The Cl content in the fly ash was very low (<0.07 wt%) when coal was co-fired up to 25 wt% SRF, indicating that the majority of the Cl in the SRF were released to gas phase during co-combustion. The formation of fouling deposits on a probe was reduced with increasing share of SRF and the resulting deposits had a very small Cl content (<0.01 wt%), suggesting a low corrosion potential on superheater tubes when coal was co-fired with up to 25 wt% SRF. On the other hand, when NaCl or PVC was added to the mixture of coal and SRF, the formation of alkali chlorides was significantly promoted, and a larger amount of deposits with higher corrosion potential was formed, suggesting the importance of controlling the Cl and alkali content in the SRF.

The partitioning of trace elements (As, Cd, Cr, Pb, Sb and Zn) during co-combustion of coal and SRF was investigated through the experiments in the EFR. They revealed that As, Cd, Pb, Sb and Zn were highly volatile during combustion, while the volatility of Cr was relatively low. Compared to dedicated coal combustion, the volatility of Cd, Pb and Zn was slightly increased in co-combustion of coal and SRF, whereas the volatility of Cr and Sb was to some extent reduced. The volatility of Cd, Pb and Zn increased significantly with the injection of Cl based additives such as PVC and NaCl, while the addition of ammonium sulphate generally decreased the volatility of trace elements. The addition of kaolinite reduced the volatility of Pb, while the effect on other trace elements was insignificant. The results generally implied that co-combustion of coal and SRF in a coal-fired power plant may increase the trace element content in the fly ash considerably, primarily due to the significantly larger trace element content in SRF compared to coal, but also related to the interactions of the fuels during co-combustion.

Full-scale tests on co-combustion of coal and SRF were carried out in a pulverized coal-fired power plant, and the formation of fine particles was evaluated by applying a low-pressure cascade impactor. Compared to dedicated coal combustion, co-combustion of coal and SRF (up to 10% thermal share) generally promoted the formation of ultrafine particles with a concentration peak around 0.1 μm, while the total concentration of $PM_{2.5}$ decreased. TEM (transmission electron microscopy) analyses indicated that the ultrafine particles with primary particle size of 10–30 nm were predominantly comprised of aggregated particles originating from homogenous nucleation, whereas the remaining submicron particles were mostly a mixture

of the aggregates and the spherical particles originating from the melted minerals, with the contribution of the latter being more significant with increasing particle size. Composition analyses showed that the Ca, S and P were significantly enriched in the ultrafine particles, indicating a high volatility of these elements in pulverized coal combustion. Compared to dedicated coal combustion, the content of the Ca, P and K was larger in the fine particles generated from co-combustion, whereas the S content was slightly smaller. During the full-scale tests, the dust emission appeared to be significantly increased during co-combustion of coal and SRF, which was presumably related to a reduction of the collection efficiency of the electrostatic precipitator (ESP).

Dust-firing of straw was performed in an entrained flow reactor, and the feasibility of utilizing spent bleaching earth (SBE) as an additive was investigated through a comparison with kaolinite. It was found that about 70% of the K in the fly ash from straw-dust firing was water soluble, and the KCl contributed more than 40% of the water soluble K. With the addition of 10-20 wt% of SBE, the Cl retention in ash was decreased, the SO_2 emission was increased, and the formation of water soluble alkali species was reduced. Compared to kaolinite, the inhibiting effect of SBE on the formation of alkali chlorides was slightly smaller when the molar ratio of K/(Al+Si) was similar in the fuel mixture. The addition of SBE significantly reduced the Cl content of the deposits collected on a probe, both due to a dilution effect and the presence of chemical reactions. Compared to pure straw combustion, the ash deposition propensity was decreased during the addition of SBE. The results generally suggested that SBE could be a promising additive to be used in straw dust-firing.

The release and transformation of inorganic elements during the combustion of a residual bran was studied through experiments and equilibrium modeling. The work revealed that the major inorganic elements released during bran combustion were K, P and S. The S was almost fully vaporized during pyrolysis at temperatures below 700 ^{o}C, whereas about 60–70 % of the K and P in the bran were released during combustion in a temperature range of 900–1100 ^{o}C. The release of K and P was attributed to vaporization of KPO_3 generated from the thermal decomposition of the inositol phosphates, which were considered as a major source of P and K in the bran. Additives such $CaCO_3$, $Ca(OH)_2$ and kaolinite generally showed some influence on the release of K and P. The Ca-based additives mostly increased the molar ratio of the released K/P, whereas the kaolinite showed an opposite effect. Thermodynamic modelling indicated that the fly ash chemistry is sensitive to the molar ratio of the released K/P. When the molar ratio of the released K/P was below 1, KPO_3 and P_4O_{10} (g) were the main stable K and P species at temperatures higher than 500 ^{o}C. Below 500 ^{o}C, the KPO_3 and P_4O_{10} (g) may be converted to H_3PO_4 (l). By increasing the molar ratio of the released K/P to above 2, the equilibrium distribution of the K and P species was changed significantly and the formation of H_3PO_4 (l) was not predicted by thermodynamic modelling.

Danish Resume

Denne Ph.D.-afhandling omhandler alternative og høj effektive metoder for anvendelse af affaldsafledte brændsler til el og varme produktion. Hovedfokus er på følgende emner: 1) Medforbrænding af kul og affaldsafledte brændsler (SRF) i støvfyrede kedler 2) Støvfyring af halm og anvendelsen af affaldsafledte materialer som additiver 3) Forbrænding af en P-rigt biprodukt fra biomasseforædling.

Medforbrænding af kul og SRF blev udført i en fastbrændselsreaktor (EFR). Arbejdet har vist at når kul bliver samfyret med op til 25 vægt-% SRF udbrændingen samt emissionerne af SO_2 og NO med stigende andel af SRF, sandsynligvis på grund af SRFs forbrændingskarakteristika og/eller interaktionen mellem SRF og kul i medforbrændingen. Analyser af sammensætningen indikerede at klorindholdet i flyveasken var meget lavt (<0.07 vægt-%) når kul blev samfyret med til op 25 vægt-% SRF, hvilket indikerer at hovedparten af klor i SRF bliver frigivet til gasfasen under medforbrænding. Dannelsen af forurenende belægninger på en dertil designet sonde reduceredes med stigende andel af SRF under samfyring. Belægningerne havde et meget lavt Cl indhold (<0,01vægt-%) hvilket tyder på et lavt korrosions potentiale på overheder rør når kul blive samfyret med op til 25 vægt-% SRF. På den anden side, når NaCl eller PVC blev tilsat blandingen af kul og SRF, fremmedes dannelsen af alkaliklorider signifikant, og der blev dannet en større mængde belægninger med højere korrosionspotentiale, hvilket viser vigtigheden af kontrol med Cl og Na indholdet i SRF.

Fordelingen af sporstoffer (As, Cd, Cr, Pb, Sb og Zn) under medforbrænding af kul og SRF blev undersøgt gennem eksperimenter i EFR en. De viste at As, Cd, Pb, Sb og Zn var yderst flygtige, mens flygtigheden af Cr var relativt lav. Sammenlignet med kulforbrænding forøgedes flygtigheden af Cd, Pb og Zn lidt ved samfyring mellen af kul og SRF, hvorimod flygtigheden af Cr og Sb blev reduceret til en vis grad. Flygtigheden af Cd, Pb og Zn steg signifikant med injektion af Cl baserede additiver såsom PVC og NaCl, mens tilsætning af ammoniumsulfat generelt reducerede flygtigheden af sporstofferne. Tilsætning af kaolin reducerede flygtigheden af Pb, mens effekten på andre sporstoffer var ubetydelig. Generelt tydede resultaterne på at samfyring af kul og SRF i kulfyrede kraftværker måske kan øge indholdet af sporstoffer i flyveasken væsentligt, primært på grund af det signifikant højere indhold af sporstoffer i SRF sammenlignet med kul, men også relateret til interaktionerne af brændslerne i medforbrændingen.

Fuldskalatests med samfyring af kul og SRF blev udført i et støvfyrede, kul kraftværk og dannelsen af små partikler blev evalueret vhja af en lavtryks kaskadeimpaktor. Sammenlignet med kulforbrænding, fremmer samfyring af kul og SRF (op til 10% termisk andel) generelt dannelsen af ultrafine partikler med diameter omkring 0.1 μm mens den totale koncentration af $PM_{2.5}$ (partikler <2.5 μm) faldt. TEM (transmissionselektronmikroskopi) analyser indikerede at de ultrafine partikler, med primær partikel størrelse mellem 10-30 nm, overvejende bestod af aggregerede partikler stammende fra homogen kimdannelse, hvorimod de resterende submikrone partikler hovedsageligt var en blanding af aggregater og sfæriske partikler stammende fra de

smeltede mineraler, og bidraget fra de sfæriske partikler blev mere signifikant med stigende partikelstørrelse.

Analyser af sammensætningen viste at Ca, S og P blev signifikant beriget i de ultrafine partikler, hvilket indikerer en høj flygtighed af disse grundstoffer i kulstøvfyring. Sammenlignet med dedikeret kulforbrænding var indholdet af Ca, P og K større i de fine partikler dannet ved samfyring, mens indholdet af S var en smule mindre. Fuldskalatestene viste at støvemissionen steg signifikant gennem medforbrændingen af kul og SRF, hvilket antageligt er relateret til en reduktion af opsamlingseffektiviteten af elektrofilteret (ESP).

Støvfyring med halm blev udført i en fastbrændselsreaktor og muligheden for anvendelse af brugt blegejord (SBE) som tilsætningsstof blev undersøgt ved en sammenligning med kaolin. Det blev fundet at omkring 70% af K i flyveasken fra halmstøvafbrænding er vandopløseligt, og at KCl bidrager med mere end 40 % af det vandopløselige K. Med tilsætning af 10-20 vægt-% af SBE, blev Cl undbinding i asken reduceret, SO_2 emissionen blev øget og dannelsen af vandopløselige alkaliklorider blev reduceret. Sammenlignet med kaolinit blev inhiberingseffekten af SBE på dannelsen af alkaliklorider lidt mindre når det molære forhold af K/(Al+Si) var svarende til forholdet i brændselsblandingen. Tilsætningen af SBE reducerede Cl-indholdet i belægninger opsamlet på en sonde signifikant, både på grund af en fortyndingseffekt og tilstedeværelsen af kemiske reaktioner. Sammenlignet med ren halmafbrænding blev tilbøjeligheden til askebelægninger mindsket gennem SBE tilsætning. Generelt tyder resultaterne på at SBE kunne være et lovende tilsætningsstof til halmstøvfyring.

Frigivelsen og omdannelsen af uorganiske forbindelser under forbrændingen af et restklid fra biomasse forædling er blevet undersøgt gennem eksperimenter og ligevægtsberegninger. Arbejdet vist at størstedelen af de uorganiske forbindelser frigivet under afbrænding af klid bestod af K, P og S. S blev næsten fuldstændig fordampet under pyrolysen ved temperaturer under 700 ^{o}C, hvorimod omkring 60-70% af K og P i kliddet blev frigivet under forbrænding i temperaturintervallet 900-1100 ^{o}C. Frigivelsen af K og P blev tilskrevet fordampningen af KPO_3 dannet fra den termiske dekomposition af inositol fosfaterne i kliddet. Generelt havde additiver som $CaCO_3$, $Ca(OH)_2$ og kaolin nogen indflydelse på frigivelsen af K og P. For det meste forøgede de Ca-baserede additiver forholdet mellem det frigivne K/P, hvorimod kaolin udviste den modsatte effekt. Termodynamisksmodellering indikerede at flyveaskekemien er følsom overfor det molære forhold af frigivet K/P. Da det molære forhold af det frigivne K/P var mindre end 1, udgjorde KPO_3 og P_4O_{10} (g) størstedelen af de stabile K og P forbindelser ved temperaturer over 500 ^{o}C. Under 500 ^{o}C kan KPO_3 og P_4O_{10} (g) omdannes til H_3PO_4 (l). Ved at hæve det molære forhold af frigivet K/P til over 2, blev ligevægtsfordelingen af K og P forbindelser ændret signifikant og dannelsen af H_3PO_4 (l) blev ikke forudset ved termodynamisk modellering.

Introduction to this Thesis

Utilization of waste and biomass in heat and power production has gained substantial interest in recently years primarily due to the demand of reducing the CO_2 emissions originating from fossil fuel consumption. However, the electrical efficiency of a dedicated waste- or biomass-fired power plant is often restricted to below 25%, which is considerably lower than that of modern coal-fired power plants. Therefore it is desirable to explore the alternative techniques which can improve the efficiency of utilizing waste and biomass in heat and power production.

Co-combustion of waste/biomass with coal in an existing dedicated coal-fired power plant is recognized as a fast, low-cost and high-efficiency method of utilizing waste/biomass energy. In Chapter 1 of this thesis, a general introduction to the field of co-combustion is given through a literature survey. This literature survey provides an outline of the fundamental fuel and ash conversion processes during co-combustion of coal and different secondary fuels under pulverized fuel combustion conditions. The knowledge can benefit the understanding of the remaining chapters in this thesis.

Chapter 2-4 deals with co-combustion of coal and solid recovered fuel (SRF) under pulverized fuel combustion conditions. Chapter 2 and 3 are based on the co-combustion experiments carried out in an entrained flow reactor, whereas Chapter 4 presents the results obtained from a full-scale pulverized coal-fired power plant. The main focus of Chapter 2 is on the general combustion and ash behavior during co-combustion of coal and SRF, and Chapter 3 primarily concerns with the partitioning of trace elements in co-combustion. The emphasis of Chapter 4 is on the formation of fine particles during co-combustion of coal and SRF in a full-scale plant, and some other technical issues are also discussed based on the tests.

Another potential approach to increase the efficiency of utilizing biomass in power production is to convert an existing pulverized coal-fired plant to a biomass dust-firing plant. Chapter 5 is concerned with the ash related issues during straw dust-firing as well as the feasibility of applying a waste-derived additive in straw dust-firing.

A special type of biomass residues which may have significant potential to be used in biomass dust-firing or co-combustion is phosphorus-rich biomass. In Chapter 6, the ash release and transformation during the combustion of a typical phosphorus-rich biomass residue are investigated.

The results presented in this thesis are based on several scientific articles that have been published or accepted by peer-reviewed journals:

- Chapter 2 has been published in *Fuel*, H. Wu, P. Glarborg, F.J. Frandsen, K. Dam-Johansen, P.A. Jensen, B. Sander, Co-combustion of pulverized coal and solid recovered fuel in an entrained flow reactor – General combustion and ash behaviour, vol. 90 (2011) 1980-1991.

- Chapter 3 has been accepted by *Fuel Processing Technology*, H. Wu, P. Glarborg, F.J. Frandsen, K. Dam-Johansen, P.A. Jensen, B. Sander, Trace elements in co-combustion of solid recovered fuel and coal (2011).
- Part of Chapter 4 has been published in *Proceedings of the Combustion Institute*, H. Wu, A.J. Pedersen, P. Glarborg, F.J. Frandsen, K. Dam-Johansen, B. Sander, Formation of fine particles in co-combustion of coal and solid recovered fuel in a pulverized coal-fired power station, vol. 33 (2011) 2845-2852
- Chapter 5 has been accepted by *Energy Fuels*, H. Wu, P. Glarborg, F.J. Frandsen, K. Dam-Johansen, P.A. Jensen, Dust-firing of straw and additives – ash chemistry and deposition behavior
- Chapter 6 has been accepted by *Energy Fuels*, H. Wu, M. Castro, P.A. Jensen, F.J. Frandsen, P. Glarborg, K. Dam-Johansen, M. Røkke, K. Lundtorp, Release and transformation of inorganic elements in combustion of a high-phosphorus fuel

Table of Contents

Abbreviations

AmSulf	Ammonium Sulphate
APH	Air Pre-heater
CCA	Chromated Copper Arsenate
CCSEM	Computer-Controlled Scanning Electron Microscopy
DSC	Differential Scanning Calorimetry
DTG	Derivative Thermogravimetric Analysis
EDS	Dispersive X-rays Spectroscopy
EFR	Entrained Flow Reactor
ESP	Electrostatic Precipitators
ESV	Esbjerg Power Station
FGD	Flue Gas Desulphurization
GFAAS	Graphite Furnace Atomic Absorption Spectrometer
IC	Ion Chromatography
ICP-OES	Inductively Coupled Plasma Optical Emission Spectrometry
LPI	Low-pressure Cascade Impactor
IRZ	Internal Recirculation Zone
LDPE	Low Density Polyethylene
MBM	Meat and Bone Meal
NAA	Neutron Activation Analysis
PIXE	Particle-induced X-ray Analysis
PM	Particulate Matter
PP	Polypropylene
PVC	Polyvinylchloride
RDF	Refuse Derived Fuel
RE	Relative Enrichment
SBE	Spent Bleaching Earth
SCR	Selective Catalytic Reduction
SEM	Scanning Electron Microscopy
SRF	Solid Recovered Fuel
STA	Simultaneous Thermal Analysis
TEM	Transmission Electron Microscopy
TGA	Thermogravimetric Analysis
XAFS	X-ray Absorption Fine Structure
XRD	X-ray Diffraction

1 Literature Survey

1.1 Introduction

Direct co-combustion of coal and secondary fuels in existing coal-fired power plants is regarded as an advantageous approach to replace part of the fossil fuel consumption by more CO_2-friendly fuels such as biomass and waste. The major advantages of this technique have been summarized by several reviews available on this subject [1-8]. Compared to dedicated biomass- or waste-fired plants, the addition of biomass or waste to high efficiency coal-fired power plants can greatly increase the electrical efficiency of utilizing these fuels [4]. Besides, the cost of retrofitting an existing coal-fired power plant to a co-combustion plant can be considerably lower than building a new dedicated biomass- or waste-fired plant [9]. Furthermore, co-combustion can be operated in a flexible mode (i.e. with different share of secondary fuels) which can minimize the fluctuating supply of some secondary fuels (such as straw) and secure the power generation [1].

Although with many advantages, co-combustion may involve a number of technical issues which need to be addressed [1,3,4]. For example, the cost of co-combustion may be considerably higher than that of dedicated coal combustion due to the relatively high price of the secondary fuels (including the transportation expense) and the cost associated with the required pretrements (such as drying, grinding and densification). In addition, co-combustion of coal and a secondary fuel in a coal-fired power plant may affect the performance of the plant, and lead to problems associated with ash deposition, fuel conversion, pollutant formation (such as NO_x, SO_2, and fine particles), corrosion, and fly ash utilization [4]. These issues have been the major technical barriers of co-combustion, and have become the topics of extensive research in the past two decades. In addition, with the growing interest in utilizing biomass and waste in heat and power production, the understanding of the fundamentals of biomass and waste combustion has improved considerably in recent years through extensive research. These advances, together with the relatively well-established knowledge on coal combustion, can generally allow us to achieve a good understanding on the co-combustion processes.

This review aims to provide an outline of the fundamental fuel and ash conversion processes during co-combustion of coal and different secondary fuels, particularly at conditions relevant to pulverized fuel combustion. Through a detailed assessment of the differences and interactions of coal and various secondary fuels in different fuel/ash conversion processes, the possible effect of co-combustion on a number of technical aspects, such as ignition, burnout, pollutants formation, ash deposition, corrosion, and ash utilization, are evaluated and interpreted based on literature.

1.2 Combustion fundamentals and gaseous emissions

1.2.1 Devolatilization

When a solid fuel particle is exposed to a high temperature environment, the organic structure can undergo thermal decomposition and release volatile matter. This process is described as devolatilization, with the major products containing light gases (mainly CO_2, CO, H_2O, H_2, CH_4 and other light hydrocarbons), tar/soot and char. The characteristics of devolatilization, such as decomposition temperature, rate and product distributions, can subsequently influence the ignition, burnout and pollutant formation during solid fuel combustion [10-12].

The devolatilization behavior of coal has been well characterized through experiments and modeling, with several detailed reviews available on this subject [10,11,13]. The major organic structures in coal can be categorized as aromatic clusters, side chains, aliphatic bridges and loops [14]. During the primarily devolatilization, the aromatic clusters are largely converted to tar and char, while the other organic structures are the main precursors of light gases [11]. The product distribution from the primary devolatilization of coal is influenced by factors such as coal properties (rank), heating rate, environmental temperature and pressure. The coals with lower rank generally produce more light gases during the primary devolatilization [10,15-18], due to the presence of smaller amount of aromatic carbon and larger amount of aliphatic chains. The formation of tar is usually most significant for the devolatilization of intermediate-rank coals (such as bituminous coals) [10,15-18], as these coals contain more aliphatic chains than the high-rank coals (such as anthracite) and more aromatic carbon than the low-rank coals (such as lignite), which favor tar formation. The formation of light gases such as CO, CO_2 and CH_4 during the primary devolatilization is reported to be promoted by increasing the temperature of the pyrolysis environment [19,20]. The formation of tar may also increase with increasing environmental temperature [19,20], whereas the effect may become insignificant when the temperature is above 800 ^oC [20]. When the primary devolatilization is carried out at elevated pressure, the formation of tar as well as the total volatile species can be inhibited to some extent [10].

Once the tar and light gases are released from the primary devolatilization of coal, they may undergo secondary reactions and produce soot and different light gases [21-24]. The secondary reactions of tar usually involve thermal cracking and/or soot formation. During the thermal cracking, the side chains and functional groups in the tar are cracked to produce light gases [25]. On the other hand, the main mechanisms of soot formation are considered to be the direct conversion of tar and the addition of light gases to soot [21].

Compared to coal, biomass and waste are often characterized by a higher volatile content and a lower char content [26]. Extensive research has been carried out on devolatilization of biomass and waste [27-31]. For biomass and biomass-originated waste, such as waste wood and paper, the major organic components are usually cellulose, hemicellulose and lignin [26,27]. During the devolatilization, the hemicellulose often decomposes at lower temperature compared to cellulose, and produces more volatiles, less tar and less char. Lignin is an amorphous cross-linked resin, which can produce more char during devolatilization than that of cellulose or hemicellulose [27]. Due to the structural differences between biomass and coal, their devolatilization characteristics are usually quite different. A typical example is given in Figure 1.1, showing that the devolatilization of the biomass mixture occurs at much lower temperature than that of coal, and

produces much more light gases and tar. The devolatilization of biomass is greatly influenced by the biomass properties and the process parameters such as environmental temperature and heating rate [28]. A higher environmental temperature usually inhibits the char yield and promotes the light gas formation. The maximum yield of tar is often observed at intermediate environmental temperature range (~500–700 ^{o}C), which is related to both the primary release and secondary reactions of tar [28]. More detailed investigations on biomass devolatilization are summarized in [27,28].

An important constituent of waste materials is highly polymerized materials such as plastics and rubbers. Compared to biomass, devolatilization of plastics and rubbers generally occurs at higher temperature and produces more volatiles. According to the thermogravimetric analysis (TGA), the devolatilization of various plastics primarily takes place in the temperature range of ~400–550 ^{o}C, while the devolatilization of biomass (lignocellulosic materials) mainly happens in the temperature range of ~200–400 ^{o}C [29-31]. PVC (Polyvinylchloride) is a special type of plastics, which starts to decompose at lower temperatures than most other plastics [29-32]. The devolatilization of PVC primarily follows two steps. The first step (dehyrochlorination) occurs in the temperature range of ~200–370^{o}C, in which a fraction of hydrocarbons is released as benzene and the Cl is almost fully released as HCl. The second step takes place in the temperature range of ~400–500^{o}C, which is accompanied by the evolution of toluene and alkyl aromatics [29-32].

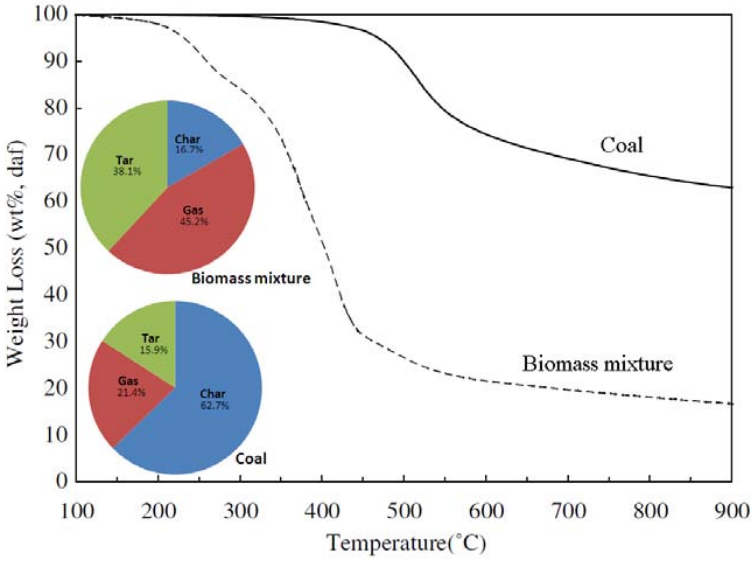

Figure 1.1 Mass loss and product distribution during devolatilization of a bituminous coal and a biomass mixture at a heating rate of 30 ^{o}C/min, adapted from [33].

The interactions between coal and biomass/waste during devolatilization have been investigated through TGA, fixed-bed, and entrained flow experiments [34-43]. A number of studies show that the interactions between coal and biomass/waste are negligible during the devolatilization [34,39,41,43,44], suggesting that the devolatilization behavior of the fuel mixture is additive (i.e. no obvious synergy effect between the fuels). On the other hand, some others report that small interactions may exist, when coal is pyrolyzed together with biomass/waste [35,36,38,40,42]. The mechanisms which may cause the interactions are discussed in the following.

When coal is pyrolyzed together with biomass, the volatiles released from biomass may react with coal or coal volatiles. These reactions may promote the formation of volatiles from the fuel mixture, and meanwhile inhibit the char yield [36,38,40,42]. A possible explanation is that the devolatilization of typical biomass/waste may produce relatively large amount of H_2, which can prevent the recombination and cross-linking reactions of free radicals, thereby suppressing the char formation [36]. Alternatively, the free radicals such as H* and CH_3* originated from the decomposition of aliphatic components of coal may react with the methoxyphenolic compounds from biomass devolatilization and form benzene substitutes [38]. The presence of such reactions may influence the distribution of volatile products from co-pyrolysis, and result in an increased formation of tar [35,42]. However, the extent of the secondary reactions among the released volatiles and the fuel mixture are to a large extent dependent on their mixing level and contacting time [39]. This may be an explanation to the insignificant synergy effect reported in other co-pyrolysis experiments [34,39,41,43,44]. The extent of synergy may be also dependent on the characteristics of the fuels, such as coal rank and biomass properties [37,40].

Besides the organic species, inorganic elements in biomass/waste may induce certain interactions during co-pyrolysis of coal and biomass/waste, since these elements may catalyze solid fuel devolatilization [45-47]. When biomass is demineralized, the initial devolatilization temperature is often increased compared to that of raw biomass, indicating that the cations in biomass, such as Ca, Mg, and K, may catalyze fuel decomposition to start at lower temperatures. Besides, the demineralization process may affect the distribution of the devolatilization products and result in an increased formation of volatiles [45-47]. As a result, when coal is co-pyrolyzed with biomass/waste of high ash content, the catalytic effect of inorganic elements may lead to interactions. As an example, during co-pyrolysis of coal and MBM (meat and bone meal), the DTG (derivative thermogravimetric analysis) curve of the mixture is found to be shifted to lower temperature, compared to that calculated from the pure fuels. This is partly explained by the catalytic effect of the inorganic elements in MBM, as the interactions are weakened in a mixture of demineralized MBM and coal [48].

Synergy effects have also been observed when coal is pyrolyzed with plastic materials, such as LDPE (low density polyethylene) and PP (polypropylene) [49-51]. At temperatures lower than the decomposition temperature of plastics, the devolatilization of the mixture is reported to be inhibited, which is probably because the softening and melting of plastics may inhibit the evolution of volatile matter during coal pyrolysis [49,51]. However, when the temperature becomes higher than the decomposition temperature of the plastics, the devolatilization of the mixture may be promoted and result in an increased formation of volatiles [49,51]. A possible explanation is that the hydrocarbon species originated from cleavage of polymer bonds may react with the radicals from coal thermal decomposition, which stabilize the primary decomposition products and thereby promote the formation of volatiles [49].

The presence of PVC in fuel mixtures may significantly affect the devolatilization behavior of other solid fuels, particularly for the lignocellulosic materials [30,52]. Co-pyrolysis of PVC and lignocellulosic materials may lower the decomposition temperature of the lignocellulosic materials and increase the char yield [30,52]. These interactions are primarily linked to the HCl released from the dehyrochlorination of PVC. The evolution of HCl may facilitate dehydration and aldehyde formation from the lignocellulosic materials, which could inhibit depolymerization and thereby promote the char formation [52].

It should be noted that the majority of the interactions during co-pyrolysis of coal and biomass/waste are observed during TGA experiments, in which fuel particles are intimately contacted and the heating rate is relatively slow. In the case of co-pyrolysis at suspension-fired conditions, the extent of interactions may be limited, due to the constraints in mixing and contacting time among the fuel particles and the volatiles.

1.2.2 Ignition and flame stability

During solid fuel combustion, ignition and flame stability are important for carbon burnout and formation of pollutants such as NO_x [53,54]. The ignition of solid fuel particles can follow two mechanisms, i.e. heterogeneous ignition and homogeneous ignition. The heterogeneous ignition usually results from the direct attack of oxygen on the fuel/char particle surface, while the homogeneous ignition describes the ignition of the volatiles released from the fuel particles [53,54]. The ignition characteristics of solid fuels, including ignition mechanism, time (delay) and temperature, are influenced by a number of factors such as fuel characteristics, particle size/shape, ambient temperature/heating rate, ambient gas compositions, particle number density and fluid flow [53-59].

In co-combustion of pulverized coal and biomass, the applied biomass particles are usually considerably larger than the coal particles [3,60-62]. Biomass is more difficult and costly to grind than coals [3,9], and the characteristics of biomass (such as the high volatile content) allows it to have a relatively large particle size in co-combustion. Due to the differences in particle size and in the inherent fuel characteristics, the ignition behavior of biomass and coal particles may be quite different, which can influence the flame characteristics in co-combustion.

With the purpose of comparing the ignition/flame characteristics of pulverized coal and biomass (sawdust), experiments have been conducted in a semi-industrial-scale reactor [63]. Compared to the coal flame, a more intense and wide flame is observed near the burner during the sawdust combustion, which is attributed to the volatiles released from the fine fraction of sawdust particles. On the other hand, a second flame stage appears downstream of the near-burner region during sawdust combustion, which is presumably related to the combustion of the large sawdust particles. These large sawdust particles usually require more devolatilization time and could more easily penetrate the IRZ (internal recirculation zone) of the burner compared to the coal particles [63].

A similar two-stage flame has been seen during co-combustion of coal and straw [64], as indicated by the O_2 and CO distributions shown in Figure 1.2. Particle sampling suggests that the second flame stage results from the large and dense straw knee particles. These particles can have sufficient momentum to penetrate the IRZ of the burner [65], and the large particle size may cause a significant intra-particle temperature gradient which prolongs the devolatilization process [66]. By decreasing the primary air flow (i.e. inertia of straw particles), the flame is found to be shortened and the second flame stage disappears, suggesting that the flame structure in co-combustion is largely dependent on the injection method of biomass [64]. This is supported by the experiments carried out in a down-fired furnace, showing that the injection method of biomass can greatly affect the burnout and NO emissions [67].

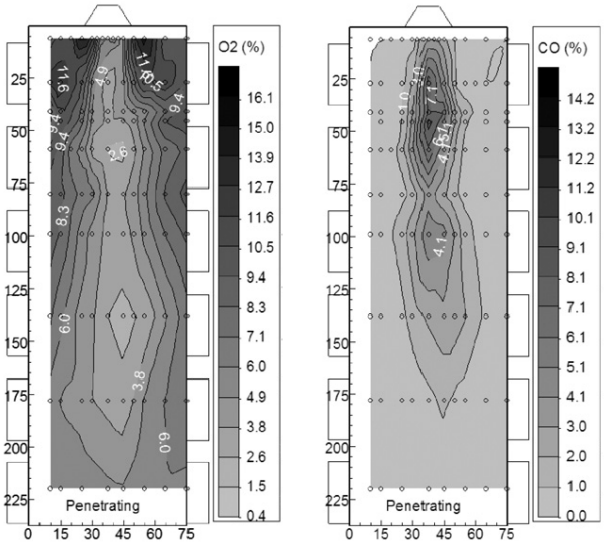

Figure 1.2 O_2 and CO distributions in a flame of co-firing coal and straw (50% thermal basis); the straw was injected through a center tube with an air flow of 16.5 kg/h and the coal was injected via an annular tube with an air flow of 15.0 kg/h [64].

The influence of co-firing coal and different biomass on the flame temperature, stability and other characteristics has been investigated by using vision-based measurement techniques on an industrial-scale combustion test facility [68]. The addition of 10% (thermal basis) biomass generally resulted in a delayed ignition of the fuel particles compared to the coal flame. This is presumably a result of the relatively large particle size and high moisture content of the biomass particles. For biomass with smaller moisture content, the ignition time is shorter than that of other co-combustion experiments. The brightness of the co-firing flames is consistently higher than that of coal flames, presumably because biomass may generate more soot with high radiant intensity. The oscillation of the co-firing flames is quite similar to a coal flame, indicating that the flame stability is not significantly affected when part of the coal is replaced by biomass [68]. The temperature of the co-firing flame is slightly greater than that of coal flame, which is attributed to a faster heat release caused by the volatiles from biomass [68]. Similar increased flame temperature is observed when coal is co-combusted with sawdust in an electrically heated drop tube reactor [69].

In general, the influence of adding biomass to a coal flame is to a large extent dependent on the physical and chemical properties of the biomass particles and their injection method. The relatively large size of biomass particles, together with a high moisture content, may result in a delayed ignition [68] or devolatilization [64,66]. If the delayed devolatilization is associated with a significant momentum of large biomass particles, it may result in a two-stage flame structure [63,64]. Besides, biomass usually contains relatively large volatile content and starts to decompose at lower temperatures [70], which is a favorable condition for generating a more intensive flame than coal flame [63,64,68,69]. The injection method of biomass particles also significantly affects the extent of fuel interactions, and subsequently impacts the ignition and flame characteristics during co-combustion [64,67,68].

1.2.3 Char reactivity and burnout

The degree of carbon burnout refers to the fraction of combustion matter in the parent fuel that is converted to gaseous products, with the remainder being left as carbonaceous residue [71]. In pulverized fuel combustion, the carbon burnout does not only influence the thermal efficiency of the plant, but also affects the quality of fly ash to be used in cement or concrete production [71,72]. The typical combustion history of a solid fuel particle is illustrated in Figure 1.3. It can be seen that the characteristic time of char oxidation is much longer than that of heating or devolatilization. Therefore the burnout in pulverized fuel combustion is to a large extent dependent on the char reactivity of the fuel particles.

The global reactivity of a char particle is governed by the mass and heat transport across the external boundary layer of the particle, by the mass and heat transport through the porous structures of the particle, and by the chemical reactions occurring between oxygen and the carbonaceous surfaces within the particle [28]. In general, the combustion of char particles can follow three regimes [28,71].When the diffusion rate is much faster than the chemical reaction rate, the combustion of char particles follows the regime I (kinetic control), which is usually established for low temperatures and small char particles. For the regime II, the chemical reaction rate becomes comparable with the pore diffusion rate. Thus the char combustion is controlled both by pore diffusion and chemical reaction. For the regime III, the char combustion is controlled by the diffusion from the bulk gas to the external surface of the particle [28,71]. During pulverized fuel combustion the char oxidation generally follows the regime I and II, whereas the regime III is often favored by fixed-bed combustion where larger particles are combusted [71].

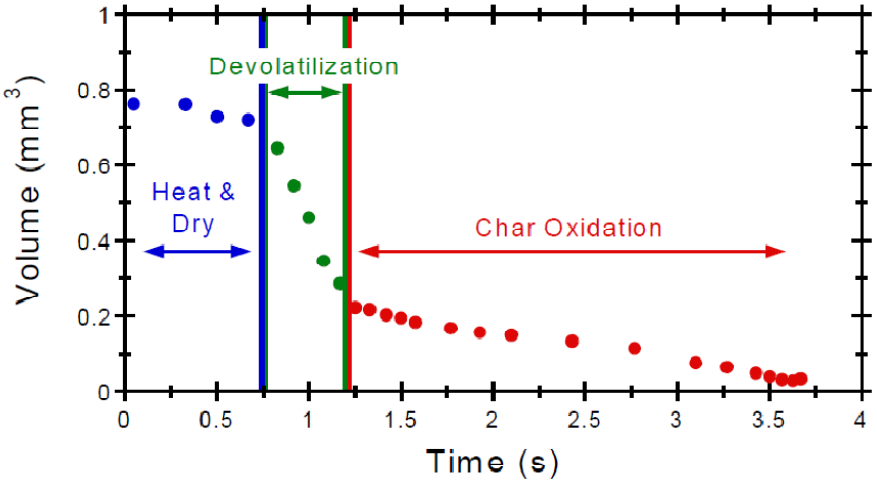

Figure 1.3 Typical combustion history of a biomass particle (switchgrass), also representative for a coal particle [3].

The reactivity of char particles can be influenced by various factors such as fuel characteristics, heating rate, temperature, and pressure [28,71]. For co-combustion where different fuel particles are combusted at similar conditions, the discrepancy in the char reactivity of different fuel particles is largely attributed to the fuel characteristics. A comparison of the char reactivity of

different solid fuels has been performed through TGA experiments at kinetic control conditions (regime I) [73]. Figure 1.4 shows the obtained reactivities for 17 char samples prepared at 1000 ^{o}C. The reactivities of different solid fuels vary almost 4 orders of magnitude under identical conditions. For coal chars, the char reactivity generally decreases with increasing carbon (daf) content of the coals, which is consistent with the tendency observed in another study [71]. The reactivity of biomass chars is generally greater than that of coal chars, which is in agreement with several other studies [74-77]. Since the non-catalytic model/pure materials (such as cellulose) shown in Figure 1.4 exhibit uniformly low char reactivity, the variations of the char reactivity of biomass and coal samples are primarily attributed to the catalytic effect of the inorganic elements (such as Ca, Mg and K) present in these fuels. The char surface area can also influence the reactivity, but this effect is believed to be less significant compared to the catalytic effect of the inorganic elements at the given experimental conditions [73].

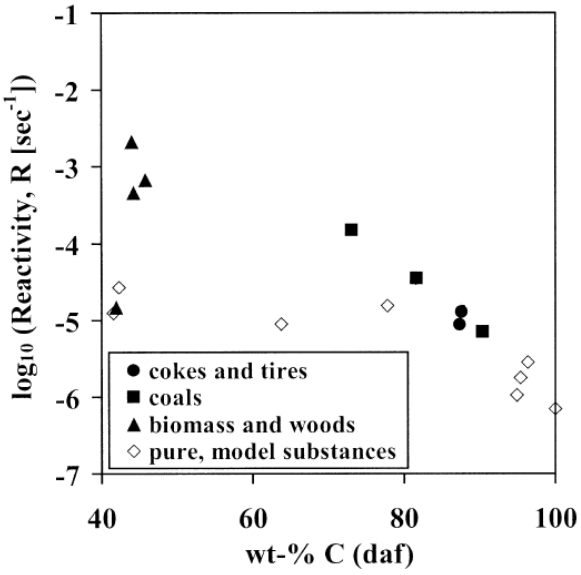

Figure 1.4 Measured reactivity of chars prepared at 1000 ^{o}C from 17 samples versus the carbon content (daf) of the fuels [73].

To investigate the catalytic effect of inorganic elements on char reactivity, Zolin et al. have carried out a detailed investigation on the char reactivity of a straw and a low rank coal [78]. For the char samples produced in a TGA, the catalytic effect of the inorganic elements appears to be significant both for the straw and the coal at heat treatment temperatures up to 1000 ^{o}C, as reflected by a much lower char reactivity of the demineralized coal and washed straw compared to raw fuels. However, when the char is produced in the TGA at temperatures higher than 1200 ^{o}C, the catalytic effect of the inorganic elements is reduced, which is interpreted by the transformation of the inorganic elements and/or the char thermal deactivation such as annealing. On the other hand, for the char produced in an entrained flow reactor (EFR) at 1200 ^{o}C/1400 ^{o}C, the reactivity of the char from raw straw is still about 30-40 times higher than that of leached straw, indicating that the reduction of the catalytic effect at high temperatures is insignificant at this condition. A possible explanation is that the time scale of the heating stage in the EFR may be shorter than that needed for the deactivation or vaporization of the inorganic catalysts. In

addition, the char sampling method in the EFR may recombine inorganic aerosols such as KCl on the char surfaces [78].

Although the reactivity of biomass char particles is generally greater than that of coals [73-78], the carbon burnout in co-combustion of coal and biomass is affected by other factors, such as the residence time, the shape, and the ignition/heating characteristics of fuel particles. The investigations on the influence of co-combustion on the burnout have been carried out on with a number of different coals and biomass [79-81]. Depending on the fuel characteristics and combustion environment, co-combustion of coal and biomass may either increase or decrease the burnout, compared to dedicated coal combustion.

During co-combustion of coal and straw in a pulverized coal-fired power plant [79], the unburnt carbon in the fly ash is found to decrease progressively with increasing share of straw. On the other hand, the unburnt carbon in the bottom ash is increased with increasing share of straw, which is interpreted as a result of insufficient residence time for some dense straw particles [79]. Similar results are obtained during co-combustion of pulverized coal and sawdust in a full-scale plant [80], showing that the residue carbon in fly ash is decreased by the addition of sawdust and some large unburnt wood particles are seen in the bottom ash. The beneficial effect of biomass addition on the burnout is also observed during co-combustion of lignite and sawdust in an isothermal flow reactor [81], during co-combustion of coal and a number of different biomass in a down-fired combustor [82], and during co-combustion of different coal and biomass both under air and oxy-fuel combustion conditions [83]. In general, the observed effect is likely a combination of several factors. Because of the catalytic effect of inorganic elements and the porous structure, the reactivity of biomass char is usually greater than that of coal char [73-78]. Besides, the biomass char particles are usually non-spherical and have large aspect ratios, which are more favorable in terms of heat transfer and residence time, compared to the equivalent spherical particles [84]. The possible higher flame temperature during co-combustion of coal and biomass may also be an advantage for the burnout [68,69]. Moreover, during co-combustion of coal and biomass, the particle size of biomass char is often larger than that of coal char, which can result in a higher slip velocity between char particles and local gas [3]. Therefore, in the same boiler, the residence time of a biomass char may be longer than that of coal char, and result in an increased burnout.

In contrast to the enhancing effect, some studies show that the addition of biomass can reduce the burnout during co-combustion. The experiments in a pulverized fuel combustion test facility reveal that co-combustion of coal and biomass (straw/wood/miscanthus) results in a reduced burnout compared to dedicated coal combustion [9]. The observed decreased burnout is primarily attributed to the large biomass particle size used in the experiments and the relative short residence time in the test facility [9]. Similar decreased burnout is observed when coal is co-fired with wood in a pulverized coal-fired power plant [85]. Generally, the decreased burnout during co-combustion of coal and biomass is most likely linked to the large particle size and high moisture content of the biomass particles, which may delay the devolatilization and subsequently the char oxidation processes [66]. Selection of biomass with suitable particle size and moisture content is therefore of key importance to ensure a satisfactory burnout in co-combustion of coal and biomass [3,9].

1.2.4 NO_x emission

The formation of NO_x during solid fuel combustion mainly follows three mechanisms, namely thermal NO, prompt NO, and fuel NO [12]. The thermal NO is formed from the reactions between N_2 and O_2, according to the so called extended Zeldovich mechanism:

$$O + N_2 \rightleftharpoons NO + N \quad (1.1)$$

$$N + O_2 \rightleftharpoons NO + O \quad (1.2)$$

$$N + OH \rightleftharpoons NO + O \quad (1.3)$$

The prompt NO formation is initiated by the attacking of hydrocarbon radicals on the N_2 triple bond. The reactions can generate cyanide species which can be subsequently oxidize to NO [12].

The fuel NO is formed from the oxidation of the nitrogen species present in solid fuels. When solid fuels are exposed to high temperature, the nitrogen species are released as volatiles or retained in char during the devolatilization stage. The volatile-N released from primary devolatilization consists of light gases (mainly HCN and NH_3) and tar-N. The tar-N may be decomposed to light gases and soot-N during secondary devolatilization. With the presence of oxygen, the nitrogen in char, soot and light gases may be oxidized to NO or recycled to N_2. The comprehensive fuel-N conversion processes during solid fuel combustion have been reviewed in [12]. The emphasis here is on identifying the possible interactions on NO_x formation during co-combustion of different solid fuels, especially coal and biomass.

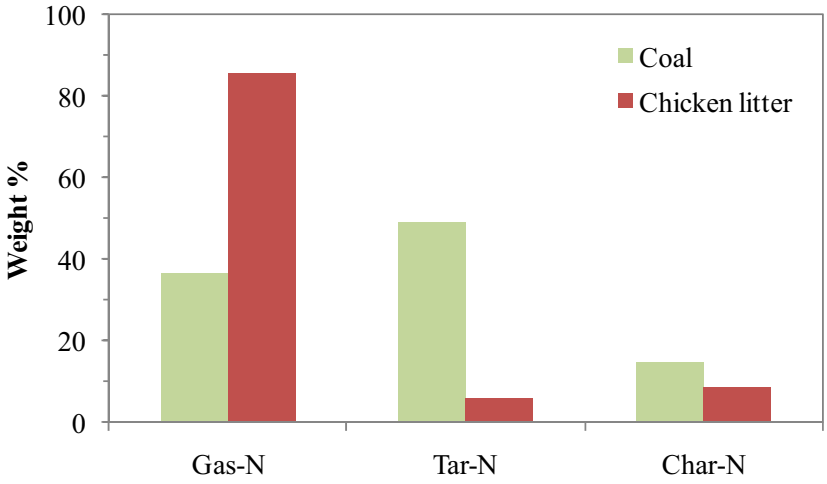

Figure 1.5 Partitioning of fuel nitrogen between gas, tar and char for coal and chicken litter obtained from an experiment carried out at a wire mesh reactor at 1300 ^{o}C [33].

For coal and biomass, the characteristics of the nitrogen species released during devolatilization are usually quite different, with respect to the onset decomposition temperature and product distributions. The release of volatile-N during biomass devolatilization may start at lower temperatures than that of coal [12,86-89]. The release of volatile-N may begin at 200-300 ^{o}C during biomass devolatilization and up to about 50-80% of the fuel-N may be released as volatile-N at 500 ^{o}C [86]. However, for coal, the onset temperature for volatile-N release is usually about 500-600 ^{o}C [33,86]. This difference may be attributed different initial

devolatilization temperatures of coal and biomass, which has been discussed previously, with a typical example given in Figure 1.5. Besides the onset temperature, the distribution of nitrogen products from coal and biomass devolatilization may also be different. A typical example of the distribution of nitrogen species from coal and biomass (chicken litter) devolatilization is given in Figure 1.5. It shows that the formation of gas-N during the biomass devolatilization is much more pronounced than that of coal, whereas the devolatilization of coal produces significantly more tar-N and slightly more char-N [33]. Other studies also support that the formation of gas-N during biomass devolatilization is more pronounced compared to coal [33,87,90]. The major gas-N species from coal/biomass devolatilization are HCN and NH_3. Compared to coal, biomass devolatilization may evolve more NH_3 [12]. This is presumably related to the presence of amino groups in biomass which may directly yield NH_3 through thermal decomposition [90]. In addition, biomass may have more oxygen functional groups that that of coal, which is a favorable condition for the hydrogenation of NH_3 from HCN [12].

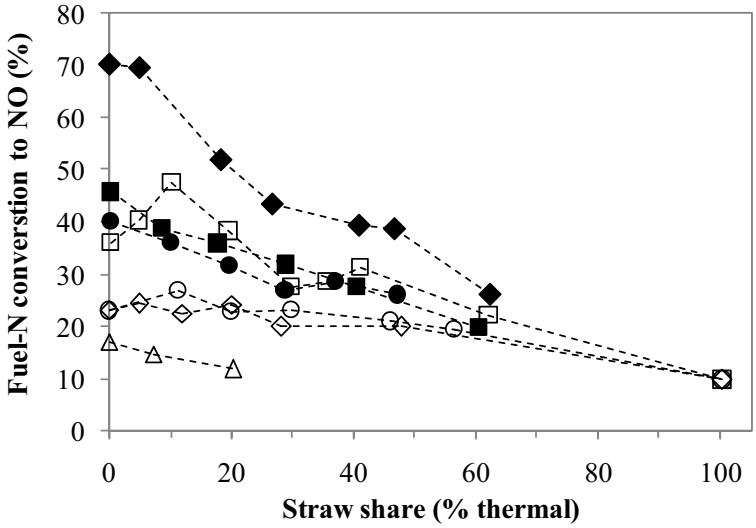

Figure 1.6 Conversion of fuel-N to NO (%) during co-combustion of different coal and straw under pulverized fuel combustion conditions. Solid symbols denote the results from high NO_x flames, while the open symbols denote the results from low NO_x flames [91].

The variations in the distribution of nitrogen species from biomass and coal devolatilization may lead to some interactions for the NO_x formation during co-combustion. In addition, the formation of NO_x during co-combustion is closely related to the flame characteristics, which are affected by the properties and injection method of the secondary fuels. Therefore, the observed effect of co-combustion on NO_x formation is often resulted from a combination of several factors. The formation of NO_x during co-combustion of straw and different coals has been studied in a pilot-scale reactor and a full-scale pulverized coal-fired power plant [91]. As shown in Figure 1.6, the conversion of fuel-N to NO generally decreases with increasing shares of straw. This is conceivably related to the higher volatile and fuel-N release at the near-burner region, which may lower the excess air ratio in the region and thereby reduce the NO formation. In addition, the observed darker flame (lower flame temperature) with increasing share of straw may also be a possible reason for the reduced NO formation. Compared to the low NO_x flames, the effect of

straw addition seems to be even more pronounced for the high NO_x flames, suggesting that burner configuration may be important to the NO_x formation in co-combustion [91]. Similar reducing effect of biomass addition on the conversion of fuel-N to NO during co-combustion has been reported in other studies [7,60,82,92], which generally support the results shown in Figure 1.6. The influence of burner configuration and air staging on NO_x formation during co-combustion is investigated [9,82]. It appears that air staging may enhance the reducing effect of biomass on NO_x formation, if the residence time in the reducing zone is sufficiently long for completing the devolatilization of biomass [9]. The influence of burner configurations on the NO_x formation may be dependent on the characteristics of secondary fuels, as different burner mode is favored when coal is co-fired with straw or sewage sludge [9].

It is worthwhile to mention that the reduced conversion of fuel-N to NO obtained during co-combustion of coal and biomass may not necessarily indicate the presence of net interactions between coal and biomass on NO_x formation. As shown in Figure 1.6, the conversion of fuel-N to NO is lower for pure straw combustion than that for coal combustion. Therefore, the observed reduced fuel-N conversion may simply be an additive effect, since the fuel-N in biomass may have a lower propensity to generate NO_x than that of coal. The experiments carried out by Robinson et al. support that the net interactions of coal and biomass on NO_x emission are insignificant [93], suggesting that the fuels in co-combustion may behave as they are combusted in isolation. However, the experimental results of Robinson et al. are obtained under carefully controlled combustion conditions [93]. In practical applications, the addition of secondary fuels may influence the temperature and stoichiometry of combustion, and certain interactions may exist. A significant reduction on NO_x formation may be achievable through optimizing the burner configurations and air staging during co-combustion [9,82]. In addition, biomass may also be applied as a reburn fuel to minimize the NO_x emission [94,95].

1.2.5 SO_x emission

During solid fuel combustion, the sulphur in the fuel may be converted to gaseous SO_2/SO_3 or partitioned to ash/aerosols. Global equilibrium calculations show that SO_2 is the only stable sulphur species at temperatures above 1200 ^oC during pulverized fuel combustion at oxidation condition [96]. At lower temperatures, part of the SO_2 may be transformed to solid phase, through reacting with inorganic elements such as Ca and K. In addition, a small fraction of SO_2 may be oxidized to SO_3, which may be further condensed as sulfuric acid at certain conditions [97]. However, the formation of SO_3 during pulverized fuel combustion is generally limited to about 0.5-1.5% of the fuel-S [97]. Thus the major SO_x emission from pulverized fuel combustion is SO_2, and the major mechanism for reducing the SO_2 emission during combustion is the reaction between SO_2 and other ash forming elements.

Compared to coal, biomass/waste is often characterized by smaller fuel sulphur content [26]. Therefore, when coal is co-fired with biomass/waste containing less sulphur, it may naturally lead to a decreased SO_2 concentration in flue gas. Beyond this dilution effect, the ash from coal and biomass/waste may have different capture capability towards the gaseous SO_2, which can further affect the SO_2 emission. A typical example of such effect is shown in Figure 1.7. Although with some experimental uncertainties (e.g. the conversion of fuel-S to SO_2 is sometimes above 100%), the general tendency shows that the conversion of fuel-S to SO_2 is decreased with increasing share of straw. This indicates that the ash from straw may be able to capture more gaseous SO_2 than that of coal ash [91]. Similar effect has been observed in other

studies, showing that the S content in the ash from co-combustion is increased with increasing share of straw [9,60,79].

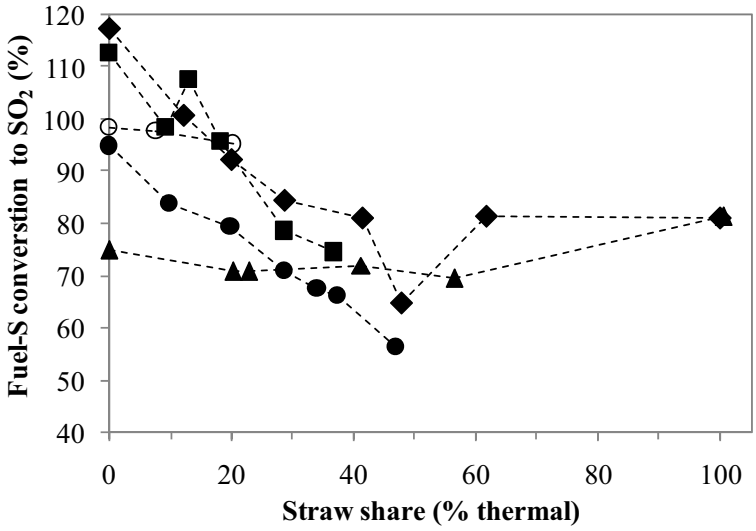

Figure 1.7 Conversion of fuel-S to SO_2 (%) during co-combustion of different coal and straw. Solid symbols denote the results from pilot-scale experiments, while the open symbols denote the results from full-scale tests [91].

The effect of straw addition on the fuel-S conversion in co-combustion is mainly attributed to the high ash and K content of straw [91]. When a secondary fuel with low ash and sulphur content (such as wood) is applied, it probably has a negligible impact on the fuel-S conversion during co-combustion [98]. Besides the properties of the secondary fuel, the fuel injection method and other combustion conditions may also play a role on the fuel-S conversion during co-combustion. Through comparing the experimental results with the predictions of global equilibrium calculations [91], it seems that the reactions between SO_2 and other ash forming elements are kinetically limited. Therefore, if sufficient mixing and long residence time can be provided, the effect of the secondary fuel on fuel-S conversion may become more significant, and vice versa.

1.3 Ash formation, deposition and utilization

Ash related issues such as slagging, fouling, corrosion and particulate emissions are of significant concerns in co-combustion of solid fuels. This is mainly because the secondary fuels applied in co-combustion, such as agricultural residues and waste-derived fuels, usually contain large amount of alkalis and chlorine that may be easily released to gas phase during combustion. The released alkali and chlorine may generate alkali chlorides and may cause severe ash deposition and corrosion on the heat transfer surfaces. In addition, the vaporized inorganic elements are a major precursor of the aerosols generated from combustion. These aerosols are not only the main source of particular matters emitted to the environment, but also a major reason for the deactivation of SCR units in the plant. Therefore, it is critical to understand and

address the ash related problems in co-combustion. With this objective, the fundamentals on ash formation, deposition, corrosion and utilization in solid fuel combustion are reviewed in this section. In addition, the possible interactions among different solid fuels on ash related issues are also evaluated. It should be noted that the present section mainly focuses on the behavior of the major ash forming elements in co-combustion, since these elements dominate the ash formation.

1.3.1 Ash forming elements in solid fuels

The ash forming elements that are significantly concerned during co-combustion of coal and biomass/waste are K, Na and Cl, since the ash related problems mentioned earlier are to a large extent induced by these elements. Despite of the diverse nature of coal, biomass and waste, the content of K, Na and Cl in these fuels shows some general tendency, which may be related to the origins/biological features of these fuels. Figure 1.8 shows the concentrations of ash, alkali (K+Na), and Cl in several different groups of biomass, waste and coals. These biomass/waste are chosen because they are extensively used in co-combustion [93,99-104]. Although the data shown in Figure 1.8 are comprehensive, they can still reveal some general features of these fuel groups. The features observed are: (1) woody biomass is generally of the lowest ash, alkali and Cl content among the fuel groups; (2) grasses usually have slightly larger ash, alkali and Cl content than that of woody biomass; (3) coals are comparable to grasses or woody biomass in terms of alkali and Cl content, but the ash content is often considerably larger and varies significantly; (4) the ash and alkali content in RDFs (refuse derived fuels) is generally within the range of coals, but the Cl content is significantly larger; (5) the straws are comparable to RDFs in terms of Cl and ash content, but have a significantly larger alkali content than that of other fuel groups.

Comparison of the alkali and Cl content of the fuel groups in Figure 1.8 indicates that straw may be the most problematic fuel group to be used in co-combustion, since it has both large Cl and alkali content. On the other hand, a fuel with large Cl and alkali contents may not necessarily lead to severe ash related problems in combustion, since the Cl and alkalis in the fuel may undergo complicated reactions with other ash forming elements during combustion. These reactions may prevent the formation of alkali chlorides, by converting the Cl and alkalis to less harmful species (such as HCl, alkali aluminosilicates/sulphates). Therefore, in addition to the content of Cl and alkali in the fuel, the content of other ash forming elements also plays an important role on the ash behavior during combustion.

One of the major inorganic elements that may influence the behavior of alkali and Cl during combustion is Si. This is because some Si containing minerals in the fuel (such as kaolinite) may react with the gaseous alkali chlorides generated from combustion, and lead to the formation of high-melting temperature alkali aluminosilicates/silicates and gaseous HCl. The molar ratios of (Na+K)/Si and Cl/Si in different fuel groups are plotted in Figure 1.9. It shows that the molar ratios of (Na+K)/Si and Cl/Si in coals are generally much smaller than that of other fuel groups, indicating that coals may contain relatively more reactive Si species than other fuel groups, which may prevent the formation of alkali chlorides during combustion. For the remaining fuel groups, the variations of the molar ratios of (Na+K)/Si and Cl/Si are significant, and no general tendency can be observed.

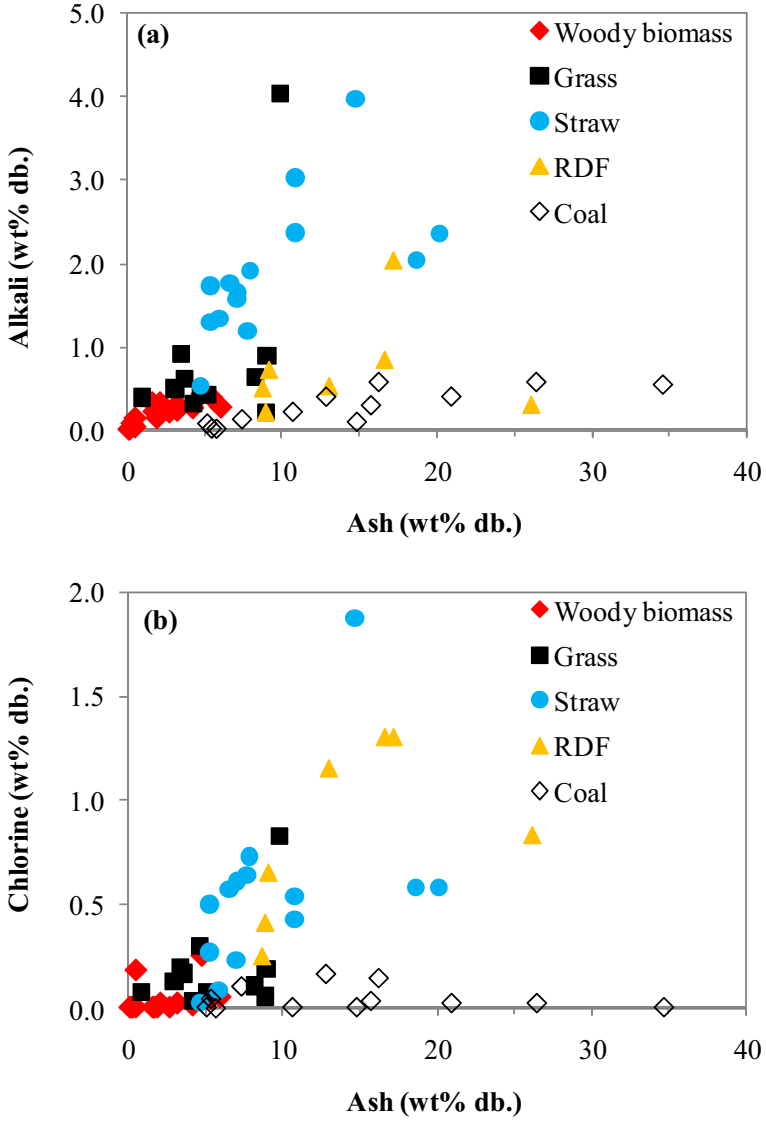

Figure 1.8 (a) alkali content (wt% db.) versus ash content (wt% db.) in different solid fuels, (b) chlorine content (wt% db.) versus ash content (wt% db.) in different solid fuels. The data are derived from open literature [26,93,99,101-106].

The fuel S content also plays an important role in mitigating the ash related problems caused by the Cl and alkali content. It is primarily because of the gaseous S (SO_2/SO_3) may react with the alkali chlorides, generating alkali sulphates which do not only have higher melting temperatures than alkali chlorides, but also are less corrosive for heat transfer surfaces. The molar ratios of (Na+K)/S and Cl/S in different fuel groups are shown in Figure 1.10. It is obvious that the coals generally have much smaller (Na+K)/S and Cl/S molar ratios compared to other fuel groups. This indicates that coal combustion may generate relatively more SO_2/SO_3, and the extent of

sulphation reaction on alkali chlorides may be more significant. For the remaining fuel groups, it seems that there is no general difference among these groups, with respect to the molar ratios of (Na+K)/S and Cl/S.

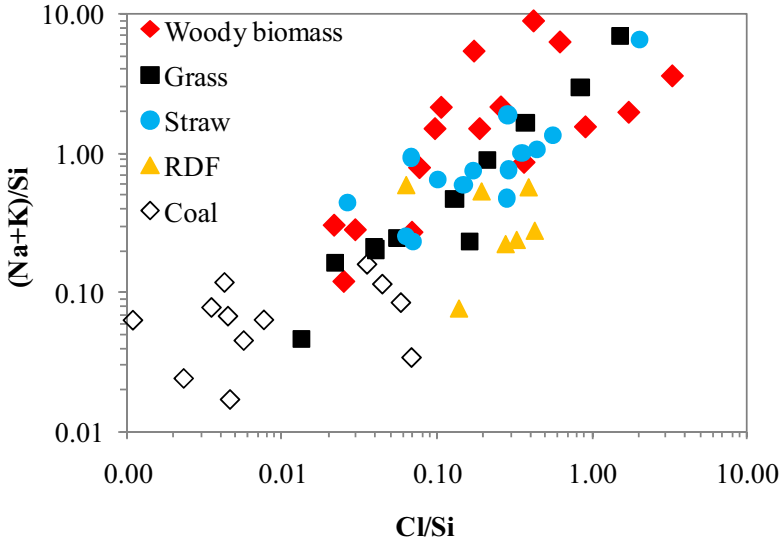

Figure 1.9 Molar ratios of (Na+K)/Si versus Cl/Si in different solid fuels. The data are derived from open literature [26,93,99,101-106].

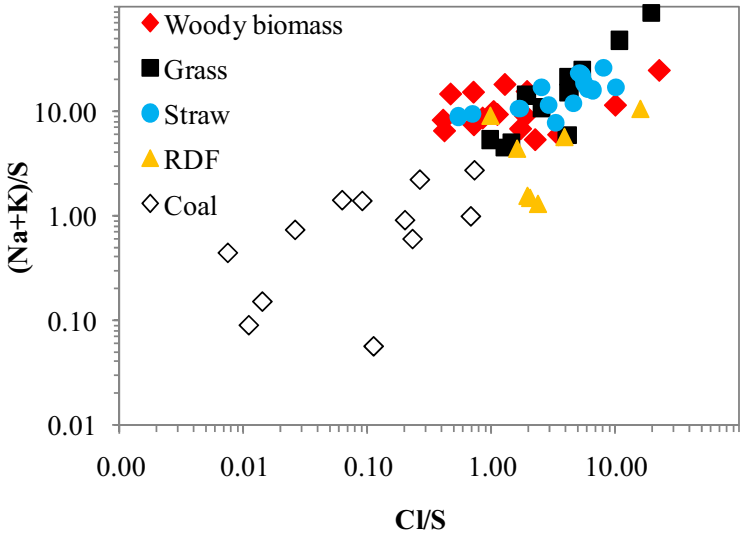

Figure 1.10 Molar ratios of (Na+K)/S versus Cl/S in different solid fuels. The data are derived from open literature [26,93,99,101-106].

Other ash forming elements may also directly or indirectly influence the behavior of alkali and Cl in combustion. For example, the Ca in the fuel may react with part of the Si or S species, which may inhibit the reactions between alkalis and these species [99]. The Al in the fuels may

to some extent affect the reactivity of the Si species on alkali chlorides, since aluminosilicates are usually more reactive than silicates [107]. However, in most cases, these ash forming elements are not the most critical elements that can induce or mitigate the ash related problems in co-combustion. Therefore, a comparison of the content of these ash forming elements in different fuel groups are not provided here. More insights to the ash properties of different solid fuels can be found elsewhere [26,105].

Besides the fuel groups mentioned earlier, there are some other biomass/waste groups which are also widely used as secondary fuels in co-combustion, such as sewage sludge, animal residue and seed-originated biomass. In general, sewage sludge is characterized by significantly larger ash content (~30–50 wt%, dry basis) than other biomass/waste groups, and the ash usually contains considerable amount of Si, Fe, Al, Ca and P [108-111]. Animal residues, such as manure or meal and bone meal (MBM), may have larger ash, Ca and P content than the typical woody/grassy biomass [112-114]. Another special group of biomass is seed-originated biomass, such as grain and rapeseed meal, which usually has significantly larger P content than that of other biomass [115-119].

1.3.2 Association of ash forming elements

The concentration of the ash forming elements in the fuel is not the only factor that influences the ash behavior during combustion. An additional factor which can play an important role is the association of these elements. Although different classification methods may be used, the ash forming elements in solid fuels can be generally categorized as organic association (elements that are organically bound, ionically bound or water dissolvable) and mineral association (elements that exist as included or excluded minerals) [120,121]. The association of the ash forming elements may not only greatly affect the vaporization behavior of these elements during combustion but also influence their reactions.

A number of methods have been applied to evaluate the association of ash forming elements in coal, such as microscopy based techniques (e.g. CCSEM) and spectroscopy based techniques (e.g. XAFS and XRD) [122,123]. However, some of these techniques developed for coal may not be appropriate for biomass, since biomass is often characterized by a low degree of mineralization. A widely used method for identifying the association of ash forming elements in biomass/waste is the chemical fractionation method, which was initially developed for coal [124,125], and later adapted to biomass/waste [126,127]. The chemical fraction method is a sequential leaching method. According to the standardization proposed by Zevenhoven et al. [127,128], the fuel sample is leached successively by water, 1 M ammonium acetate and 1 M hydrochloric acid, and then the concentrations of ash forming elements in these solutions as well as in the residue are analyzed. The partitioning of the ash forming elements to different fractions can provide information about the occurrence mode of these elements. In general, it is considered that the easily soluble salts such as alkali chlorides and sulphates would appear in the water soluble fraction; the organically associated ions would be mostly present in the ammonium acetate solution; the acid solution would consist of acid-soluble salts or minerals like earth alkaline carbonates and sulphates; and the residues would be primarily comprised of mineral materials such silicates or aluminosilicates [127,129]. It has to be mentioned that the interpretations to the chemical fractionation results are quite fuel/element specific, and there is no general agreed guidelines for quantifying the results [129]. Nevertheless, the chemical fractionation analysis is still considered to provide valuable information about the speciation of

ash forming elements in different solid fuels, and the information is important for understanding the behavior of these elements during combustion [128].

Based on the chemical fractionation analysis [130-134], the association of some critical ash forming elements in different solid fuels is compared in Figure 1.11–Figure 1.13. In the figures, the fractions that are leached by water and ammonium acetate are summed together, since these fractions are considered to behave similarly during combustion (i.e. relatively easier to be released to gas phase). The remaining fractions, i.e. acid soluble fraction and residue fraction, are considered to be more difficult to be released during combustion.

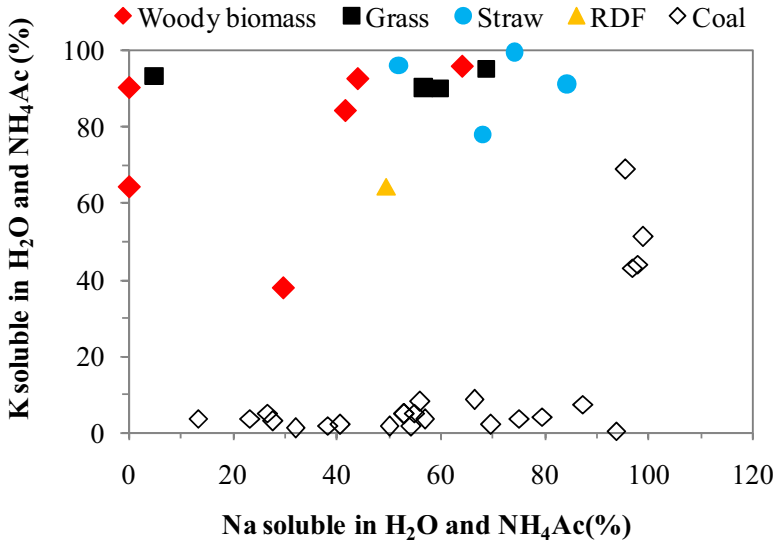

Figure 1.11 Percentage of K and Na (%) that appears as H_2O and NH_4Ac (ammonium acetate) soluble in different solid fuels. The data are derived from open literature [130-135].

From Figure 1.11, it is seen that the majority of the K (60–100%) in biomass/waste is leachable by water and ammonium acetate, while this fraction in most coals is usually less than 10% (except for some low rank coals). This indicates that the association of K in biomass/waste may be quite different from that of coal. In live plants, such as wood and straw, the K may predominantly exist as mobile ions surrounded by water molecules, or present as organically associated K such as oxalates and oxygen-containing functional groups. When the plants are harvested and dried, part of the K ions may be converted to KOH, KCl and K_2CO_3, and the remaining may still be dissolved in water, depending on the extent of the drying process [136]. The K species mentioned above are mostly leachable by water and ammonium acetate. However, the K in coals may be mainly present as minerals, such as illite and muscovite [131,136-138], which are difficult to leach by water and ammonium acetate. However, for some low rank coals, such as lignite, a considerable fraction of K may exist as water and ammonium acetate soluble [135]. Compared to K, the fraction of water/ammonium acetate soluble Na in coals is larger (20–100%) and shows greater variations. This is presumable because a certain fraction of Na in coals is present as water soluble salts such as NaCl or organically associated [131,139]. For biomass/waste, the percentage of Na that is leachable by water and ammonium acetate varies significantly for different biomass/waste, and no general tendency is observable.

Figure 1.12 shows the percentage of Cl and Si that are present as water and ammonium acetate soluble in different solid fuels. It is seen that the Cl is almost fully soluble in water and ammonium acetate in different solid fuels. This may be explained by the association of Cl in these fuels. In coals, the Cl may exist as chloride anions in moisture, inorganic chlorides (such as NaCl and KCl), or organic chlorine compounds (such as covalently bonded Cl or Cl combined to organic complexes) [140]. For biomass, the majority of Cl may be associated with the nutrient cycle and the living portion of the biomass materials [140], in forms of free anions or loosely bound to exchange sites [141]. These Cl species are generally leachable by water and acetate solution. However, for some plastics materials, such as PVC, the Cl may not be soluble in water and acetate solution, but still can be released to gas phase during combustion [131]. This may explain the large fraction of insoluble (by water and acetate) Cl found in RDF in Figure 1.12. Besides, in some coals, the Cl may be associated with minerals such as sodalite ($Na_8(AlSiO_4)_6Cl_2$) [140], which may be a possible explanation for the insoluble Cl part. It has to be mentioned that there are some limitations in determining the partitioning of Cl through the chemical fractionation analysis [131,132]. For some low-Cl fuels, such as coal and wood, the concentration of Cl in the water or acetate solution may be below the detection limit of the analysis method, and the analysis uncertainties may be considerably high [129]. Besides, since it is not possible to determine the fuel-Cl that is leached by the HCl solution and the Cl content in the residue is often greatly influenced by the HCl leaching process, the reliability of the chemical fractionation method on Cl partitioning may not be evaluated through mass balance calculations. These limitations need to be considered when evaluating/utilizing the results from chemical fractionation analysis.

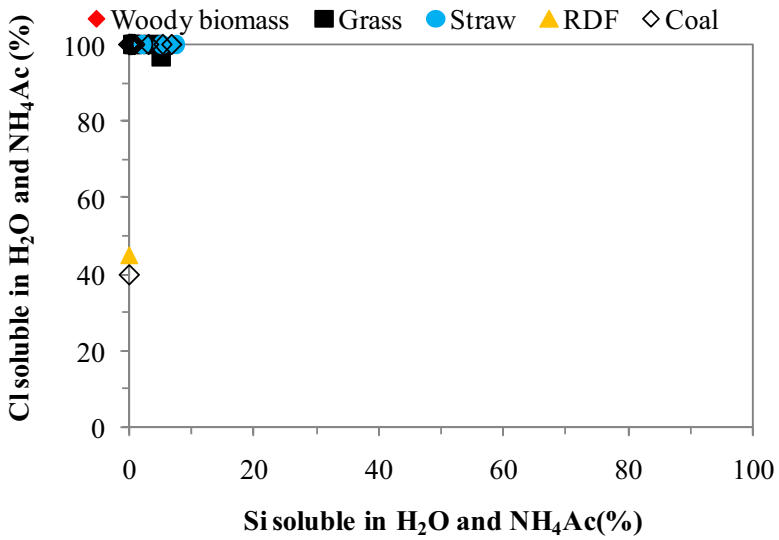

Figure 1.12 Percentage of Cl and Si (%) that appears as H_2O and NH_4Ac (ammonium acetate) soluble in different solid fuels. The data are derived from open literature [130-135].

In contrast to Cl, the Si in different solid fuels is mostly (>90%) not soluble by water and ammonium acetate, as shown in Figure 1.12. For coals, the Si may predominantly exist as minerals such as quartz, kaolinite and illite [137]. In biomass, the Si may be present as polymerized silicic acid, which is an amorphous mineral of silica with varying amount of crystal

water ($SiO_2 \cdot nH_2O$) [129,141]. In addition, a certain fraction of Si in biomass may be from the soil contaminations during the collection process, which may exist as quartz and clay materials [142].

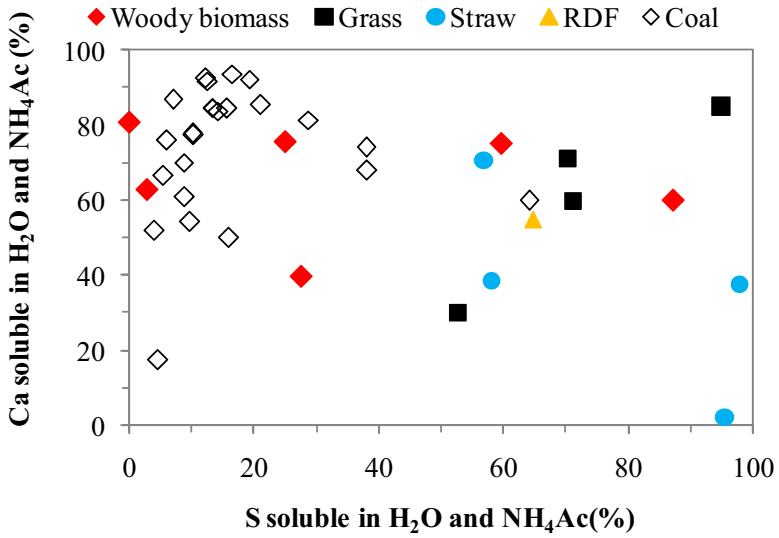

Figure 1.13 Percentage of Ca and S (%) that appears as H_2O and NH_4Ac (ammonium acetate) soluble in different solid fuels. The data are derived from open literature [130-135].

Figure 1.13 shows the percentage of S and Ca that is present as water and ammonium acetate soluble in different solid fuels. It appears that coals generally contain less water and acetate soluble S than that of grasses and straws, indicating that the association of S may be different in these fuels. In coals, the S may be mainly present as minerals (mainly as pyrite but also as other sulfides and sulphates) or organically associated with aliphatic, aromatic, and heterocyclic structures. The sulphide minerals, which are usually the dominant inorganic S components in coals, are largely insoluble in water or ammonium acetate solutions. In addition, the organically associated S in coals is also found to have a low solubility in water or other organic solutions [143]. This may explain the relatively small fraction of the water and ammonium acetate soluble S found in coals. On the other hand, the S in biomass may be mainly present as inorganic sulphates or organically associated S with aliphatic nature such as in proteins, sulphate ester and sulphur lipids [141,142]. The sulphates may be easily leachable by the water and ammonium acetate solution, whereas the organically associated S may be difficult to be dissolved in these solutions [129]. For annual crops such as straw and grass, a large fraction (>50%) of S in these biomass may be present as sulphates, as indicated by the S release characteristics during the pyrolysis of these biomass [144]. However, for woody biomass, the majority of S may be organically associated, thus the water and ammonium acetate soluble fraction is usually only around 25% [129]. Compared to S, the percentage of Ca that is present as water and ammonium acetate soluble varies significantly for different fuels, and no tendency can be seen for different fuel groups. In biomass, the Ca that is leachable by water and ammonium acetate may be mainly ionic Ca (acting as counter ions for organic and inorganic anions such as malate and nitrate), Ca oxalate and other calcium salts of carboxylic acids [131,141]. In coals, the majority of Ca that is water and ammonium acetate leachable may be present as carboxylic groups and carbonate [131].

1.3.3 General ash formation mechanism

The ash formation mechanism in pulverized fuel combustion has been well-established [121,139,145-151]. As shown in Figure 1.14, the ash particles generated during pulverized fuel combustion primarily originat from excluded minerals, included minerals and organically associated ash forming species in the fuel particles. When the fuel particles are combusted, a fraction of the included minerals and organically associated ash forming elements may be released to gas phase, either through a direct release mechanism or a mechanism involving reducing reactions. After that, the vaporized inorganic elements may nucleate to ultrafine particles, condense on the surface of the existing particles, or chemically react with other particles. The partitioning of the vaporized inorganic elements may be dependent on the fuel properties and the combustion conditions such as cooling rate and particle density in the flue gas [121]. The ultrafine particles generated from the nucleation of inorganic vapors may aggregate/coalesce with themselves to form larger particles, which are usually an important source of submicron ash particles formed during pulverized fuel combustion. On the other hand, the ultrafine particles may also attach to the surface of the existing large fly ash particles, which may therefore partition to the supermicron ash particles.

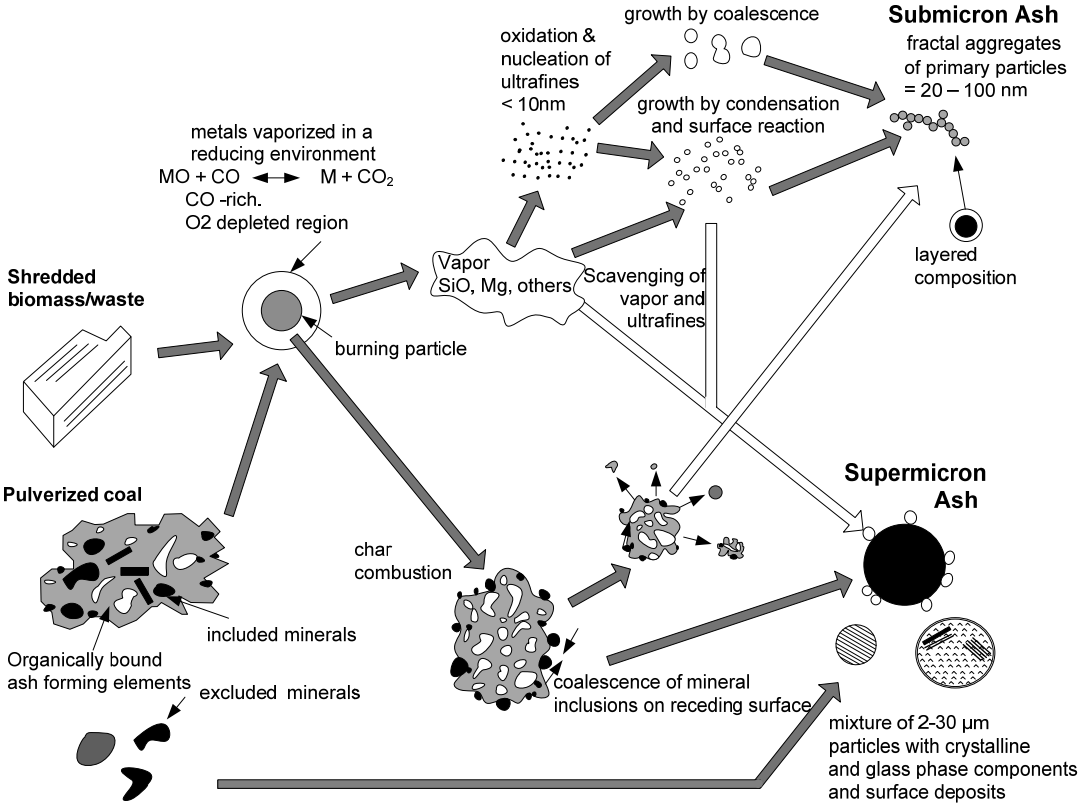

Figure 1.14 Ash formation pathways during solid fuel combustion, adapted from [121] .

In addition to the fraction that is vaporized, the remaining minerals and organically associated ash forming elements in the fuel particles may undergo fragmentation, melting and coalescence

during the fuel conversion process. The majority of these ash forming elements may result in the formation of supermicron ash particles, while a small fraction may contribute to the formation of submicron ash particles, probably via the fragmentation mechanism. The excluded minerals may also experience melting and a small extent of fragmentation/coalescence (depending on the mineral type), and may be converted mainly to supermicron ash particles during the combustion process.

Figure 1.14 shows that ash formation during solid fuel combustion is a complicated physical and chemical process, and may be affected by a number of factors. In the following sections, the release and transform of ash forming species during solid fuel combustion will be described in detail, with a special focus on the possible interactions during different fuels.

1.3.4 Release of ash forming elements

As mentioned earlier, the release of ash forming elements during pulverized fuel combustion may follow a direct release mechanism or a mechanism involving reducing reactions. The direct release mechanism may involve the release of organically associated elements during devolatilization or char oxidation, and the direct vaporization of some volatile inorganic species, such as NaCl and KCl. The reducing mechanism is usually applied for the species having low vapor pressure during combustion, such as SiO_2 and CaO. With the reducing environment generated by devolatilization or char oxidation, these oxides may be reduced to more volatile sub oxides or elemental vapor, which would facilitate the vaporization of these elements [149,150,152,153].

The vaporization of ash forming elements during pulverized coal combustion has been studied extensively through experiments and modeling [152,154-161]. These studies generally suggest that the vaporization of refractory oxides (such as SiO_2, Al_2O_3, CaO and MgO) during pulverized coal combustion is mainly achieved through the reducing mechanism described by the following global reaction:

$$MO_n(c) + CO \rightleftharpoons MO_{n-1}(v) + CO_2 \tag{1.4}$$

where MO_n and MO_{n-1} refer to the refractory oxide and the corresponding volatile suboxide or metal vapor, respectively. In the modeling approach of Quann and Sarofim [152], it is assumed that the equation above is in equilibrium on the surface of mineral inclusions in the char particle and the CO_2 is only produced from the reaction above (i.e. the vapor pressure of MO_{n-1} and CO_2 is the same). With these assumptions, the vapor pressure of MO_{n-1} on the surface of the mineral inclusions can be predicted from the partial pressure of CO and the equilibrium constant of the reaction. By taking into account the internal and external diffusion of the vaporized MO_{n-1} in the char particle as well as the interactions between different mineral inclusions, the vaporization of MO_n during pulverized coal combustion has been reasonably well modeled [152]. However, as pointed out later by some following work [156,157,160], there are some limitations in the model developed by Quann and Sarofim [152]. In their model, the vapor pressure of CO_2 on the mineral inclusion surface may be underestimated, which may result in an over estimation of the vapor pressure of MO_{n-1} [156,157]. Besides, the model also neglects the enlargement of the pores and the corresponding increase in effective diffusivity near the surface of burning char particle, which may overestimate the diffusion resistance to vaporization [160].

In addition to the reducing mechanism mentioned above, direct release mechanism may also play a role, particularly for low rank coals, such as lignites, which contain substantial amount of alkali and earth alkali metals. A typical example is the release of Na during the combustion of low rank coals [139,153,162,163]. The Na in low-rank coals may be primarily associated with organic matter or exist as halide (NaCl) [139,153]. During combustion this organically associated Na and halide may be vaporized to gas phase as metal, oxide or chloride, due to the high vapor pressure of these species [153]. For lignite, above 40% of the Na in the fuel was found to be vaporized at a furnace temperature of 1477 ^{o}C and at 20% O_2 condition [153]. A significant percentage (~18%) of the Mg was also found to be vaporized at the same experimental condition, consistent with the large amount of organically associated Mg in the low rank coal [152]. However, the vaporization of organically associated Mg may still follow a reducing mechanism, but with significantly reduced diffusion resistances compared to mineral inclusions [152].

The vaporization of ash forming elements during pulverized coal combustion may be influenced by various factors. In general, with higher combustion temperature, the vaporization of ash forming elements through the reducing mechanism can be promoted [152,160], whereas the vaporization of alkali metals (such as Na) may be reduced by an increased reaction rate between the vaporized alkali metals and silicates/aluminosilicates in the coal [153,163]. The particle size of coal may affect the vaporization of refractory oxides as well. With decreasing particle size, the vaporization of refractory oxides through the reducing mechanism may be promoted, presumably related to distribution of mineral inclusions in the particle [152]. The gas environment may also play an important role on the vaporization of ash forming elements. According to the model developed in [152], it is obvious that a more reducing environment is favorable for the vaporization of refractory oxides, when the combustion temperature is fixed. The association of ash forming elements also greatly influences their vaporization behavior. The organically associated elements are usually easier vaporized compared to mineral associations [152,153]. On the other hand, the distribution between excluded and included minerals may also have some impact. A positive correlation may be found between the vaporization of refractory oxides and their association as included minerals [152,164]. This is likely because included minerals may experience higher combustion temperature and more reducing conditions that of excluded minerals.

It should be noted that in the majority of the studies mentioned ealier, the vaporization of ash forming elements is quantified by sampling fine particles after combustion [152,154-161]. Therefore, the obtained vaporization results are naturally interfered by the secondary reactions between the vaporized species and other ash forming species. Such influence is particularly pronounced for the vaporized alkali species [153,163]. These possible secondary reactions will be discussed in detail in the following section.

Compared to pulverized coal combustion, the vaporization of ash forming elements during pulverized biomass/waste combustion has been less investigated and literature on this subject is scarce. Recently, Shah et al. has attempted to quantify the release of inorganic elements during pulverized biomass combustion, by performing experiments in a lab-scale combustion simulator with high initial heating rate (10^5 ^{o}C/S) and temperature (1450–1600 ^{o}C) [165,166]. The release of inorganic elements is quantified by assuming the elements present in vapor phase and in the submicron aerosols are vaporized during the combustion. The results obtained after complete combustion (with a residence time of about 1300 ms) are shown in Figure 1.15. It can be seen that the release of S and Cl is fairly complete (>80%) during the combustion of pulverized

biomass or coal, and no significant deviation is observed for different biomass or coal. However, the release behavior of alkali metals is considerably different for coals and biomass. For K, it appears that above 90% of the K in woody biomass has been released to gas phase, which is only slightly higher than that of straw (~80%) but significantly greater than that of coals (<20%). Such difference may be primarily related to the different associations of K in biomass and coal, as illustrated in Figure 1.11. In addition, the secondary reactions between the vaporized K and the mineral matters in the fuels may also influence the K release obtained in the experiments. Compared to the K release, the deviations between the Na release in biomass and coal seem to be less significant, which may be explained by the variety of the Na association in coals, as shown in Figure 1.11. Compared to alkali metals, the release of Mg and Ca is generally less pronounced during pulverized biomass/coal combustion. However, for woody biomass, a considerable fraction of the Mg and Ca (20-50%) may still be released to gas phase during combustion. For Al and Si, the release is generally found to be negligible for different fuels [165,166].

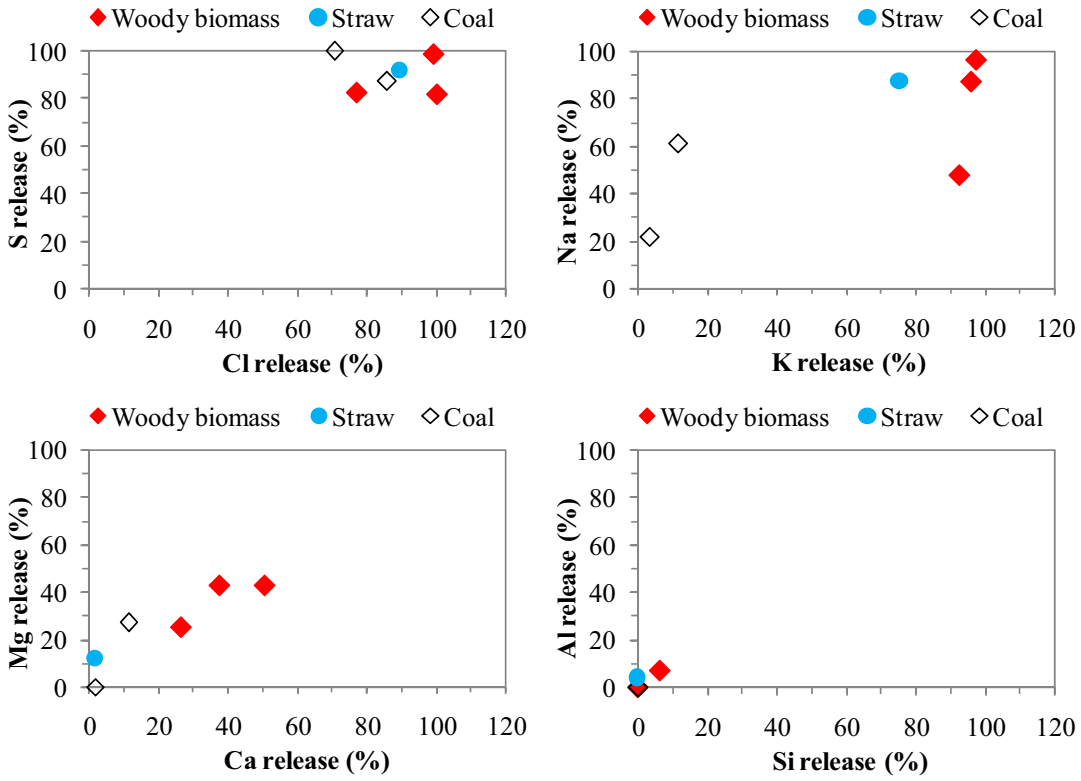

Figure 1.15 Release of ash forming elements under pulverized fuel combustion condition. The data are derived from [165,166], with a residence time of about 1300 ms (almost complete combustion). The woody biomass refers to bark, wood chips and waste wood, and the coals are a UK and a Polish coal.

The release of ash forming elements during biomass/waste combustion has been better characterized at grate-firing conditions [128,141,142,144,167-173]. Although the results may not be directly transferred to pulverized fuel combustion conditions, these studies can provide valuable insights to the release mechanisms of these elements, and the guidelines for the

important parameters that may influence the release.

Figure 1.16 shows the release of Cl at a function of temperature during the combustion of different biomass groups such as straw and woody biomass as well as some waste materials such as fiber board and PVC [142,168,172]. The results presented are obtained from the same laboratory-scale reactor and the experimental conditions are similar for different fuels. Thus the deviations shown in the figure mainly result from the different fuel characteristics. From the figure, it is seen that approximately 20-60% of the Cl is released from straw at a combustion temperature of 500 °C, and the remaining Cl is mostly released in a temperature range of 500–800 °C. For woody biomass, the release of Cl (>80%) seems to be greater than that of straw at 500 °C. However, the quantification of Cl release during wood combustion is usually rather difficult to perform due to the low Cl content in most of woody biomass, thereby only very limited woody biomass data are shown in Figure 1.16. Different from the woody biomass and straw, the Cl in the fiber board/PVC is almost completely released at a combustion temperature of 500 °C.

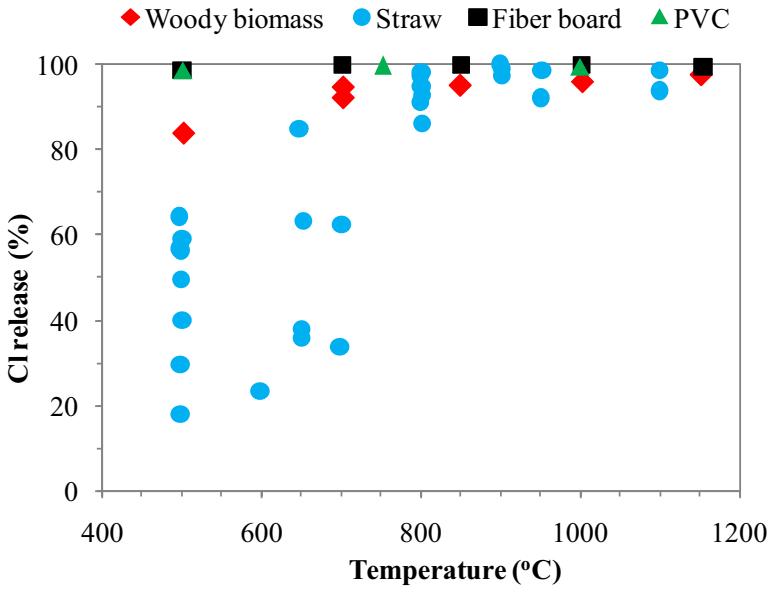

Figure 1.16 Release of Cl at different temperatures under grate-firing conditions [142,168,172].

The release of Cl at combustion temperature below 500 °C is primarily due to the vaporization of HCl (g) [141,142,167,168,172]. Since the majority of Cl in straw or woody biomass is leachable by water [131,174], it is suggested that the Cl in straw or woody biomass may predominantly exist as KCl. Thus a major mechanism for the release of Cl at temperatures below 500 °C is considered to be the reaction between KCl and the carboxylic groups of the fuel, which could result in the formation of HCl (g) and char-K [141,142,167,168,172]. The presence of such a reaction is supported by the considerable Cl release observed at 400 °C, when pure KCl is mixed with wood or cellulose [175]. However, the extent of the reaction may be confined by the available proton-donating sites in the char/fuel. In general, a negative correlation is found between the Cl release at 500 °C and the Cl content in straw [142]. This indicates that for a fuel with high Cl content compared to the number of proton-donating sites, the conversion of KCl to

HCl (g) may be relatively low. This may be an explanation to the observed deviations of the Cl release at 500 °C in Figure 1.16, especially the general difference between the low-Cl woody biomass and the high-Cl straw. On the other hand, a small fraction of Cl in biomass may be combined to the organic structures. The Cl may be released directly during the devolatilization, either in tar or decomposed to HCl (g) [142,173]. A typical example of the release of the organically associated Cl is the combustion of PVC. As shown in Figure 1.16, almost all of the Cl in PVC is released to gas phase at 500 °C, which is because the organically bound Cl has been decomposed to HCl (g) during devolatilization in a temperature range of ~200–370°C [29-32].

The second stage of Cl release during biomass combustion, which mainly happens in the temperature range of 500–800 °C, is mostly a result of KCl or NaCl vaporization [141,142,167,168,172]. The vaporization of KCl and NaCl during biomass combustion has been detected directly by a molecular beam mass spectrometer system [174]. It should be noted that at lower temperatures, such as 650 °C, the vaporization of KCl may be limited by the diffusion resistances, particularly in the reactor used in [142,168,172]. However, at higher temperatures, such as 800 °C, the diffusion resistances would become negligible, due to the high vapor pressure of KCl [167].

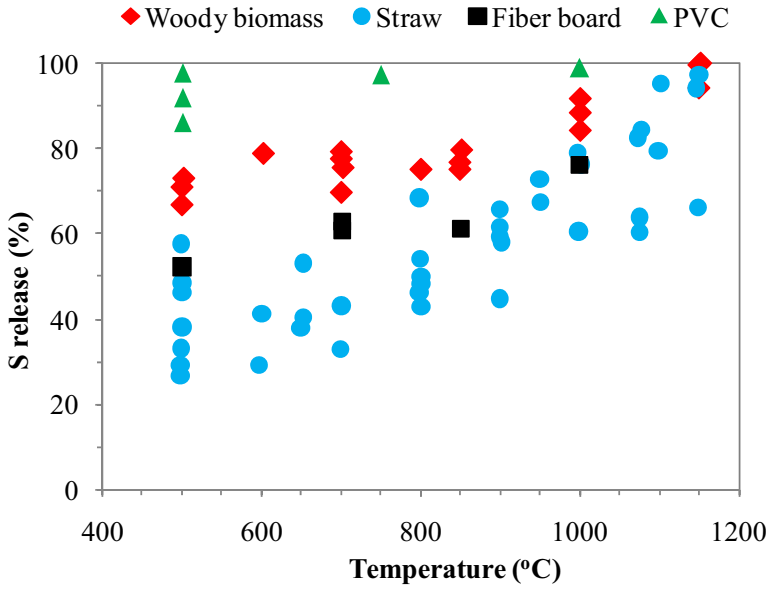

Figure 1.17 Release of S at different temperatures under grate-firing conditions [142,168,172].

Figure 1.17 shows the release of S during the combustion of biomass and waste materials at different temperature [142,168,172]. For straw, it appears that approximately 20–60% of the S is released at 500 °C. With increasing temperature, the release of S increases progressively and for most of straw the S is almost completely released at a combustion temperature of 1150 °C. Compared to straw, the release of S during woody biomass combustion is generally greater in the temperature range of 500–1000 °C. At 500 °C, the S release for woody biomass is mostly in the range 60–80%, and the release is not significantly increased up to 850 °C. In the temperature range of 850–1150 °C, a considerable increase of the S release is observed for woody biomass, and an almost complete release is achieved at 1150 °C. Different from biomass, the S release

during PVC combustion seems to be completed already at 500 °C. For fiber board, the characteristics of the S release are quite similar to that of straw.

The release of S during biomass combustion at temperatures below 500 °C is mainly attributed to the release of organically associated S during the devolatilization process [141,142,167,168]. This is supported by the fact that the S release obtained during straw pyrolysis and combustion is similar at 500 °C [142]. In addition, the S release obtained during woody biomass combustion at 500 °C seems to be correlated well with the organic S fraction derived from the chemical fractionation analysis [168]. Thus the deviations of the released S at 500 °C for different woody biomass and straw may be explained by the different S associations in these fuels.

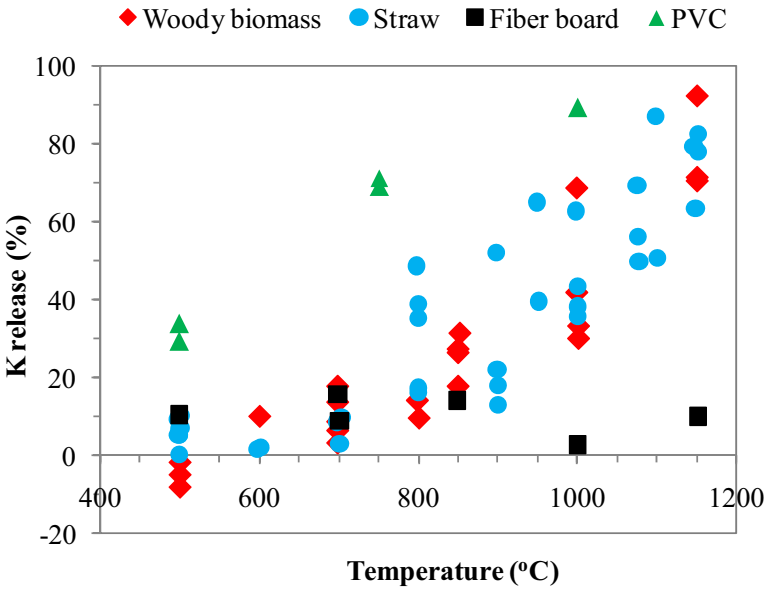

Figure 1.18 Release of K at different temperatures under grate-firing conditions [142,168,172].

The release of S at higher temperatures may follow more complicated mechanisms. For straw with relatively high Si content, the reaction between K_2SO_4 and silicates may contribute to the S release at temperatures above 700–800 °C, through the formation of K-silicates and SO_2 (g). The contribution of this reaction to the S release may be greatly affected by the molar ratio of K/Si in the fuel [142]. Besides, the Cl in the fuel may also indirectly affect the S release at temperatures above 500 °C. With a greater Cl/K molar ratio in the fuel, the S release in the temperature range of 700–950 °C is found to be increased, presumably due to the fact that part of the alkali sulphate is converted to alkali chloride and SO_2 [142]. On the other hand, the direct vaporization or decomposition of sulphate (such as K_2SO_4 or $CaSO_4$) may also constitute an important S release mechanism at high temperatures, particularly for fuels with relatively low Si and Cl content (such as woody biomass) [142,168]. However, in most cases, the contribution of this mechanism to S release is insignificant at temperatures below 1000 °C, due to the low vapor pressure and high thermal stability of the sulphates. At higher temperatures, this mechanism becomes increasingly important, and contributes greatly to the almost complete S release at about 1150 °C.

The release of K during the combustion of biomass and waste materials at different temperature

is shown in Figure 1.18. It is seen that for the majority of the woody biomass and straw, the release of K is insignificant at temperatures below 600 ^{o}C. Most of the K in woody biomass and straw is released in the temperature interval of 700–1150^{o}C. At 1150 ^{o}C, the release of K from woody biomass and straw is found to be in a range of 60–90%. In general, large deviations are observed for different biomass with respect to the K release and no general tendency is seen between straw and woody biomass. Compared to biomass, the K release in PVC seems to be greater and occurring at lower temperatures. For the fiber board, a general low K release is seen up to 1150 ^{o}C, which may be related to the high Ti content in the fuel [168].

Several different mechanisms may contribute to the K release during woody biomass and straw combustion. At temperatures below 500 ^{o}C, although the release of K is generally insignificant and may be greatly affected by the experimental uncertainties, a small fraction of K (0–10%) may still be released due to the decomposition of organically associated K [142,168]. In the temperature range of 500–800 ^{o}C, the release of K for Cl rich biomass is mainly via the vaporization of KCl, which is supported by the fact that the molar ratio of the released K/Cl is about 1 [142]. The release of K through KCl vaporization may be promoted by increasing the molar ratio of Cl/K in the fuel [142]. On the other hand, for biomass with relatively low Cl content such as wood, the contribution of KCl vaporization to K release is rather limited. Thus the major K release mechanism for these biomass during 500–800 ^{o}C is considered to be the decomposition of the K associated with the char matrix or the decomposition of K_2CO_3 [167,168]. At temperatures above 800 ^{o}C, irrespective of the original Cl content in the fuel, a major K release mechanism is considered to the vaporization of K or KOH originated from the decomposition of K_2CO_3 or the char associated K. In a dry environment, the decomposition of K_2CO_3 may produce elemental K, which may be vaporized and subsequently react with other gaseous species. With the presence of water vapor, the K_2CO_3 may be decomposed to KOH (g), which may considerably promote the release of K [167,169]. However, the K release during biomass combustion may be adversely affected by the reaction between the vaporized K and the silicates in the ash. The extent of such reaction is closely related to the availability of reactive silicates in the fuel and the contacting and reaction rate between the silicates and vaporized K. At higher combustion temperatures, the vaporization rate of K may greatly exceed the reaction rate of K and silicates, which could be an explanation to the increasing K release observed in the temperature range of 900–1150 ^{o}C. On the other hand, the presence of other inorganic elements, such as Ca and Mg, may compete with K for reacting with silicates, thus may promote the release of K to some extent [167-169].

In addition to S, Cl and K, the release of Na is also found to be significant during biomass/waste combustion at grate-firing conditions [168,171,172]. However, the Na content in most biomass is considerably lower than that of K. Thus a detailed quantification of Na release is difficult to achieve via experiments. Besides, the mechanisms for Na release during biomass combustion are in most cases analogous to that of K. Therefore, a detailed discussion on the Na release is not performed here, but can be found elsewhere [168,172]. Besides the elements mentioned above, the release of other elements such as Si, Al, Ca and Mg during biomass/waste combustion are generally found to be negligible [142,168,172]. An additional element which may exhibit high volatility during biomass/waste combustion is phosphorus. However, detailed investigations on the release characteristics of phosphorus are scarce in literature.

1.3.5 Interactions in ash chemistry

During pulverized fuel combustion, complicated interactions may occur among the ash forming elements, which cannot only alter the chemical form of these elements in the flue gas but also greatly affect the partitioning of these elements into fly ash of different particle size. These interactions are mostly achieved through gas-gas reactions of the vaporized ash forming elements, or the gas-solid reactions between the solid ash particles and the vaporized ash forming elements. The major vaporized ash forming elements during pulverized coal combustion can be categorized as S, Cl, refractory metals (such as Si, Al, Fe, Ca and Mg), and alkali metals (such as K and Na). Since the refractory metals are mostly vaporized through a reducing mechanism, these metals are usually quickly re-oxidized at the vicinity of a burning char particle and nucleate to small solid/liquid ash particles [155]. Thus the major vaporized ash forming elements, which may have relatively long residence time during pulverized coal combustion, are S, Cl and alkali metals. Since these elements are also the major ash forming elements released from biomass or waste combustion and are the most critical elements for ash deposition and corrosion in pulverized fuel combustion, the possible reactions of vaporized alkali metals, S and Cl are mainly emphasized in this section.

1.3.5.1 Reactions between vaporized alkali metals and kaolinite

The vaporized alkali metals during pulverized coal combustion usually exist as alkali hydroxides or alkali chlorides. These alkali species may react with the coal minerals at high combustion temperature, resulting in the formation of alkali aluminosilicates/silicates as well as gaseous HCl/H_2O. A typical example is the reaction between vaporized Na species and kaolinite, which has been the subject of extensive research [146,163,176-184]. At combustion temperatures and particle residence times similar to pulverized coal combustion, the kaolinite ($Al_2O_3{\cdot}2SiO_2{\cdot}2H_2O$) particles can be readily converted to metakaolinite ($Al_2O_3{\cdot}2SiO_2$), however further conversion to mullite ($3Al_2O_3{\cdot}2SiO_2$) may be greatly confined by the residence time. The formed metakaolinite can react with the vaporized sodium species (such as NaOH or NaCl), and generate sodium aluminosilicates such as nephelite and carnegieite (both with a chemical form of $Na_2O{\cdot}Al_2O_3{\cdot}2SiO_2$). The transformation from kaolinite to metakaolinite and then to sodium aluminosilicates may cause some free silica to be released. Thus some sodium silicates may be formed initially along with the sodium aluminosilicates. As the reaction proceeds, the basic metakaolinite crystal structure may break down into silicates and aluminates, allowing accommodating more vaporized sodium species than the predicted product ($Na_2O{\cdot}Al_2O_3{\cdot}2SiO_2$). It should be noted that the initial generated sodium aluminosilicates can form an eutectic with the remaining metakaolinite, and cause melting. This melt can enhance the reaction rate between the kaolinite and vaporized sodium by breaking apart and opening up the tightly parked metakaolinite crystal structure, and by inducing a surface renewal to allow access to the unutilized metakaolinite buried under the unexposed platelet layers [180]. On the other hand, as the reaction progresses, the entire kaolinite particle may transform to a catastrophic melt, which can deactivate the reaction by closing the pores [176].

The reactions between the kaolinite and vaporized sodium are influenced by different factors such as temperature, particle size, molar ratio between the sodium and kaolinite, residence time, and gas environment [163,179,180]. The optimum temperature window for the reaction between the vaporized sodium and kaolinite has been proposed to be 900–1100 ^{o}C [179], since a higher

temperature may result in a significant melt-induced deactivation, particularly when the molar ratio of the vaporized sodium and kaolinite is high [180,185]. The particle size of kaolinite may also impact the reaction rate. Under the same experimental conditions, the conversion of submicron kaolinite particles is found to be at least 6 times greater than the particles around 9 μm [179]. The results suggest that the reaction between vaporized sodium and kaolinite particles in the range of 3–9 μm are controlled by pore diffusion, whereas the smaller particles (0.65–3μm) are in a transition of pore diffusion and reaction control [179]. A lower molar ratio between the vaporized sodium and kaolinite is usually preferable in order to completely capture the sodium, but the effect becomes less significant when the molar ratio is already below 0.5 [180]. The presence of gaseous Cl and S may inhibit the reaction between the vaporized Na and kaolinite [163,179].With the presence of gaseous Cl, part of the vaporized Na may be converted to NaCl [162], which may react much slower with kaolinite than that of NaOH [163]. On the other hand, the presence of gaseous S may result in the formation of sodium sulphate, which may condense at higher temperature and reduce the residence time for the gas–solid reaction [179].

Several mathematical models have been proposed to simulate the reaction between kaolinite and vaporized sodium [163,177,179,180,182]. Punjak et al. have developed a model which describes the simultaneous diffusion and reaction of sodium vapor in a porous kaolinite particle [182,183]. The model fits well with the experimental data obtained at 800 ^{o}C, but it did not take into account the possible deactivation at higher temperatures [182,183]. Recently, Gale and Wendt have proposed a model which utilizes two global reactions to describe the reaction between kaolinite and sodium vapor as well as the deactivation at high temperature [180]. The simulation results are in good agreement with the experimental results, and the feature of the high temperature deactivation has been well-characterized by using the two-step approach [180].

The reactions between the vaporized K species and kaolinite are generally analogous to that of kaolinite and vaporized Na species [107,184,186,187]. A direct comparison indicated that the adsorption rate of kaolinite on NaCl and KCl was similar at 850 ^{o}C [184]. The experiments carried out by Tran et al. show that kaolinite can capture vaporized potassium (such as KCl and KOH) both by chemical reaction and physical adsorption at 850 ^{o}C [186]. In the temperature range of 750–950 ^{o}C, the capture efficiency of kaolinite on KCl is found to decrease with increasing temperature, which is explained as an increased desorption rate of KCl at higher temperatures, since the kaolinite sintering is insignificant at the experimental temperature range. The influence of different K species on the capture efficiency is also investigated, showing that the K capture efficiency is similar for KCl and KOH but significantly lower for K_2SO_4 [186].

Zheng et al. have studied the reactions between kaolinite and vaporized potassium at a temperature range of 900–1500 ^{o}C [107]. They reveal that in the temperature range of 900–1300 ^{o}C, the amount of potassium captured by kaolinite decreases with increasing temperature, which is explained as a higher degree of sintering in the kaolinite pellet with increasing temperature. However, at temperatures above 1300 ^{o}C, the amount of potassium captured by kaolinite starts to increase with increasing temperature. This is presumably because of the appearance of a molten phase in the kaolinite pellet at temperatures above 1300 ^{o}C, which could facility the transportation of KCl and increase the reaction rate. A mathematical model similar to that in [182,183] is developed to describe the diffusion and reaction between vaporized KCl and kaolinite pellet at 900 ^{o}C [107]. However, this model neglects the effect of sintering and melting, which limits its application at higher temperatures.

1.3.5.2 Reactions between vaporized alkali metals and other minerals

In addition to kaolinite, other minerals in coal may react with the vaporized alkali metals. Punjak et al. have compared the capture efficiency of kaolinite, emathlite and bauxite on the vaporized Na at 800 ^{o}C, showing that all of these minerals could capture the vaporized Na through chemical reactions [182,183]. In comparison with kaolinite, bauxite shows a higher initial capture rate and a lower ultimate capture capability (mass basis). However, the capturing of vaporized Na by bauxite is partly attributed to physical adsorption, which is different from the other two minerals where chemical reaction is dominated. The initial capture rate of emathlite is similar to that of kaolinite, while the capture capability of emathlite is close to that of bauxite. XRD (X-ray diffraction) analysis suggests that the formation of nephelite, carnegieite and glassy silicates may be responsible for the sodium capture by bauxite, whereas the formation of abite ($Na_2O{\cdot}Al_2O_3{\cdot}6SiO_2$) may account for the sodium captured by emathlite [182,183].

Silica (SiO_2) is able to react with the vaporized sodium or potassium, although the reaction rate is usually much lower than that of kaolinite [107,163]. A direct comparison of the reaction rate of kaolinite and SiO_2 under conditions similar to pulverized coal combustion indicates that the reaction rate of NaCl and kaolinite is 5–8 times higher than that of NaCl and silica [163]. A similar tendency is observed in fixed-bed experiments [107], showing that much less vaporized K is captured by silica compared to kaolinite and the capture efficiency of silica is almost not influenced by the exposure temperature in the range of 900–1500 ^{o}C.

There are other mineral matters that could react with the vaporized alkali species. Kyi et al. have tested the reactions between sodium species (NaCl, NaOH and Na_2SO_4) and minerals such as kaolinite, bentonite, diatomite, miclay, pumice and pyrophyliite at 1000 ^{o}C and 1200 ^{o}C, showing that these Si and Al containing minerals generally exhibit a high reactivity that is comparable to kaolinite [188]. Mullite ($3Al_2O_3{\cdot}2SiO_2$) is usually considered to be an inert material towards vaporized alkali species. However, experimental results in a fixed bed reactor indicated that reaction starts to take place between mullite and vaporized potassium at temperatures above 1300 ^{o}C, possibly related to the formation of a molten phase inside the mullite pellet which reduces the transportation limitations [107]. Alumina (Al_2O_3) is found to be an effective sorbent to capture vaporized alkali species at moderate temperatures (e.g. <1000 ^{o}C). However, the alkali species captured by alumina is primarily achieved by physical adsorption, rather than chemical reactions [107,189]. Besides Si or Al based minerals, calcium phosphates, such as $Ca(PO_3)_2$, could also react with K species (such as K_2CO_3 and KCl) at 900–1000 ^{o}C through the formation of $(K_2O)_k{\cdot}(CaO)_l{\cdot}(P_2O_5)_m$ structures, but such reactions may be greatly influenced by the temperature and the applied Ca/P molar ratio [169].

Direct study on the reactions between the vaporized potassium and coal ash has been carried out [107], showing that a Columbia bituminous coal (COPRIB) ash exhibits a capture behavior that is similar to kaolinite, both with respect to the capture efficiency on the vaporized potassium and its dependence on the exposure temperature. The capture efficiency of the COPRIB ash decreases with increasing temperature in the range of 900–1200 ^{o}C, but it increases significantly when the temperature becomes 1300 ^{o}C. The similarity between the capture efficiency of COPRIB ash and kaolinite is considered to be related to their similar Al and Si content. On the other hand, the lignite ash exhibits a much lower capture efficiency than the COPRIB ash, which is possibly related to the relatively small Si and Al content in the lignite ash. In addition, the lignite ash contains relatively large content of Ca and Mg, which may compete with K to react

with the alumina and silica [107]. The competition between Ca and K on reacting with silica is further demonstrated through fixed bed experiments, showing that less K is captured by silica with the dosage of Ca [169]. The influence of coal ash properties on reaction with alkali species has been further studied through co-firing different coals with chlorine rich biomass [134], showing that the coal with a larger Al and Si content and a smaller K content reacts more easily with the gaseous alkali chlorides. CCSEM analysis of the fly ash from lignite combustion shows that the majority of the Na is combined to Al and Si (rather than Si alone), suggesting that the aluminosilicates are the preferred scavengers during coal combustion [178]. This conclusion is in agreement with experimental results obtained from different coal ashes [107,134], and the tendency indicated by global equilibrium calculations [96].

When the vaporized potassium and sodium are presented in the flue gas at the same time, they may interact with each other in reacting with minerals. The capture rates of an Al and Si based sorbent on vaporized KCl, NaCl and their mixture have been compared in fixed-bed experiments at 800 ^{o}C [190]. It is shown that the sorbent could capture KCl much faster than NaCl. For the mixture of NaCl and KCl, the observed capture rate is lower than the summation from pure components, indicating that the capturing of KCl by the sorbent may be inhibited by the presence of NaCl and the overall capture rate becomes similar to that of NaCl [190]. On the other hand, when a sorbent containing potassium (emathlite) is exposed to NaCl vapor at 800 ^{o}C, the potassium content in the sorbent is found to be decreased, indicating that a significant amount of potassium is released to the gas phase with the presence of NaCl vapor [183]. This tendency is supported by coal combustion experiments under suspension-firing conditions [146], showing that the vaporization of potassium is not closely related to the association of potassium and the amount of silicates in the coal, but rather exhibiting a positive correlation with the vaporization of sodium. This indicates that that vaporized sodium may be able to displace some mineral bound potassium and facilitate its vaporization to gas phase [146].

1.3.5.3 Reactions between alkali metals and gaseous sulphur

During pulverized fuel combustion, significant interactions can occur between the vaporized alkali species and the gaseous sulphur such as SO_2/SO_3. The reactions between the vaporized alkalis (such as alkali chlorides) and the gaseous sulphur could potentially minimize the risk of ash deposition and corrosion in pulverized fuel-fired boiler, since alkali sulphates usually have much higher melting temperature and are less corrosive than alkali chlorides. The sulphation reactions of alkali species have been studied both through experiments and detailed kinetic modeling [191-199]. According to the detailed gas phase mechanism proposed by Hindiyarti et al. [194], the formation of K_2SO_4 at 1100 ^{o}C may follow the reaction pathways shown in Figure 1.19. It can be seen that the sulphation of KCl to K_2SO_4 may proceed with and without the presence of SO_3/OH radical as an intermediate. At low temperatures (e.g.< 900 ^{o}C), the pathway involving the formation of $KHSO_3$ is considered to be the major pathway, with the reaction from $KHSO_3$ to $KHSO_4$ being the rate-limiting step. However, at higher temperatures (e.g. > 1100 ^{o}C), the other pathways may also become important for K_2SO_4 formation, probably related to an increased generation of radicals at these temperatures. The mechanism proposed by Hindiyarti et al. [194] is found to be consistent with several experimental results [63,173,191], although further experiments in a rigorously homogeneous system are still needed for obtaining more insights into the mechanism [194].

In addition to the homogeneous mechanism, the formation of alkali sulphates may also follow a heterogeneous mechanism involving the condensation of alkali containing species (such as alkali chlorides or hydroxides) on a surface and the subsequent sulphation in liquid or solid phase. According to the experimental and modeling studies carried out by Steinberg and Schofield [195,200-202], the formation of Na_2SO_4 (g) under fuel lean-flame conditions is considered to be kinetically limited through an analysis of the detailed reaction mechanism. Therefore they suggest that the heterogeneous sulphation mechanism is responsible for the formation of Na_2SO_4 at these conditions. This hypothesis is supported by the Na_2SO_4 formation rate obtained on a deposition probe, which is proportional to the total sodium content in the flame, but is independent of the fuel type, equivalence ratio, flame temperature and sulphur concentration [195]. The heterogeneous sulphation of alkali chlorides has been studied directly through fixed-bed experiments in a temperature range of 400–850 ^oC [203,204]. It is revealed that the sulphation rate of the solid NaCl is very slow at temperatures below 600 ^oC, with only 0.5–1.1% of the NaCl being converted to Na_2SO_4 in 3 h. At these temperatures, the rate-limiting step is considered to be the adsorption of SO_2 on the NaCl surface [203]. One the other hand, the sulphation rate of KCl or NaCl is increased considerably at temperatures above 650 ^oC, which is probably caused by a change in the reaction mode from a gas-solid to a gas-liquid and/or a gas phase reactions [204]. However, even at 850 ^oC, a quite large residence time (~hours) is needed in order to fully convert the alkali chlorides to sulphates [204].

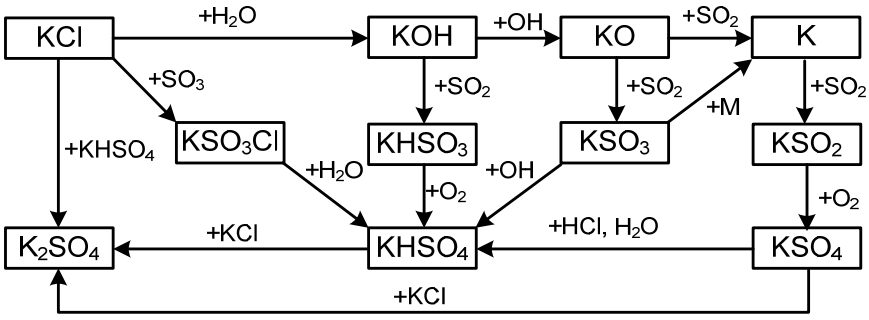

Figure 1.19 Pathway diagram for potassium transformation at 1100 ^oC (under the conditions of Iisa et al. [191]) [194].

The sulphation of KCl particles has been studied by Iisa et al. in a laminar entrained-flow reactor at 900–1100 ^oC, with the residence times of 0.2–1.2 s [191]. The results reveal that up to 100% conversion can be achieved for the vaporized KCl in the reactor, whereas only about 0.5–2% conversion is obtained for the melted KCl. This suggests that at residence times similar to pulverized fuel combustion condition, the homogeneous sulphation rate would be significantly higher than that of heterogeneous sulphation [191]. The importance of the the homogeneous sulphation mechanism over heterogeneous mechanism at entrained flow conditions is further supported by studying aerosol formation through laboratory-scale experiments and modeling [205,206]. The significant increase of the aerosol number concentration observed by adding SO_2 to NaCl and KCl vapor indicate that the alkali sulphates result from the homogeneous sulphation of the vaporized alkali chlorides, rather than the heterogeneous sulphation of the condensed alkali chlorides [205]. However, it should be noted that the conversion of the vaporized alkali chlorides to sulphates may be thermodynamically limited at high temperatures (e.g. >1000 ^oC)

[191,206,207]. Thus a high conversion of vaporized alkali chlorides to sulphates may be only achievable at moderate temperature (e.g. ~900 ^{o}C) [191].

The reactions between the alkali species and gaseous sulphur have been investigated in practical combustion systems, mostly through the injection of sulphur based additives (such as elementary sulphur, SO_2, and ammonium sulphate) during the combustion of high alkali fuels such as straw [197,198,208-210]. These studies generally reveal that the addition of sulphur based additives can effectively reduce the concentration of alkali chlorides in the flue gas. However, among the different additives, ammonium sulphate seems to be more effective than other additives such as SO_2 and elemental S [199]. It is probably because that the decomposition of ammonium sulphate could generate SO_3 which can react with alkali chlorides more efficiently than that of SO_2 [191,192].

1.3.5.4 Ash interactions during co-combustion of coal and high alkali biomass/waste

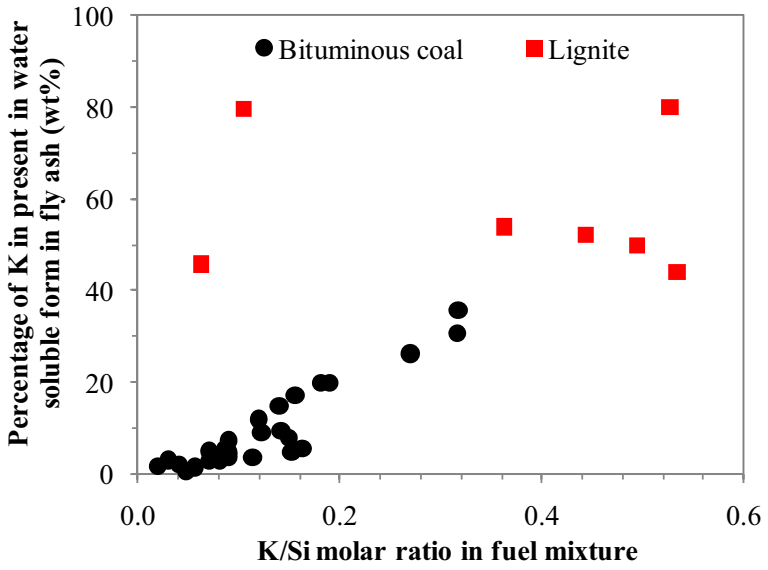

Figure 1.20 The percentage of K present as water soluble form in fly ash (wt%) versus the K/Si molar ratio in the fuel mixture. The results are derived from laboratory- and full-scale co-combustion of straw and different coals [99].

It has been shown earlier that the vaporized alkali species, minerals, and gaseous sulphur can lead to significant interactions during combustion. Therefore, when coal with relatively large mineral and sulphur content is co-combusted with biomass containing large alkali and chlorine content, significant interactions may take place between the alkali species released from the biomass and the minerals and sulphur in the coal. A typical example of such interactions is co-combustion of straw and coal, which has been studied extensive through laboratory-, pilot-, and full-scale experiments as well as modeling [60-62,79,96,100,211]. Figure 1.20 shows the influence of the silicate based-minerals in coal on the partitioning of K in the fly ash [99]. The percentage of the water soluble K in the total K in fly ash provides an approximation of the percentage of K appearing as KCl and K_2SO_4 in the fly ash. It can be seen that when straw is co-

fired with bituminous coals, the percentage of K present as water soluble form in the fly ash generally decreases with decreasing K/Si molar ratio in the fuel mixture. This indicates that the formation of KCl and K_2SO_4 may be inhibited when straw is co-fired with a bituminous coal with large amount of silicate based-minerals, due to the formation of water insoluble K aluminosilicates. On the other hand, when straw is co-fired with lignite, it appears that the influence of K/Si molar ratio in the fuel mixture is insignificant for the formation of water soluble K in the fly ash. This is probably because the relatively high Na and Ca content in the lignite could inhibit the reactions between the alkali species from the straw and the Si-based minerals in the lignite [99].

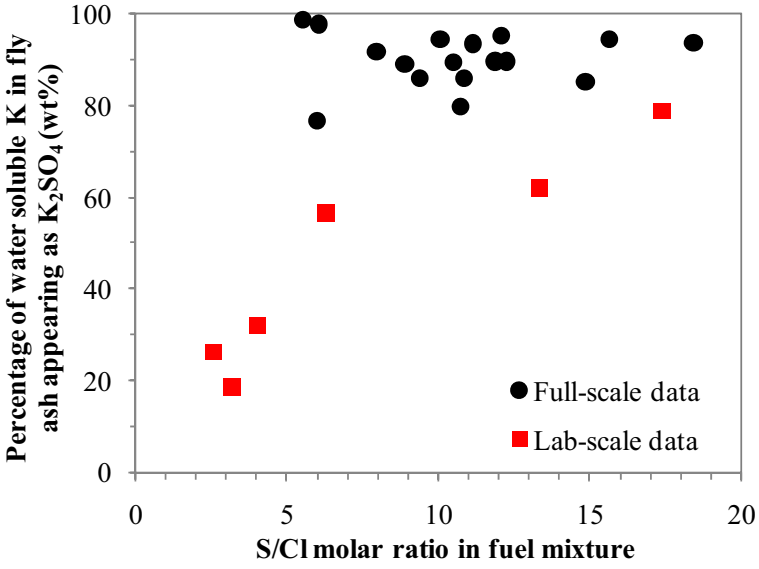

Figure 1.21 The percentage of water soluble K appearing as K_2SO_4 in the fly ash from full-scale and lab-scale co-combustion of coal and straw [99].

As shown in Figure 1.20, although the majority of the K in the fly ash is present in water insoluble form during co-combustion of straw and bituminous coal, a certain percentage of K (up to ~30 wt%) still exists in water soluble form. The water soluble K in the fly ash may primarily be present as KCl and K_2SO_4, and the distribution between these two species would be greatly influenced by the sulphation reactions of the vaporized alkali species and the gaseous sulphur. The effect of co-combustion of coal and straw on the formation of K_2SO_4 is shown in Figure 1.21 [99]. It is seen that when straw is co-fired with coal, the molar ratio of S/Cl in the fuel mixture is in most cases above 5. This is considerably larger than that of pure straw, which normally has a S/Cl molar ratio below 1 (see Figure 1.10). During co-combustion of coal and straw in full-scale pulverized coal-fired plants, it appears that approximately 80–100% of the water soluble K in the fly ash is present as K_2SO_4, and the influence of the S/Cl molar ratio seems to be insignificant on the formation of K_2SO_4 when it is above 5. On the other hand, in the laboratory scale experiments, it seems that the percentage of water soluble K appearing as K_2SO_4 in the fly ash is increased with increasing S/Cl molar ration in the fuel mixture, and is considerably lower than that of full-scale data. This indicates that in laboratory experiments, the formation of K_2SO_4 may be kinetically limited, possibly due to the short residence time in the

temperature range of 1300–500 °C (~0.1 s) [99]. According to the global equilibrium calculations performed by Wei et al. [96], the formation of K_2SO_4 during co-combustion of hard coal and straw seems to be only thermodynamically feasible at temperatures below 1000 °C. This indicates that the sulphation reaction in co-combustion may only happen at a certain temperature range, since the reaction would be thermodynamically restricted at high temperature and kinetically limited at low temperature. Thus a relatively long residence time at moderate temperature is preferable for the sulphation reaction. This is supported by the results obtained from fluidized bed combustion, where the residence time at around 800 °C is relatively long. Under these conditions, a significant reduction on the gaseous KCl concentration is seen when sulphur based additives are injected during biomass combustion, particularly during the addition of ammonium sulphates or other sulphates [197-199,212]. In contrast to the sulphation reaction, the reaction between alkali species and Si-based minerals is likely not thermodynamically limited at high temperature [96]. This may explain the similarity of the full-scale and laboratory-scale results with respect to the reaction between alkali species and Si-based additives [99].

1.3.6 Fine particle formation

The formation of fine particles, here defined as particles with aerodynamic diameters less than 2.5 μm [151], is a significant concern in pulverized fuel combustion. This is primarily because these particles can much more easily penetrate the electrostatic precipitator (ESP) of a pulverized coal-fired power plant than larger particles, and dominates the particulate matter (PM) emission from the plant [121]. In addition, the fine particles are often rich in trace elements which are highly toxic to the environment [213-215]. Besides the influence on the PM emission, the formation of fine particles during pulverized fuel combustion may also significantly affect the performance of the SCR (selective catalytic reduction) catalyst [216,217]. Extensive studies have been carried out to study the formation of fine particles during pulverized coal combustion through laboratory- and pilot-scale experiments [138,145,151,155,164,218-224] as well as full-scale sampling [213,214,225-228]. These studies generally lead to a well established mechanism of fine particle formation during pulverized coal combustion, with several reviews available on this subject [121,149-151]. On the other hand, the formation of fine particles in pulverized biomass/waste combustion is generally less studied, with only a few laboratory- or pilot- scale investigations available on this subject [109,208,209,229-231]. The fine particle formation during co-combustion of pulverized coal and biomass/waste has also been investigated in laboratory- and pilot-scale reactors as well as full-scale power plants [109,208,226,227,232]. In this section, the mechanism of fine particle formation during pulverized fuel combustion will be introduced, and the effect of co-combustion on fine particle formation will be assessed based on literature.

1.3.6.1 Fine particle formation in pulverized coal combustion

The mass-based particle size distribution of the fly ash from pulverized coal combustion is conventionally considered to be bimodal, i.e. a fragmentation mode which is mainly responsible for the formation of supermicron particles and normally has a peak concentration at around 20 μm, and a vaporization mode primarily contributes to the formation of submicron particles and usually has a concentration peak around 0.1 μm [213,233,234]. Recently, it is proposed that the particle size distributions in the fly ash from pulverized coal combustion may be trimodal [151,222-224]. In addition to the two modes mentioned earlier, a fine fragmentation mode,

which is normally between approximately 0.7 and 3.0 μm, is suggested to be present in pulverized coal combustion [151].

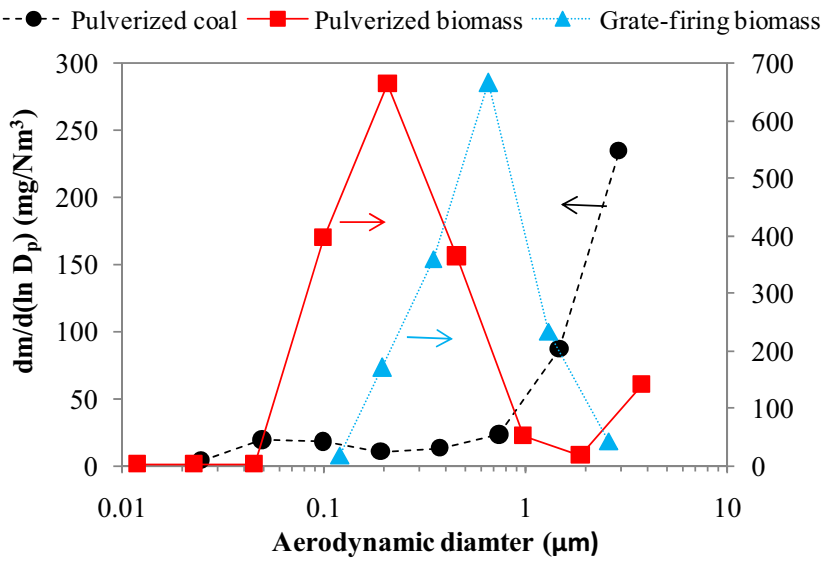

Figure 1.22 Typical mass-based particle size distributions of the fine particles from pulverized coal and biomass combustion as well as grate-firing of biomass. The pulverized coal data is derived from a pulverized coal-fired power plant [235]; the pulverized biomass data is obtained from an entrained flow reactor using Orujillo (a residue of olive oil production process) as fuel and combusted at 1300 ^{o}C [236]; and the grate-firing biomass data is derived from a full-scale grate-firing plant using straw as fuel [237].

A typical particle size distribution of the fine particles formed from a pulverized coal-fired power plant is shown in Figure 1.22 [235]. Consistent with the results shown in [151], a small peak is seen at around 0.1 μm, and the mass-based particle concentration is significant at around 3 μm. As mentioned earlier, the ash particles around 0.1 μm is mainly generated from the inorganic elements in coal which are vaporized through a reducing mechanism [152]. According to the experimental and theoretical analyses conducted by Helble and Sarofim [155], the inorganic elements vaporized in a suboxide or elemental form during char oxidation can be quickly re-oxidized in the boundary layer of the char particle. This will lead to a supersaturation followed by nucleation. With sufficiently high temperature and short coalescence time, these nucleated particles would grow through a Brownian collision and coalescence mechanism, which can either occur through solid state diffusion or viscous flow. The resulting primary particle size is found to increase with increasing gas and char particle temperature. Besides, the addition of sodium to a silicon system is also seen to greatly increase the primary particle size of the particles, by decreasing the viscosity of the nucleated particles and therefore permitting coalescence at lower temperatures. On the other hand, with low temperature at which the time needed for coalescence is comparable to the time between collisions, the colliding particles would generate aggregates, which may be preserved if the temperature reduction is sufficiently rapid [155]. According to the TEM analysis on the ultrafine particles from pulverized coal-fired power plant, the primary particle size (diameter) of these vaporization mode particles is mostly

found to be in the range of 10-30 nm [225,238]. These primary particles are mostly present in a form of aggregates and result in a peak concentration around an aerodynamic diameter of 0.1 μm [213,225].

In addition to the ultrafine particles generated from the vaporized inorganic elements, the remaining fine particles, which dominate the mass of the fine particles from pulverized coal combustion, are mainly generated from the fragmentation and coalescence of coal minerals [149,151]. For excluded minerals, the fragmentation is usually insignificant for silicate minerals, quartz, illite and muscovite. On the other hand, excluded pyrite or carbonate particles may experience a large extent of fragmentation at a high heating rate, due to the evolution of CO_2 or gaseous sulphur [149]. However, according to the modeling and experimental analyses in a drop tube furnace [239], it appears that the fragmentation of excluded minerals may influence the particle size distribution above 20 μm. The results indicate that the formation of fine particles from fragmentation of excluded minerals may be quite limited [239], although this process may be largely affected by the particle size and the composition of the originally excluded minerals as well as the combustion conditions.

Included minerals in coal particles may undergo a significant extent of fragmentation and coalescence during char oxidation, and result in the formation of fine particles [149,151,240]. Helble and Sarofim propose that the char fragmentation is the main mechanism responsible for the formation of ash particles in the range of 1–5 μm [240]. Therefore the porosity of a char particle may greatly influence the number of the ash particles produced from one char particle as well as the ash particle size distribution. This is supported by the observations that the macroporous synthetic char doped with sodium silicate yields about 75 ash particles per char particle, whereas the non-macroporous char doped with sodium silicate only yield one ash particle per char particles. The results obtained by Helble and Sarofim [240] indicate that the shedding of liquid minerals from the surface of a rotating char particle would not occur during pulverized coal combustion. However, some other studies advocate that the shedding of ash from rotating char particle may be an important mechanism for the formation of fine particles from pulverized coal combustion [151,224]. In addition, the fragmentation of char cenospheres from combustion may also contribute to the formation of fine particles during pulverized coal combustion, as summarized in [149,151].

1.3.6.2 Fine particle formation in pulverized biomass combustion

The fine particle formation during pulverized biomass combustion is considerably different from that of pulverized coal combustion. An example of the fine particles formed from pulverized biomass combustion is shown in Figure 1.22, which is obtained from combustion of Orujillo (a biomass with ash rich in K, Cl, Ca and Si) in an entrained flow reactor [236]. The particle size distribution is considered to be representative for a number of biomasses tested in the same reactor [209,231,236]. Compared to pulverized coal combustion, the fine particles from pulverized biomass combustion appear to have a significantly larger concentration peak at around 0.1–0.2 μm. Chemical composition analyses of these particles reveal that they are almost only composed of alkali, Cl, S and P, indicating that the observed concentration peak is a result of the vaporization of the inorganic elements during biomass combustion. Based on the molar ratios of the inorganic elements and the results from XRD (X-ray diffraction) analysis, the dominant species in these particles are found to be KCl and K_2SO_4 during the combustion of pulverized Orujillo [231]. The similarity of the compositions of submicron particles in different

size implies that the submicron particles are primarily generated from the vaporized inorganic elements. On the other hand, the composition of the supermicron particles is found to be closer to the fuel ash composition, suggesting that to a large extent these ash particles may be formed from the coalescence of the minerals in biomass, which is supported by the spherical appearance of the supermicron particles [231].

The formation of fine particles during pulverized biomass combustion seems to be analogous to that of biomass grate-firing, in terms of the mass-based particle concentration as well as the chemical composition. In Figure 1.22, the particle size distribution of the fine particles from grate-firing of straw [237] is compared with that of pulverized combustion of Orujillo [236]. It can be seen that the peak concentration of the fine particles is similar (~ 700 mg/Nm^3) during grate-firing of straw and pulverized combustion of Orujillo. In addition, the composition of the submicron particles from grate-firing of straw is comprised of K, Cl, S and P [237], which is also quite similar to the submicron particles obtained during Orujillo combustion [236]. These similarities suggest that the fine particle formation mechanism in pulverized Orujillo combustion [231] may be analogue to that of grate-firing of straw, which has been characterized extensively through full-scale measurements [207,237,241], laboratory-scale experiments [205,242] and modeling [206,242]. According to these experimental and theoretical investigations [205-207,237,241,242], the formation of fine particles during grate-firing of straw is believed to be initiated by the homogeneous nucleation of K_2SO_4 from the gas phase, followed by condensation of KCl and K_2SO_4 on the nucleated sulphate seeds. Therefore the number concentration of the fine particles is mainly dependent on the formation of gaseous alkali sulphate, whereas the concentration of alkali chloride may only change of the mass concentration of the aerosols. The contribution of the homogeneous nucleation of alkali chlorides is considered to be negligible for the formation of fine particles during grate-firing of straw, due to the presence of other seed particles [205-207,237,241,242]. The fine particle formation mechanism derived from grate-firing of straw seems to reasonably well explain the formation of fine particles during pulverized Orujillo combustion, in which only K_2SO_4 nucleates is obtained at a sampling temperature of 900 ^oC and the condensation of KCl is only found to be significant below 560 ^oC [231]. For other biomass with different fuel properties, homogeneous nucleation of K_2SO_4 followed by condensation of KCl/K_2SO_4 is still considered to be an important fine particle formation mechanism, although these processes may initiate at different temperatures for different biomass [231]. Besides homogeneous nucleation of K_2SO_4, homogeneous nucleation of K-phosphates may also take place at high temperature during the combustion of phosphorus rich biomass, and contribute to the formation of fine particles [230,231]. For biomass containing relatively large amount of Na, the formation and homogeneous nucleation of Na-species (such as Na_2SO_4), may also significantly contribute to the formation of fine particles, although detailed investigations are still lacking [231].

1.3.6.3 Fine particle formation in co-combustion o f pulverized coal and biomass

When coal is co-fired with biomass, the formation of fine particles would be greatly influenced by the interactions between the coal and biomass. Therefore the obtained particle size distribution of the fine particles can be significantly different from that added from the pure fuels. A typical example of fine particle formation during co-combustion of coal and biomass is shown in Figure 1.23, where different thermal shares of straw (10% and 20%) are co-fired with coal in a pulverized coal-fired power plant [235]. It can be seen that the mass-based particle size

distribution from co-combustion of coal and straw is quite similar to that of dedicated coal combustion. The significant submicron concentration peak appearing during dedicated biomass combustion (see Figure 1.22) is not observed in co-combustion of coal and straw (up to 20 th%). This indicates that the minerals in the coal (South American bituminous coal) can effectively react with the alkali species vaporized during straw combustion. As a result, the majority of the alkali species released from straw combustion would partition to coal mineral particles with relatively large particle size, thus inhibiting the homogenous nucleation of these vaporized alkali species. This is supported by fact that the composition of the submicron particles from co-firing of coal and different share of straw (up to 20 th%) is generally quite similar [235]. Nevertheless, during co-firing of coal and 20 th% straw, a considerable increase of the K and S content in the submicron particles, particularly in the ultrafine particles around 0.1 μm, has been observed for different coals and at different boiler loads [235]. This indicates that the formation of K_2SO_4 may have been promoted during co-firing of coal and 20 th% straw, which is probably linked to the alkali species released from straw and the relatively high sulphur content in the coal. The K_2SO_4 would prefer to partition to fine particles either through homogeneous nucleation or condensation on existing ash particles. However, according to the particle size distribution shown in Figure 1.23, the influence of the increased K_2SO_4 formation is insignificant on the particle size distribution during co-combustion of coal and straw (up to 20 th%) . It should be noted that the results shown in Figure 1.23 are closely associated to the properties of the fuels used in co-firing as well as the operation conditions [235]. With different fuels or operation conditions, the influence of co-firing on the formation of fine particles may become more significant, and possibly result in a larger concentration of fine particles

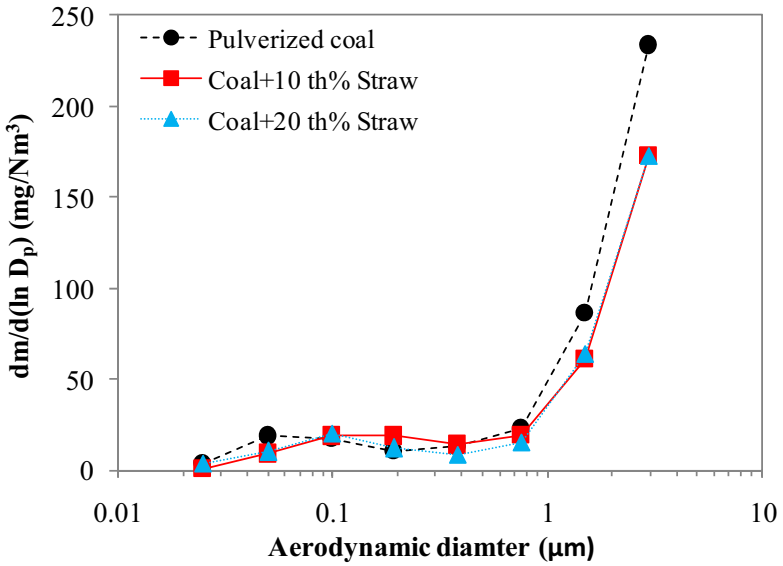

Figure 1.23. Mass-based particle size distributions of the fine particles from dedicated coal combustion, co-combustion of coal and 10% (thermal basis) straw, and co-combustion of coal and 20% straw. The data are derived from an impactor measurement in a full-scale pulverized coal-fired power plant at 100% load [235].

1.3.7 Ash deposition

1.3.7.1 Ash deposition mechanisms

Ash formed during pulverized fuel combustion may deposit on the furnace or heat exchange surfaces of the boiler. The formed deposits are usually classified as slagging and fouling, where the slagging is defined as the formation of fused or sintered deposits on the heat-transfer surfaces and refractory in the furnace subjected to radiant heat exchange, and fouling describes the deposition of ash in the non-radiant convective heat-transfer portion of the steam generator immersed in the flue gas [243]. The major ash deposition mechanisms during coal and biomass combustion are inertial impaction, thermophoresis, condensation and chemical reaction [244].

Inertial impaction describes the deposition of ash particles which have sufficient inertia to traverse the stream lines around a tube (e.g. a superheater tube in the boiler) and deposit on the tube surface. The deposit formation through this mechanism is mainly dependent on the impaction efficiency and the capture efficiency of the ash particles. The impaction efficiency, defined as the ratio of the number of particles that impact on the tube surface to the number that are directed at the tube in the free stream, is influenced by various factors such as ash particle size, density, and gas flow properties. One the other hand, the capture efficiency, which describes the propensity of the impacted particles to stay on the surface, is greatly affected by factors such as composition, morphology and viscosity of the particles and deposits. During pulverized fuel combustion, the formation of deposits through inertial impaction is usually most important for large particles (>5–10 μm), and the formed deposits typically have an elliptic shape on the windward side of the tube [244,245].

Thermophoresis describes the particle transport from the bulk gas to the heat transfer surface by local temperature gradients. This process results from the collisions of gas molecules having different kinetic energy on the surface of a particle, and is influenced by different factors such as particle diameter, gas properties, and temperature gradient. In general, thermophoretic deposition is most important for small ash particles (<3 μm), and the formed deposits are fine-grained and evenly distributed around the whole circumference of the tube [244-246].

Condensation is a process by which vapors are liquefied on the surfaces cooler than the surrounding gas. Thus it is closely related to the concentration of the vaporized inorganic species in the flue gas as well as the gas and surface temperatures. The deposits formed by condensation often consist of a uniform layer extending the entire circumference of the tube. Although the mass fraction of the deposits formed by condensation may not be significant, the condensed inorganic species may lower the porosity of a granular deposit and increase the contact area between the deposit and surface, thus greatly influencing the strength and thermal conductivity of the deposit. Besides, the condensed inorganic species may be molten at the surface temperature, which may enhance the capture efficiency of the impacted particles [244,245].

Once deposits are formed through the mechanisms mentioned above, they may further react with the gaseous species in the flue gas. The presence of such chemical reactions can influence both the mass and the composition of the deposits. Typical examples are the sulphation of the condensed alkali chlorides and the oxidation of the deposited carbon particles [244,245].

The mechanisms mentioned above are recognized as the major mechanisms for the buildup of deposits during biomass and coal combustion. On the other hand, it should be noted that the

deposits buildup may occur simultaneously with the deposits shedding. The deposit shedding mechanisms have been reviewed recently by Zbogar et al. [247], and will not be described in detail in this work.

1.3.7.2 Influence of co-combustion on deposition rate/tendency

The influence of co-combustion on ash deposition under pulverized fuel combustion conditions has been investigated extensively through full-scale measurements and laboratory-/pilot-scale experiments [62,93,99-101,246,248-259]. These studies mainly focus on co-combustion of coal with different biomass, but other secondary fuels, such as sewage sludge and refuse derived fuel (RDF), have also been investigated. The major research emphases are on the effect of the secondary fuels on the ash deposition rate/tendency as well as the chemical and physical characteristics of the deposits. Since the ash deposition rate/tendency can differ by several orders of magnitude for different secondary fuels [100,254], the main emphasis here is on the secondary fuels with high deposition tendency/rate, such as straw [99,100,254]. The secondary fuels with relatively low deposition rate/tendency, such as sawdust, are not focused, since co-firing coal with these secondary fuels would not significantly influence or even decrease the ash deposition rate/tendency [101,256].

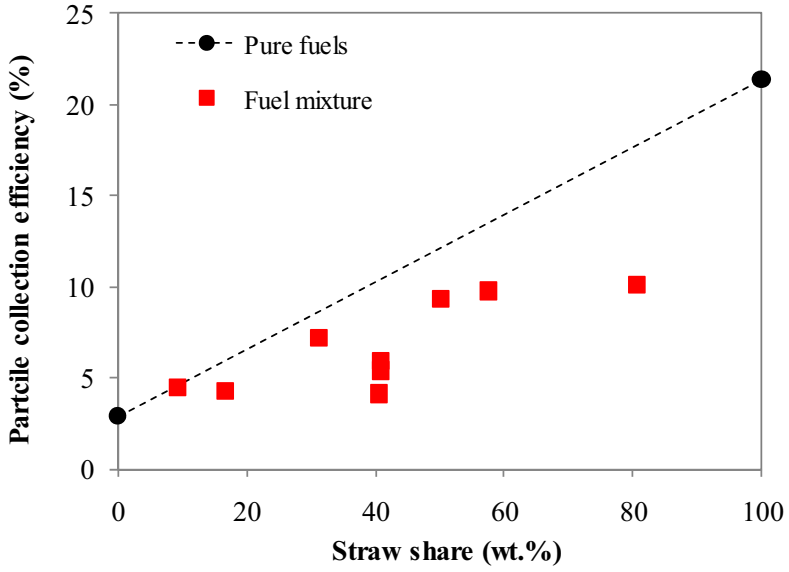

Figure 1.24. Particle collection efficiency on a probe during combustion of a bituminous coal, a wheat straw and their mixtures in a pilot-scale reactor simulating pulverized fuel combustion conditions [100].

Figure 1.24 shows the particle collection efficiency (ash deposition rate/mass fraction of ash in the fuel) on a probe during co-combustion of coal and different mass share of straw in a pilot-scale reactor [100], which is a representative case for co-firing coal with biomass having a high fouling tendency. It is shown that the particle collection efficiency of pure straw combustion is remarkably higher than that of dedicated coal combustion. A primary reason is that straw combustion may result in a large concentration of KCl in the flue gas. At the given experimental

conditions (i.e. a flue gas temperature of 1000 ^{o}C and a probe surface temperature of 540 ^{o}C), part of the gaseous KCl may condense on the probe and result in partially melted deposits which would significantly increase the capture efficiency of the impacted fly ash particles. The particle collection efficiency during co-combustion of coal and straw is between those of pure fuels. With increasing straw share, an increasing tendency is seen for the particle collection efficiency. However, the collection efficiency obtained in the experiments is generally lower than that interpolated from the pure fuels, and the difference is not due to the experimental uncertainties. This implies that the interactions between the coal and straw have affected the ash deposition. As discussed earlier, the KCl released from straw combustion may react with the aluminosilicates in the coal, which would result in the formation of K-aluminosilicates with high melting temperature and gaseous HCl. On the other hand, the relatively high S content in the coal may promote the conversion of KCl to K_2SO_4. These reactions would generally deplete the concentration of KCl in the flue gas, thus reducing the stickiness of the fly ash and deposits, as compared to the combustion in isolation [100].

Similar to the deposition tendency shown in Figure 1.24, non-linear ash deposition behavior has been observed in other co-combustion experiments [99,249-251,256,259]. According to a detailed investigation on co-firing peat and straw [249,250,259], the obtained ash deposition rate in co-firing is almost the same as that of pure peat combustion, when the mass share of straw is below 70 wt%,. However, when the mass share of straw is between 70 wt% and 100 wt%, a significant increase of the ash deposition rate is observed. This non-linear ash deposition behavior during co-firing of peat and straw is presumably caused by the reactions between gaseous alkali from straw and Si-Al compounds from peat, rather than the sulphate reactions of the alkali chlorides. In addition, the erosion effect of the peat ash may also play a role on the observed non-linear ash deposition behavior [249,250,259]. On the other hand, when peat is co-fired with bark, the obtained non-linear ash deposition behavior seems to be governed by the interactions between Cl and S, i.e. a larger extent of sulphation may reduce the melted fraction of the deposits at the experimental conditions thus decreasing the ash deposition [249,250,259].

1.3.7.3 Influence of co-combustion on deposit properties

In addition to the deposition rate/tendency, the influence of co-firing on the chemical and physical properties of the fouling deposits has also been evaluated through laboratory-scale experiments and full-scale measurements [62,99,100]. The full-scale investigations of co-firing coal with straw (10% and 20%, thermal basis) in a pulverized coal-fired power plant [62] reveal that the amount and tenacity of the fouling deposits collected at the probe position 1–3 (with flue gas temperature of ~1250–900 ^{o}C and probe surface temperature of ~620–540 ^{o}C) are generally increased with increasing share of straw, although the effect of straw may vary for different coals. Chemical analyses of the deposits indicate an increased K and S content during co-combustion of coal and 20% straw, and the presence of Cl is negligible. Thus the increased tenacity of the deposits obtained during co-combustion is attributed to an effect of K_2SO_4 melting, which is believed to be a main species that consolidates the mature deposits [62].

The influence of co-firing on fouling deposit composition has also been characterized under well-controlled conditions during laboratory-scale experiments [99,100]. During co-combustion of coal and straw, it appears that the composition of the deposits obtained from co-combustion somehow deviates from that predicted from pure fuels [100]. In comparison with the deposit composition interpolated from the pure fuels, the S content is significantly enhanced and the Cl

content is considerably decreased in the deposits collected from the co-combustion experiments, whereas the content of Al, Fe, Ca and Si appears to be similar. The observed tendency of the S and Cl content in deposits is mainly attributed to the interactions between the alkali chlorides from straw and the sulphur from coal. When the ratio of the fuel-S to available alkali is in excess of 5 times the S-to-alkali stoichiometric ratio, the Cl content in the fouling deposits is found to be negligible, indicating that part of the vaporized alkali chlorides from straw may have been converted to sulphates during co-combustion [100]. One the other hand, through comparing the composition of the deposits and the fly ash obtained in entrained flow co-combustion of coal and straw [99], it is evident that the Cl content in the deposits is smaller than that of fly ash, whereas the S content is much larger. This implies that sulphation of the condensed alkali chlorides on the deposition probe may also contribute to the small Cl content in the deposits. However, compared to the effect of Si and Al species, the reducing effect of SO_2 on the gaseous KCl seems to be less significant in the experiments, even at a high ratio of the fuel-S to available alkali [99].

Besides the effect on fouling, the influence of co-firing on the formation of slagging deposits has been investigated either by directly deposit sampling during combustion experiments [101,246,248] or indirectly by measuring the properties of the fly ash samples from co-combustion [253,257,258]. Heinzel et al. have evaluated the impact of co-firing coal and straw on slagging in a pilot-scale test facility by using deposition probes [248]. When coal is co-fired with 50% straw (thermal basis), a sintered layer is observed on the probe placed at a flue gas temperature of 1050 ^{o}C. This is quite different from dedicated coal combustion and co-firing of coal with 25% straw, where no slagging is detected. Through the analyses in a hot stage microscopy, the soften temperature of the ash from coal and straw blends (up to 50%) appears to be similar to that of coal ash, whereas the fluidization temperature is considerably lower in the blended ash, which may induce a higher slagging risk in co-firing [248].

Similar conclusions have been made when the fly ashes from full-scale co-firing of coal and straw are analyzed by using a CCSEM (computer-controlled scanning electron microscopy), a STA (simultaneous thermal analysis) and the viscosity calculations based on the fly ash compositions [253]. In comparison with dedicated coal combustion, the initial melting temperature of the fly ash from 20% straw (thermal basis) co-combustion is about 150 ^{o}C lower, whereas the value in 10% straw co-combustion is similar. The difference in the melting temperature of the fly ash appears to be in good agreement with the observed ash deposition tendency in the full-scale plant. CCSEM analysis indicates that the formation of K-aluminosilicates is increased when coal is co-fired with straw. These K-aluminosilicates particles may have relatively low viscosity and thus more likely form deposits on the heat transfer surfaces compared to the unreacted aluminosilicates. The viscosity of the fly ash from different tests has been evaluated by using a viscosity model, showing that the viscosity of the fly ash from co-combustion is considerably lower than that of dedicated coal combustion, which may not only increase the tendency of slagging formation, but also lower the sintering temperature of the deposits [253]. The viscosity of the fly ash from co-combustion of coal and straw has been directly measured by using a high temperature viscometer [257,258], which supports that co-firing coal with straw may lower the ash viscosity and lead to a higher stickiness of the ash particles.

Kupka et al. has studied the slagging formation during co-combustion of a bituminous coal and sewage sludge or refuse derived fuel (RDF) in a pilot-scale reactor [246,260]. The deposition rate on a slagging probe is considerably increased when coal is co-fired with sewage sludge (up

to 20%, thermal basis) or 5% RDF. The results are compared with the predictions by a slagging index based on the ratio of fluxing oxides to sintering oxides, showing that intensive slagging has been observed when the index is in the range of 0.75–2 range. The slagging intensity is decreased when moving away from this range in either direction [246,260].

1.3.8 High temperature corrosion

1.3.8.1 Corrosion mechanisms

High temperature corrosion in the superheater region of a pulverized fuel-fired power plant may be induced by the sulphur and/or chlorine species generated from combustion. In conventional coal-fired boilers, the corrosion of superheater tubes is mainly caused by the presence of molten alkali-metal-trisulfates [261,262]. During pulverized coal combustion, the interactions between the vaporized alkali species and the gaseous sulphur may generate alkali sulphates, which can deposit on the superheater tubes either through condensation or thermophoresis. The deposited alkali sulphates may react with SO_2 and iron oxide to generate alkali-iron-trisulfates. This reaction often requires a relatively high concentration of SO_3, which may be generated from the catalytic oxidation of SO_2 in the deposits. The resulting alkali-iron-trisulfates may form a molten layer at the outer surface of the oxide layer, which can increase the sulfidation potential of the superheater tubes and promote corrosion. The rate of corrosion on superheater tubes appears to be temperature dependent, often showing a bell-shaped curve in the temperature range of 600–750 ^{o}C. At low metal temperature (e.g. <550 ^{o}C), the ash deposit is normally a porous layer allowing relatively free gas diffusion between the tube surface and the bulk gas, thus the corrosion rate can be approximately correlated to the gas phase oxidation rate of the metal. At higher metal temperatures, the corrosion rate can be significantly increased by the appearance of a molten layer of alkali-metal-trisulfates adjacent to the tube surface. When the metal temperature is further increased (e.g. >700 ^{o}C), the stability of the iron sulphates can be decreased due to thermodynamic limitations, thus leading to a decreased corrosion rate [261].

In biomass-fired boilers, the deposits formed on the superheater tubes may contain a considerabe amount of alkali chlorides, which can cause higher corrosion rates than alkali sulphates. The mechanisms of the chlorine associated corrosion in biomass combustion have been reviewed in [140,261]. The corrosion can be either induced by the gaseous chlorine species (such as HCl or Cl_2) or the solid/molten alkali chlorides deposited on the superheater tubes. The HCl and Cl_2 in the flue gas may diffuse to the interface of scale and metal, where they react with the metal alloys to form metal chlorides. The depletion of the oxygen at the interface of scale and metal favors the metal chlorides to be present in a vapor phase. Once generated, these volatile metal chlorides may diffuse to the flue gas and gradually being oxidized to solid metal oxides, since the oxygen concentration is increased with increasing distance from the metal surface. The formed metal oxides usually have a very loose structure providing limited protection for further attack. On the other hand, the chlorine released from the oxidation reaction may diffuse back to the metal surface and lead to further corrosion. However, the corrosion mechanism described above requires a relatively high gaseous chlorine concentration in the flue gas, which may not be achieved during biomass combustion. Alternatively, the relatively high chlorine concentration may result from the sulphation of the deposited alkali chlorides. Such reactions are thermodynamically favorable at the temperatures of the superheater region, and can result in a significantly high local gaseous chlorine concentration. Once the gaseous chlorine is formed

through the sulphation reactions, the corrosion would follow the same mechanism as described earlier [261].

Besides the corrosion caused the attacking of gaseous chlorine, the presence of molten chlorine species may also cause a fast corrosion rate on superheater tubes [261]. These molten chlorine species are usually not only alkali chlorides, but rather a mixture of alkali chlorides and other chlorides (such as $FeCl_2$), which can form low-temperature eutectics. The presence of these low-temperature eutectics may induce some direct corrosion reactions and in general results in a remarkably high corrosion rate [261]. In addition to the major mechanisms mentioned above, some other chlorine associated mechanisms may also contribute to the corrosion of superheater tubes. These mechanisms are described in more detail in [261].

1.3.8.2 Influence of co-combustion on corrosion

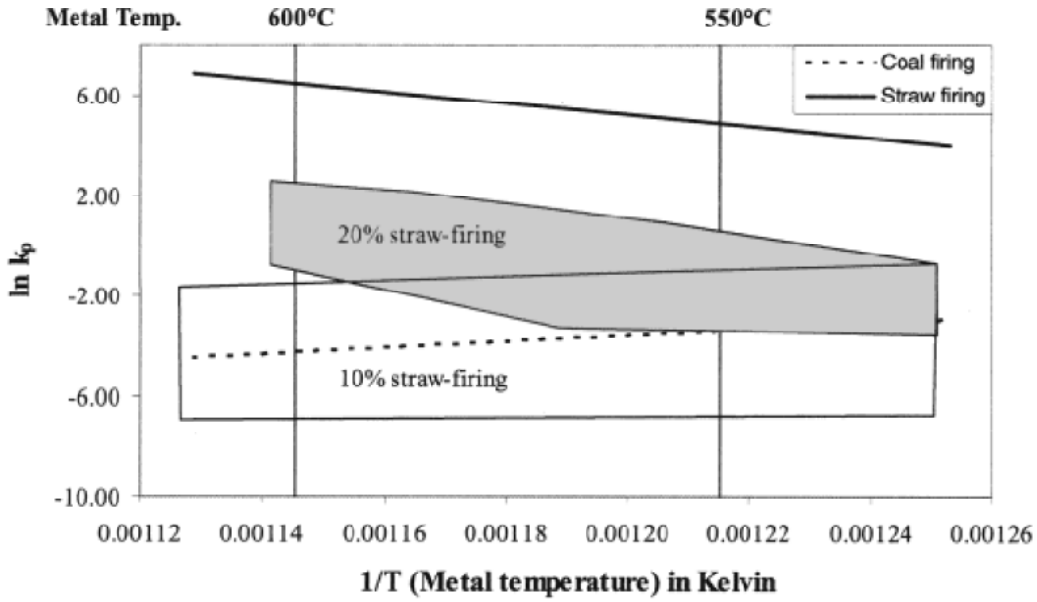

Figure 1.25. Arrhenius plot showing the corrosion rate of TP347HFG during 100% coal firing, 100 straw firing and co-firing of coal and straw [263] .

The most practical approach to assess the influence of co-combustion on corrosion is to insert corrosion probes in a full-scale co-combustion plant and to conduct long-term tests. This has been carried out during co-combustion of coal and straw in pulverized coal-fired power plants, with controlled probes at different locations of the superheater region [79,263,264]. Figure 1.25 shows the corrosion rate obtained on the probes made of TP347HFG under different co-firing conditions at the Studstrup power plant Unit 1, in which 10% and 20% (thermal basis) of straw is co-fired with coal [263]. The co-firing results are obtained at an exposure time of about 3000 h and are compared with that of dedicated coal and straw combustion. It appears that when coal is co-fired with 10% straw, the corrosion rates are similar to dedicated coal combustion at all temperatures. On the other hand, when coal is coal-fired with 20% straw, a slight increase

compared to 10% straw co-firing is observed, particularly at high metal surface temperatures. Nevertheless, the corrosion rate in co-firing of coal and 20% straw is remarkably lower than that of 100% straw combustion, and is considered to be comparable to that of medium-corrosive coals [79]. The main corrosion mechanism for dedicated coal combustion and co-firing of coal and 10% straw is believed to be sulphidation and oxidation. The oxidants needed by these reactions originate from the potassium sulphate present in the deposits, and the corrosion products are Fe_2O_3 and FeS. However, for 20% straw co-firing, low temperature hot corrosion constitutes an additional important corrosion mechanism, especially at high metal surface temperatures. This mechanism is induced by a melt formed by a mixture of iron sulphate and potassium sulphate, which can considerably increase the corrosion rate through increasing the dissolution of gaseous oxidants at the salt-flue gas interface and the transport of oxidants (e.g. SO_3) to the salt-oxide interface. The chlorine associated corrosion is found to be negligible in co-firing of 10% or 20% straw [263].

The effect of 10% straw co-firing on the corrosion of superheater tubes has been tested at longer exposure time (7231 h, 17719h and 22597h) in the Studstrup power plant Unit 4 [264]. The results also support that sulphidation and oxidation is the main corrosion mechanism, and the contribution of low temperature hot corrosion is negligible. However, compared to the results obtained in unit 1 of the Studstrup power plant [263], high corrosion rate is observed in this longer test, which is attributed to the occurrence of internal sulphidation [264].

1.3.9 Fly ash utilization

Fly ash from pulverized coal combustion can be used in concrete or cement production [72,265]. In Europe, the standardizations EN 197-1 and EN 450-1+A1 have specified the requirements of utilizing coal fly ash in cement and concrete production, respectively [266,267]. The utilization of fly ash from co-combustion of coal and secondary fuels in cement production is restricted in EN 197-1. However, the recently released EN 450-1+A1 permits the utilization of fly ash from co-combustion in concrete production when the criteria are fulfilled. In order to meet the requirements of EN 450-1+A1, the amount of the secondary fuels used in co-combustion must not exceed 20 wt%, and the contribution of the secondary fuels to the fly ash must not exceed 10 wt%. The types of the secondary fuels allowed by En 450-1+A1 include vegetable materials like wood chip and straw, green wood and cultivated biomass, animal meal, municipal sewage sludge, paper sludge, petroleum coke, and virtually ash free liquid and gaseous fuels [267]. Besides the specific requirements mentioned above, the fly ash from co-combustion must also meet the general requirements for the fly ash properties, which are partly given in Table 1.1. The parameters given in Table 1.1 may be affected when coal is co-fired with a secondary fuel, particularly when the secondary fuel has relatively large ash content. A typical example is straw, which does not only have an ash content comparable to coal, but also contains considerable amount of K and Cl. Thus co-firing of coal and straw may increase the Cl and K content in the fly ash, which may confine the utilization of fly ash in concrete production. Based on the fly ash composition obtained from full-scale co-firing of coal and straw [79], the chlorine and alkali content in the fly ash is found to meet the criteria of EN 450-1+A1, even at about 25 wt% straw condition. However, the results are limited to the fuels in the plant and the applied operation conditions [79]. Different results may be achieved for different coal/secondary fuels and different operation conditions [60].

Table 1.1 Chemical and physical requirement for the fly ash used in concrete production based on EN 450-1+A1 [267].

Properties	Concrete Criteria (EN 450-1+A1)
Loss on ignition	≤ 5 (wt%), Category A
	2-7 (wt%), Category B
	4-9 (wt%), Category C
Chloride (Cl-)	≤ 0.1 (wt%)
Sulfuric anhydride (SO_3)	≤ 0.1 (wt%)
Free CaO	≤ 2.5 (wt%)
Reactive CaO	≤ 10 (wt%)
Reactive SiO_2	≤ 25 (wt%)
SiO_2+Al_2O_3+Fe_2O_3	≥ 70 (wt%)
Total alkali	≤ 5 (wt%)
MgO	≤ 4 (wt%)
Soluble phosphate (P_2O_5)	≤ 0.01 (wt%)
Fineness	60 (wt%) ≤ 0.045 mm, Category N
	88 (wt%) ≤ 0.045 mm, Category S
Activity index	≤ 75% at 28 days and ≤ 85% at 90 days
Soundness	expansion ≤ 10 mm for a mixture of 30 wt% fly ash and 70 wt% test cement*
Particle density	deviate no more than ± 200 kg/m^3 from the declared value
Initial setting time	initial setting time for a mixture of 25 wt% fly ash and 75 wt% test cement ≤ twice of the time of the test cement
Water requirement	≤ 95 (wt%), Category S

* Only needed when free CaO > 1 (wt%)

The influence of the fly ash from co-combustion on the quality of concrete has been investigated by Wang et al. [268] through replacing 25 wt% of cement by different fly ashes. In their tests, the fly ash from co-firing of coal and 10 wt% or 20 wt% switchgrass is compared with the coal ash of the same class (Class F according to the ASTM C618). In addition, the ash from pure wood combustion (20 wt%) is blended with two different coal fly ash (Class C and Class F, respectively), and compared with the original coal fly ash. The results reveal that the fly ash from co-firing and the blended fly ash exhibit slightly greater water demand than the traditional Class C and Class F fly ash, but the difference is marginally significant. Compared to pure cement, the air-entraining agent demand and the setting time are increased, when part of the cement is replaced by different ashes. The increased air-entraining agent demand is presumably related to the relatively high loss of ignition in the co-firing or blended ash. Up to 7 days, the compression strength of the concrete produced by pure cement seems to be higher than that produced by the addition of ashes. However, the difference in compression strength becomes insignificant from 28 days to one year. The impact of fly ash addition on the 56 day flexure strength is insignificant with respect to pure cement. Based on their results, it was concluded that the co-firing fly ash and the blended fly ash used in tests is similar to pure coal fly ash, with respect to the properties of the produced concrete [268]. However, care must be taken to prepare the concrete since the fly ash from co-firing or the blended fly ash may increase the amount of air-entraining agent needed to meet the requirement of the air content percentage in the concrete mix [268].

2 Co-Combustion of Coal and Solid Recovered Fuel: General Combustion and Ash Behavior

Abstract

Co-combustion of a bituminous coal and a solid recovered fuel (SRF) was conducted in an entrained flow reactor, and the influence of additives such as NaCl, PVC, ammonium sulphate, and kaolinite on co-combustion was investigated. The co-combustion experiments were carried out with SRF shares of 7.9 wt%, 14.8 wt% and 25 wt%, respectively. The effect of additives was evaluated by maintaining the share of the secondary fuel (mixture of SRF and additive) at 14.8 wt%. The experimental results showed that the fuel burnout, NO and SO_2 emission in co-combustion of coal and SRF were decreased with increasing share of SRF. The majority of the additives inhibited the burnout, except for NaCl which seemed to have a promoting effect. The impact of additives on the NO emission was mostly insignificant, except for ammonium sulphate which greatly reduced the NO emission. For the SO_2 emission, it appeared that all of the additives increased the S-retention in ash. Analysis of the bulk composition of the fly ash from different experiments indicated that the majority of the S and Cl in the fuels were released to gas phase during combustion, whereas the K and Na in the fuels were mainly retained in ash. When co-firing coal and SRF, approximately 99 wt% of the K and Na in fly ash was present in water insoluble form such as alkali aluminosilicates. The addition of NaCl, PVC, and AmSulf generally promoted the vaporization of Na and K, resulting in an increased formation of water soluble alkalis such as alkali chlorides or sulphates. The vaporization degree of Na and K was found to be correlated during the experiments, suggesting an interaction between the vaporization of Na and K during pulverized fuel combustion. By collecting deposits on an air-cooled probe during the experiments, the ash deposition propensity in co-combustion was found to be decreased with increasing share of SRF. The addition of NaCl and PVC significantly increased the ash deposition propensity, whereas the addition of AmSulf or kaolinite showed a slight reducing effect. The chlorine content in the deposits generally implied a low corrosion potential during co-combustion of coal and SRF, except for the experiments with NaCl or PVC addition.

2.1 Introduction

Direct co-combustion of coal and secondary fuels in a pulverized coal-fired power plant is recognized as one of the most convenient and advantageous methods to replace part of coal consumption by less CO_2-emitting fuels such as biomass and waste [1]. Besides the effect on net CO_2 reduction, co-combustion of coal and secondary fuels may influence the operation and

performance of a boiler. In order to evaluate the possible impact of adding a secondary fuel to a pulverized coal-fired power plant and to optimize the technology, a number of co-combustion investigations have been carried out in full-scale boilers [7,60,62,85], pilot-scale reactors [9,93,99-101,255], and laboratory-scale setups [253,269]. The commonly tested secondary fuels were straw [9,60,62,93,99], wood [7,9,85,101], sewage sludge [101,108,217], and waste derived fuels [101,103,270]. The investigations addressed the fuel burnout [9,60], SO_2 and NO emission [7,9], ash deposition and corrosion [62,99-101,255], fly ash qualities [99,271], formation and emission of fine particles [217,227], and the performance of SCR system in co-combustion [217].

Solid recovered fuel (SRF) derived from nonhazardous waste streams such as industrial waste and bulky waste is considered as an advantageous secondary fuel to be co-fired in pulverized coal-fired power stations [272]. Although waste is normally regarded as a highly heterogeneous fuel with low thermal value, the production technologies of SRF can significantly improve the combustion properties of the waste. After processing steps such as screening, mechanical sorting and size reduction, the lower heating value of SRF can become approximately 20 MJ/kg (dry basis) [272], which is comparable to biomass such as straw and wood. Besides, SRF can be produced as a fluffy form, and it has the possibility to be injected into a pulverized coal-fired boiler directly, by using a similar injection method that has been applied for ground straw particles [61]. Moreover, since SRF normally contains 40-80 wt% of biogenic components [272], co-combustion of coal and SRF will reduce the net CO_2 emissions from a pulverized coal-fired power plant. This technique also has the potential to increase the efficiency of utilizing waste fuels, as the electrical efficiency of a pulverized coal-fired plant is usually 10-20% higher than that of a dedicated waste incineration plant. Furthermore, if the SRF contains lower nitrogen and sulphur contents than coal, the emission of NO_x and SO_x from the coal-fired boiler may be decreased by co-firing coal with the SRF.

Besides the advantages mentioned above, several technical issues may be associated with co-combustion of coal and SRF. In comparison with coal, SRF is usually characterized of high chlorine content (0.3-0.8 wt%, dry basis [272,273]). When coal is co-fired with SRF, the high chlorine content in SRF may aggravate the ash deposition and corrosion problems in the boiler, since the organically associated alkalis in coal and SRF may react with gaseous chlorine and generate alkali chlorides which could promote the deposit formation and corrosion of superheater tubes. Besides, the content of trace elements in SRF may be considerably higher (sometimes 1 order of magnitude higher) than that of coal [272,273]. This is likely due to the fact that SRF may contain waste fractions with high trace element concentration, such as CCA (chromate copper arsenate) impregnated wood and plastics with stabilizers [171]. Therefore, co-combustion of coal and SRF may significantly increase the trace element emission from a pulverized coal-fired power plant, and generate fine particles which are potentially more harmful than those from coal combustion [103]. In addition, since SRF is a more heterogeneous fuel than coal, the variation of SRF properties may be significant in practical operations and may greatly influence co-combustion of coal and SRF. Furthermore, co-firing of coal and SRF may affect the fly ash quality, fine particle formation, and the performance of the SCR system in a pulverized coal-fired power plant. As a consequence, a systematic evaluation of co-combustion of coal and SRF is necessary in order to apply this technique in a full-scale plant.

In order to investigate co-combustion of coal and SRF, it is desirable to study the combustion behavior of the fuel mixture in conditions similar to a pulverized coal-fired plant. With this purpose, co-combustion of a bituminous coal and a SRF was carried out in an entrained flow

reactor (EFR) in this work. During the experiments, the coal was co-fired with different share of SRF (7.9 wt%, 14.8 wt%, and 25 wt%). Besides, in order to evaluate the possible influence of SRF property variation, additives such as NaCl, PVC, $(NH_4)_2SO_4$ (AmSulf), and kaolinite were blended with the mixture of coal and SRF, and combusted in the reactor. Based on the experimental results, the impact of co-combustion on fuel burnout, NO and SO_2 emissions, fly ash properties, and deposit formation is investigated in the present chapter. The influence of co-combustion on the partitioning of trace elements will be addressed in next chapter.

2.2 Experimental

2.2.1 Fuels and Additives

A Columbian bituminous coal and a SRF mainly consisting of waste paper, plastic and wood were chosen as the fuels. The investigated additives included PVC, NaCl, AmSulf and kaolinite. The properties of the fuels and additives are given in Table 2.1. It can be seen that the SRF is of higher volatile, Cl and Ca content than the coal, while it is of lower ash, N, S, Si, Al, K and Fe content. The additives used in this study are pure compounds from chemical companies, with chemical compositions shown in Table 2.1.

Table 2.1 Properties of fuels and additives.

Properties	Coal	SRF	PVC*	NaCl	AmSulf	Kaolinite
LHV (MJ/kg wet)	26.53	20.86	19.88	-	-	-
Moisture (wt% wet)	5.25	5.20	1.10	0.04	0.08	0.98
Volatiles (wt% wet)	34.11	72.05	98.90	-	99.92	-
Ash (wt% wet)	10.42	5.69	-	99.96	-	85.20
C (wt% dry)	71.00	58.00	38.40	-	-	-
H (wt% dry)	4.90	6.60	4.80	-	5.33	1.55
N (wt% dry)	1.50	1.00	-	-	30.67	-
S (wt% dry)	0.70	0.42	-	-	21.33	-
Cl (wt% dry)	0.03	0.28	56.80	60.68	-	-
Si (wt% dry)	3.06	1.08	-	-	-	22.75
Al (wt% dry)	1.21	0.21	-	-	-	20.05
Mg(wt% dry)	0.15	0.09	-	-	-	0.17
P (wt% dry)	0.02	0.02	-	-	-	-
Ca (wt% dry)	0.18	0.67	-	-	-	0.03
Na (wt% dry)	0.07	0.11	-	39.32	-	0.58
K (wt% dry)	0.21	0.09	-	-	-	1.32
Fe (wt% dry)	0.60	0.28	-	-	-	-

* The heating value of PVC is estimated from [32].

To be able to feed into the reactor, both the coal and SRF were pulverized by an Alpine® pin mill Although the SRF is normally regarded as a heterogeneous fuel, the grinding process has significantly improved the homogeneity of the SRF. For confirmation, the Si and Al content in the SRF has been analyzed by 3 times and the average deviation were found to 9% and 13%, respectively. This indicates that the SRF is quite homogeneous. The homogeneity of the SRF has

been further evaluated by performing repeating co-combustion experiments, showing a good reproducibility of the NO and SO_2 emission (average deviation <2%) during co-combustion of coal and SRF.

The particle size distribution of the fuels and additives was determined by a laser diffraction method (Malvern Mastersizer 2000 particle size analyzer). It was found that the d_{50} (meaning that 50 vol% of the particles is below this size) of SRF is approximately 164 μm, while the d_{50} of coal is about 19 μm. The d_{50} of PVC, NaCl, AmSulf, and kaolinite is approximately 104 μm, 259 μm, 222 μm, and 8 μm, respectively. The detailed particle size distribution of the fuels and additives is depicted in Figure 2.1. It should be noted that the SRF particles used in this work form agglomerates more easily than the coal particles. Thus, the actual particle size of SRF in the experiments may be larger than that obtained by the particle size analyzer.

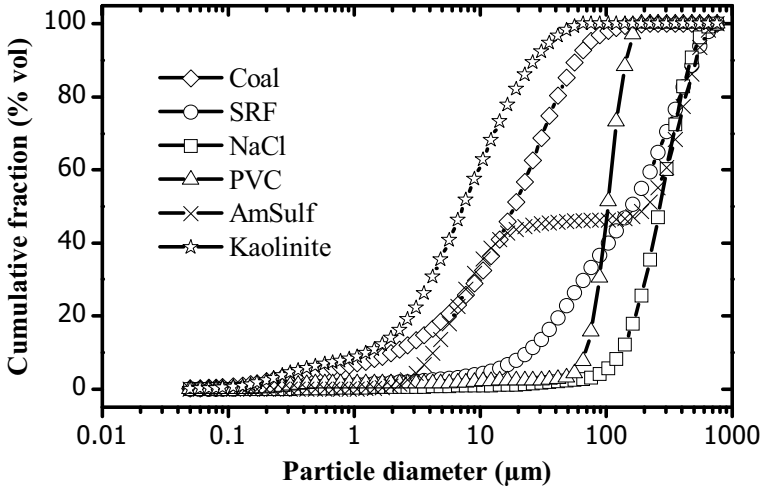

Figure 2.1 Particle size distribution of the fuels and additives.

2.2.2 Setup

The experiments were carried out in an entrained flow reactor (EFR) designed to simulate the combustion environment of a suspension fired boiler. A schematic drawing of the setup is shown in Figure 2.2. The setup consists of a gas supply system, a fuel feeding system, a gas preheater, a 2-meter long vertical reactor which is electrically heated by 7 heating elements, a bottom chamber, a particle and gas extraction system, and a deposition system which aims to simulate deposit formation on the superheater tubes of a boiler. The vertical reactor, which contains the combustion zone, is made of silicon carbide (SiC), and has an inner diameter of 0.08m. A more detailed description of the reactor can be found in [99].

In the co-combustion experiments, the premixed fuels were injected into the reactor together with the primary air. In order to have a comparable residence time (~1s) in different experiments, the flow rate of the primary air and total air was maintained at 13 Nl/min and 95 Nl/min respectively. The feeding rate of the fuel particles was controlled by a gravimetric screw feeder, and was adjusted for different experiments in order to control the excess air ratio to be approximately 1.43. The injected fuel particles were mixed with the preheated secondary air at

the inlet of the vertical reactor, and subsequently combusted in the reactor. The temperature of the heating element in the preheater was 900 °C, and the wall temperature of the vertical reactor was set to 1000–1300 °C for all of the experiments, similar to the conditions used in [99].The mean gas velocity in the reactor is approximately 1.7 m/s, assuming an average gas temperature of 1200 °C.

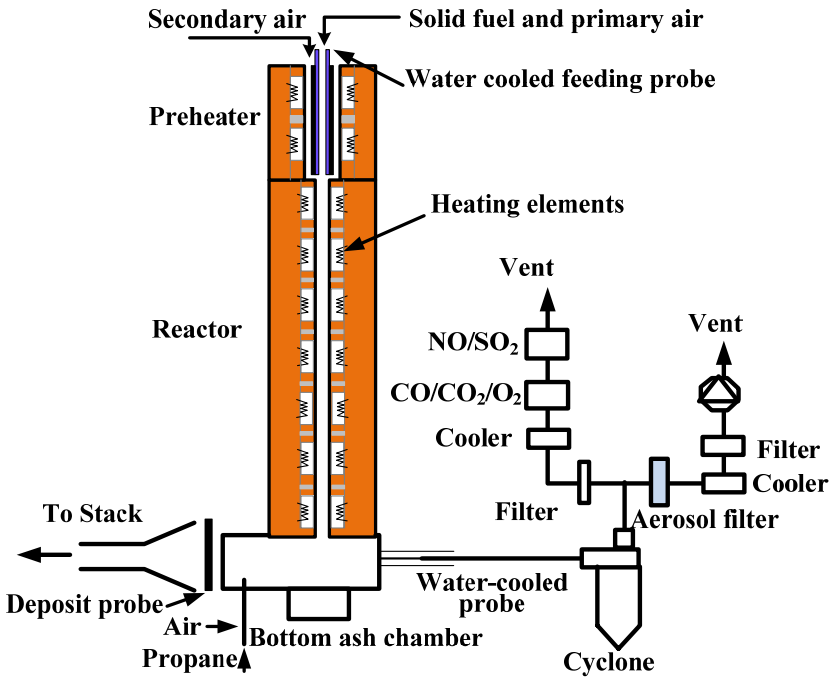

Figure 2.2 Schematic drawing of the entrained flow reactor (modified from [99]).

During the combustion experiments, the bottom ash was collected in a metal collector placed at the bottom chamber. The flue gas from combustion was separated into two fractions. As illustrated in Figure 2.2, a minor part of the flue gas was drawn to an extraction system through a water-cooled probe. The water-cooled probe was placed perpendicular to the direction of the flue gas and the sampling position was located close to the center of the reactor tube. The probe has an outer diameter of 6.4 mm and an inner diameter of 4.4 mm. The flue gas temperature at the sampling point was about 600 °C, which was rapidly cooled to about 100 °C in the water-cooled probe. It should be noted that the significant temperature gradient between the flue gas and the surface of the water cooled probe may induce thermophoresis and lead to deposition of aerosols on the probe surface. These deposited aerosols and other fly ash particles in the cooling probe were collected after the experiment, and were considered as part of the cyclone ash. The large fly ash particles passing through the water-cooled probe were collected by a cyclone with a cut diameter of 2.5 μm, and the fine fly ash particles passing through the cyclone were gathered in an aerosol filter using a polycarbonate membrane with a pore size of 0.1 μm. The concentration of CO, CO_2, O_2, NO and SO_2 was measured in the extraction system by two gas analyzers.

Apart from the flue gas drawn by the extraction system, the remaining flue gas from the combustion was directed toward a deposit probe which simulated a superheater tube in a boiler.

In front of the deposition probe, a propane burner was mounted to control the flue gas temperature to be 800 °C. It should be noted that the flue gas introduced by the propane burner lowered the concentration of fly ash and vaporized inorganic species in flue gas. The dilution influenced the ash deposition rate on the probe. However, since the propane burner was operated at similar conditions at different experiments, the ash deposition results from different experiments would be comparable. As a result, it is suggested that the tendency of the ash deposition results should be focused in this work, rather than the detailed numbers. The air-cooled deposit probe is made of stainless steel, with an outer diameter of 1 cm and a length of 10 cm. The probe was placed in front of the exit slit of bottom chamber which has a size of 4*8 cm^2. By adjusting the temperature of air preheater and the heating tape connected to the probe, the surface temperature of the deposit probe was controlled to be 550 °C during the experiments.

The duration of an experiment was 1.5 hours. In order to achieve a stable combustion condition, the reactor was preheated to operational temperatures and kept over-night, and the fuel injection began 40 minutes prior to the start of an experiment. After the experiment, the deposits on the probe, the ash from the extraction tubes, cyclone, aerosol filter, and bottom chamber were collected, weighted and preserved for chemical analysis. In order to minimize the influence of deposit built-up inside the reactor, the reactor was heated to 1400 °C for 20 hours after every experiment to perform high temperature cleaning.

2.2.3 Experimental Matrix

Table 2.2 Experimental matrix and excess air ratios.

Experiment	Fuel composition wt%						Feeding rate (kg/h)	Excess air ratio
	Coal	SRF	NaCl	PVC	AmSulf	Kaolinite		
1*	100	-	-	-	-	-	0.582	1.44
2*	92.1	7.9	-	-	-	-	0.594	1.43
3*	85.2	14.8	-	-	-	-	0.607	1.42
4*	75	25.0	-	-	-	-	0.629	1.39
5*	85.2	13.8	1.0	-	-	-	0.623	1.42
6	85.2	12.8	2.0	-	-	-	0.615	1.42
7*	85.2	12.8	-	2.0	-	-	0.604	1.43
8	85.2	10.8	-	4.0	-	-	0.604	1.43
9	85.2	10.8	-	-	4.0	-	0.618	1.42
10	85.2	10.8	-	-	-	4.0	0.631	1.42

*Repetition experiments have been performed.

The experimental matrix and the excess air ratio of different experiments are shown in Table 2.2. When co-firing coal and SRF, the mass share of SRF was chosen as 7.9 wt% (wet basis), 14.8 wt% and 25.0 wt%, which corresponded to a thermal share of 6.3 th%, 12.0 th% and 20.8 th%, respectively. In the additive experiments, the mass share of coal was maintained at 85.2 wt%, meaning that the mass share of the secondary fuel (SRF + additive) was kept at 14.8 wt%. With fixed mass share of coal, the addition of additives simulated a variation of SRF properties. The addition of NaCl (1 wt% and 2 wt%) simulated a SRF with a high alkali chloride content, while the addition of PVC (2 wt% and 4 wt%) enhanced the chlorine content of SRF. The addition of AmSulf and kaolinite allowed us to study the co-combustion behavior of SRF with a coal rich in sulphur or aluminosilicates contents. In order to ensure the experiments were carried out at

similar combustion conditions, the excess air ratio for different experiments was controlled at around 1.43, as shown in Table 2.2.

2.2.4 Ash and Deposit Analysis

The ash/deposit samples from the experiments were analyzed at the Enstedværket Laboratory, DONG Energy A/S. The content of Al, Ca, Fe, K, Mg, Na, P, Si, Ti, S, and Cl in the bottom ash, cyclone ash, and filter ash was analyzed by ICP-OES (inductively coupled plasma optical emission spectrometry). Furthermore, the water soluble K, Na, Cl and S content in the cyclone ash and deposit was analyzed by ICP-OES/IC. During the analysis of water soluble elemental content, the ash/deposit sample was dissolved in ultra-pure water at 120 ^{o}C for 1 hour, and then the solution was filtered and analyzed by ICP-OES/IC. Besides the bulk chemical analysis, the typical morphology and composition of the fly ash from the experiments were characterized by using TEM-EDS (transmission electron microscopy and dispersive X-rays spectroscopy).

2.3 Results and Discussion

2.3.1 Carbon Burnout

Figure 2.3 shows the carbon burnout from different experiments, which is determined by the ash tracer method [274]:

$$B = \left[1 - \frac{A_0}{100 - A_0} \times \frac{100 - A_i}{A_i}\right] \times 100 \tag{2.1}$$

where B (%) is the carbon burnout, A_0 (wt%) is the ash content of the dry fuel/fuel mixture, and A_i (wt%) is the weighted mean ash content of different ash fractions (bottom ash, cyclone ash, and filter ash) collected from the experiment. The ash content of different ash fractions is obtained by keeping the ashes at 750 ^{o}C for two hours and measuring the Loss-On-Ignition [275].

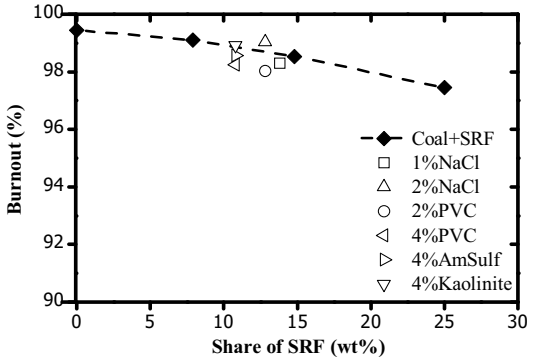

Figure 2.3 Carbon burnout at different experiments (open symbols denote the experiments with additives).

From Figure 2.3, it can be seen that when coal is co-fired with SRF, the burnout decreases with increasing share of SRF. The burnout in EFR is about 99.5% for coal combustion, whereas it decreases to 97.5% when co-firing of 25 wt% SRF with coal. Such a tendency is consistent with

the CO emission from EFR. The average CO emission in coal combustion is 23 ppmv (dry, 6% O_2), while the average CO emission in co-firing of 25wt% SRF and coal increases to 153 ppmv (dry, 6% O2). The reduced burnout during co-combustion of coal and SRF may be partly related to the particle size of SRF, which is significantly larger than that of coal. Therefore, the SRF particles may require more time to be heated up and combusted. In addition, the SRF particles are found to be partly agglomerated during injection. This would increase the particle size of SRF and lead to a less stable fuel injection condition. Therefore the relatively low burnout observed during co-combustion of coal and SRF may be also related with the lower stability during fuel injection. With higher share of SRF, the fluctuation of CO_2 concentration in the flue gas is increased progressively, which supports the hypothesis of less stable fuel injection.

As shown in Figure 2.3, the additives generally show a slight reduction effect on the burnout, except for the addition of 2 wt% NaCl. For the addition of kaolinite and AmSulf, it may be the case that the flame temperature is reduced and result in a slightly lower fuel burnout than that seen from the mixture of coal and SRF. This is likely to happen, since both kaolinite and AmSulf can be decomposed at high temperature and the reactions are endothermic. Compared with the addition of kaolinite and AmSulf, more significant reduction effects can be seen with the addition of 2 wt% or 4 wt% PVC. It is likely that the addition of PVC has affected the reactivity of the chars from coal and SRF. In [276], it was found that the presence of PVC could increase the char yield of municipal waste and reduce the char reactivity. In the present work, similar effects may be present and responsible for the reduced burnout during PVC addition. The addition of NaCl may have two contrary effects on burnout. The vaporization of NaCl may result in a lower flame temperature and adversely affect fuel burnout, whereas the catalytic effect of alkali metals on char reactivity may improve burnout [78]. With the addition of 2 wt% NaCl, the catalytic influence on the char reactivity may become dominant and lead to the observed increased fuel burnout.

2.3.2 NO Emission

The NO emission (ppmv, dry, 6% O_2) from different experiments is shown in Figure 2.4a. It can be seen that the NO emission from co-combustion of coal and SRF decreases with increasing share of SRF, which is in agreement with the lower nitrogen content in SRF compared to coal. The addition of NaCl, PVC or kaolinite shows insignificant effect on NO emission, whereas the addition of AmSulf reduces the NO emission greatly. The reduction is likely linked to the NH_3 yielded by the thermal decomposition of AmSulf, which would occur at temperature higher than 257 ^oC [277], with products of NH_3, SO_3 and H_2O [140]. The released NH_3 may go through two major pathways, i.e. either reaction with O_2 to form NO, or reaction with NO to form N_2 [12]. For the AmSulf used in the present work, the reaction between NO and NH_3 is probably the dominant pathway, which results in a significantly reduced NO emission. In order to further investigate the behavior of AmSulf particles in the experiments, it is necessary to know the decomposition rate of AmSulf particles at different temperatures as well as the temperature profile of the particles in the reactor, which are outside the scope of this work.

In order to neglect the dilution effect caused by the fuel nitrogen content, the percentage of fuel nitrogen that has been converted to NO is calculated for different experiments, by assuming all NO in the flue gas is formed from fuel nitrogen. From Figure 2.4b, it can be seen that the conversion of fuel nitrogen to NO decreases with increasing share of SRF. This is in line with the results from co-combustion of coal and straw/wood, which showed decreased fuel nitrogen

conversion to NO with increasing share of straw/wood [91]. The reduced conversion of fuel nitrogen to NO in co-combustion of coal and SRF is likely related to the high volatile content of SRF, with which a reduction zone with lower excess air ratio may be generated near the burner, when part of the coal is replaced by SRF. The lower oxygen concentration in the reduction zone may inhibit the conversion of fuel nitrogen to NO, resulting in reduced NO formation [91]. In addition, since the formation of thermal NO may not be negligible in the EFR, it may be the case that co-combustion of coal and SRF would result in a lower flame temperature compared to coal combustion, thus leading to a reduced formation of thermal NO. This hypothesis is possible as the flame temperature of a refuse derived fuel (RDF) is found to be 200–300 ^{o}C lower than the coal flame, given the same excess ratio condition [260].

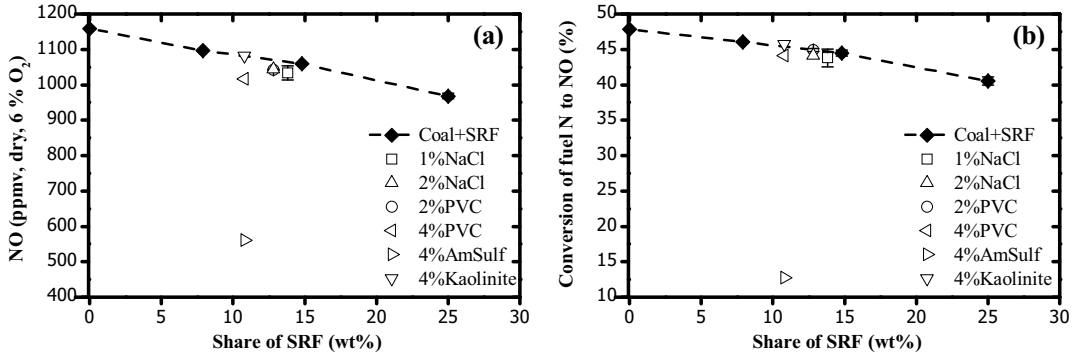

Figure 2.4 (a) NO emission (ppmv, dry, 6 % O_2) from EFR experiments with different share of SRF and additives, (b) Conversion of fuel nitrogen to NO (%) in EFR experiments with different share of SRF and additives, by assuming the NO generated during combustion is only from fuel nitrogen.

2.3.3 SO_2 Emission

Figure 2.5 shows the SO_2 emission (ppmv, dry, 6 % O_2) from different experiments. It can be seen that the SO_2 emission decreases slightly with increasing share of SRF. This is consistent with the fuel properties, i.e. the SRF contains less sulphur than the coal. With the same mass share of secondary fuels, the addition of NaCl, PVC or kaolinite does not significantly affect the SO_2 emission. However, the addition of 4 wt% AmSulf greatly increases the SO_2 emission, indicating the majority of the SO_3 released from the decomposition of AmSulf has been converted to SO_2 during the experiment.

In order to further investigate the influence of co-combustion on the behavior of sulphur, the percentage of sulphur that is retained in ash is calculated from different experiments, based on the sulphur content and feeding rate of the fuel mixture as well as the composition and amount of the collected bottom ash, cyclone ash and filter ash. As shown in Figure 2.5b, the sulphur retention in ash generally increases with increasing share of SRF. A primary reason is that the SRF contains more calcium than the coal, which would favor the formation of calcium sulphate and retain more sulphur in ash. Similar effect has been seen when coal is co-fired with wood of high calcium content [9]. The additives also influence the sulphur retention in ash. For the addition of NaCl, the sulphur retention is increased compared to co-combustion of coal and SRF. This is probably related to the sulphation reaction between the gaseous sulphur and the added

NaCl. Similar effects have been observed in straw and coal co-combustion, where the retention of sulphur was found increased in co-combustion due to the high potassium content in straw [91]. With the addition of AmSulf, a significant increase of sulphur retention in ash is observed in Figure 2.5b. The higher extent of sulphation reactions between gaseous sulphur and alkali/earth alkaline is probably a primary reason for the increased sulphur retention in ash. In addition, it is likely that part of gaseous sulphur may form H_2SO_4 during flue gas cooling and condense on the surface of ash particles [121]. In the combustion of bituminous coal in a pulverized coal-fired power plant, it was found that approximately 1% of the sulphur in the fuel could end up as SO_3 [97]. If the same percentage is applied in this work, the concentration of SO_3 in the flue gas would be around 15 ppmv during 4 wt% AmSulf addition. According to the estimated SO_3 concentration and dew point of SO_3 in flue gas [97], condensation of H_2SO_4 would likely occur on the surface of the cyclone and filter ash, as these ash particles are collected at a temperature of ~100 ^oC during the experiments. For other experiments, the condensation of H_2SO_4 is probably negligible, as the SO_3 concentration in the flue gas is probably below 5 ppmv.

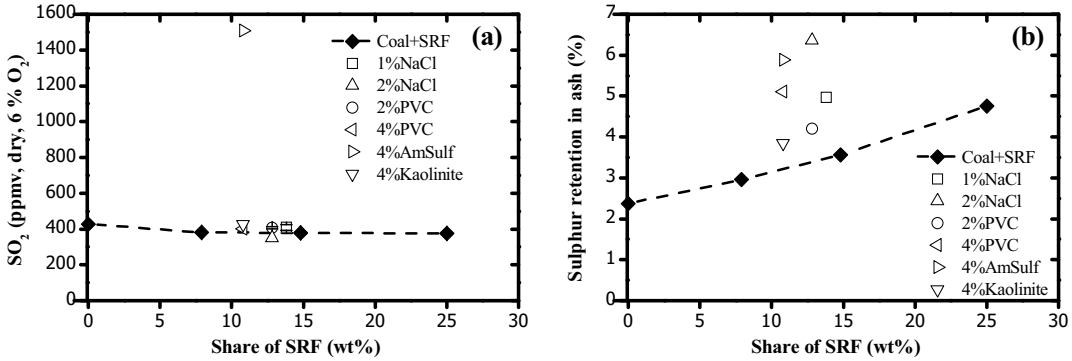

Figure 2.5 (a) SO_2 emission (ppmv, dry, 6 % O_2) from EFR experiments with different shares and types of secondary fuels, (b) the percentage of sulphur retained in the ashes collected from the EFR experiments.

When PVC is added to the mixture of coal and SRF, it is seen that the sulphur retention in ash is slightly increased, and the effect becomes more pronounced with an increasing share of PVC. A possible explanation is that the vaporization degree of alkalis may be promoted by the addition of PVC, as more gaseous alkalis may be released from the fuels due to the formation of alkali chlorides. These alkali chlorides may further react with the gaseous sulphur in the flue gas and form alkali sulphates. As a result, more alkali sulphates would be formed, leading to more pronounced sulphur retention in ash. For the addition of 4 wt% kaolinite, a slight increase of the sulphur retention in ash compared to the estimations is seen, which may be linked to the capture effect of the impurities in kaolinite such as K and Na.

2.3.4 Typical Fly Ash Morphology and Composition

The morphology of fly ash particles from the EFR experiments has been characterized by transmission electron microscopy (TEM) and dispersive X-rays spectroscopy (EDS). Figure 2.6 shows the TEM pictures of the filter ash collected from co-combustion of coal and 14.8 wt% SRF, which are representative for the fly ash morphology obtained from the EFR. It can be seen that the fly ash particles generally consist of two parts i.e. spherical particles and aggregated

nucleates. The spherical particles, which dominate the mass of the fly ash, are mainly formed from the fragmentation, melting and coalescence of the minerals in coal and SRF [278]. The particle size of the spherical particles is normally larger than 0.5 μm. The majority of these particles have nearly perfect spherical shape, implying that the combustion temperature in the EFR is sufficiently high to melt the minerals in the coal and SRF. Different from the spherical particles, the nucleates are primarily generated from the vaporized inorganic species via vaporization, reaction, homogeneous nucleation, and aggregation mechanisms [278]. The primary particles of nucleates usually have irregular shapes with a typical size around 10–30 nm. These nucleates can either form aggregates by themselves or attach to the surface of existing spherical particles. The contribution of nucleates is generally negligible to the formation of supermicron particles. However, for submicron particles, the contribution of nucleate increases progressively with decreasing particle size, and becomes the dominant component for the formation of ultrafine particles around 0.1 μm [278].

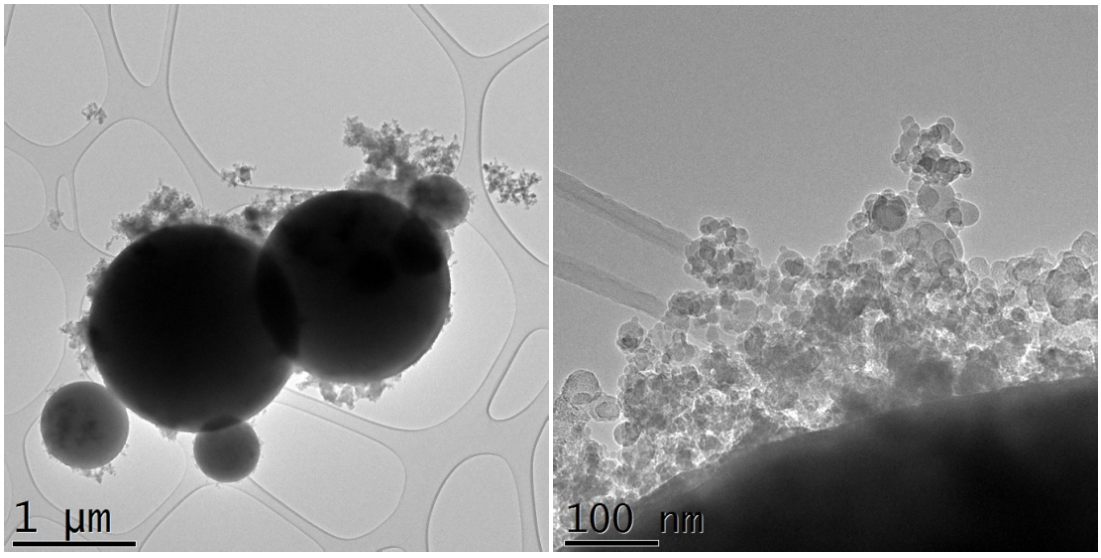

Figure 2.6 Typical morphology of the fly ash particles from the entrained flow reactor.

The composition of the spherical particles and nucleates from different experiments has been characterized by TEM-EDS. Figure 2.7 shows the typical results from three different experiments. One should be aware that TEM-EDS is a semi-quantitative method which to a large extent depends on the samples selected for analysis. Although the results presented in Figure 2.7 are average values from a number of analyses, it is still suggested to focus on the tendencies shown by the figure, rather than the precise numbers. From Figure 2.7, it can be seen that the composition of spherical particles and nucleates has some general differences. The nucleates are normally characterized of higher Ca, Mg, S and P content, whereas the spherical particles usually have higher Si, Al and K content. Such tendencies are generally in agreement with the fine particle measurement carried out in a full-scale co-combustion test with similar fuels, see details in Chapter 4. The influence of SRF and PVC on the composition of the spherical particles and the nucleates is reflected in Figure 2.7. Compared with coal combustion, co-combustion of coal and 14.8 wt% SRF seems to decrease the Si and S content and increases the K, Na, P and Cl content in the nucleates. The tendencies are mostly consistent with the findings in Chapter 4.

When 2 wt% PVC is added to the coal and SRF mixture, the Si and S content seems to be further decreased in nucleates, while the content of Ca, K, Na, P and Cl is increased. In general, the influence of SRF and PVC addition is found to be more significant on the composition of nucleates than that of spherical particles. This implies that the vaporization of inorganic species may be affected to a large extent when coal is co-fired with SRF and additives, whereas the influence on bulk ash composition is less pronounced.

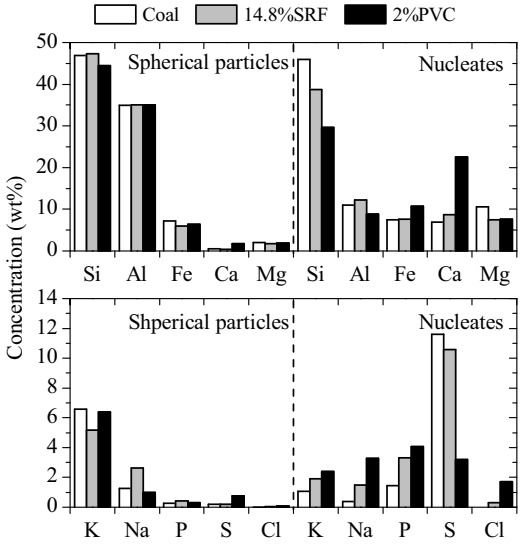

Figure 2.7 Typical composition of the spherical particles and nucleates from the experiments with coal, coal+14.8 wt% SRF, and coal+SRF+2 wt% PVC.

2.3.5 Bulk Fly Ash Composition

2.3.5.1 Ash composition from coal and SRF co-combustion

In Figure 2.8, the bulk composition of the cyclone ash and filter ash from co-combustion of coal and SRF is illustrated. It can be seen that the composition of cyclone ash varies progressively with increasing share of SRF. Most of the variations are consistent with the ash composition of the two fuels, such as the tendencies for Al, Fe, K and Ca. However, the tendency for S deviates from the fuel properties. This is primarily due to that the S content in ash is more closely related with the sulphur retention capability of ash, rather than the fuel sulphur content. As aforementioned, the cyclone ash from co-combustion of coal and SRF has higher Ca content than that of coal combustion, which is capable of retaining more gaseous S in ash.

Compared to cyclone ash, the filter ash collected from co-combustion of coal and SRF has slightly larger K, Na, P, and S content. The cyclone ash and filter ash collected in this work are separated by a cyclone with cut-off diameter of ~2.5 μm. As indicated from the TEM analysis, although the contribution of the nucleates to ash formation becomes more significant for smaller particles, the collected filter ash is still dominated by spherical particles formed from the minerals in coal and SRF. Therefore, a possible explanation to the observed higher K and Na

content in the filter ash is that the filter ash may react more effectively with gaseous K and Na than the cyclone ash, as the influence of particle size on the reactions between aluminosilicates particles and gaseous alkali has been well-demonstrated [146,179]. The relatively higher S content in filter ash as compared to cyclone ash may be related to several reasons. The reactions between the ash and gaseous sulphur may be more efficient for smaller ash particles. In addition, the smaller ash particles would also contain more nucleates which are enriched in S (as illustrated in Figure 2.7). For the higher P content in the filter ash, it is primarily due to that the filter ash contain more nucleates compared to cyclone ash.

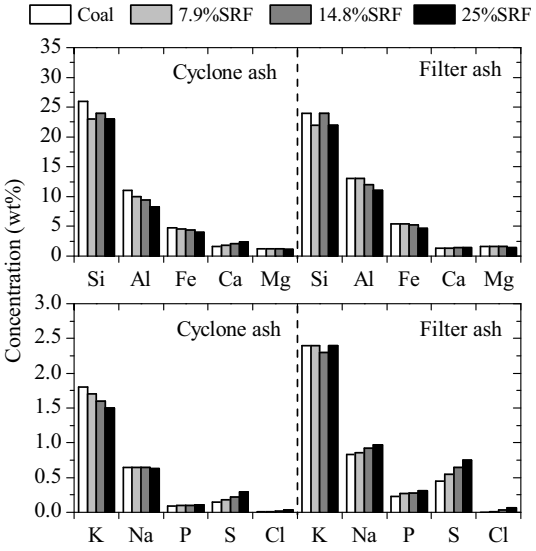

Figure 2.8 Bulk composition of the cyclone ash and filter ash collected from co-combustion of coal and different share of SRF.

Different SRF shares also influence the filter ash composition. With increasing SRF share, the content of Na, P and S seems to increase progressively. The Cl content in filter ash is also increased slightly with higher share of SRF. However, in general, the Cl content in filter and cyclone ash is below 0.065 wt% during co-combustion of coal and SRF (up to 25 wt%), indicating that the majority of the chlorine in the two fuels is released to gas phase during co-combustion.

2.3.5.2 Ash composition from the additive experiments

Figure 2.9 depicts the influence of the additives on the K, Na, S and Cl content in the cyclone ash and the filter ash. With the addition of NaCl, it can be seen that the content of K, Na, S, and Cl is generally increased in the filter ash and the cyclone ash. This demonstrates the effect of NaCl addition on co-combustion of coal and SRF. When NaCl is injected together with the coal and SRF mixture, a major part of the NaCl would be vaporized, and the gaseous NaCl may subsequently react with the fly ash and the SO_2/SO_3 in flue gas. As a result, part of the vaporized NaCl could be fixed in fly ash as sodium silicates or sodium aluminosilicates; whereas part of the NaCl would be converted to sodium sulphate which may further generate nucleates or condense

on the surface of existing ash particles. Both mechanisms would release the chlorine to the flue gas. For the remaining vaporized NaCl which has not undergone reaction, it may either generate nucleates or condense on the surface of the existing fly ash particles. Therefore, the observed larger Na content in the cyclone and filter ash during NaCl addition is likely due to a combination of the mechanisms mentioned above. Besides the Na content, the K content in fly ash, particularly in filter ash, is also increased during NaCl addition. It may be the case that the addition of NaCl has promoted the reaction between gaseous sodium and fuel minerals, resulting in fewer minerals available for reacting with the gaseous potassium released from the fuels. In addition, the gaseous sodium may displace part of the potassium bound in minerals, which would not otherwise be expected to vaporize [146]. Therefore the vaporization degree of K may be enhanced by NaCl addition, and lead to an increased K content in the filter ash. The S content in fly ash is not significantly increased during NaCl addition, implying the reaction between the added NaCl and the gaseous sulphur is limited. The Cl content in the filter/cyclone ash is increased during the addition of NaCl, particularly with the addition of 2 wt% NaCl. This indicates that the minerals in the coal and SRF may not be sufficient to fully convert the added 2 wt% NaCl, i.e. a certain fraction of the 2 wt% NaCl would remain unreacted during combustion. However, for the addition of 1 wt% NaCl, the fraction of the unreacted NaCl is much smaller, as the capture effect of minerals would be more pronounced in this condition. During the NaCl addition, the Cl content in filter ash is generally found to be significantly higher than that in cyclone ash, suggesting most of the chlorine would partition to ash through nucleation and/or condensation mechanisms.

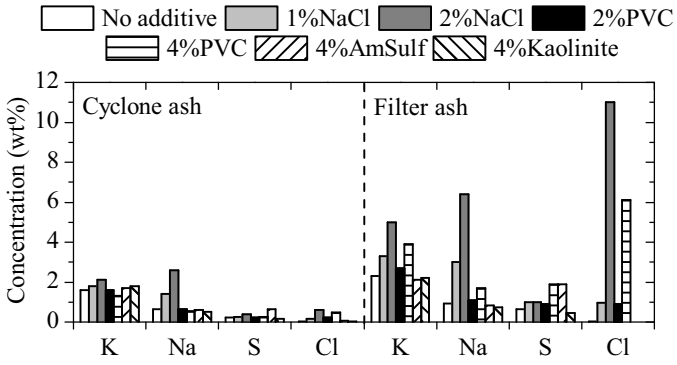

Figure 2.9 The content of the K, Na, S and Cl in the cyclone ash and filter ash collected from the experiments with additives, the experiments are all based on a coal share of 85.2 wt% and a total share of 14.8 wt% secondary fuels.

The addition of PVC does not show a notable effect on the composition of cyclone ash. However, for the filter ash, it is clearly seen that the K, Na and Cl content is increased by the PVC addition. It is known that the main gaseous product from the pyrolysis and combustion of PVC is HCl [279]. The higher alkali content obtained during PVC addition implies that the vaporization degree of Na and K may be increased by the presence of HCl. The reaction between the released gaseous alkali and HCl would form alkali chlorides, which may hinder the reaction between gaseous alkali and minerals, since the reaction rate of alkali chlorides and coal minerals is lower than that of alkali hydroxide and coal minerals [163,179]. Furthermore, the gaseous HCl may react with the mineral associated alkalis and result in a higher vaporization degree of alkalis. The

influence of different PVC share is obvious in Figure 2.9. By increasing the PVC share from 2 wt% to 4 wt%, the contents of K, Na and Cl in the filter ash are increased accordingly. The significantly higher Cl content in the filter ash from 4 wt% PVC addition is likely not only related to an increased formation of alkali chlorides, but also to the formation of calcium chlorides. This hypothesis is supported by the fact that the calcium content in the filter ash is increased from 1.7 wt% to 3.7 wt%, when the PVC share is increased from 2 wt% to 4 wt%. Moreover, at 2% PVC addition, the molar ratio of water soluble (K+Na)/Cl in filter ash is found to be 0.46, which also suggests that the presence of calcium chlorides is possible.

With the addition of 4 wt% AmSulf, it is noticed that the S content in both cyclone ash and filter ash is increased. As described earlier, the higher S content obtained during AmSulf addition is likely a result of the enhanced sulphation reactions between gaseous sulphur and fly ash, and a condensation of H_2SO_4 during flue gas cooling. The influence of AmSulf addition on the K, Na and Cl content in fly ash is generally not significant. With the addition of 4 wt% kaolinite, the variations of the K, Na and S content are mostly not significant. However, the Cl content in the cyclone ash and filter ash is below detection limit of the instruments, indicating that almost all of the chlorine in the fuels is released to gas phase during the addition of kaolinite.

2.3.5.3 Water soluble alkalis in fly ash

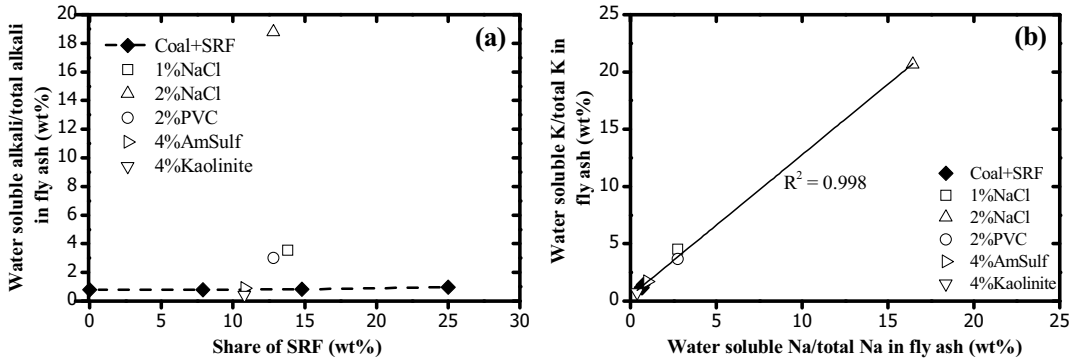

Figure 2.10 (a) percentage of water soluble alkali in the fly ash from EFR experiments with different share and type of secondary fuels, (b) comparison of the percentage of water soluble K/total K and the percentage of water soluble Na/total Na in the fly ash.

The results presented in the previous section show that the chlorine based additives (NaCl and PVC) can significantly increase the chlorine and alkali content in fly ash, particularly for the case with 2 wt% NaCl or 4 wt% PVC addition. It is well-known that the presence of a large quantity of alkali chlorides in flue gas can cause severe ash deposition and corrosion problems during pulverized fuel combustion [140,211]. To investigate the existing forms of alkalis in fly ash, the water soluble alkalis in fly ash have been analyzed for different experiments. In pulverized fuel combustion, the alkalis in the fuels can be converted into water soluble alkalis and water insoluble alkalis. The water soluble alkalis would mainly consist of alkali chlorides and sulphates, whereas the water insoluble alkalis would be dominated by alkali silicates or aluminosilicates. From a practical point of view, it is desirable to convert the alkalis to water insoluble forms, as water soluble alkalis may introduce operation problems such as deposition and corrosion in the boiler and deactivation of the SCR units [99]. Figure 2.10a shows the percentage of water

soluble alkali/total alkali in the fly ash collected from different experiments. The fly ash composition is calculated from the composition and mass fraction of the collected filter ash and cyclone ash. From Figure 2.10a, it can be seen that during co-combustion of coal and SRF, less than 1 wt% of alkalis appears as water soluble form in fly ash. It implies that majority of the fuel alkalis in co-combustion of coal and SRF would present as insoluble forms such as alkali silicates or aluminosilicates. With increasing share of SRF, the change of the percentage of water soluble alkali/total alkali in fly ash is insignificant.

The effect of additives on the percentage of water soluble alkali/total alkali is illustrated in Figure 2.10a as well. With the addition of 1 wt% NaCl, the percentage of water soluble alkali/total alkali in fly ash increases to approximately 4 wt%. By increasing the NaCl addition to 2 wt%, the percentage of water soluble alkali/total alkali in the fly ash is increased further to about 19 wt%. This demonstrates that addition of NaCl can increase the percentage of alkalis present in a water soluble form. Furthermore, it appears that the increase of the percentage of water soluble alkali is not linearly correlated with the added amount of NaCl, since the percentage of water soluble alkali/total alkali in the fly ash becomes approximately 5 times higher when the addition of NaCl is increased from 1 wt% to 2 wt%. In order to explain this, both the release and conversion of alkalis during pulverized fuel combustion need to be considered. When NaCl is added to the mixture of coal and SRF, it would significantly increase the release of Na to gas phase. A certain fraction of the released gaseous alkalis would react with the minerals in the fuels and result in water insoluble alkalis. However, the remaining gaseous alkalis would either stay un-reacted or react with gaseous S and Cl, which would result in water soluble alkalis. With the addition of 1 wt% NaCl, although the percentage of the released gaseous alkalis is increased significantly, the minerals in the fuels may still be able to react with the majority of the released alkalis, resulting in the percentage of water soluble alkali/total alkali in fly ash to be around 4 wt%. However, when 2 wt% NaCl is added to the fuel mixture, the fraction of the released gaseous alkali that are converted to insoluble alkali may be significantly reduced, due to the limited amount of the reactive minerals in the fuels. Therefore, a much larger percentage of water soluble alkali/total alkali (~19 wt%) in fly ash is obtained. However, it should be noted that the percentage of water soluble alkali/total alkali in the fuel mixture is larger than 75 wt% for the experiment with 2 wt% NaCl addition. The significant difference between the percentage of water soluble alkali in the fuel mixture and the collected fly ash suggests that a significant fraction of the injected NaCl has been converted to water insoluble alkalis by the minerals in the coal and SRF during co-combustion.

As can be seen in Figure 2.10a, the addition of 2 wt% PVC slightly increases the percentage of water soluble alkali/total alkali in fly ash. With the addition of PVC, the release of alkali may be slightly increased, due to the possible interaction between the gaseous chlorine from PVC combustion and the mineral form alkalis. Furthermore, the gaseous chlorine generated from PVC combustion would compete with the fuel minerals for reacting with the released gaseous alkali. With the increased gaseous chlorine concentration, the formation of alkali chlorides would become more pronounced, leading to a higher percentage of water soluble alkali/total alkali in the fly ash. It should be noted that the results for 4 wt% PVC is not shown in the figure, due to the analysis of filter ash from that experiment is not available.

As shown in Figure 2.10a, the addition of 4 wt% AmSulf also slightly increases the fraction of water soluble alkali/total alkali in fly ash. Similar to the PVC case, the increased concentration of the gaseous sulphur from AmSulf decomposition may compete with the reaction between

gaseous alkali and fuel minerals, resulting in a slightly increased formation of water soluble alkalis. With the addition of 4 wt% kaolinite, a slight decrease of the percentage of water soluble alkali/total alkali in fly ash is seen. It is likely because that the addition of kaolinite increases the amount of minerals for reacting with the released gaseous alkalis. However, the effect of kaolinite addition is not significant, implying the minerals in the fuel mixture are sufficient for reacting with the majority of the released gaseous alkalis.

To study the behavior of Na and K separately rather than the total alkalis, the percentage of water soluble Na/total Na in the fly ash is plotted against the same parameter of K in Figure 2.10b. A positive correlation is seen between the two parameters, including the cases with NaCl addition. The results shown in Figure 2.10b demonstrate that NaCl addition does not only increase the vaporization degree of Na, but also enhances the vaporization of degree K in fuel mixture. The results clearly illustrate that the addition of NaCl may increase the vaporization of K through reacting with the mineral associated K [146], and inhibiting the reaction between gaseous K and reactive minerals. By performing equilibrium calculations in the program HSC 6.1, it is found that the addition of 1 wt% or 2 wt% NaCl may significantly increase the fraction of K/Na that is present as KCl (g)/NaCl (g) at temperatures above 800 ^{o}C. This further supports that the addition of NaCl may increase the release of K, through displacing the mineral associated K radicals by Na radicals.

2.3.6 Ash Deposition

2.3.6.1 Ash deposition rate and propensity

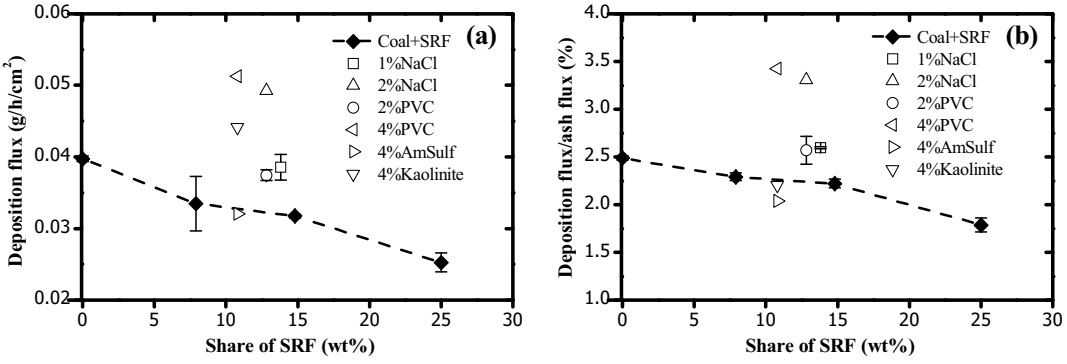

Figure 2.11 (a) Deposition fluxes (g/h/cm^2) from EFR experiments with different shares and types of secondary fuels, (b) The values of deposition flux/ash flux (%) from experiments with different shares and types of secondary fuels.

In order to evaluate the influence of coal and SRF co-firing as well as different additives on the deposit formation in the convective part of a boiler, deposits are collected during the EFR experiments by using an air-cooled deposit probe. The average deposition flux obtained from different experiments is shown in Figure 2.11a. It can be seen that when coal is co-fired with SRF, the deposition flux generally decreases with increasing share of SRF. By fixing the total share of secondary fuels to 14.8 wt%, it is seen that the addition of NaCl/PVC enhances the deposition flux and the effect is more pronounced with higher share of NaCl/PVC. The addition of 4 wt% kaolinite to the mixture of coal and SRF also increases the deposition flux considerably.

However, with the addition of 4 wt% AmSulf, the obtained deposition flux is similar to that of co-combustion of coal and SRF.

The deposition fluxes shown in Figure 2.11a would be primarily affected by two factors i.e. the ash flux to the probe and the deposition propensity of the ash. For different experiments, the ash flux to the probe would vary due to the variations in the fuel ash content. In order to minimize the effect of ash flux, the obtained deposition flux is divided by the calculated ash flux that is directed to the probe. The obtained deposition flux/ash flux (%) is a parameter that gives implication about the deposition propensity of the fly ash. Figure 2.11b shows the deposition flux/ash flux from different experiments. It is seen that when coal is co-fired with SRF, the obtained deposition flux/ash flux decreases with increasing share of SRF. This implies that co-combustion of coal and SRF may reduce the deposition propensity of the fly ash, in comparison with coal combustion. The reduced ash deposition propensity may be related to the relatively high calcium content in the ash of SRF, which may generate calcium components with high melting temperature and decrease the fouling tendency of fly ash. Moreover, the average particle size and/or density of the fly ash from co-combustion of coal and SRF may be smaller than those from coal combustion, as the coalescence degree of the ash from SRF would be lower than the coal ash due to the higher char fragmentation degree of the SRF. With smaller fly ash particle size and/or lower density, the inertial impaction efficiency would be decreased and result in reduced ash deposition rate [244].

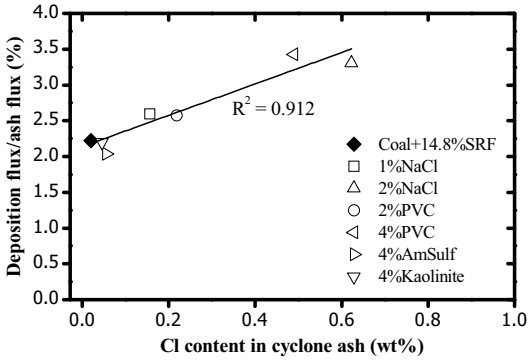

Figure 2.12 A comparison of the deposition flux/ash flux (%) from different EFR experiments and the Cl content of the cyclone ash obtained in the experiments. The results shown in the figure are carried out with the same total share of secondary fuels (14.8 wt%) but different additives.

With the addition of NaCl or PVC, it is seen that the obtained deposition flux/ash flux is higher than that of co-combustion of coal and SRF, and the effect is more significant with increasing share of NaCl/PVC. However, with the addition of AmSulf/kaolinite, the obtained deposition flux/ash flux is slightly smaller than that of co-combustion of coal and SRF. To further investigate the possible reasons for the increased or decreased deposition propensity of fly ash, the deposition flux/ash flux obtained from the EFR experiments carried out at 14.8 wt% secondary fuel is plotted against the Cl content of the cyclone ash, which is the major mass constituent of deposits. As shown in Figure 2.12, a positive correlation is found between the deposition flux/ash flux and the Cl content in cyclone ash. This indicates that the increased deposition flux/ash flux during the addition of NaCl/PVC is likely linked to the increased concentration of chlorides in the fly ash. It is well-known that alkali chlorides generally have low

melting temperatures, thus can significant increase the stickiness of deposits and fly ash particles, and enhance the ash deposition rate [100,128]. However, when the Cl content in cyclone ash is lower than 0.1 wt%, it is seen that the deposition flux/ash flux decreases slightly with increasing Cl content in cyclone ash. It implies that the influence of other factors (such as the particle size and density of the fly ashes, etc.) may become more significant for the deposition propensity of fly ash, when the Cl content in cyclone ash is remarkably low. One should be aware that the deposition rates obtained in this study are based on an experimental period of 1.5 hours, which is quite different from the deposit build-up time scale in a real boiler. In addition, the ash deposition rate in the experiments is affected by the dilution effect caused by the propane burner. Therefore, it is considered that the results shown in Figure 2.12 would provide information about the deposition propensity of the fly ash from co-combustion of coal and SRF as well as the effect of additives. However, the detailed numbers may deviate from the ash deposition rates in a practical boiler.

2.3.6.2 Deposit composition

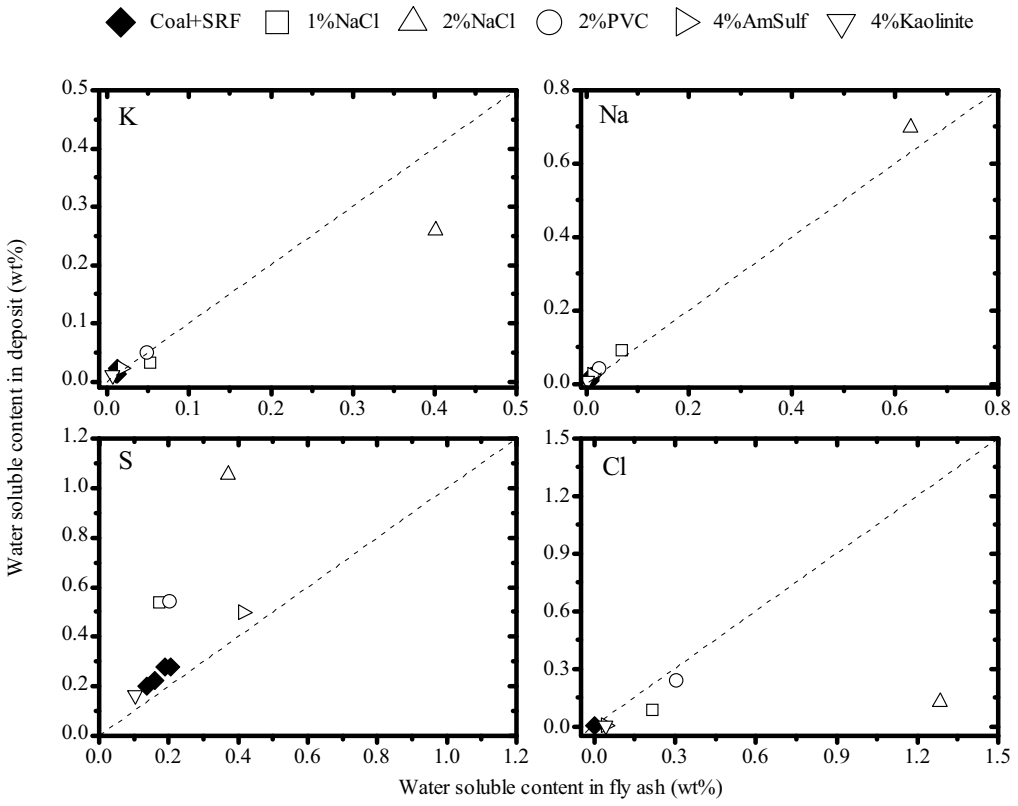

Figure 2.13 The content of water soluble K, Na, S and Cl from different experiments.

Besides the deposition rate/propensity of fly ash, the composition of the deposits is of importance, since it is closely related to the corrosion potential of the superheaters [140]. In Figure 2.13, the content of water soluble element in fly ash is plotted against the content of water

soluble element in deposits. It can be seen that the content of water soluble K and Na in deposits is generally similar to that in the fly ash. This tendency is consistent with a previous study on deposit composition from co-firing of coal and straw [99]. The only case that deviates from this tendency is the experiment with 2 wt% NaCl. In this experiment, the K content in the deposit is lower than that in the fly ash, whereas the Na content in the deposit is slightly higher. According to Figure 2.10, it is known that approximately 20 wt% of Na and 17 wt% of K in fly ash would exist as water soluble form in this experiment. The results shown in Figure 2.12 indicate that the deposition propensities for the water soluble Na and K may be quite different. This is likely linked with the different condensation characteristic of NaCl and KCl. By performing equilibrium calculation in HSC 6.1, it is found that the condensation temperature of KCl is lower than NaCl, and can be below 800 ^{o}C. In the EFR experiments, the flue gas temperature around the deposition probe is about 800 ^{o}C. At this temperature, part of the KCl in flue gas may not be condensable, resulting in a depletion of water soluble K in the deposits as compared to that of fly ash. However, the majority of NaCl would be condensable at 800 ^{o}C, thus no depletion of Na is observed.

The water soluble sulphur is also generally enriched in deposits compared to that of fly ash. A possible mechanism for the enrichment of sulphur is that condensed phase sulphation reaction may occur on the deposits, which could convert a fraction of chlorides in the deposits to sulphates. Such reactions could be significant at temperature higher than 750 ^{o}C [204]. An exceptional case shown in Figure 2.13 is that when AmSulf is added to the fuel mixture, the content of water soluble sulphur in fly ash becomes similar to that in the deposits. In this situation, due to the high gaseous sulphur concentration, it is likely that condensation of H_2SO_4 could occur on the surface of the collected fly ash particles and increase the content of water soluble sulphur, whereas the condensation of H_2SO_4 cannot occur on the deposits due to the high gaseous/surface temperature. This may lead to the content of water soluble S in the cyclone ash being similar to that of deposits.

Different from sulphur and alkalis, the content of water soluble Cl is mostly depleted in deposits, in comparison with that of fly ash. This implies that the initially formed deposits would probably contain similar water soluble Cl as the fly ash. However, as discussed previously, the deposited chlorine may undergo sulphation reaction with the gaseous sulphur in the flue gas. Such gas-solid sulphation reaction would result in a depletion of the water soluble Cl in the deposits compared to fly ash. Although the sulphation reaction is present, it can still be seen that the deposits from the experiments with NaCl/PVC addition have considerably larger chlorine content than that from co-combustion of coal and SRF. Furthermore, it was observed during the experiments that the deposition probe was slightly corroded with the NaCl/PVC addition, implying that the corrosion potential on superheater tubes would be higher when the SRF contains significant high alkali chlorides or chlorine content. However, without the additives, the content of water soluble chlorine is generally lower than 0.1 wt% in deposits, indicating a low potential for corrosion [140].

2.4 Conclusion

In this chapter, co-combustion of a bituminous coal and a solid recovered fuel (SRF) was carried out in an entrained flow reactor, and the effect of additives such NaCl, PVC, ammonium sulphate

(AmSulf), and kaolinite on co-combustion was investigated. The experimental results showed that when coal was co-fired with SRF, the carbon burnout decreased with increasing share of SRF. The addition of additives generally reduced the burnout, except for the case with 2 wt% NaCl which showed a promoting effect. The NO emission in co-combustion of coal and SRF decreased with increasing share of SRF. The additives generally did not affect the NO emission significantly, expect for the AmSulf which greatly inhibited the NO formation. The SO_2 emission in co-combustion of coal and SRF also decreased with increasing share of SRF. And consequently the retention of sulphur in ash was found to increase with increasing share of SRF, which was likely linked to the high calcium content in the SRF. All of the additives increased the retention of sulphur in ash, either due to chemical reaction or physical absorption.

The typical fly ash morphology and composition were characterized by TEM-EDS. The fly ash from the experiments mainly consisted of spherical particles and aggregated nucleates, with the latter being more important for the formation of submicron particles. The nucleates were normally characterized by higher Ca, Mg, S and P content, whereas the spherical particles usually have higher Si, Al and K content. Such findings are in agreement with a full-scale fine particle measurement carried out on similar fuels (see details in Chapter 4). Analysis of the bulk fly ash composition from the experiments showed that the most S and Cl in the fuels was released to the gas phase during combustion, while the K and Na in the fuels were mainly retained in ash. In co-combustion of coal and SRF (up to 25 wt%), most K and Na (~99 wt%) appeared in the fly ash in a water insoluble form i.e. as aluminosilicates or silicates. The addition of NaCl, PVC, and AmSulf generally increased the vaporization of K and Na, resulting in an increased formation of water soluble alkalis, whereas the addition of kaolinite showed a slight inhibiting effect. The experimental results demonstrated that the minerals in coal and SRF would be able to react with part of the gaseous alkalis released from the additives. Furthermore, the vaporization degree of Na and K was found to be correlated, suggesting an interaction between the vaporization of Na and K during pulverized fuel combustion.

Ash deposits were collected on an air-cooled probe in order to simulate boiler deposit formation. The ash deposition rate and the deposition propensity of fly ash in co-combustion were found to decrease with increasing share of SRF. The addition of NaCl and PVC increased the ash deposition propensity, and a positive correlation between the ash deposition propensity and the Cl content in cyclone ash was found. The Cl content in the deposits generally indicated low corrosion potential during co-combustion of coal and SRF (up to 25 wt%). However, for the experiments with NaCl and PVC addition, the corrosion potential on superheater tubes would be considerably high. The water soluble alkali content in deposits was generally similar to that in the fly ash. Higher water soluble sulphur content and lower water soluble chlorine content were found in the deposits than that of the fly ash, suggesting the presence of gas-solid sulphation reaction in deposits.

The results from this work indicate that co-combustion of coal and SRF may not put any additional burden on the NO and SO_2 emissions of a pulverized coal-fired power plant. The burnout in the plant may be affected by co-combustion. The selection of a suitable SRF particle size is desirable, but it would to a large extent depend on the physical properties (such as density and shape) of the SRF [269,280], the detailed configuration of the plant and the injection method of the SRF [281]. By using the coal and SRF used in this work, co-combustion of coal and up to 25 wt% SRF may not cause severe ash deposition and corrosion problems in the convective part of the boiler, possibly due to the positive synergy effects between the coal ash and the inorganic

components in SRF. This work also implies that in order to minimize ash deposition and corrosion problems in co-combustion, it is important to control the quality of the SRF, especially the chlorine and alkali contents. Lastly, it should be noted that results obtained in this work are from a lab-scale reactor with some conditions deviate from the real plants. In order to transfer the lab-scale results to a practical situation, these condition differences need to be considered.

Acknowledgment

The work is part of the CHEC (Combustion and Harmful Emission Control) Research Center. The present work is sponsored by The Technical University of Denmark (DTU), ENERGINET.DK, and BiofuelsGS-2 (Nordic Graduate School in Biofuel Science and Technolog-2). DONG Energy Power A/S is gratefully acknowledged for providing the fuels and for the fuel/ash analysis at Enstedværket Laboratory. We thank Thomas W. Hansen at DTU CEN for the TEM-EDS analysis.

2.5 Appendix: calculation methods for different parameters

Excess air ratio

$$\lambda = \frac{\text{Oxygen Supply by air}}{\text{Oxygen required by complete combsution}} = \frac{2P_0\dot{V}_{air}y_{O_2,air}/R/T_0}{\dot{m}_{fuel}(1-X_{moisture,fuel})(X_{H,fuel}+X_{C,fuel}/6+X_{N,fuel}/14+X_{S,fuel}/16-X_{O,fuel}/16)} \quad (2A.1)$$

where:

$\dot{V}_{air}$ = Volumetric flow rate of the air in the experiments (Nm^3/s)

$\dot{m}_{fuel}$ = Fuel feeding rate in the experiments (g/s)

$X_{moisture,fuel}$ = Moisture fraction in the fuel

$X_{i,fuel}$ = Mass fraction of element *i* in the dry fuel

P_0 = Pressure (101325 Pa)

T_0 = Temperature (273.15 K)

R = Gas constant (8.3145 J/mol-K)

$y_{O_2,air}$ = Mole fraction of O_2 in air (20.95 %)

Dry flue gas flow rate

$$\dot{V}_{fg,dry} = \frac{y_{(N_2+Ar),air}\dot{V}_{air}}{1-y_{O_2,fg}-y_{NO,fg}-y_{CO,fg}-y_{SO_2,fg}-y_{CO_2,fg}} \quad (2A.2)$$

where:

$\dot{V}_{fg,dry}$ = Dry flue gas flow rate (Nm^3/s)

$y_{(N_2+Ar),air}$ = Mole fraction of N_2+Ar in air (80.97 %)

$y_{m,fg}$ = Measured mole fraction of *m* gas in the flue gas

Ash balance

$$Ash_{Balance} = \frac{m_{Ash,out}}{m_{Ash,in}} \quad (2A.3)$$

$$m_{Ash,in} = \dot{m}_{fuel}X_{Ash,fuel}t_{\exp} \quad (2A.4)$$

where:

$m_{Ash,in}$ = Ash input during the experiment (g)

$X_{Ash,fuel}$ = mass fraction of ash in the wet fuel

$t_{\exp}$ = Total experiment time (5400 s)

$$m_{Ash,out} = m_{large\ fly\ ash} + m_{fine\ fly\ ash} + m_{bottom\ ash} \quad (2A.5)$$

$$m_{large\ fly\ ash} = (m_{cyclone\ ash} + m_{pipe\ ash})\frac{\dot{V}_{fg,dry}}{\dot{V}_{ext,dry}} \quad (2A.6)$$

where:

$m_{large\ fly\ ash}$ = mass of the large fly ashes (d_{cut}≥2.5 µm) produced in an experiment (g)

$\dot{V}_{ext,dry}$ = total extracted dry flue gas flow (Nm^3/s)

$m_{cyclone\ ash}$ = collected mass of fly ash in the cyclone in an experiment (g)

$m_{pipe\ ash}$ = collected mass of fly ash in the extraction pipes before cyclone (g)

$$m_{fine\ fly\ ash} = m_{filter\ ash} \frac{\dot{V}_{fg,dry}}{\dot{V}_{fil,dry}} \tag{2A.7}$$

where:

$m_{large\ fly\ ash}$ = mass of the fine fly ashes (d_{cut}<2.5 µm) produced in an experiment (g)

$\dot{V}_{fil,dry}$ = extracted dry gas flow to the aerosol filter (Nm^3/s)

$m_{filter\ ash}$ = collected mass of fly ash in the aerosol filter in an experiment (g)

$$m_{bottom\ ash} = m_{collected\ bottom\ ash} \frac{m_{fuel,exp}}{m_{fuel,total}} \tag{2A.8}$$

where:

$m_{collected\ bottom\ ash}$ = total mass of ash collected in the bottom of reactor in an experiment (g)

$m_{fuel,exp}$ = mass of fuel used after start sampling (g)

$m_{fuel,total}$ = total mass of fuel used in an experiment (g)

Note: the mass balance for the ash forming elements is calculated the same way as ash balance.

Ash flux

$$Ash\ flux = \frac{m_{large\ fly\ ash} + m_{fine\ fly\ ash}}{b_{slit} h_{slit} t_{\exp}} \tag{2A.9}$$

where

$Ash\ flux$ = average ash flux at the flue gas outlet during an experiment ($g/cm^2/h$)

b_{slit} = width of the flue gas outlet (4 cm)

h_{slit} = height of the flue gas outlet (8 cm)

Deposit flux

$$Deposit\ flux = \frac{m_{deposit} \dot{V}_{fg,dry}}{(\dot{V}_{fg,dry} - \dot{V}_{ext,dry}) \frac{\pi d_{probe} h_{slit}}{2} t_{\exp}} \tag{2A.10}$$

where:

$Deposit\ flux$ = average flux of the deposits formed at the probe ($g/cm^2/h$)

$m_{deposit}$ = mass of collected deposits (g)

d_{probe} = external diameter of the probe (1 cm)

3 Co-Combustion of Coal and Solid Recovered Fuel: Trace Element Behavior

Abstract

This chapter investigates the trace element partitioning in co-combustion of a bituminous coal and a solid recovered fuel (SRF), based on the experiments carried out in Chapter 2. The trace elements studied were As, Cd, Cr, Pb, Sb and Zn, since these elements were significantly enriched in the SRF as compared to the coal. It was found that when the coal was co-fired with up to 25 wt% SRF, the As, Cd, Pb, Sb and Zn content in the filter ash/cyclone ash increased almost linearly with their content in the fuel ash. This linear tendency was affected when the fuels were mixed with additives, such as PVC, NaCl, ammonium sulphate and kaolinite. The volatility of trace elements during combustion was assessed by applying a relative enrichment (RE) factor, and TEM-EDS analysis was conducted for providing qualitative interpretations. The results indicated that As, Cd, Pb, Sb and Zn were highly volatile when co-firing coal and SRF, whereas the volatility of Cr was relatively low. Compared to coal combustion, co-firing of coal and SRF slightly enhanced the volatility of Cd, Pb and Zn, but reduced the volatility of Cr and Sb. The Cl-based additives increased the volatility of Cd, Pb and As, whereas the addition of ammonium sulphate generally decreased the volatility of trace elements. The addition of kaolinite reduced the volatility of Pb, while the influence on other trace elements was insignificant. The results from the present work imply that trace element emission would be significantly increased when coal is co-fired with SRF, which may greatly enhance the toxicity of the dusts from coal-fired power plant. In order to minimize trace element emission in co-combustion, in addition to lowering the trace element content in the SRF, utilizing SRF with low Cl content and coal with high S and aluminosilicates content would be favorable.

3.1 Introduction

Trace element emission is one of the major environmental concerns for pulverized coal-fired power stations. During pulverized coal combustion, the trace elements in the fuel usually undergo complicated chemical and physical transformations, and a fraction is eventually emitted to the atmosphere as dust or vapor [108,120,146,282-285]. Due to the adverse health effect [146], it is desirable to control the emission of trace elements from coal-fired power stations.

Co-combustion of coal and secondary fuel such as biomass and waste is recognized as a promising approach to reduce the CO_2 emission from pulverized coal-fired power stations [1]. The typical secondary fuels are biomass such as straw [60,99] and wood [9], and waste derived fuels such as sewage sludge [108] and refuse derived fuels [270,278,286,287]. When biomass is used as the secondary fuel in co-combustion, the emission of trace elements is usually not of great concern, since the trace element content in most biomass is much lower than that of coal. In

contrast, waste derived fuels are often characterized by significantly larger trace element concentration than coal [108,270]. Thus it is of importance to characterize the behavior of trace elements during co-combustion of coal and waste derived fuel.

The behavior of trace elements during pulverized fuel combustion is well-known to be influenced both by the fuel properties and combustion conditions. The trace elements present in the fuels can be categorized as organic association (elements that are organically bounded, ionically bounded, or water soluble) and mineral association (elements that are present as included or excluded minerals) [120]. Extensive studies on the association of trace elements in different coals have been performed [120,146,284,288,289]. Similar investigations were also carried out on waste derived fuels such as sewage sludge [283] and refuse-derived char [290]. These studies generally suggest that the organically associated trace elements are easier to be vaporized during combustion than those associated with minerals [146]. On the other hand, the vaporization behavior of trace elements is also influenced by conditions such as combustion temperature, transport/mixing phenomena, oxidizing/reducing condition, and the presence of gaseous species such as HCl and SO_2 [282]. In most cases, the presence of gaseous chlorine may shift the distribution of trace elements such as Pb and Cd towards more volatile chlorides, thus promoting the vaporization [146,282,291]. However, the presence of SO_2 may result in the formation of sulphates with relatively low vapor pressure [291].

After being vaporized from the fuel, the trace elements may undergo reactions both with the ash particles and the gaseous species in the flue gas [176,291]. The reactions between the vaporized trace elements and the ash particles constitute an important mechanism for the retention of trace elements in large fly ash particles that are easier to be captured by the air pollution control systems [120,146]. Typical examples are the reactions between trace elements such as Cd and Pb and aluminosilicates such as kaolinite [176]. Such reactions may primarily occur on the particle external surface and may result in trace element concentration in the ash particle being proportional to $1/d_p$ (particle diameter) [121,146,292,293]. On the other hand, the vaporized trace elements may also react with other gaseous species in the flue gas, such as HCl and SO_2. These reactions may alter the condensation behavior of the trace elements. In addition, they may also influence the reactions between the vaporized trace elements and ash particles, since trace element in different gaseous forms (such as chlorides or hydroxides) may have different reaction rates with the ash particles [146].

When the flue gas temperature becomes lower than the dew point of a trace element species, condensation may occur on the surface of the existing ash particles. For ash particles in the continuum regime (supermicron particles with $Kn<<1$) condensation may lead to the trace element concentration in the ash particles being proportional to $1/d_p^2$, while for particles in the free molecular regime (ultrafine particles with $Kn>>1$) the concentration of the condensed trace element may be proportional to $1/d_p$ [121,292,293]. One should be aware that the correlations mentioned above are based on several assumptions which may deviate from practical situations, such as perfect spherical and nonporous particles [121]. Therefore care must be taken in applying these theoretical correlations in practice.

All of the mechanisms mentioned above can influence the partitioning of trace elements in combustion. For a practical combustion system, the partitioning of trace elements involves complex processes such as vaporization, reaction, nucleation, condensation and coagulation. These processes may become more complicated when a secondary fuel is introduced to the system, since it may have different fuel properties and combustion behavior as compared with

the primary fuel. In order to evaluate the behavior of trace elements during co-combustion in a pulverized coal-fired plant, performing controlled experiments at combustion conditions similar to a practical plant is an advantageous approach.

The objective of this chapter is to study the partitioning of trace elements in co-combustion of coal and solid recovered fuel (SRF) at conditions similar to a pulverized coal-fired plant. This was achieved by evaluating the trace element partitioning in the different ash fractions (bottom ash, cyclone ash and filter ash) collected during the experiments in Chapter 2. It should be noted that the conditions in the entrained flow reactor are not fully representative of a pulverized coal-fired plant with respect to particle residence time, temperature profile and fluid flow. Therefore the results from this chapter may not fully represent the practical situation. The trace elements studied were As, Cd, Cr, Pb, Sb and Zn. These elements were focused since their content in the SRF was significantly (~5–150 times) larger than that of coal. The emphasis of this chapter is on the trace element behaviors during co-combustion of coal and different share of SRF as well as on the effect of additives such as NaCl, PVC, ammonium sulphate, and kaolinite. These additives may have notable effect on the partitioning of trace elements [176,291]. Therefore the results from the present work could provide suggestions for trace element emission control in co-combustion of coal and SRF.

3.2 Experimental

Table 3.1 Properties of coal and SRF

Properties	Coal	SRF	Properties	Coal	SRF
LHV (MJ/kg wet)	26.53	20.86	Mg(wt% dry)	0.15	0.09
Moisture (wt% wet)	5.25	5.20	P (wt% dry)	0.02	0.02
Volatiles (wt% wet)	34.11	72.05	Ca (wt% dry)	0.18	0.67
Ash (wt% wet)	10.42	5.69	Na (wt% dry)	0.07	0.11
C (wt% dry)	71.00	58.00	K (wt% dry)	0.21	0.09
H (wt% dry)	4.90	6.60	As (ppm dry)	3.71	18.9
N (wt% dry)	1.50	1.00	Cd (ppm dry)	0.20	1.1
S (wt% dry)	0.70	0.42	Cr (ppm dry)	15.2	178.0
Cl (wt% dry)	0.03	0.28	Pb (ppm dry)	7.35	206.1
Si (wt% dry)	3.06	1.08	Sb (ppm dry)	1.0	51.5
Al (wt% dry)	1.21	0.21	Zn (ppm dry)	25.2	3500

The detailed experimental procedures and matrix can be found in Chapter 2. The additional information provided here are the trace element concentrations in the coal and SRF. The other fuel properties are also listed here, in order to provide a direct comparison of the two fuels. From Table 3.1, it can be seen that the trace element content in the two fuels is significantly different. The content of As, Cd and Cr in the SRF is 5–10 times larger compared to the coal. For Pb, Sb and Zn, the content in the SRF is 30–150 times larger than that of coal. The trace element concentrations in the fuels as well as in the ash fractions collected during the experiments is analyzed by using ICP-OES (inductively coupled plasma optical emission spectrometry). In addition, TEM-EDS analysis has been carried out on the collected ash samples, in order to provide qualitative explanations to the observed trace element behavior.

3.3 Results and Discussion

3.3.1 Mass balance

The mass balance for different experiments has been calculated based on the fuel and ash composition, the fuel feeding rate, the amount of the collected ash and the corresponding flue gas flow rate. Figure 3.1 shows the mass balance of ash, Si, and trace elements. It is seen that the ash balance for most of the experiments is between 80% and 90%. The ash balance is all below 100%, primarily due to the deposition of ash in the reactor tube which can be observed after experiments. In addition, although the ash is collected carefully during the experiments, some fly ash may remain in the sampling system after collection, which also influences the ash balance. The mass balance for the major inorganic elements is mostly between 70% and 90%, which is similar to the ash balance. As an example, the mass balance of the element Si and Al is shown in Figure 3.1.

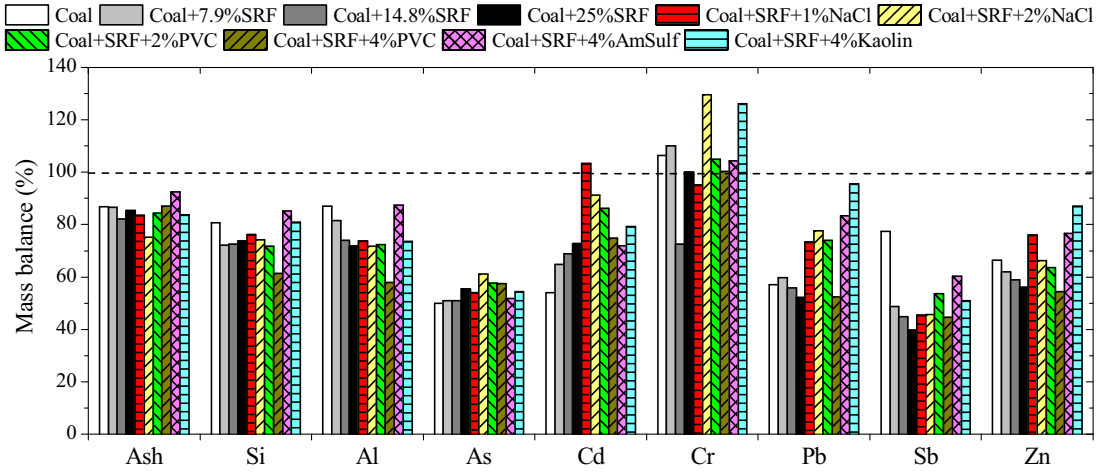

Figure 3.1. Calculated ash and elemental mass balances for different experiments.

In comparison with the major inorganic elements, the mass balance of the trace elements is generally less satisfactory. This is presumably related to the analysis uncertainties of the trace element concentrations in the SRF. It is well-known that the content of trace elements in different waste fractions can deviate significantly [171]. Although the SRF used in the experiments has been homogenized through the production and grinding processes, the SRF sample selected for analyzing trace element content may not be fully representative, primarily due to the small amount (~0.4 g) of sample selected for analysis. This may be reflected by the increased mass balance of Cd with increasing share of SRF, which suggests that the Cd content in the SRF might be under-estimated. For Sb and Zn, the decreasing tendency with increasing share of SRF indicates that the content of Sb and Zn in SRF may be over-estimated. Besides the analysis uncertainties, the collection efficiency of different ash fractions may also influence the mass balance, since the distribution of trace elements in different ash fractions is more uneven compared to the major inorganic elements. Considering the uncertainties, it is suggested to focus on the tendencies shown in this chapter, rather than the accurate numbers.

3.3.2 Trace element content in the cyclone ash and filter ash

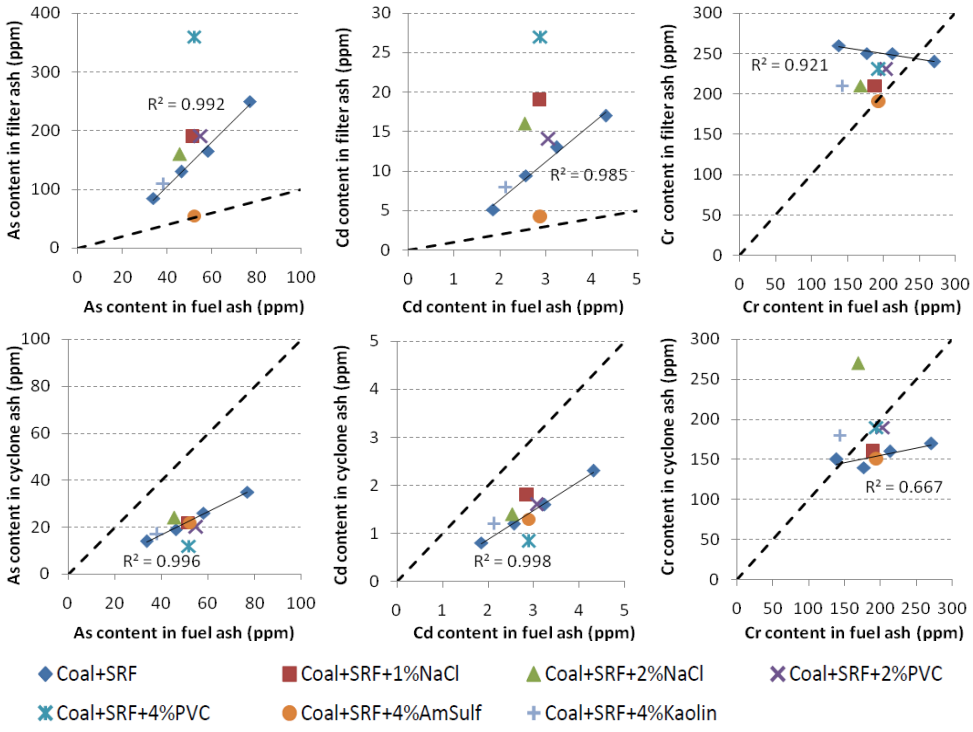

Figure 3.2 The content of As, Cd and Cr in the filter ash and cyclone ash collected from different experiments versus their content in the fuel ash.

In order to assess the influence of co-combustion on the trace element content in the fly ash, the trace element content in the filter ash and the cyclone ash collected from the experiments are plotted versus the content in the fuel ash, as shown in Figure 3.2 and Figure 3.3. The trace element content in fuel ash was calculated from the fuel properties, i.e. the ash and trace element content in fuel/fuel mixture. It can be seen that when coal is co-fired with SRF (i.e. without additive), the content of As, Cd, Pb, Sb and Zn in filter ash/cyclone ash increases almost linearly with their content in fuel ash, which is a strong indication that the SRF used in the experiments is considerably homogeneous. Compared with the content in fuel ash, the As, Cd, Pb, Sb and Zn content in filter ash is typically 2–5 times larger, whereas the content in cyclone ash are usually 40-60% smaller. The observed enrichment of As, Cd, Pb, Sb and Zn elements in filter ash is qualitatively in agreement with literature, where these elements were classified as volatile trace elements in pulverized coal combustion [120]. The depletion of these trace elements in cyclone ash may be primarily related with two reasons. For elements such as As and Sb, the mass balance shown in Figure 3.1 is mostly around 50%. This suggests that the As and Sb content in fuel ash may be over-estimated, thus resulting in the trace element content in cyclone ash being 40-60% lower than that in fuel ash. In addition, for elements such as Cd, Pb, Sb and Zn, the content in the bottom ash collected from co-combustion experiments is notably higher (~1–3 times) than that in fuel ash. This would adversely affect the partitioning of trace elements to cyclone ash, thus lower the trace element content in cyclone ash. The high trace element content found in the bottom ash

from co-combustion experiments may be related with the physical properties of the SRF particles. The SRF particles used in experiments are larger than the coal particles, and tend to form agglomerates during injection. As a result, the burnout degree of the SRF particles may be lower than for the coal particles in the reactor, and part of the unburnt SRF particles may end up as bottom ash with relatively high trace element content. This explanation is supported by the fact that the total amount of bottom ash collected during co-combustion experiments is increased with increasing share of SRF, and the overall burnout is decreased with higher share of SRF [286].

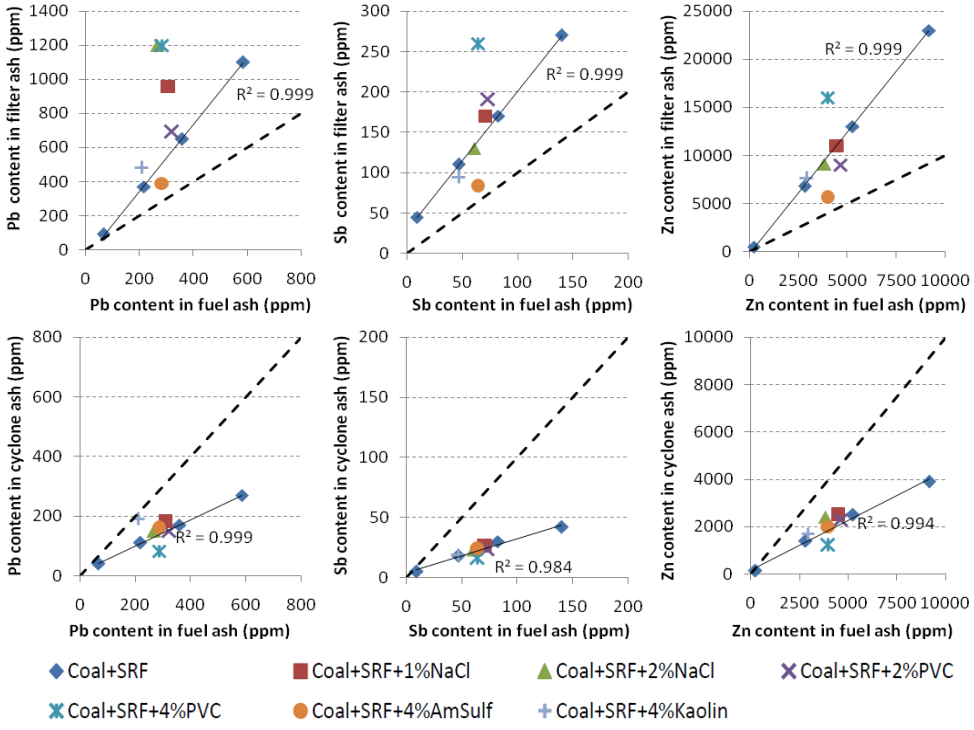

Figure 3.3 The content of Pb, Sb and Zn in the filter ash and cyclone ash collected from different experiments versus their content in the fuel ash.

In comparison with the trace elements mentioned above, the behavior of Cr is significantly different. During co-firing coal and SRF, the Cr content in filter ash decreases slightly with increasing Cr content in fuel ash, whereas the Cr content in cyclone ash increases slightly with increasing Cr content in fuel ash. In comparison with other trace elements, the content of Cr in cyclone ash seems to be much closer to the content in fuel ash. This is probably linked to the mass balance of Cr shown in Figure 3.1, which is close to or even higher than 100%. The Cr content in the bottom ash from co-combustion of coal and SRF is found to be larger than that of fuel ash. This may explain the slightly lower Cr content in cyclone ash, with respect to that in fuel ash.

The effect of additives on trace element partitioning is also illustrated in Figure 3.2 and Figure 3.3. The main tendency is that the Cl-based additives (NaCl or PVC) generally increase the content of As, Cd, Pb and Sb in filter ash. This effect is particularly pronounced for the addition

of 4 wt% PVC. However, the influence of Cl-based additives on Zn and Cr is somewhat different. For Zn, most of the Cl-based additives do not have a significant impact on the Zn content in filter ash, except for the addition of 4 wt% PVC which shows a pronounced enhancing effect. For Cr, the Cl-based additives appear to have a reducing effect on the content in filter ash. Compared with the influence on filter ash, the effect of Cl-based additives on cyclone ash chemical composition is generally less significant. However, a noticeable effect is that the As, Cd, Pb, Sb and Zn content in cyclone ash is lowered by the addition of 4 wt% PVC, suggesting a promoted vaporization of these elements which has shifted the partitioning from cyclone ash to filter ash. Besides, the addition of NaCl seems to slightly increase the content of some trace elements such as Cd and Zn in cyclone ash. For Cr, it is found that most of the Cl-based additives have a promoting effect on the Cr content in cyclone ash.

Compared to Cl-based additives, the addition of kaolinite shows insignificant effect on the content of As, Cd, Sb and Zn in cyclone ash and filter ash. For Pb, it seems that the addition of kaolinite significantly enriches the Pb content in cyclone ash and slightly increases the content of Pb in filter ash. For Cr, the addition of kaolinite shows a reducing effect on the content in filter ash and an enhancing effect on the content in cyclone ash. The addition of 4 wt% ammonium sulphate (AmSulf) generally lowers the concentration of different trace elements in filter ash. However, the impact of ammonium sulphate on the trace element content in cyclone ash is almost negligible. The results present in Figure 3.2 and Figure 3.3 demonstrated the influence of additives on the trace element content in cyclone ash and filter ash. However, further discussions on the effect of additives on the partitioning of trace elements as well as the underlying mechanisms will be given in the following section.

3.3.3 Volatility of the trace elements

To assess the relative volatility of trace elements in pulverized coal combustion, a widely applied method is the enrichment of trace elements in different ash fractions with respect to fuel ash [108,292]. However, the results shown in the previous section reveal that such enrichment in the present work may be interfered by the mass balance of trace elements which is considerably lower than 100% (as indicated by Figure 3.1) and the unreacted trace elements partitioned to bottom ash. To minimize those influences, the following relative enrichment (RE) factor is introduced to evaluate the volatility of trace elements at different experiments:

$$RE\ factor = \frac{C_i\ in\ filter\ ash / C_{Al}\ in\ filter\ ash}{C_i\ in\ cyclone\ ash / C_{Al}\ in\ cyclone\ ash} \tag{3.1}$$

where C_i is the content of element i and C_{Al} is the content of Al.

Similar as the relative enrichment factor used in [294,295], the equation above uses Al as a reference element, as Al is usually considered as an abundant and nonvolatile element with relative even distribution at different particle size. The RE factor of an element indicates whether the element is enriched (RE factor>1) or depleted (RE factor <1) in filter ash, with respect to the content in cyclone ash.

It should be noted that the filter ash and the cyclone ash collected in the present work are separated by a cut-off diameter of 2.5 μm. The cyclone ash particles mostly consist of spherical particles formed by the melting of included/excluded minerals, whereas the filter ash contain both spherical particles formed by the melted minerals and the nucleates generated from

homogeneous nucleation and coagulation of the vaporized major inorganic elements [278,286]. The trace elements vaporized during combustion would partition to the cyclone ash and filter ash through condensation and/or gas-solid reactions. Both mechanisms would favor the enrichment of trace elements in filter ash [121,146,292,293], and the RE factor would increase with increasing vaporization degree of trace elements. However, if the vaporization degree of a trace element is fixed, a shift from gas-solid reaction mechanism to condensation mechanism may also result in a higher RE factor. This is primarily due to the fact that the gas-solid reaction mechanism would lead to trace element concentration proportional to $1/d_p$, whereas the condensation mechanism would cause a trace element concentration proportional to $1/d_p^2$ in the continuum regime (larger than 0.5-1μm) [121,292,293]. Therefore, the condensation mechanism would result in a higher enrichment of trace element in small particles (around 0.5-2.5μm), compared to the reaction mechanism. In addition, there are probably more particles available for condensation than for gas-solid reaction, which would further promote the enrichment of trace elements in smaller particles when the condensation mechanism is important. As a consequence, an increased RE factor of a trace element can be read as a higher vaporization degree of the trace element and/or a shift from reaction to condensation mechanism. Both influences need to be considered in interpreting the results. From a practical point of view, a higher RE factor indicates an increased partitioning of trace element to fly ash particles smaller than 2.5 μm. Compared with large particles, fly ash particles smaller than 2.5 μm are generally easier to penetrate the air pollution control system in a coal-fired power plant [121]. Thus, with a higher RE factor, the penetration of trace element through the air pollution control system may be promoted and result in increased trace element emission.

3.3.3.1 Volatility of Si and Cr

The RE factors of Si and Cr in different experiments are present in Figure 3.4. It can be seen that the RE factors of Si are rather consistent in the experiments, which are mostly between 0.7 and 0.8. The results are in line with a number of studies, showing that Si is of low volatility in pulverized coal combustion and the content of Si in submicron particles are slightly lower than that in larger fly ash particles [225,278]. The results also indicate that the additives do not have significant effect on the volatility of Si.

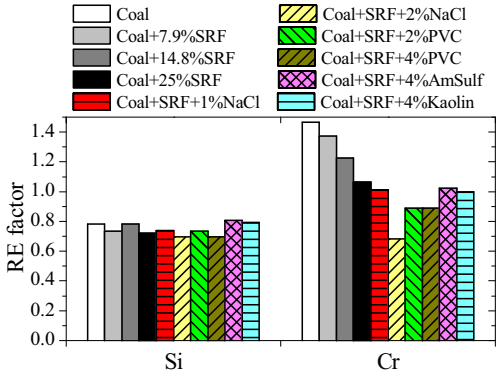

Figure 3.4 RE factor of Si and Cr in different experiments.

For Cr, it can be seen the RE factor of Cr in coal combustion is about 1.5, indicating that the volatility of Cr is only slightly higher than that of Al or Si. Similar low volatility of Cr has been

observed in other studies [293,295]. When coal is co-fired with SRF, the RE factor of Cr decreases with increasing share of SRF. Similar reducing effect on the volatility of Cr has been seen when coal was co-fired with sewage sludge [108] or RDF [270]. The reduced volatility of Cr in co-firing coal and sewage sludge was attributed to the lower flame temperature in co-combustion [108]. For co-combustion of coal and SRF, it can be presumed that the flame temperature would also decrease with increasing share of SRF, as the flame temperature of a similar waste derived fuel (RDF) is found to be 200–300 ^{o}C lower than a coal flame with same excess air ratio [260]. The sensitivity of Cr vaporization on temperature has also been demonstrated by thermodynamic calculations [108,296]. In addition to the flame temperature, the association of Cr may also be different in the coal and SRF and has an impact on the RE factors. However, the study of trace element association in coal and SRF is outside the scope of the present work.

For different additives, it can be seen that the RE factor of Cr is reduced with the addition of Cl-based additives, especially for 2 wt% NaCl addition. The addition of 4 wt% AmSulf or 4 wt% kaolinite also appears to have a reducing effect on the RE factor of Cr, but not as significant as the Cl-based additives. For the addition of NaCl, AmSulf and kaolinite, it may be that the flame temperature is further decreased compared to co-firing coal and SRF, since the vaporization of NaCl and the decomposition of AmSulf and kaolinite are all endothermic processes. For the addition of PVC, some thermodynamic calculations predicted that the vaporization of Cr could be significantly enhanced with a large increase of HCl concentration in flue gas, due to the formation of CrO_2Cl_2 [146]. However, such an effect is not observed in the present work, indicating the vaporization of Cr is not sensitive to the chlorine concentration in flue gas.

In general, the results shown in Figure 3.4 reveal that Cr does not have a high volatility when co-firing coal and SRF. The volatility of Cr decreases with increasing share of SRF, and is further reduced by the additives used in the experiments. This suggests that the flame temperature may be the most significant parameter for the vaporization of Cr. A relatively low flame temperature would be favorable in order to reduce the Cr vaporization/emission.

3.3.3.2 Volatility of Cd and Pb

The RE factors of Cd and Pb are shown in Figure 3.5a. When coal is co-fired with SRF, the RE factor of Cd is in the range of 5-7, and tends to increase slightly with increasing share of SRF. The effect of the Cl-based additives is significant on the RE factor of Cd. With the addition of 1 wt% and 2 wt% NaCl, the RE factor of Cd is increased to about 8 and 10, respectively. With the addition of 2 wt% and 4 wt% PVC, the RE factor of Cd becomes about 6 and 23, respectively. In order to further illustrate the impact of chlorine on the volatility of Cd, the RE factor of Cd from different experiments is plotted versus the RE factor of Cl in Figure 3.5b (the experiments with AmSulf and kaolinite are excluded due to chlorine content in the ash from these experiments is below the detection limit). A positive correlation is found between the RE factor of Cd and the RE factor of Cl, suggesting that the partitioning of Cd is closely related with that of Cl. If the experiment with 4 wt% PVC is excluded, the correlation is almost linear. However, in the case with 4 wt% PVC addition, a considerably higher RE factor of Cd is obtained, which deviates from the tendency predicted by other experiments. The influence of Cl-based additives may be primarily related with the formation of $CdCl_2$, which is a volatile and thermodynamically favorable compound when chlorine is present in the flue gas [282,291]. Although most of the thermodynamic calculations predicted that Cd would be totally volatilized (mainly as gaseous Cd)

at combustion temperature [282,291], retention of Cd at high temperature is observed [291], possibly related with the association form of Cd in the fuel and the limitation on the reaction time and/or mixing in a combustor. For the experiments in the present work, it may be the case that the injected Cl-based additives could react with some of the stable Cd species in the fuel and increase the overall vaporization degree of Cd. Such effect would be particularly pronounced with the addition of 4 wt% PVC, due to the significantly high concentration of HCl in flue gas, which may increase the reaction rates considerably.

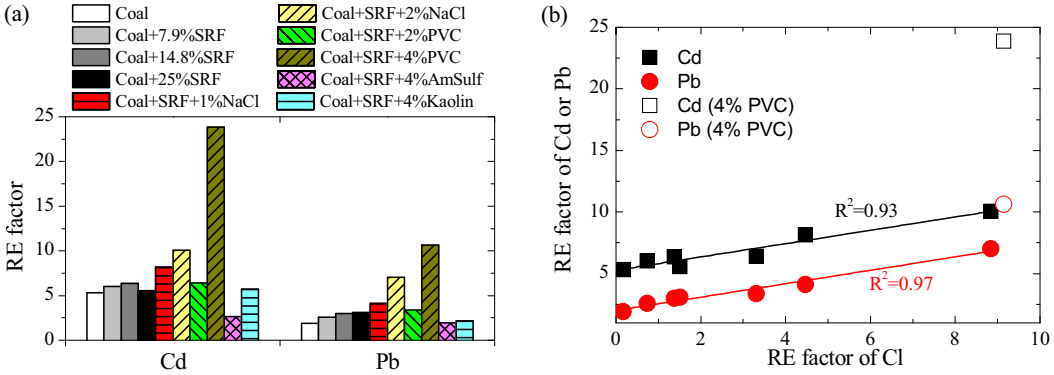

Figure 3.5 (a) the RE factor of Cd and Pb in different experiments; (b) comparison of the RE factors of Cd and Pb versus the RE factor of Cl from different experiments (the open symbols denote the results from the addition of 4 wt% PVC).

The influence of Cl on the partitioning of Cd is qualitatively illustrated by the TEM-EDS analysis shown in Figure 3.6. It is seen that when coal is co-fired with 14.8 wt% SRF, the content of Cd in the aerosols from the vaporization mode (see Spectrum 2 and 3 in Figure 3.6a) is negligible, consistent with the negligible Cl content found in these aerosols. However, when 1 wt% NaCl or 2 wt% PVC is added to the mixture of coal and SRF, the Cl content in the aerosols from the vaporization mode (see Spectrum 2 in Figure 3.6b and Spectrum 3 in Figure 3.6c) is increased significantly to about 6 wt% and 2 wt%, respectively. Under these conditions, despite of the small Cd content in the fuel mixture, approximately 1 wt% of Cd is found in the vaporized aerosols. The results indicate that the addition of Cl-based additive may increase the vaporization of Cd during combustion, presumably related to the formation of $CdCl_2$. However, detailed investigations on the exact chemical form of the Cd present in these aerosols are not possible from the TEM-EDS analysis.

On the other hand, with the addition of 4 wt% ammonium sulphate, the RE factor of Cd is decreased notably, indicating a reduced vaporization degree of Cd. The reduction may be both related with the possible lower flame temperature caused by the decomposition of ammonium sulphate and the reactions between the ammonium sulphate and the Cd species in fuel. The thermal decomposition of ammonium sulphate may increase the concentration of SO_2 in flue gas. The SO_2 would compete with gaseous chlorine for reacting with the stable Cd species in the fuel, thus inhibit the formation of $CdCl_2$. The formed $CdSO_4$ would have lower vapor pressure than $CdCl_2$, thus are more probably to be retained in the char/ash particles. According to thermodynamic calculation [282], the presence of $CdSO_4$ is only found at temperatures below 700 ^{o}C. However, the formation of $CdSO_4$ at higher temperatures may be possible to occur in practice, as residence time and/or transport limitations may prevent the reactions to reach global

equilibrium. The addition of 4 wt% kaolinite also shows a slight reducing effect on the RE factor of Cd. It is most likely that part of the vaporized Cd has been reacted with the injected kaolinite particles, which are mostly particles larger than 2.5 μm. The presence of such reactions has been observed in [176], where kaolinite was found to react with vaporized Cd.

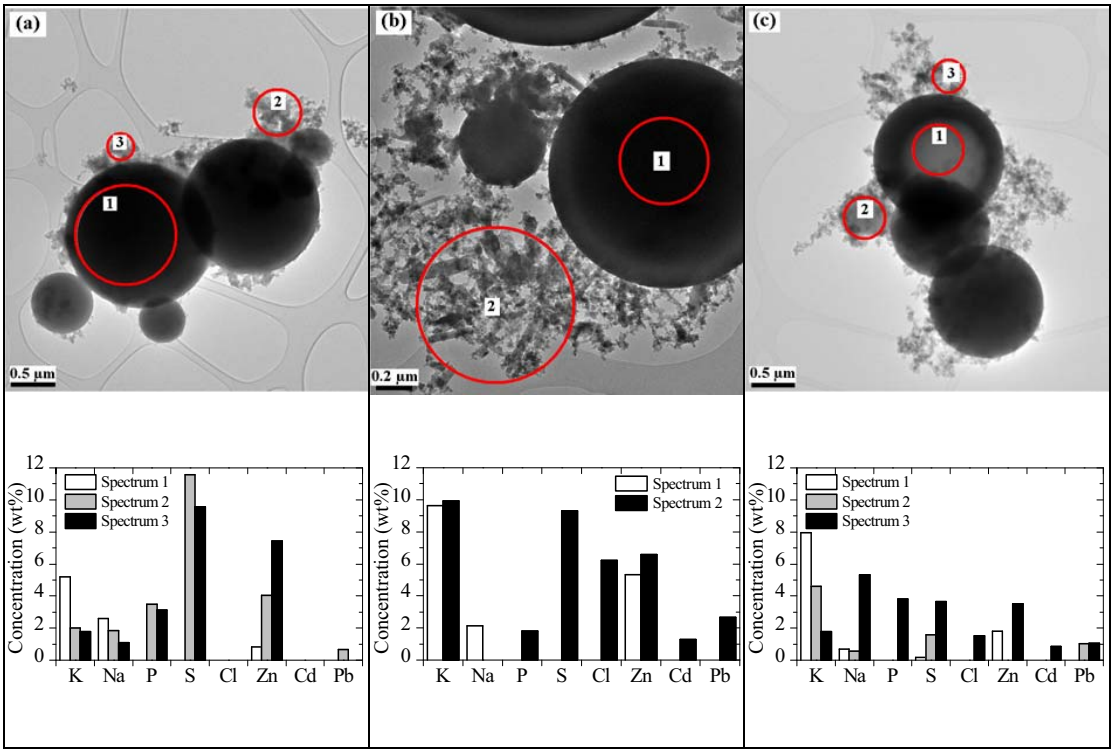

Figure 3.6 (a) morphology and composition of the filter ash collected from co-combustion of coal with 14.8 wt% SRF; (b) morphology and composition of the filter ash collected from co-combustion of coal with13.8 wt% SRF and 1 wt% NaCl; (c) morphology and composition of the filter ash from co-combustion of coal with 12.8 wt% SRF and 2 wt% PVC. The results are obtained from the TEM-EDS analysis, and only the compositions of K, Na, P, S, Cl, Zn, Cd, Pb are presented. The elemental content below 0.5 wt% is considered to be not reliable, thus is neglected in the figure.

As shown in Figure 3.5a, the RE factor of Pb is in the range of 2-3 during co-combustion of coal and SRF, and it increases slightly with increasing share of SRF co-fired. The addition of the Cl-based additives generally enhance the RE factor of Pb, particularly for the addition of 4 wt% PVC. Similar as Cd, the RE factor of Pb is plotted versus the RE factor of Cl in Figure 3.5b. It can be seen that positive correlation generally exists between the two factors. If the results of 4 wt% PVC addition are not considered, the RE factor of Pb increases almost linearly with that of Cl. However, for the case with 4 wt% PVC addition, the RE factor of Pb is higher than that predicted from the tendency of other experiments. According to thermodynamic calculations [282,291], the presence of chlorine in the combustion would favor the formation of $PbCl_2$/PbCl, which are volatile at flue gas temperature higher than 700 ^oC. Thus, it may be the case that the injection of Cl-based additives would promote the Pb vaporization via the formation of $PbCl_2$/PbCl. Furthermore, with the addition of Cl-based additives, the distribution of vaporized

Pb compounds may be shifted from PbO to $PbCl_2$/PbCl. This transition may inhibit the reactions between vaporized Pb and coal minerals such as kaolinite [110,146,176], and cause a shift of the reaction mechanism to the condensation mechanism, which would also increase the RE factor of Pb.

The effect of Cl on the partitioning of Pb is also reflected in Figure 3.6. It is seen that with a large Cl content in the vaporization mode aerosols (see Spectrum 2 in Figure 3.6b), a considerably large Pb content (~3 wt%) is also found. This suggests that vaporization of Pb may have been promoted by the addition of chlorine based additives, as discussed previously. However, for vaporized aerosols with negligible Cl content (see Spectrum 2 in Figure 3.6a), a certain amount of Pb (~0.8 wt%) is also observed in the aerosols. This indicates that part of the vaporized Pb may be present in other forms, such as PbO.

Different from the Cl-based additives, the addition of AmSulf and kaolinite both have reducing effect on the RE factor of Pb. For the addition of AmSulf, similar explanations that have been used for Cd may be applied here, i.e. lower flame temperature and chemical effect caused by the SO_2 from ammonium sulphate decomposition. The lower Pb volatility during kaolinite addition is probably related with the reaction between the vaporized Pb species and kaolinite [176]. In comparison with Cd, the reducing effect of kaolinite is more significant for Pb, which is consistent with the different capture efficiency/rate found between these two trace elements and kaolinite [146,176].

The results shown in Figure 3.5 suggest that Cd and Pb are highly volatile when co-firing coal and SRF, and the volatility is increased with increasing share of SRF. A most probable reason for the increased volatility is the chemical effect of the chlorine in SRF, which may promote the formation of volatile chlorides such as $CdCl_2$ and $PbCl_2$. Such an effect is clearly demonstrated in experiments with Cl-based additives. The addition of ammonium sulphate and kaolinite both reduce the volatility of Cd and Pb, which is most likely because of the chemical reactions between the trace elements and the additives. From a practical point of view, it seems that lowering the Cl-content in SRF and utilizing coal with high sulphur and aluminosilicates content are possible countermeasures for reducing the emission of Cd and Pb in co-combustion.

3.3.3.3 Volatility of As, Sb and Zn

Figure 3.7 shows the RE factor of As, Sb and Zn. It can be seen that the RE factor of As is around 5 when coal is co-fired with SRF. No obvious effect is seen for different share of SRF. However, for the Cl-based additives, the RE factor of As is generally increased. This effect is particularly significant with the addition of 4 wt% PVC, in which the RE factor of As becomes about 22. The increased RE factor of As during the injection of Cl-based additives is in line with other studies which found that the injection of HCl enhanced the condensation of As on small fly ashes [291].This may be related to the formation of $AsCl_3$ (g), which is a volatile compound at combustion temperature and could increase the vaporization degree of As [297]. Thermodynamic calculations indicate that the presence of other major inorganic elements (such as Na and K) may decrease the concentration of gaseous chlorine available for reacting with As [297]. This may explain the high volatility of As found in the injection of 4 wt% PVC, since the effect of the major inorganic elements would become less significant in this condition and a large amount of gaseous chlorine would be available for reacting with As. For the addition of 4 wt% AmSulf, it can be seen that the RE factor of As is reduced significantly. This result is in agreement with a

study showing that the injection of SO_2 increased the retention of As in ash by 30% [291]. Since the sulphur retention effect was not predicted by thermodynamic calculation [291], it was suggested there may be some As compounds which have not been taken into account in the thermodynamic calculations. These compounds may have high condensation temperature and would decrease the vaporization degree of As. The addition of 4 wt% kaolinite does not show a noticeable effect on the RE factor of As.

For Sb, it is shown that the RE factor in dedicated coal combustion is about 7.5, which is significantly higher than that in co-combustion of coal and SRF. The significant difference may be related with the association form of Sb in two fuels. It was found that the Sb in coal may be primarily associated with pyrite or organically bound, which would be easy to vaporize during combustion [292]. For SRF, the Sb may be inorganically bound with more stable species. However, this explanation needs to be confirmed by performing analysis on the trace element association in two fuels, which is outside the scope of the present work. As shown in Figure 3.7, the addition of NaCl does not have an obvious effect on the RE factor of Sb, whereas the addition of PVC appears to increase the RE factor of Sb. Since the addition of PVC can significantly increase the HCl concentration in flue gas, it suggests that the vaporization of Sb may be enhanced with the presence of a large amount of HCl, although such effect has not been predicted by thermodynamic calculations in [298]. For the addition of AmSulf, it can be seen that the RE factor of Sb is reduced. However, the addition of kaolinite does not show an evident influence on the RE factor of Sb.

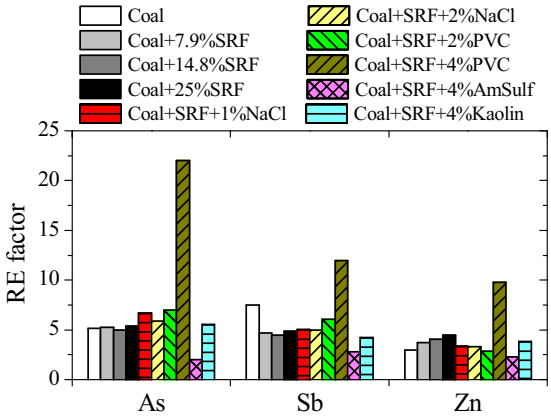

Figure 3.7 RE factor of As, Sb and Zn in different experiments.

The RE factor of Zn is found to increase slightly with increasing share of SRF, when the coal is co-fired with SRF. The observation is in line with the results from co-combustion of coal with sewage sludge [108]. The increased RE factor in co-combustion may be related with the association of Zn in SRF and coal. It has been found that Zn in municipal waste can be associated as pigments for waste wood or stabilizers for plastic [171], which would be easier to vaporize than the silicates associated Zn in coal [292]. For the addition of NaCl or 2 wt% PVC, the RE factor of Zn is slightly decreased compared in the experiment without additives. For NaCl, this may be partly related with the lower flame temperature in the experiment, which would adversely affect the vaporization of Zn. During the addition of 4 wt% PVC, the RE factor of Zn is considerably increased. In this experiment, the HCl concentration in flue gas would be significantly high, which may shift the distribution of Zn from relatively stable ZnO to more

volatile $ZnCl_2$ [299]. The addition of kaolinite shows an insignificant effect on the RE factor of Zn, However, the addition of AmSulf provides a reducing effect, which is likely related with the possible low flame temperature at this condition, since the chemical effect of SO_2/SO_3 would probably not be significant for the vaporization of Zn, both confirmed by experiments and thermodynamic calculations [291].

The TEM-EDS results shown in Figure 3.6 may provide some indications on the partitioning of Zn at different experimental conditions. It is seen that the Zn content is considerably large (>4 wt%) in the vaporized mode aerosols from co-combustion of coal and 14.8 wt% SRF (see Spectrum 2 and 3 in Figure 3.6a). Since the presence of Cl is negligible in these aerosols, it clearly the vaporized Zn species is probably present in other forms, such as ZnO. With the addition of Cl based additives, a large content of Zn can still be found in the aerosols from the vaporized mode (see Spectrum 2 in Figure 3.6b and Spectrum 3 in Figure 3.6c), but the Zn content in these aerosols is not much greater than that in Figure 3.6a. This implies that at these experimental conditions, the effect of Cl based additives on Zn vaporization is probably rather limited, especially compared to the obvious effect observed on Cd and Pb.

The results present in Figure 3.7 indicate that the volatility of As and Sb is unaffected or even decreased in co-firing coal and SRF, compared to coal combustion. However, the volatility of Zn is increased in co-combustion, which is likely linked with the association of Zn in SRF. The effect of Cl-based additive is generally not significant on the volatility of Sb and Zn, but slightly increased the volatility of As. However, in the extreme case with 4 wt% PVC addition, the volatility of As, Sb and Zn is increased significantly. The addition of ammonium sulphate generally reduces the volatility of As, Sb, and Zn, whereas the effect of kaolinite addition is insignificant. From a practical point of view, the results imply that utilizing coal with relatively high sulphur content may be favorable for reducing the volatility of As, Sb and Zn in co-combustion. The volatility of As, Sb and Zn in co-combustion is generally not sensitive to the chlorine or aluminosilicates content in the fuel mixture, expect for the case with extremely high chlorine content.

3.4 Conclusion

The partitioning of As, Cd, Cr, Pb, Sb and Zn in co-combustion of coal and SRF in suspension has been studied in an entrained flow reactor. The influence of NaCl, PVC, ammonium sulphate and kaolinite on trace element partitioning was investigated. By analyzing the ash fractions from different co-combustion experiments, it was found that the As, Cd, Pb, Sb and Zn content in cyclone ash (fly ash particles with diameter above ~2.5 μm) and filter ash (remaining fly ash particles with diameter below ~2.5 μm) were almost proportional to their content in fuel ash, and the content in filter ash was significantly higher than that in cyclone ash. The partitioning of trace elements was influenced by additives. In general, the Cl-based additives (NaCl and PVC) enriched the content of As, Cd, Pb and Sb in filter ash, and reduced the Cr content. The addition of ammonium sulphate showed a general reducing effect on all of the trace elements in filter ash. Most of the additives had an insignificant impact on the trace element content in cyclone ash, whereas the addition of kaolinite increased the Pb content in the cyclone ash.

The volatility of trace elements was investigated by introducing a relative enrichment (RE) factor, which compared the trace element content in filter ash with that in cyclone ash. It revealed that

the volatility of Cr was much lower than the other studied trace elements. The volatility of As, Cd, Pb, Sb and Zn was generally high, suggesting a large fraction of these elements was vaporized during combustion. Compared to coal combustion, the volatility of trace elements was affected by co-firing of coal and SRF. For Cd, Pb and Zn, the volatility in co-combustion of coal and SRF was slightly higher than that in coal combustion, which might promote the emission of trace elements. For trace elements such as Cd, Pb and As, the volatility was increased significantly by the addition of Cl-based additives. However, the volatility of trace elements was generally reduced with the addition of ammonium sulphate. For the addition of kaolinite, a notable reducing effect was seen on the Pb volatility, whereas the effect on other trace elements was minor.

The results from the present work imply that co-combustion of coal and SRF in a coal-fired power plant may increase the trace element content in fly ash particles greatly, primarily due to the significantly larger trace element content in SRF compared to coal. In addition, SRF may have relatively larger Cl-content and contain more organically associated trace elements than coal, which may further promote the emission of trace elements such as As, Cd, Pb and Zn, and alter the chemical form of the emitted trace elements to more volatile species such as $AsCl_3$, $CdCl_2$ and $PbCl_2$. An increased trace element emission together with a change of the trace element chemistry may greatly increase the toxicity of the dusts from a coal-fired power plant [103]. In order to minimize the trace element emission during co-firing coal and SRF, besides reducing the trace element content in SRF, utilizing coal with high S and aluminosilicates content and SRF with low Cl-content would be desirable.

Acknowledgment

This work is part of the CHEC (Combustion and Harmful Emission Control) Research Centre. The present work is funded by DTU, Energinet.dk and BiofuelsGS-2 (Nordic Graduate School in Biofuel Science and Technology-2). DONG Energy Power A/S is acknowledged for providing the fuels and for the fuel/ash analysis at Enstedværket Laboratory.

4 Formation of Fine Particles in Full-Scale Co-combustion of Coal and Solid Recovered Fuel

Abstract

Fine particles formed from combustion of a bituminous coal and co-combustion of coal with up to 10% (thermal percentage) solid recovered fuel (SRF) in a pulverized coal-fired power plant were sampled and characterized in this chapter. The particles from dedicated coal combustion and co-combustion both showed an ultrafine mode centered at approximately 0.1 μm. Compared with coal combustion, co-combustion of coal and SRF generally increased the formation of submicron particles, especially ultrafine particles below 0.2 μm. The morphology of the particles indicated that supermicron particles were primarily formed by the melting of minerals. The ultrafine particles were generated through homogeneous nucleation and coagulation of the vaporized inorganic species, while for the particles in between supermicron and ultrafine particles, condensation of the vaporized species or aggregation of the nucleates on the existing spherical submicron particles may also be an important formation mechanism. The elemental composition of the particles from coal combustion showed that S and Ca were significantly enriched in ultrafine particles and P was also enriched considerably. However, compared with supermicron particles, the contents of Al, Si and K were depleted in the ultrafine particles. The observed high volatility of Ca was attributed to the high combustion temperature and relative low oxygen condition in the boiler which may promote vaporization of Ca during char oxidation. The discrepancies on the observed volatilities of Ca and alkalis between some laboratory experiments and full-scale measurements were discussed. The composition of the fine particles from co-combustion was generally similar to those from coal combustion. The ultrafine particles from co-combustion were of slightly higher Ca, P, and K contents, and lower S content. The practical implications related to the fine particle formation in co-combustion of coal and SRF were discussed based on the full-scale results.

4.1 Introduction

Co-combustion of coal and solid recovered fuel (SRF) derived from nonhazardous waste streams is recognized as a promising method to both reduce the CO_2 emission from pulverized coal-fired power stations and increase the efficiency of utilizing waste fuels [272]. One of the major technical concerns for applying such a technology is the influences of coal and SRF co-combustion on the emission of fine particles from the power plant, since coal-fired power stations are important sources of fine particles in the atmosphere [300]. Although modern coal-fired power stations are usually equipped with efficient flue gas treatment equipment such as

electrostatic precipitator (ESP) and wet flue gas desulphurization (FGD) that can remove the majority of the particles in the flue gas [301], a considerable fraction of the submicron particles can still penetrate the flue gas treatment system and emit to the atmosphere [145,225,300,301]. These fine particles are often rich in trace elements that are highly toxic to the environment [213,214].

It is well-known that the dominant formation mechanism for supermicron particles from pulverized coal combustion is the fragmentation, melting, and coalescence of coal inherent and excluded minerals [145,151,221]. This mechanism usually results in a composition of the supermicron particles that is not significantly dependent on particle size [151,214,223,225]. For ultrafine particles below or around 0.1μm whose composition and morphology are significantly different from those of supermicron particles, the primarily formation mechanism is believed to be the vaporization, reaction, nucleation, coagulation and condensation of inorganic species in coals [151,152,214,218,221,223,238,302]. For particles in between ultrafine and supermicron particles, recent studies indicate that the aggregation or condensation of the vaporized species on the existing submicron ash particles would be a major formation mechanism [147,223,303]. This proposed mechanism is supported by the observed progressive change of the particle composition with particle size [214,223,225] and the reported morphologies of submicron particles [225,238,302]. The existing submicron ash particles, which provide the surfaces for condensation or aggregation, may be a result of the fine fragmentation mode as proposed in [151].

The inorganic elements which are important for the formation of submicron particles in pulverized coal combustion can be categorized as refractory metals (such as Si, Al, Fe, Ca and Mg), alkali metals (such as K and Na), S, P, and Cl [147]. The vaporization degree of different inorganic elements and their contribution to the formation of submicron particles are largely dependent on coal properties and combustion conditions. The coals with a higher fraction of organically associated components or salts from inorganic elements would likely have a higher overall vaporization degree of the ash forming matters [152,218]. Distribution of inorganic elements between inherent and excluded minerals may also influence their vaporization degree [164]. Particle combustion temperature is an essential factor for the vaporization of ash forming matters. With higher particle combustion temperature, the vaporization degree of ash forming matters and the formation of submicron particles usually increases [147,152,153,218,219,304,305]. However, the vaporization degree of alkali metals may be reduced with increasing combustion temperature [153], due to the reactions between these components and coal minerals [163,178,179]. The oxygen concentration near the char particles may influence the vaporization of refractory metals, since the reduction of metal oxides during char oxidation is an important ash vaporization mechanism [152].

Because of the significance of combustion conditions to the formation of fine particles, direct sampling of fine particles from a full-scale plant is probably the most reliable method to study fine particle formation in pulverized coal combustion. In this work, fine particles formed in a pulverized coal-fired power station in Denmark are sampled by using a low-pressure cascade impactor (LPI). The power station was operated at both dedicated coal combustion conditions and under conditions with co-combustion of coal and up to 10 th% (thermal percentage) SRF. The objective of this work is to explore the impact of SRF co-combustion on the formation of fine particles, based on the particle size distribution, morphology and elemental compositions of the fine particles collected from a real power plant. In addition, the formation mechanism of fine

particles in a pulverized coal-fired power plant is discussed according to the full-scale results. Furthermore, the practical implications related to the fine particle formation in co-combustion of coal and SRF is also discussed.

4.2. Experimental

4.2.1 Full-scale co-combustion tests

The coal boiler at the Esbjerg Power Station (ESV) has a production capacity of 378 MW_{el} and 460 MJ/s district heating. The steam data are: 304 kg/s at 251 bar and 560 ^{o}C. The combustion chamber is equipped with 24 coal burners, placed in tangential formation in the four corners, to ensure optimal turbulence and combustion. The coal burners are placed in 6 burner levels (named 10, 20, 30, 40, 50 and 60). Oil burners are placed between level 10 and 20, and in levels 30, 40, 50, 60. The coal burners each consists of two "sub-burners", one "rich" and one "lean". The coal is distributed from the coal mills to the (sub) burners (together with the primary air) through an "enricher", in a ratio of app. 80/20 %. The coal consumption at 100 % load is 120 t/h. The plant is equipped with an SCR for NO_x reduction, electrostatic precipitators (ESP) and wet flue gas desulphurization (FGD).

4.2.2 Fuels

The fuels used during the present measurements comprised a high-volatile bituminous coal from South America, and two types of SRF obtained from different suppliers. The SRF was co-fired with the coal in shares up to 10 % (thermal basis). The SRF, which had a fluffy morphology, was injected through special tubes, into the "lean" part of the existing coal burners, at either burner level 20 or 30. The influence of SRF particle size (10 mm or 20 mm average particle size) was also investigated. In the present work, only the results of one SRF were focused since the observed tendency is generally consistent with that of the other SRF. The composition of the coal and the SRF focused in this work is given in Table 4.1. It is seen that the SRF is characterized by high Cl and Ca contents, while the coal has relatively larger S, Al and Si content than the SRF.

Table 4.1 Fuel composition (wt%, dry fuel basis), the oxygen content is calculated by difference.

	Coal	SRF		Coal	SRF
Ash	12.81	12.90	Ca	0.32	2.39
C	72.01	52.66	Fe	0.64	0.27
H	4.74	6.61	K	0.24	0.12
N	1.49	1.09	Mg	0.2	0.23
S	0.69	0.31	Na	0.08	0.23
Cl	0.07	1.02	P	0.02	0.03
Al	1.48	0.70	Si	2.92	2.33
O	15.02	31.74	Ti	0.07	0.25

4.2.3 Particle measurement system

Fine particle measurements are carried out by using a 10-stage Berner LPI with an aerodynamic diameter range of 0.03-12.7μm and a sampling system described in detail elsewhere [225,306]. A schematic drawing of the setup is shown in Figure 4.1. During the measurement, flue gas with

a temperature around 380 ^{o}C is withdrawn by a gas ejector located downstream of the SCR unit of the plant. The ejector capillary, which is the inlet of the flue gas, performs as a prefilter with a cutoff diameter of ~2.5μm [225,306]. The sampling position in this study is chosen according to the availability of the ports in the plant. It should be noted that the particles collected at this sampling position would be slightly smaller than that obtained at lower temperature (e.g. at the inlet of ESP), due to the shorter residence time for the coagulation of ultrafine particles [232]. The extracted flue gas is diluted by dry and filtered air, in order to reduce the coagulation of inorganic species and extend the sampling time. The selection of air as dilution gas is based on the availability of gas in the power plant. The reaction between the fine particles and dilution air is considered to be negligible, due to the relative low flue gas temperature (~380^{o}C) at the sampling point and the fast cooling rate during the dilution process. The dilution ratio is determined by measuring the CO_2 concentrations in the raw flue gas and diluted flue gas. During the measurement, the dilution ratio is between 15 and 25. By directing the flue gas to the LPI, the particles are collected on aluminum foils coated with a thin film of Apiezon H grease.

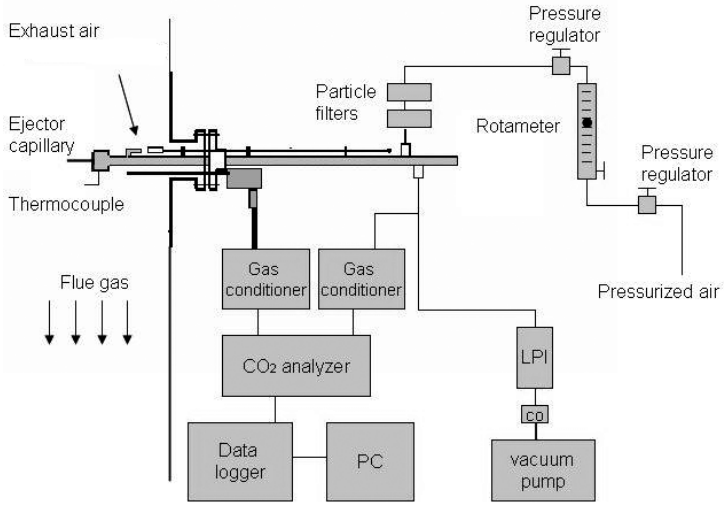

Figure 4.1. Ejector diluter and low-pressure cascade impactor for aerosol measurements.

The duration of one measurement is around 30 minutes, and one or two repetitions are normally performed at the same combustion condition. After the measurement, the particles deposited on the aluminum foils are weighted to obtain the mass-based particle size distribution. The morphology and the elemental composition of the collected particles are analyzed by Scanning Electron Microscopy (SEM) and Transmission Electron Microscopy (TEM), both equipped with Energy Dispersive Spectroscopy (EDS) for elements quantification. The particles for TEM analysis are transferred from the Al-foils to the TEM-grid by touching the TEM grid to the surface of the deposits on the Al-foils.

4.3. Results and Discussion

4.3.1 Mass-based particle size distribution

Table 4.2 Experimental matrix for the present experiments and the resulting $PM_{2.5}$ (as measured by the LPI). High and low injection position corresponds to burner level 30 and 20, respectively.

	Coal	Co-firing with SRF			
SRF particle size (mm)	-	10	10	10	20
Injection position	-	High	High	Low	High
SRF thermal fraction (%)	-	7	10	10	3
$PM_{2.5}$ (mg/m^3)	362±36	304±11	253±16	222±21	268±50

The experimental conditions included in the present study are summarized in Table 4.2, together with the corresponding results for the total aerosol mass load (PM2.5), as measured by the LPI. As mentioned earlier, the cut-off diameter for particles extracted by the ejector is approximately 2.5 µm, meaning that the results for the mass-based size distribution are not accurate above this size. From Table 4.2, it can be seen that the total mass load of $PM_{2.5}$ is quite stable with dedicated coal combustion ($PM_{2.5}$: 362±36 mg/m^3). When coal is co-fired with SRF, the mass load of $PM_{2.5}$ is generally decreased (range: 222 – 304 mg/m^3), while the influence of detailed co-firing conditions, such as SRF share, injection position, thermal fraction and particle size is not apparent based on the current results.

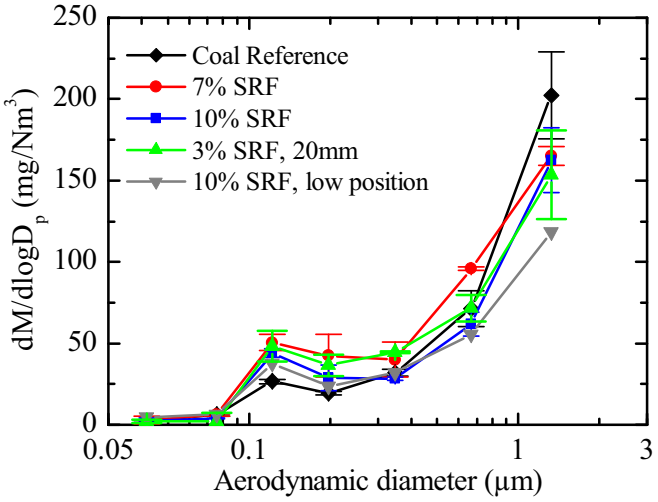

Figure 4.2 Mass-based particle size distribution from coal combustion and co-firing of coal and SRF at different conditions listed in Table 4.2.

Figure 4.2 shows the average mass-based particle size distribution obtained from the impactor stage 1-7 during coal combustion and co-combustion of coal and SRF at different conditions. The standard deviations shown in the figure indicate that the measurement uncertainties are not significant, especially for the submicron particles. In Figure 4.2, a peak particle size distribution is seen at average aerodynamic diameter (d_{ae}) around 0.1 µm. This peak is evident both for the coal reference case and the co-combustion cases. The obtained results are consistent with a

number of full-scale and lab-scale studies where fine particles from pulverized coal combustion containing an ultrafine mode centered at approximately 0.1 μm were reported [151,214,225].

As shown in Figure 4.2, co-combustion of coal and SRF has an impact on the fine particle formation. When coal is co-fired with SRF, the mass concentration of the submicron particles is generally increased, especially the ultrafine particles below 0.2 μm. Compared to the coal reference case, the amount of the particles collected on impactor stage 7 (mean d_{ae}=1.32 μm) is generally reduced in co-combustion. The increased formation of submicron particles in co-combustion of coal and SRF may result in higher dust emission from the power plant, since the submicron particles usually have a high probability to penetrate particle collection devices in power plants [121]. Furthermore, the increased formation of submicron particles in co-combustion of coal and SRF may lead to a significant increase of the trace element emission from the power plant, as the trace element contents in SRF are normally much higher than those in coals [272]. The co-combustion results shown in Figure 4.2 are obtained from different thermal fraction, particle size and injection position conditions. However, the influence of these factors on the particle size distribution is not clear from our results, presumably related to the highly heterogeneous characteristics of the SRF.

4.3.2 Typical morphology and composition of the fine particles

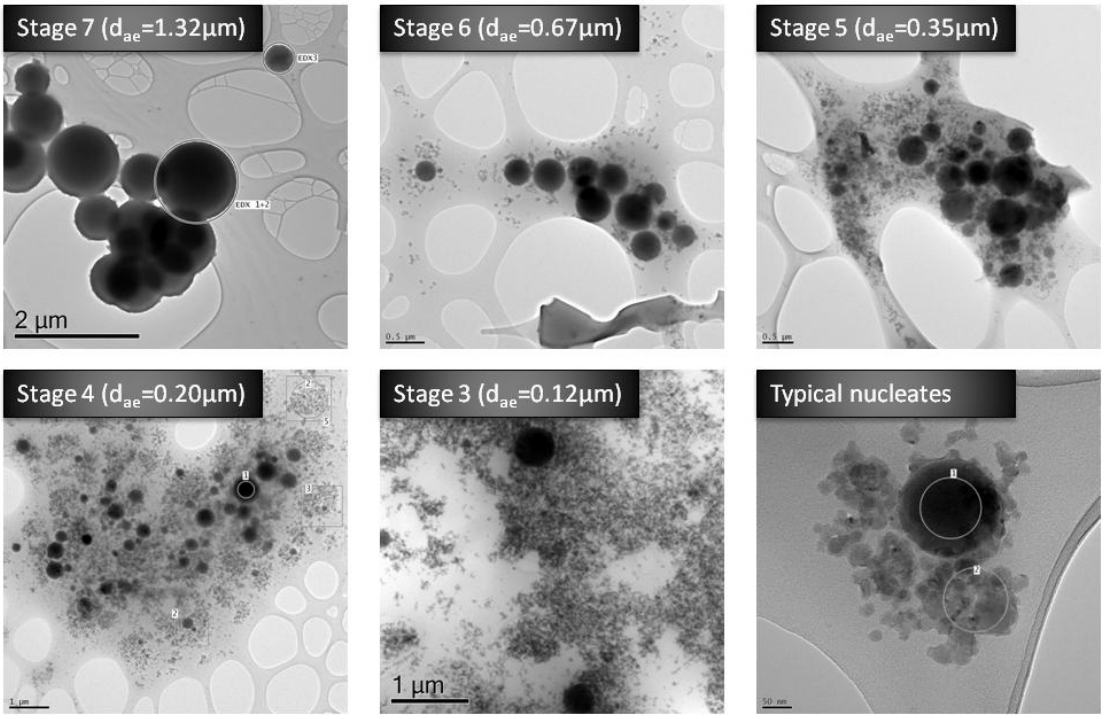

Figure 4.3. Typical morphology of the particles collected from co-combustion of coal and 7th% SRF.

The morphology of the collected fine particles is characterized by SEM and TEM. No obvious difference between the morphology of the particles from co-combustion and dedicated coal combustion was found. The TEM pictures of the fine particles collected from co-combustion of

coal and 7%th SRF are presented in Figure 4.3. These morphologies are also considered to be representative for the particles from coal combustion.

From Figure 4.3, it is seen that the supermicron particles (collected on LPI stage 7) primarily consist of individual spherical particles. The nearly perfect spherical appearance of the particles implies that the minerals in coal or SRF are almost completely melted during combustion. Although some small aggregates exist, the surfaces of these particles are normally quite smooth, indicating that the aggregation and condensation of vaporized species are not significant for the formation of supermicron particle. The morphology suggests that the supermicron particles are primarily generated from the minerals in coal and SRF that are melted during the combustion in the boiler. The formation mechanisms may involve the coalescence of inherent minerals, the fragmentation of chars, and the melting of excluded minerals [145,151,221,307]. The contribution of different mechanisms to the formation of supermicron particles is difficult to distinguish from the present results.

The morphology of the submicron particles collected during co-combustion of coal and 7 th% SRF is also shown in Figure 4.3. It is seen that the particles on the LPI stage 6 and stage 5 are still dominated by individual spherical particles. However, the surfaces of the majority of the submicron particles are to a large extent covered by small aggregates. Those small aggregates may either originate from the direct condensation of vapor phase species or from the aggregation of nucleates generated from inorganic vapors. Similar spherical submicron particles coated by inorganic aggregates have been seen in [225,302]. The morphology of the particles from stage 6 and stage 5 indicates that for particles in between supermicron and ultrafine particles, condensation of vapor phase species or aggregation of nucleates on the surface of existing submicron particles is an important formation mechanism. This formation mechanism would be closely related to the surface area of the particles. For spherical particles, the specific surface area of particles increases with decreasing particle diameter. Therefore this mechanism would be more pronounced for smaller particles, i.e. the contribution of vaporized species/nucleates would be more significant for the formation of smaller particles. It should be noted that some of the particles generated by homogeneous nucleation may coagulate and grow to a particle larger than 0.1 μm [238], which is observable in the Figure 4.3. Those particles may also contribute to the formation of particles between supermicron and ultrafine modes. However, the contribution of the nucleated particles is likely negligible for the formation of large particles close to 1 μm, but becoming more and more important to the formation of smaller particles. For the particles collected on stage 4 of the LPI (with average d_{ae} about 0.2 μm), the contribution of the nucleated particles appears to be more significant than that of the fragmented/coalesced spherical particles.

The morphology of the ultrafine particles collected on stage 3 of the impactor is presented in Figure 4.3. It is obvious that the morphology of these ultrafine particles differs significantly from the particles collected in other stages. These ultrafine particles almost only consist of irregular shape particles that are largely aggregated. Although these particles may be aggregated after being collected in the LPI, a remarkable difference between the morphology of the ultrafine particles and the supermicron particles is seen and indicates a different formation mechanism. As the morphology of ultrafine particles observed in this study is similar to those obtained in [238,302], it is suggested that the ultrafine particles are predominantly formed by the vaporized inorganic species. According to the detailed TEM analysis in [238], the observed ultrafine particles with irregular shapes are a result of the collision and partial fusion of tiny particles below 10 nm, which were from homogeneous nucleation. The results shown in Figure 4.3

suggest that these primary particles are usually in an irregular shape and the primary particle size is often between 10 and 30 nm.

EDS analyses have been performed on a number of spherical particles and nucleates observed by TEM. The average composition of the analyzed spherical particles and nucleates is depicted in Figure 4.4, with the error bars indicate the standard deviation of a number of analyses (>20). It can be seen that there are some general differences between the compositions of the spherical particles and the nucleates. The spherical particles generally contain relatively large Al and Si content, whereas the nucleates are characterized of larger S, P, and Ca content. The composition differences of the elements mentioned above are beyond the deviations shown in the figure. The detailed interpretations will be given in the following sections. On the other hand, considerable deviations are seen for different elements in Figure 4.4, indicating that particle to particle difference would be rather significant.

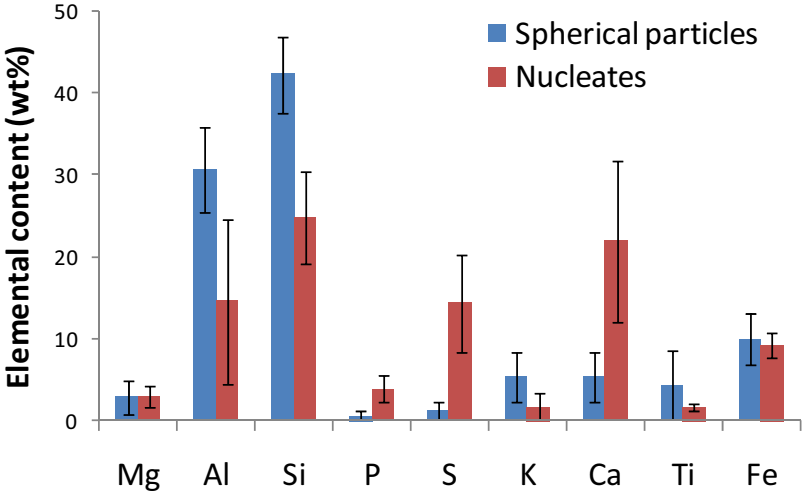

Figure 4.4 Typical composition of the spherical particles and nucleates observed by TEM analysis.

4.3.3 Bulk composition of the fine particles from coal combustion

The bulk elemental compositions of the fine particles from coal combustion have been analyzed by SEM-EDS and the results are presented in Figure 4.5. The oxygen and carbon contents in the particles are not included, as the measurement uncertainties on these two elements are larger than for other elements and the carbon content may be affected by the carbon coating used in sample preparation. In addition, the elements that mostly have contents lower than 1wt% (such as Na) are not presented in Figure 4.5, as the analysis uncertainties are high for such elements. From the figure, it can be seen that the supermicron particles are dominated by Si and Al, with approximate contents of 50 wt% and 20 wt%, respectively. With decreasing particle size, the content of Si and Al in the particles decreases. For the ultrafine particles collected on impactor stage 2, the contents of Si and Al become about 27 wt% and 13 wt%, respectively. The K content also decreases with decreasing particle size. The K content in the supermicron particles is around 7 wt%, while its content in the ultrafine particles decreases to about 1 wt%.

Different from Si, Al and K, the contents of Ca, S and P generally increase with decreasing particle size. For supermicron particles collected on impactor stage 8, the contents of Ca, S and P are approximately 5 wt%, 1 wt% and 1.7 wt%, respectively, while for ultrafine particles collected on impactor stage 2, the values increase to about 21 wt%, 19 wt% and 5 wt% respectively. Compared with the supermicron particles, the enrichment of Ca and S in the ultrafine particles is significant, with an approximate factor of 4 and 19 respectively, while the enrichment of P is by a factor of 3.

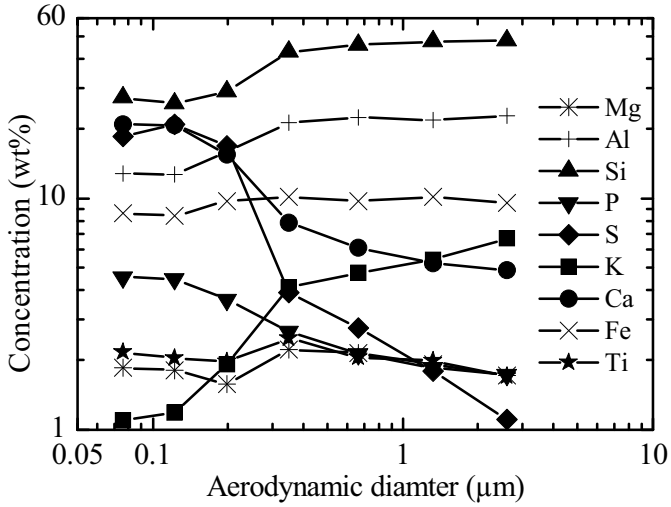

Figure 4.5. Elemental composition of the particles from COCERR coal combustion.

Compared with other elements shown in Figure 4.5, the contents of Fe, Mg and Ti are more evenly distributed over different particle size. In addition to the elements shown in Figure 4.5, Na and Cu have been detected in the particles collected on different impactor stages, and Mn and Cl are observed on some impactor stages. However, the contribution of these elements to the formation of particles is less significant and the analysis uncertainties are larger, compared with the elements shown in Figure 4.5.

The elemental compositions of the particles obtained in this study are in general consistent with the results obtained from other full-scale measurements [214,225-227]. Those measurements generally show that Ca and S are significantly enriched in ultrafine particles. The measurements in two pulverized coal-fired power plants in Denmark which fired Polish bituminous coal and a mixture of Polish and American bituminous coals and pet-coke showed that compared with supermicron particles, Ca and S were enriched by a factor of 5-20 in the ultrafine particles collected before the ESP [225]. Similar results on a Polish bituminous coal were obtained by a field study carried out in Finland where it was found that Ca and S were of higher volatility than other major inorganic elements and considerably enriched in the ultrafine particles collected after the ESP [214]. Significant enrichment of S and Ca in ultrafine particles was observed in other full-scale measurements carried out in a Denmark with a Columbia bituminous coal, a South Africa bituminous coal, and an American bituminous coal (Illinois) [226,227]. In [308], the distributions of different alkali and refractory metals in the fine particles from the combustion of a bituminous coal in a pulverized coal-fired power plant showed that volatility of Ca was much higher than other refractory and alkali metals, which moved the distribution of Ca towards

ultrafine particles. Elemental composition of the submicron particles collected from a pulverized coal utility boiler fired subbituminous coal were analyzed in [228]. The results implied that the enrichment factors of Ca, S, P and Mg in ultrafine particles are higher than that of Fe, while Al, Si, and K had lower enrichment factors than Fe.

The significant enrichment of S in ultrafine particles has also been observed in a number of laboratory-scale studies [147,158,164,218,221,223,303,305]. The importance of sulphur to the formation of ultrafine particles may be primarily related to the sulphation reactions between vaporized metal species and SO_2/SO_3 in the flue gas [164,192]. Another possibility is that sulfuric acid can be formed during the cooling of flue gas and may condense on the fine particle surfaces or form nucleates [121,309].

Laboratory experiments have indicated that the volatility of Ca is low and its contribution to ultrafine particle formation is insignificant [147,152,158,218,304,305]. The discrepancy on the Ca volatility between these results and the full-scale experiments are likely related to the differences in combustion conditions. Pulverized coal combustion would favor vaporization of Ca due to the high combustion temperature and local reducing condition in the char particles [152]. Equilibrium calculation showed that the vaporization of calcium was negligible at temperature lower than 1973K. When the temperature increased to 2073K, the vaporization degree of calcium was significantly increased [305]. With increased particle combustion temperature, enhanced contribution of Ca to the formation of fine particles below 0.3 μm has been observed [147]. In laboratory-scale reactors, it may be difficult to achieve conditions comparable to power plants in terms of temperature and oxygen level. A typical temperature of burning coal particles in a pulverized coal fired power plant is about 2000K [152], which can be achieved in the plant at oxygen concentrations of 4-6% [310]. However, in laboratory-scale reactors where coal particles are combusted in a dilute atmosphere with high excess air ratio [152,218,305], similar particle combustion temperature can be obtained at bulk oxygen concentration of about 20% [152]. Since the ratio of CO/CO_2 in a burning char particle increases with decreasing bulk oxygen concentration [311], it is likely that the local reducing condition of the char particles in laboratory-scale reactors would be less pronounced than that in full-scale plants, at the same particle combustion temperature condition. Besides, an extended reducing zone with high temperature is usually present at the near burner region of a full-scale plant, which would also be a favorable condition for the vaporization of Ca. Therefore, even though the particle combustion temperature in some laboratory experiments is comparable to that in full-scale plants [152,218,305], the high bulk oxygen concentration and dilute combustion condition in those experiments may result in Ca vaporization degree less significant than that in full-scale plants. However, for some pilot-scale experiments carried out in temperature and bulk gas conditions close to real boiler, significant vaporization of Ca has been obtained [219,303].

Coal properties may also play a role in the discrepancy found on Ca volatility between laboratory-scale and full-scale experiments. Some laboratory studies were performed with low rank coals such as lignite [152]. The association and composition of the ash forming elements may be quite different for bituminous coals and lower rank coals [139]. Still, it should be noted that the performed full-scale measurements are based on a number of different bituminous coals [214,225-227]. It may be the case that for the volatility of Ca, the impact of combustion conditions is more pronounced than that of coal properties. A range of analysis methods is applied in the full-scale studies including SEM-EDS [225-227], particle-induced X-ray analysis (PIXE) and graphite furnace atomic absorption spectrometer (GFAAS) [214], and neutron

activation analysis (NAA) [226]. This shows that the observed high volatility of Ca is not related to the analysis method. Fundamental studies on the volatility of Ca species at elevated temperature and different gaseous environment may be necessary to fully understand the significant enrichment of Ca in ultrafine particles collected in this and other full-scale studies [214,225-227].

In addition to Ca and S, P is also enriched in ultrafine particles in this study. The high volatility of P, which has been shown in other laboratory-scale and full-scale studies [147,164,218,227,303], is possibly due to that part of the phosphorus in the coals present in a form that can be vaporized at combustion temperature [164].

In Figure 4.5, it is seen that the K content in the fine particles decreases with decreasing particle size. The low volatility of K may be related to the fact that the majority of K in bituminous coals exists as minerals (such as illite) which are difficult to vaporize during combustion [137,138]. In addition, the reactions between gaseous K and coal minerals may take place in the boiler. The existence of such reactions in pulverized coal-fired boilers has been demonstrated through co-combustion of coal and straw [99]. The reactions between Na and coal minerals are to some extent similar to those between K and coal minerals. This is a potential reason for the relatively low Na volatility obtained in this study compared with some laboratory-scale experiments [147,152,218,305]. The high combustion temperature, long residence time, and turbulent conditions in the real boilers are favorable for the reactions between alkalis and coal minerals.

As shown in Figure 4.5, although Si and Al have lower volatilities than S, Ca and P, high contents of Si and Al are still found in ultrafine particles. The parts of Si and Al, which are vaporized and contribute to the formation of ultrafine particles, are likely due to the reduction reactions between Si and Al oxides with the CO produced from char oxidation [152,218]. In addition, organically associated Si and Al may contribute to a small fraction of vaporization [218]. Direct vaporization of SiO_2 may be another possible route [160]. Fe and Mg are also found in the ultrafine particles. The major vaporization mechanism for Mg is most likely the reduction of MgO during char oxidation [152]. For Fe, vaporization is possibly facilitated by reduction of iron oxides with the CO formed during char oxidation, as well as reduction of mineral-bound iron to Fe and FeC during the pyrolysis of coal [304].

4.3.4 Effects of co-combustion on fine particle composition

Figure 4.6 provides a comparison of the particle composition from dedicated coal combustion and co-combustion of coal with 7th% SRF, which is a representative case for evaluating the effect of co-combustion on the fine particle composition. Only the elemental contents of Si, P, S, K and Ca are presented in the figure, since the levels of other major inorganic elements (Al, Fe, Mg and Ti) are quite similar regardless of SRF addition. From Figure 4.6, it can be seen that the tendency of the elements in co-combustion of coal and SRF is quite similar to that in dedicated coal combustion, i.e. the contents of Si and K increase with increasing particle size while the contents of P, S, and Ca decrease with increasing particle size. In comparison with dedicated coal combustion, the particles from co-combustion generally have higher contents of Ca, P and K, and lower contents of Si. For S, it can be seen that the ultrafine particles (<0.2 μm) from dedicated coal combustion are of higher S content than those from co-combustion, while the S contents in larger particles are quite similar in those two cases. Although the SRF used in this work has relatively high Cl content, the presence of Cl in the fine particles is generally negligible,

indicating the majority of the Cl in the SRF is released to gas phase as HCl during co-combustion.

The higher Ca contents in the ultrafine particles from co-combustion are likely related to the high Ca content in the SRF, which may be vaporized and form ultrafine particles during combustion. However, the higher P and K contents may be explained by the higher content of organically associated phosphorous and potassium in the SRF compared to the coal, which can be easier vaporized and thereby contribute to the formation of ultrafine particles. The decreased S content in ultrafine particles from co-combustion is likely related to the relatively low S content and high Ca content in the SRF, which would reduce the formation of ultrafine particles from sulfuric acid [121]. Comparison of the particle composition from co-combustion and dedicated coal combustion indicates that the increased formation of ultrafine particles during co-combustion is related to the higher Ca and P contents in the SRF. Further interpretation of the results requires more detailed characterization of the SRF and the coal as well as studying the combustion behavior of SRF in a pulverized coal boiler, which are rarely studied and outside the scope of this study. To the author's knowledge, the only work that attempted to characterize the flame of refuse derived fuels is [260]. The heterogeneous characteristics of the SRF may be another difficulty for interpreting the results. Although the SRF was sampled carefully, the obtained composition might still deviate from the actually composition of the SRF and the variations from time to time would not be negligible during the measurement.

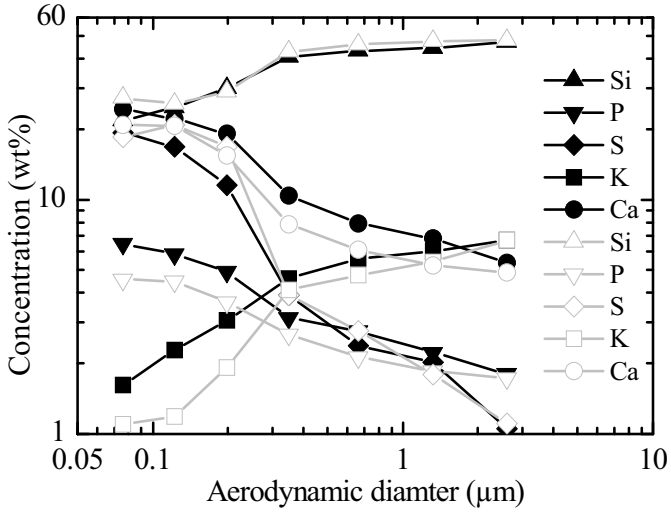

Figure 4.6. Comparison of the particle elemental compositions from co-combustion of coal with 7th% SRF (solid symbol) and coal combustion (open symbol).

4.3.5 Effects of co-combustion on the composition of ESP ash

During the full-scale tests, the fly ashes from the electrostatic precipitator (ESP) were collected and analyzed. Table 4.3 compares the composition of the fly ashes from the ESP during dedicated coal combustion and co-firing of coal and SRF. It is noticed that the concentration of S tends to be increased in the fly ashes from co-firing, as compared to the coal reference case, in spite of a lower initial concentration in SRF (Table 4.1). Thereby, the overall picture seems to indicate that for co-firing of coal with SRF, a relatively larger fraction of the S is "captured",

primarily in the coarser particles, as compared to dedicated coal combustion. This may be a consequence of the increased Ca concentration in the fly ashes from SRF co-firing (Table 4.3). CaO can readily react with SO_2/SO_3 in the gas phase, forming $CaSO_4$ [9,225]. This, in turn, may decrease the concentration of SO_2/SO_3 in the flue gas, while increasing the concentration of S in the fly ash [9]. Such effects have previously been observed during co-combustion of coal and SRF in the entrained flow reactor in Chapter 2. In addition, some other experimental observations also support the observed results. Spliethoff and Hein [9] studied effects of co-combustion of biomass in pulverized fuel furnaces and found that, since biomass in most cases contains considerably less sulphur than coal, an increasing biomass share made the SO_2 emissions decrease proportionally. In addition, biomass co-combustion enhanced the content of S in the ash, due to capture by CaO and MgO in the biomass ash [9]. Unfortunately, no data for the SO_2/SO_3 concentrations in the flue gas during the present SRF co-firing campaign are available.

Table 4.3 Comparison of the ESP fly ash composition from dedicated coal combustion and co-combustion of coal and SRF. Analysis method: wet chemical (acid digestion and ICP-OES).

Concentration in ESP ash (wt%)	Coal reference	Co-firing with SRF
Ca	1.61	2.16 – 3.65
S	0.32	0.36 – 0.52
P	0.12	0.20 – 0.45
K	1.74	1.83 – 2.17

The P and K content in the fly ashes from co-combustion also appears to be increased compared to dedicated coal combustion. The increased P content may be attributed to the relatively larger P content in the SRF (see Table 4.1). On the other hand, the fuel analysis shows that the K content of the SRF is much lower than that of the coal, while the K content in the fly ash from co-combustion is generally larger than that of coal fly ash. A possible explanation is that the K content of the SRF may not be analyzed accurately due to the heterogeneous characteristics of the SRF. The actual K content of the SRF may be larger than that of coal, which may be an additional explanation to the observed tendency of K in Figure 4.6.

4.3.6 Link to overall plant performance: increased dust emissions

During the present co-firing campaign, it was observed that the dust concentration in the stack (after ESP and wet FGD) increased significantly. The dust emissions were increased by a factor of up to 8 as compared to "normal levels" (which is approximately 5 mg/Nm^3) for the power plant. Consequently the emission of several particle-born trace elements (such as Zn) was also increased. There was no obvious explanation for this increase, and the emissions decreased to the normal levels again at the end of the campaign.

We have analyzed the plant's emission data during the co-firing campaign and looked for possible explanations for the increased dust emissions. While we have found no significant correlations between the dust emissions and the amounts of aerosols formed, there may be a link between the increased dust emissions and the behavior and fate of Ca and S in the boiler:

It has been reported in the literature that replacement of high-sulphur coals with low-sulphur coals has led to decreased efficiencies of the electrostatic precipitators, and this has been explained by the lower concentrations of SO_2/SO_3 in the flue gas while firing low-sulphur coals

[312]. Small amounts of SO_3 are needed for proper electrostatic precipitator performance, as SO_3 reacts with moisture and forms a conductive film of sulfuric acid on the fly ash when the flue gas cools. Without this conductive layer, ash resistivity increases, limiting the transfer of particle charge over the particle surface to the grounded collection plates. As a result, the collected ash forms a charged layer on the collection plates, repelling other charged particles [312].

Hence, the presence and fate of SO_3, in particular, seems to be a "key parameter" for efficient ESP performance. The formation of SO_3 is determined by the oxidation of SO_2 to SO_3, and this step is most evidently kinetically limited [209]. During pulverized coal combustion, the majority of the fuel-sulphur is converted into SO_2, with only a few % converted into SO_3 [97,209]. This results in quite low SO_3 concentrations in the flue gas, approximately 10 ppm by volume for coal containing 0.5 – 5 wt % sulphur [97].

Cao et al. [97] studied the fate of SO_3 in different coal-fired boilers, burning high-sulphur (> 3.5 % S) bituminous coal and low sulphur (~0.4 % S) sub-bituminous coal, respectively. They reported that different interaction mechanism between SO_3 and fly ash applies for the different-rank coals, as temperature changes: under higher temperature ranges (> ~300 ^oC), alkali earth metal (Ca + Mg) constituents in fly ash are active on capturing SO_3 through chemical reactions, to form sulphate salt. Sub-bituminous coal generally has higher alkali earth metals in their fly ash, which allows the SO_3 in their flue gas to be captured effectively in the higher temperature zone (> 300 – 350 ^oC) prior to the air pre-heater (APH). Under lower temperature ranges, on the other hand (below the dew-point of SO_3 which is ~150 ^oC), the carbon residue in the fly ash functions as major adsorption sites for SO_3 condensation. Bituminous coal generally has high carbon-residue content in fly ash but lower occurrence of alkali earth metal constituents, which allows the SO_3 to be captured effectively through condensation, in the lower temperature zone after the APH.

If these effects also apply to co-firing of coal with SRF (as in our case), this means that SO_3 could be effectively captured by reaction with Ca in the fly ash, at relatively high temperatures, to form $CaSO_4$. This, in turn, would suppress the condensation of sulfuric acid on the surface of the fly ash particles at lower temperatures, especially if the rate of oxidation of SO_2 to SO_3 is much slower than the reaction between SO_3 and CaO, which is very likely. This may lead us to suggest that the increased dust emission observed during the present SRF co-firing campaign is linked to a deficiency of SO_3 in the flue gas, due to enhanced capture by CaO in the fly ash.

4.4 Conclusion

The formation of combustion aerosols (i.e. particles with an aerodynamic diameter below 2.5 μm) during co-firing of coal and solid recovered fuel (SRF) was studied through direct sampling in a pulverized coal-fired power plant. During the measurement campaign, the plant was operated at both dedicated coal combustion conditions and under conditions with co-firing of up to 10 % (thermal basis) of SRF. The influence of particle size, and injection position was also investigated. The SRF was characterized by high contents of Cl, Ca, Na and trace metals, while the coal (a bituminous coal from South America) had relatively larger S, Al, Fe and K contents.

The mass-based particle size distribution of the fine particles was generally found to have an ultrafine (vaporization) peak centered around 0.1 μm. The total fine particle mass load was quite stable when no SRF was introduced ($PM_{2.5}$: 362±36 mg/m^3). Co-firing of coal and SRF tended to

increase the ultrafine peak, while decreasing the total mass load of $PM_{2.5}$. The influence of SRF thermal fraction, size, and injection position was not evident from our data, probably due to the inhomogeneous characteristics of the SRF.

TEM analyses revealed that the difference between the morphology of the fine particles from dedicated coal combustion and co-combustion was insignificant. In general, the supermicron particles primarily consisted of individual spherical particles formed from fragmentation, melting and coalescence of the minerals in the coal or SRF. The submicron particles collected on stage 6 and stage 5 (mean d_{ae} of 0.67–0.35 μm) of the LPI were also dominated by individual spherical particles, but the surfaces of the majority of these particles were covered by small nucleates. For the particles collected on stage 4 (mean d_{ae} of 0.20 μm) of the LPI, a major fraction was formed directly by the nucleates, whereas the fragmented/coalesced spherical particles were still present in this stage. The ultrafine particles collected on stage 2 of the LPI (mean d_{ae} of 0.12 μm) almost only consisted of irregularly shaped nucleated particles that were aggregated. These particles were mainly generated from the vaporization and homogeneous nucleation of the inorganic elements present in the fuels. The primary particle size of the nucleates was found to be in a range of 10-30 nm, and the nucleates were generally enriched in Ca, S, and P compared to the spherical particles originating from melted minerals.

The bulk elemental composition of the fine particles from coal combustion showed that Ca, S and P were significantly enriched in the ultrafine particles. The high volatility of Ca found in the full-scale measurements was attributed to the high combustion temperature and relatively low oxygen concentration in the boiler. The content of K, Al and Si was found to decrease with decreasing particle size. The low volatility of K was probably due to the association of K in the bituminous coal and the reactions between the gaseous K and the coal minerals.

The effect of co-combustion of coal and SRF on the composition of the fine particles was evaluated. It was revealed the overall composition of the fine particles from co-combustion was similar to that of coal combustion. However, the content of Ca, P, and K in the fine particles from co-combustion was generally larger than that from coal combustion. For ultrafine particles, the S content was slightly smaller in the particles from co-combustion. Further investigations are needed in order to fully understand and interpret the influences of SRF and coal co-combustion on the formation of fine particles. Besides the fine particles, the influence of co-combustion on the composition of fly ashes collected by ESP has also been evaluated. It appeared that the contents of S, P, Ca and K in the fly ash were generally increased when coal was co-fired with SRF. The increased S content was attributed to the enhanced capture by the calcium in the fly ash.

A reduced collection efficiency of the electrostatic precipitator was observed during co-firing of SRF. Based on our results, we suggest that the increased dust emission while co-firing SRF is presumably linked to a deficiency of SO_3 in the flue gas. A relatively high content of Ca in the fly ashes from SRF co-firing would promote the effective capture of SO_3 at relatively high temperatures (> 300 ^{o}C) through chemical reactions, to form $CaSO_4$. Consequently, SO_3 is exhausted from the flue gas, and subsequent condensation of sulfuric acid on the surface of the fly ash particles is suppressed. Small amounts of SO_3 are needed for proper electrostatic precipitator performance, as SO_3 condenses as a conductive layer of sulfuric acid on the ash during cooling of the flue gas.

In conclusion, we have found that the formation of fine particles is to some extent influenced by co-firing of coal with SRF, both with respect to the amount and the chemical composition. However, further investigations are needed in order to evaluate the effect of parameters such as SRF type, share, size, and injection position. Laboratory investigations on char reactivity and burn-out may serve to clarify the ash formation mechanisms during co-firing of coal with SRF, as well as the effect of initial particle size distribution and injection position of the SRF. A significant increase of the dust emission was observed during the full-scale co-combustion of coal and SRF. A conceivable explanation is that the formation of SO_3 in the flue gas is inhibited by the calcium in the SRF, thus resulting in a reduced collection efficiency of the ESP. Further investigations are needed in order to support the explanation. This increased dust emission may greatly increase the emission of trace elements, since the volatility of some trace elements, such as Cd and Pb, may be increased during co-combustion of coal and SRF, according to the results in Chapter 3.

At this point we have identified no serious technical obstacles for co-firing of coal with SRF at the investigated conditions. Potential dust emission problems may probably be solved by using a coal with higher sulphur content, or alternatively by injection of a fly ash conditioning agent, as e.g. SO_3, upstream of the ESP.

Acknowledgment

The work is part of the CHEC (Combustion and Harmful Emission Control) Research Center. The present work is sponsored by The Technical University of Denmark and co-funded by Energinet.dk. DONG Energy A/S is acknowledged for providing the opportunity to perform the measurement. Laila Leth and Thomas W. Hansen are acknowledged for the SEM-EDS and TEM-EDS analyses, respectively. We thank Jacob Zeuthen for his help to initiate the measurements.

5 Utilization of Spent Bleaching Earth as an Additive in Dust-Firing of Straw

Abstract

In the present chapter, the ash chemistry and deposition behavior during straw dust-firing were studied by performing experiments in an entrained flow reactor. The effect of using spent bleaching earth (SBE) as an additive in straw combustion was also investigated by comparing with kaolinite. During dust-firing of straw, the large (>~2.5 μm) fly ash particles generated were primarily molten or partially molten spherical particles, rich in K, Si and Ca, supplemented by Si-rich flake-shaped particles. The smaller fly ash particles (<~2.5 μm) were predominantly formed from the nucleation, condensation and coagulation of the vaporized K, Cl, S and P species. Approximately 70% of K in the fly ash from straw combustion was water soluble, and KCl was estimated to contribute to more than 40% of the water soluble K. With the addition of SBE to straw dust-firing, the Cl retention in ash was reduced, the SO_2 emission was increased, and the formation of water soluble alkali species was decreased. Compared to kaolinite, the inhibiting effect of SBE on alkali chloride formation seemed to be slightly smaller, at similar K/(Al+Si) molar ratio of the fuel mixture. The addition of SBE to straw dust-firing significantly decreased the Cl content of the deposits collected on a probe, both due to a dilution effect and chemical reactions. Compared to pure straw combustion, the deposition rate was slightly increased during the SBE addition, despite of the considerably decreased deposition propensity. The results from the present work suggest that SBE could be a promising additive to be used in straw dust-firing.

5.1. Introduction

In order to achieve the European targets regarding reduction of greenhouse gases and increasing the use of renewable energy in 2020 [313], an important measure is to use biomass as fuel in high-efficiency centralized electrical power plants. In Denmark, the utilization of biomass in power production has been primarily based on dedicated grate-fired power plants and co-firing in coal-fired power plants [99,211,278,286,314]. With an aim of increasing the biomass share in power production, an attractive solution is to convert the existing coal-fired power plants to 100% biomass dust-firing plants. Compared to traditional grate-fired plants, biomass dust-firing plants has higher load flexibility, which can compensate the power production uncertainties induced by increasing wind power production in Denmark [315].

Since biomass is fundamentally different from coal in terms of fuel properties and combustion behavior [26], dust-firing of biomass may raise several technical challenges, such as flame stability and burnout, ash deposition and corrosion, deactivation of SCR catalyst, and ash utilization. Most of these issues are linked to the inorganic constituents in biomass. Compared to

coal, biomass is often characterized by the large content of critical inorganic elements that may be easily vaporized during combustion [128,167,168,170]. The released critical inorganic elements, such as alkalis and chlorine, may form alkali chlorides and may lead to severe ash deposition and corrosion of superheaters in the boiler [6,140,211,250,261,316-318], thus restricting the electrical efficiency of biomass-fired plants [314]. Compared to grate-firing, ash deposition of biomass dust-firing may be more severe, due to the higher concentration of fly ash in the flue gas. Besides, the vaporized inorganic elements from biomass combustion may result in high concentrations of submicron particles in the flue gas [207,237,241,278]. These particles may deteriorate the performance of SCR catalysts, through physical deposition and blocking of channels as well as chemical poisoning and deactivation [216,319-321].

One possible approach to minimize the ash related problems during biomass combustion is to use additives that can convert the vaporized inorganic species to less harmful forms [116,187,197-199,237,322-324]. The usable additives can be approximately categorized as Al-Si-based, S-based, P-based, and Ca-based, according to the major elements present in the additives. A typical example of the Al-Si-based additives is kaolinite, which has been proven to be very effective in minimizing the gaseous alkali concentration in the flue gas, through the formation of alkali-aluminosilicates with high melting temperature [107,177,179,182,191]. Other Al-Si-based additives such as Bauxite [182], Emathlite [182], Bentonite [237], clay [237], quartz [169] and coal ash [107] also show some extent of decreasing effect on the gaseous alkali concentrations. For S-based additives, the main effect is to convert the gaseous alkali chlorides in the flue gas to alkali sulphates, which are less harmful with respect to ash deposition and corrosion [191,192]. A typical S-based additive is ammonium sulphate, which cannot only convert the gaseous alkali chlorides to sulphates, but also reduce the NO_x concentration in the flue gas [198,199]. Other examples of S-based additive are aluminum sulphate [197], ferric sulphate [197], and elemental or gaseous sulphur [99,199]. P-based additives usually refer to Ca-phosphates which are capable of capturing gaseous alkali through the formation of alkali-Ca-phosphates [169,237]. Besides, a recent study showed that the addition of ammonium phosphate could also decrease the concentration of alkali chloride in flue gas, presumably through the formation of alkali phosphates [325]. For biomass with large chlorine and alkali content, utilization of Ca-based additives such as $Ca(OH)_2$ or $CaCO_3$ normally do not greatly influence or can even increase the concentration of alkali chlorides/fine particles in the flue gas [237]. However, for biomass rich in P and alkalis, a significant decreasing effect on the fine particle formation may be achieved by using Ca-based additives [116,324]. In general, with the purpose of minimizing ash related problems in biomass combustion, additives which have a pronounced decreasing effect on the harmful species (e.g. alkali chlorides) in the flue gas are desirable. Besides, an ideal additive is also expected to be cheap and easy to handle, and should not significantly influence the fuel combustion behavior and ash utilization.

The aim of the present work is to provide a systematic evaluation of the ash morphology, chemistry, and deposition behavior during dust-firing of straw. In addition, the feasibility of utilizing spent bleaching earth (SBE) as an additive in straw dust-firing was examined, through comparison with kaolinite. The SBE is a powdery residual product from vegetable-oil production, which is considered to be an applicable additive in straw dust-firing, because of the relatively high heating value, cheap price, and the relatively large Si content. To achieve the objective of this work, dust-firing of straw was performed in an entrained flow reactor (EFR), at different shares of SBE and kaolinite, respectively. The composition of different ash fractions from the experiments was analyzed, and the ash chemistry in dust-firing of straw with and without

additives was investigated. By collecting ash deposits on a probe with controlled conditions, the influence of additives on deposition rate and deposit composition was examined.

5.2 Experimental Section

5.2.1 Fuel and additives

The straw used in the present work was a Danish wheat straw, with compositions listed in Table 5.1. It is seen that the most abundant inorganic elements in the straw are Si, K, Ca and Cl. Compared to the Danish straw used in other studies [60,99,237,317,323], the Cl content in this straw is relatively low, whereas the K content is comparable.

Table 5.1.Properties of the fuel and additives.

Properties	Straw	SBE	Kaolinite
LHV (MJ/kg wet)	16.28	16.13	-
Moisture (wt% wet)	7.22	3.48	0.98
Ash (wt% wet)	3.87	44.44	85.20
C (wt% dry)	47.50	38.90	-
H (wt% dry)	6.00	5.40	1.55
O* (wt% dry)	43.49	33.29	53.49
N (wt% dry)	0.43	-	-
S (wt% dry)	0.08	0.18	-
Cl (wt% dry)	0.16	0.01	-
Si (wt% dry)	1.20	16.50	22.75
Al (wt% dry)	0.01	3.00	20.05
P (wt% dry)	0.06	0.02	0.03
Fe (wt% dry)	0.01	0.86	0.58
Ca (wt% dry)	0.29	0.24	0.03
Mg (wt% dry)	0.06	0.56	0.17
Na (wt% dry)	0.01	0.27	0.03
K (wt% dry)	0.70	0.77	1.32

*The oxygen content is calculated by difference of the elemental content.

Bleaching earth refers to clays that are capable of absorbing coloring matters and undesirable residues during the processing of edible oils as well as the production of oleochemicals [326]. The spent bleaching earth (SBE) used in this work was from a Danish company producing vegetable oil (Aarhus Karlshamn AB). The price of the SBE was approximately 40 DKK/GJ, which was considered to be similar to the price of straw in Denmark [327]. Since the received SBE contained some vegetable oil (~ 10 wt%) which agglomerated the particles, the SBE was dried at 80 ^{o}C for 4 hours. The resulting SBE was a mixture of bleaching earth (~50 wt%), activated carbon (~ 25 wt%), and cellulose-based filter aid (~ 25 wt%), with compositions listed in Table 5.1. It is seen that the SBE has a large ash content, and the ash is dominated by Si. The heating value of the SBE is comparable to straw. An additional characteristic of the SBE is that the trace element content in the SBE is usually negligible [327]. This is favorable, since the concentration of trace elements is a major limiting factor for utilizing the residue ash from biomass combustion as fertilizer [314]. The kaolinite used in the present work was a pure

compound, with analyzed compositions listed in Table 5.1. The kaolinite has larger ash, Al and Si content than that of SBE.

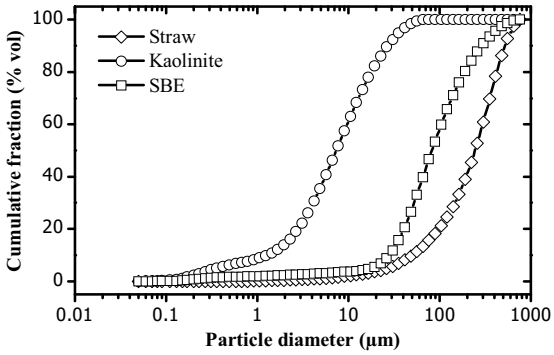

Figure 5.1.Particle size distribution of the straw, kaolinite and SBE.

In order to facilitate fuel feeding, the straw was ground at an Alpine® pin mill. The SBE and kaolinite were received as small particles which did not require further treatment. The particle size distribution of the straw and additives was analyzed by a laser diffraction method with the Malvern Mastersizer 2000 particle size analyzer. The measured particle size distribution is depicted in Figure 5.1. It is seen that the straw particles have a d_{50} (meaning that 50 vol% of the particles are below this size) of about 285 μm. The SBE particles are much smaller than the straw particles, having a d_{50} of about 95 μm. The kaolinite particles are extremely fine particles, with a d_{50} of approximately 8 μm.

5.2.2 Experimental setup and procedures

The experimental setup used in this work is the entrained flow reactor described in detail in Chapter 2. The experimental procedure is almost identical to that in Chapter 2. The only exception is that the surface temperature of the deposit probe was controlled to be around 470 ^{o}C in the experiments of this work. This temperature was chosen according to the typical superheater temperature in a straw dust-firing plant [314]. In addition, the flue gas temperature was controlled collected to be 750 ^{o}C.

5.2.3 Experimental matrix

Table 5.2. Experimental matrix and conditions.

Experiment NO.	Fuel	Excess air ratio	Molar ratios in fuel			
			K/Si	K/(Al+Si)	K/Cl	K/(Cl+2S)
1	Straw*	1.62	0.42	0.42	4.08	1.90
2	Straw+5wt% kaolinite	1.62	0.25	0.17	4.51	2.10
3	Straw+10wt% kaolinite	1.62	0.18	0.11	4.99	2.32
4	Straw+10wt% SBE*	1.58	0.26	0.17	4.54	1.88
5	Straw+20wt% SBE	1.57	0.19	0.10	5.11	1.85

*Repetition experiments have been performed.

The experimental matrix is shown in Table 5.2. It is seen that the excess air ratio in different experiments is maintained around 1.6. In addition to pure straw combustion, the straw has been co-fired with different mass share of kaolinite or SBE. The added SBE was 10 wt% and 20 wt%, respectively. The addition kaolinite was chosen to be 5 wt% and 10 wt%, respectively, in order to perform the experiments at similar K/(Al+Si) molar ratio as that of SBE addition.

5.2.4 Ash/deposit analysis

The fuel, ash, and deposit samples from the experiments were analyzed at the Enstedværket Laboratory, DONG Energy A/S. The content of Al, Ca, Fe, K, Mg, Na, P, Si, Ti, S, and Cl in the different fuels and ash fractions were analyzed by inductively coupled plasma optical emission spectrometry (ICP-OES). The water soluble K, Na, Cl and S content in the cyclone ash and deposit was analyzed by ICP-OES/IC. In this analysis, the ash/deposit sample was dissolved in ultra-pure water at 120 ^{o}C for 1 hour, and then the solution was filtered and analyzed by ICP-OES/IC. Besides the bulk chemical analysis, the typical morphology and composition of the fly ash particles from the experiments were characterized by using scanning electron microscopy and dispersive X-rays spectroscopy (SEM-EDS).

5.3 Results and discussion

5.3.1 Ash behavior during straw dust-firing

5.3.1.1 Mass balance

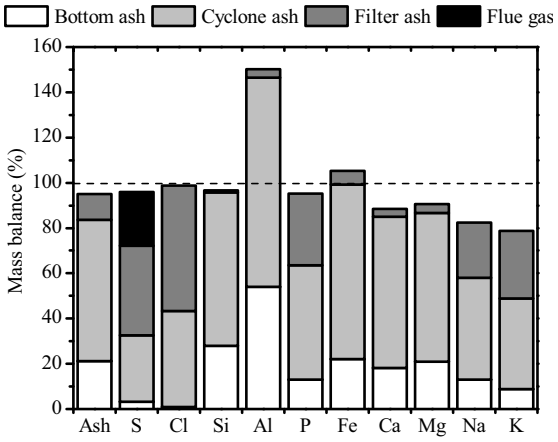

Figure 5.2. Ash and elemental mass balance during straw dust-firing.

The ash and elemental mass balance in dust-firing of straw has been calculated based on the fuel and ash composition, the fuel feeding rate, the flue gas composition, and the amount of the collected ash and the corresponding flue gas flow rate. The results are depicted in Figure 5.2. It can be seen that the overall ash balance is around 95%. Approximately 20% of the fuel ash is partitioned to bottom ash, with the remaining being fly ash particles. The percentage of the filter

ash and the cyclone ash in the fly ash is about 15% and 85%, respectively. The ash distribution indicates that the fly ash concentration in the flue gas is significantly increased in dust-firing of straw, compared to the grate-firing of straw where only about 10-20% of the fuel ash is partitioned to the fly ash [328]. The increased fly ash concentration may lead to more ash deposition in the superheater region. In addition, a significant fraction (~15%) of the fly ash is found to be present as fine particles smaller than 2.5 μm, which is considerably higher than during pulverized coal combustion in the same reactor (~8%) [286].

Similar to the ash balance, the mass balance of the major inorganic elements is mostly above 90%, except for Al, Na and K. The mass balance of Al is much higher than 100%. This is probably because of the Al content in straw is very small (see Table 5.1), and the influence of the analysis uncertainties may be significant. The mass balance of Na and K is around 80%, implying that part of the Na and K in straw may have been deposited on the reactor tube during the experiment. This hypothesis is supported by the deposits observed on the reactor tube after the experiment. One the other hand, although the collection of ash particles in the sampling system has been carried out carefully, a fraction of the ash particles may still not be collected, particularly for the aerosols deposited in the water-cooled probe via thermophoresis.

The partitioning of inorganic element to different ash fractions is illustrated in Figure 5.2. It is seen that approximately 99% of the Cl in straw is found in ash, suggesting the presence of HCl (g) in the flue gas may be negligible in this experiment. The observed significant Cl retention in ash is probably linked to the high K/Cl molar ratio in the straw (>4), which may favor the formation of KCl. The Cl distribution also indicates that Cl is significantly enriched in the filter ash, whereas the presence of Cl is negligible in the bottom ash. For the S distribution, it seems that about 70% of the S is retained in the ash, with the remaining being gaseous S (mainly as SO_2) in the flue gas. Similar to the Cl distribution, a significant enrichment of S is found in the filter ash, while the partitioning of S to the bottom ash is minor. The distribution of the other inorganic elements generally represents the ash partitioning. However, for elements such as P, Na and K, a slight enrichment in the filter ash is noticeable.

5.3.1.2 Typical fly ash morphology and composition

SEM-EDS has been used to characterize the morphology and composition of the fly ash particles from straw dust-firing. Figure 5.3 illustrates the observed typical fly ash morphologies (the results are considered to be representative for a large number of analyses performed), with the corresponding spot-analysis compositions given in Figure 5.4. It is generally found that the cyclone ash from straw dust-firing is dominated by molten or partially molten spherical particles. The large spherical particles, as illustrated in Figure 5.3b, often consist of K-silicates or K-Ca-silicates (see the composition of spot 1 and 4 in Figure 5.4b). In addition, there are some relatively smaller spherical particles which are rich in Si, P, K and Ca (see spot 2 and 3 in Figure 5.3a and Figure 5.4a). Besides the spherical particles, some flake-shaped particles are also observed in the cyclone ash (see spot 1 and 5 in Figure 5.3a). These particles typically have a high Si content (>90 wt%), which may explain the appearance of the particles, as the melting temperature of silicon oxide is considerably higher than that of K-silicates or K-Ca-silicates [126].

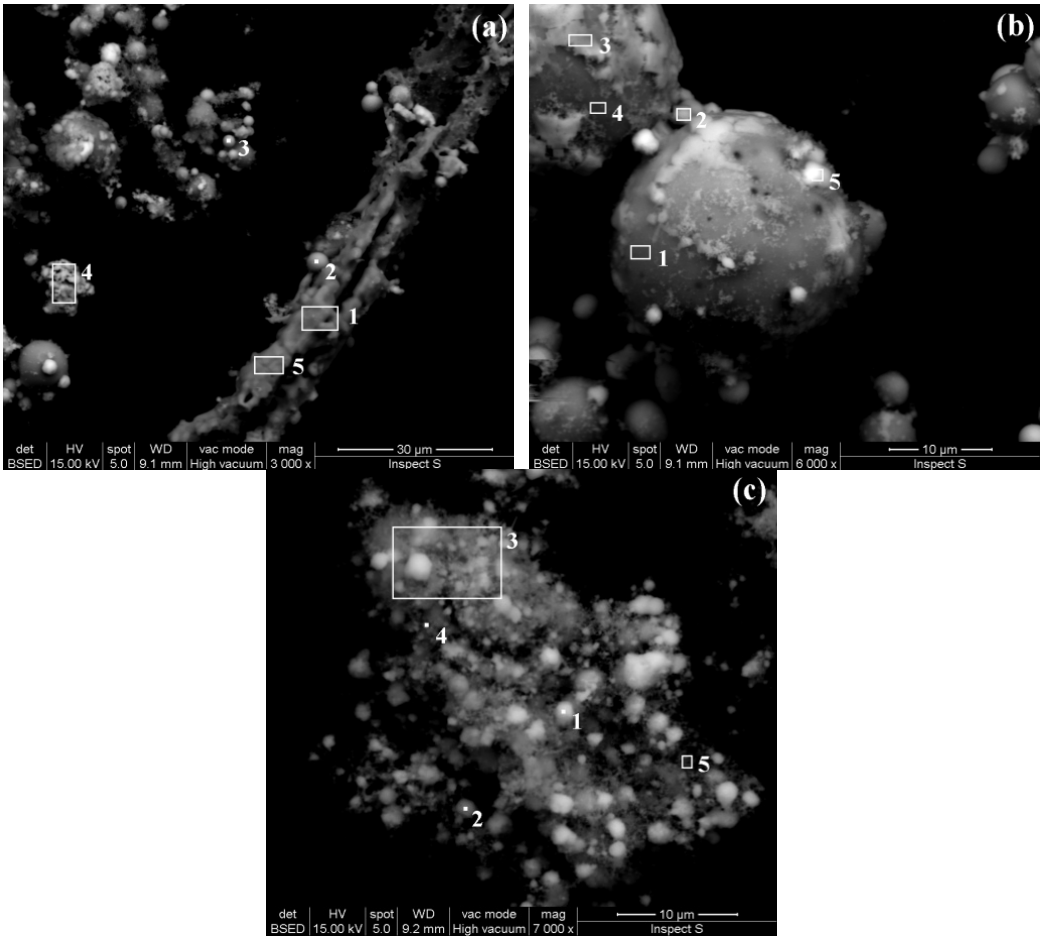

Figure 5.3 SEM pictures of the fly ash particles from dust-firing of straw, (a) and (b) are from the cyclone ash, and (c) is from the filter ash.

Compared to the cyclone ash shown in Figure 5.3a and Figure 5.3b, the morphology of the filter ash shown in Figure 5.3c is significantly different. The filter ash primarily consists of small and irregularly shaped particles, which are likely formed from the nucleation, condensation and aggregation of the vaporized inorganic species. The large particles seen in Figure 5.3c are probably a result of particle impaction in the filter, as the composition of the large particles is quite similar to that of small nucleates. As shown in Figure 5.4c, the composition of the filter ash is dominated by vaporized inorganic elements such as K, Cl, P and S, which supports its formation mechanism. Besides converting to filter ash, some of the vaporized inorganic species may also condense or attach to the existing ash particles, as illustrated by spot 2, 3 and 5 in Figure 5.3b and Figure 5.4b.

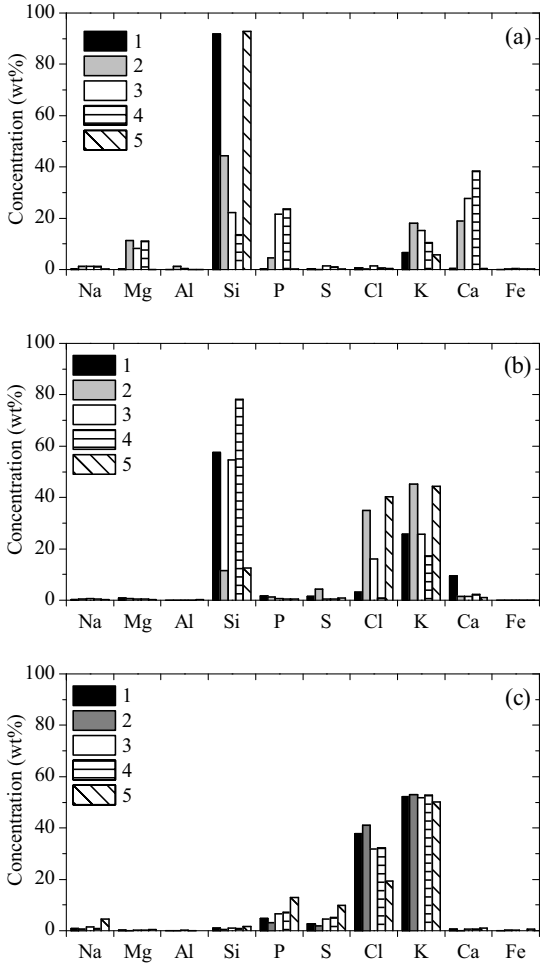

Figure 5.4 Inorganic compositions (i.e. the O and C content is neglected) of the spots shown in Figure 5.3.

5.3.1.3 Bulk ash composition

Figure 5.5 depicts the bulk composition of the bottom ash, the cyclone ash and the filter ash collected from straw dust-firing. For comparison, the fuel ash composition, which is calculated from the straw properties, is also shown. It can be seen that the bottom ash from straw dust-firing is dominated by Si, K and Ca. Compared with the fuel ash, the bottom ash is slightly enriched in Si, but depleted in Ca and K. The presence of S and Cl is almost negligible in the bottom ash, which may be explained by the high volatility of S and Cl during straw combustion.[167] The cyclone ash composition generally represents the fuel ash composition. Compared to the fuel ash, the volatile inorganic elements such as S, Cl, P, Na and K are slightly depleted in the cyclone ash, whereas the nonvolatile elements such as Si, Al, Fe, Ca and Mg are slightly increased. The filter ash primarily consists of the volatile inorganic elements K, Cl, S and P, which contribute to more than 90% of the inorganic elements in the filter ash. The composition of the filter ash obtained

from two repeating experiments is almost identical, which supports the reliability of the results. Both the composition and the morphology of the filter ash suggest that during straw-dust firing, the ash particles smaller than 2.5 μm are predominantly generated from vaporized inorganic elements. Since the composition of the filter ash obtained in this work is close to the composition of the aerosols from grate-firing of straw [207,241], the particle formation mechanism in the two cases is presumably quite similar. During grate-firing of straw, the formation of aerosols is considered to be initiated by the homogeneous nucleation of K_2SO_4, followed by the condensation of KCl and K_2SO_4 as well as coagulation [205,206]. This mechanism may greatly contribute to the formation of the filter ash obtained in this work. On the other hand, a small fraction of the filter ash, which contains relatively large content of the non-volatile elements such as Si and Al, may result from the small mineral particles present in the original straw or generated by the fragmentation of included or excluded minerals. In pulverized coal combustion, the fragmentation mechanism is found to be an important $PM_{2.5}$ formation mechanism [151]. However, in straw dust-firing, the contribution of this mechanism is limited to the formation of $PM_{2.5}$, as indicated by the composition of the collected filter ash.

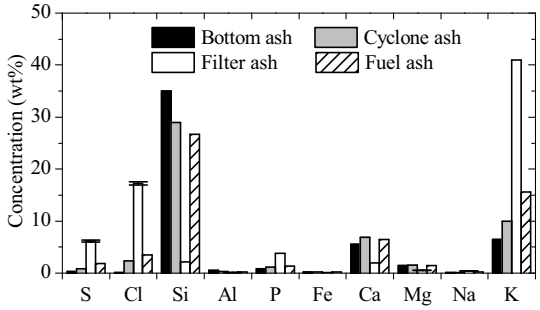

Figure 5.5 Bulk composition of the bottom ash, cyclone ash, filter ash and fuel ash during straw dust-firing, the error bars on the filter ash composition show the deviations of two repetition experiments.

Besides the bulk ash composition, a useful parameter to evaluate the deposition/corrosion potential of fly ash from straw dust-firing is the water soluble alkali concentration [99]. The water soluble alkalis, such as alkali chlorides, are normally more corrosive than water insoluble alkalis such as alkali silicates [140,261]. In the present work, the water soluble K and Na content in the cyclone ash has been analyzed, showing that about 53% of the K and 41% of the Na in the cyclone ash are water soluble. Besides, since the filter ash is dominated by volatile species such as Cl, S, P and K which normally form water soluble species, it is reasonable to assume that the alkalis in the filter ash are totally water soluble. With this assumption, the water soluble K and Na content in the fly ash can be calculated based on the ash composition shown in Figure 5.5 and the mass balance given in Figure 5.2. The calculation reveals that about 73% of K and 62% of Na in the fly ash from straw dust-firing are water soluble. The molar ratio of the (water soluble K+Na)/(Cl+2S+P) in the fly ash is about 0.98, suggesting the water soluble K and Na in the fly ash are most likely present as chlorides, sulphates and phosphates. The molar ratio of Cl/(water soluble K+Na) is about 0.46, indicating that approximately 46% of the water soluble alkalis in the fly ash may be alkali chlorides.

5.3.2 Effect of additives on straw dust-firing

5.3.2.1 Ash chemistry

Figure 5.6 shows the influence of kaolinite and SBE addition on the cyclone and filter ash composition during straw dust-firing. It is seen that the variation of the cyclone ash composition generally reflects the ash composition change in the fuel mixture. With the addition of kaolinite, the Al content in the cyclone ash is increased significantly, whereas the content of S, Cl, Ca, P and K is reduced because of the dilution effect. The decreasing effect on the S and Cl may be also associated with the chemical reactions between kaolinite and the vaporized S/Cl species, which release SO_2/HCl to the flue gas. Similar to kaolinite, the addition of SBE also reduces the content of S, Cl, Ca, P and K in the cyclone ash. The Si and Al content in the cyclone ash is increased with SBE addition, which reflects the difference in the ash composition of the SBE and straw.

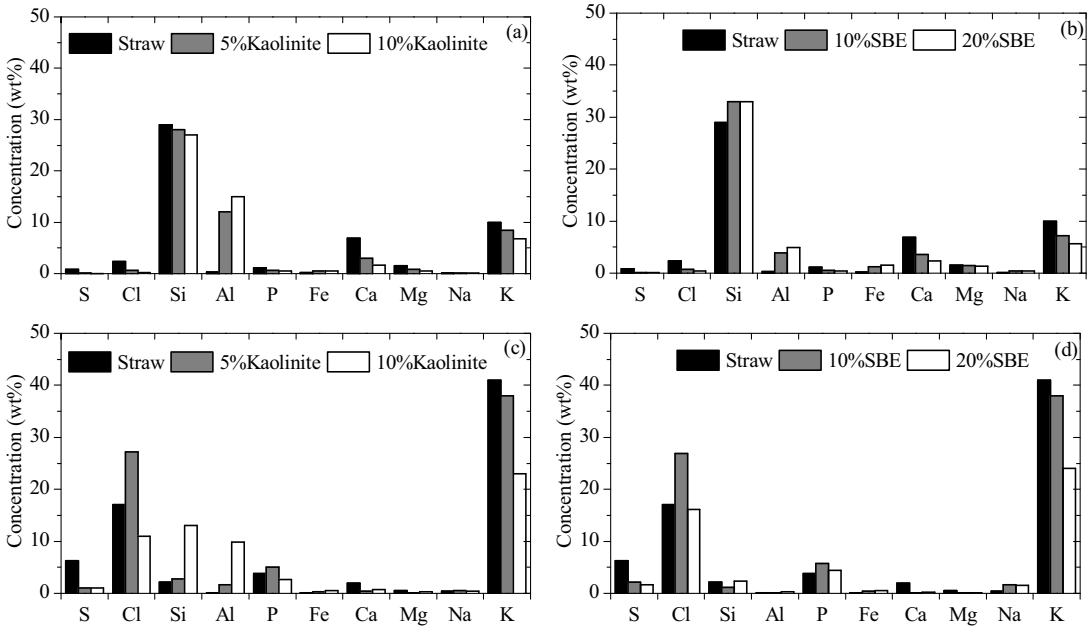

Figure 5.6. Influence of kaolinite and SBE addition on cyclone a) b) and filter ash c) d) composition.

Compared to the cyclone ash, the influence of kaolinite and SBE addition on the filter ash composition shows some different tendencies. With the addition of 5 wt% kaolinite, the S content in the filter ash is decreased compared to pure straw combustion, whereas the Cl content is increased. Similar tendency is observed with the addition of 10 wt% SBE. However, the increased Cl content does not necessarily mean that the formation of KCl is increased with the addition of 5 wt% kaolinite or 10 wt% SBE. During dedicated straw combustion, the collected filter ash contributes to about 10% of the fuel ash (see Figure 5.2), while this contribution becomes about 2.5% and 1.9% respectively during the addition of 5 wt% and 10 wt% SBE,

which is significantly beyond the dilution effect caused by these two additives. This indicates that the formation of KCl is actually decreased with the addition of 5 wt% kaolin or 10 wt% SBE. On the other hand, with the addition of 10% kaolinite, both the Cl and K content in the filter ash is decreased compared to 5% kaolinite addition, while the Si and Al content is increased. This suggests that a fraction of the kaolinite particles is partitioned to filter ash under this condition. The molar ratio of (K+Na)/(Cl+2S+P) in the filter ash from 10 wt% kaolinite addition is about 1.3, implying that part of the K and Na (about 25%) in the filter ash is probably presented as Na- or K-aluminosilicates. Compared to 10 wt% SBE addition, a considerable decrease of the Cl and K content is observed in the filter ash collected from 20 wt% SBE addition. Since an increase of other inorganic elements is not observed, it is likely that the decrease of Cl and K content is linked to an increased formation of soot/small residual carbon under this condition. For other experiments, the contribution of inorganic elements/oxides to the formation of the filter ash is generally rather consistent.

The results shown in Figure 5.6 indicate that the composition of fly ash may be affected both by the dilution effect of the additives or by chemical interactions. In order to better evaluate the chemical effect of kaolinite and SBE addition on the S partitioning, the percentage of fuel S emitted as SO_2 is calculated based on the measured SO_2 concentration in the flue gas. From Figure 5.7a, it can be seen that both the addition of kaolinite conversion of fuel S to SO_2. Since the presence of S is found to be negligible in the kaolinite (see Table 5.1), the results imply that the formation of alkali sulphates is inhibited. The inhibiting effect of kaolinite on alkali sulphate formation has been reported in other work [196]. It is likely that the added kaolinite has reacted with the KOH/KCl released from straw combustion [167], thereby reducing the sulphation reaction between gaseous alkali and SO_2/SO_3. In addition, the alkali sulphate may react with kaolinite directly and release SO_2 [186]. However, the formation of alkali sulphate in straw combustion is usually thermodynamically favored at temperatures lower than 1000 ^oC [210,329,330]. In the EFR, the residence time in the temperature range of 1300 ^oC – 600 ^oC (sampling point) is rather short (in an order of 0.1s). This indicates that the direct reaction between alkali sulphate and kaolinite probably is not important for the increased SO_2 formation observed in the present work. Therefore, the primary mechanism for the increased SO_2 formation is the reaction between the added kaolinite particles and the vaporized KOH/KCl. For different shares of kaolinite, the effect is particularly pronounced with the addition of 5 wt% kaolinite, as compared to pure straw combustion. However, when the kaolinite share is increased from 5 wt% to 10 wt%, the decreasing effect is only slightly promoted.

Similar to kaolinite, the addition of SBE increases the formation of SO_2. A possible reason is that part of the Si and Al in SBE reacts with the gaseous KOH/KCl released from straw combustion, forming stable K-silicates or K-aluminosilicates. Such reactions have been reported to be thermodynamically feasible, when straw is co-fired with a fuel with high Si and Al content [96,99,329]. As shown in Figure 5.7a, the conversion of fuel S to SO_2 is increased approximately from 24% to 49%, with the addition of 10 wt% SBE. By increasing the SBE addition to 20 wt%, the conversion of fuel S to SO_2 is increased further to about 71%. Through comparing the results from kaolinite and SBE addition, it appears that the effect of kaolinite is more significant than that of SBE, when applying the same molar ratio of K/(Al+Si) in fuel mixture, such as 5 wt% kaolinite versus 10 wt% SBE, or 10 wt% kaolinite versus 20 wt% SBE (see Table 5.2). However, when the molar ratio of K/(Al+Si) is around 0.10, i.e. 10 wt% kaolinite or 20 wt% SBE addition, the difference between the two additives becomes minor, as illustrated in Figure 5.7a.

In order to investigate the impact of kaolinite and SBE on the Cl partitioning, the percentage of fuel Cl retention in the ash is calculated for different experiments through a mass balance calculation. As shown in Figure 5.7b, the Cl retention in ash is reduced significantly with the addition of kaolinite/SBE. The results imply that a fraction of the alkali chlorides formed during straw combustion has reacted with the injected kaolinite/SBE particles, and releasing the Cl as gaseous HCl. The mechanism of the reactions between alkali chlorides and kaolinite has been studied extensively [107,177,179,182,191]. The results of the present work show that the addition of 5 wt% and 10 wt% kaolinite during dust-firing of straw decreases the Cl retention in ash by approximately 55% and 82%, respectively. Compared to kaolinite, the effect of SBE is less pronounced, when the molar ratio of K/(Al+Si) is similar in the fuel mixture. With the addition of 10 wt% and 20 wt% SBE, the Cl retention in ash during straw dust-firing is reduced by about 39% and 67%, respectively. The observed relatively lower reactivity of SBE may be linked both to the physical characteristics and the surface reaction kinetics of kaolinite and SBE. According to the particle size distribution shown in Figure 5.1, the kaolinite particles are much smaller than the SBE particles. Thus, the kaolinite particles likely have larger specific surface area and less transport limitations than the SBE particles, which are favorable for gas-solid reactions. Besides, the surface reaction rate between the gaseous alkali and kaolinite may be greater than that of SBE. It has been reported that the surface reaction rate of kaolinite was much higher than that of silicon oxide, when reacting with alkali chlorides [107,163,331]. Since the SBE used in the present work is dominated by Si, it is possible that the surface reaction rate between SBE and alkali species is slower than that of kaolinite.

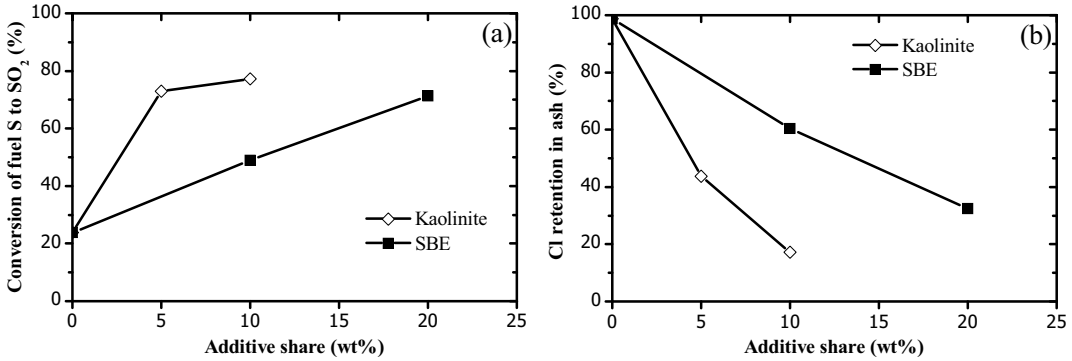

Figure 5.7. (a) Conversion of fuel S to SO_2 (%) during the addition of kaolinite or SBE, (b) Cl retention in ash (%) during the addition of kaolinite or SBE.

The influence of kaolinite and SBE addition on the partitioning of alkali species is assessed by calculating the fraction of water soluble K and Na in the fly ash. The calculation is based on the analyzed water soluble alkali content in cyclone ash and the assumption that the alkali species in the filter ash are fully water soluble. The results are presented in Figure 5.8. It can be seen that the addition of kaolinite and SBE both reduce the percentage of K/Na present as water soluble form in fly ash. This indicates that the formation of water insoluble alkalis, such as alkali aluminosilicates or alkali silicates, is promoted by kaolinite and SBE addition. With the addition of 5 wt% and 10 wt% kaolinite, the percentage of K present as water soluble form in the fly ash is reduced by approximately 62% and 78%, respectively, in comparison with that of pure straw

combustion. With the addition of 10 wt% and 20 wt% SBE, the percentage of water soluble K present in the fly ash is decreased by about 49% and 71%, respectively. At similar molar ratios of K/(Al+Si) in the fuel mixture, the decreasing effect of kaolinite is more significant than that of SBE, which is conceivably linked to the different physical characteristics and surface reaction kinetics of the two additives, as discussed earlier. On the other hand, the decreasing effect of kaolinite and SBE addition on the percentage of water soluble K may be partly related to the K present in kaolinite and SBE, which can be rather stable and difficult to vaporize during combustion. For 5 wt% kaolinite or 10 wt% SBE addition, the K in the additive may at maximum contribute to 10% of the K in fly ash. This implies that the chemical reactions would still play a dominant role on the reduction of water soluble K under these conditions. However, for 10 wt% kaolinite or 20 wt% SBE addition, the K in the additives may contribute to maximum 20% of the K in fly ash. Thus the observed further reduction on water soluble K, when the addition of kaolinite is increased from 5 wt% to 10 wt% (or the addition of SBE is increased from 10 wt% to 20 wt%) , may be primarily due to the stable K presented in the kaolinite/SBE, rather than promoted chemical reactions. In order to interpret the results shown in Figure 5.8 better, a detailed analysis of the association and release of K in SBE/kaolinite is needed, which is outside the scope of this work.

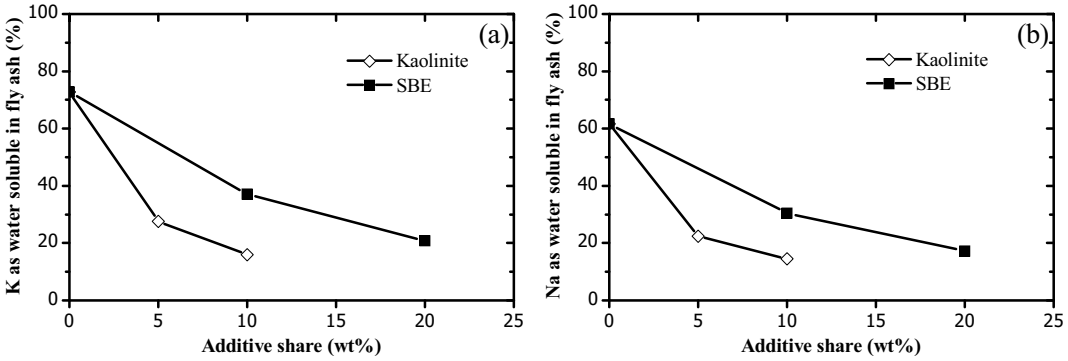

Figure 5.8 (a) Percentage of K present as water soluble form in fly ash, (b) percentage of Na present as water soluble form in fly ash.

The behavior of Na is quite similar to that of K. However, the percentage of Na present in water soluble form is generally lower than that of K. This may imply that the formation of Na aluminosilicates or silicates may be more favorable than that of K, which seems to be in agreement with the observations in literature [146,286]. On the other hand, as shown in Table 5.1, the SBE has much higher Na content than that of straw, which can contribute to about 90% of the Na in fuel mixture during 20 wt% SBE addition. Thus the observed behavior of water soluble Na during SBE addition may be greatly influenced by the release of Na from SBE, which requires further investigations. For kaolinite addition, the Na in kaolinite would not play a significant role, thus the observed results are mainly attributed to chemical reactions.

One should be aware that the results shown in Figure 5.8 are obtained by assuming all of the alkali in the filter ash is water soluble. This assumption may not be appropriate for 10 wt% kaolinite addition, as indicated by the filter composition shown in Figure 5.6. As mentioned previously, the Na-/K-aluminosilicates may contribute to 25% of the alkali in the filter ash under this condition. Therefore, the actual amount of the water soluble alkali during 10 wt% kaolinite would probably be lower than that shown in Figure 5.8.

In general, the results present in Figure 5.7, and Figure 5.8 demonstrate that the injected SBE particles have reacted with the gaseous alkali released from straw combustion, resulting in a reduced Cl retention in ash, increased SO_2 emission, and decreased formation of water soluble alkalis. According to the Cl retention in the ash shown in Figure 5.7b, it seems that the addition of 10 wt% and 20 wt% SBE could reduce the alkali chloride formation in straw dust-firing by about 39% and 67%, respectively. Although the effect of SBE addition is slightly less significant, it is still comparable to the effect of kaolinite addition at similar molar ratio of K/(Al+Si) in the fuel mixture.

5.3.2.2 Ash deposition

In order to evaluate the influence of the additives on deposit formation in the convective part of a straw dust-firing boiler, deposits are collected during the EFR experiments by using an air-cooled deposit probe. The deposition flux obtained from the experiments is shown in Figure 5.9a. It can be seen that the deposition flux increases with the addition of SBE. This is probably linked to the high ash content in the SBE, which has significantly increased the ash flux towards the probe. The reliability of the results of deposition flux is reflected by the small deviations of the repetition experiments performed on pure straw combustion and co-combustion of straw and 10 wt% SBE. For kaolinite addition, the deposition flux is decreased compared to pure straw combustion.

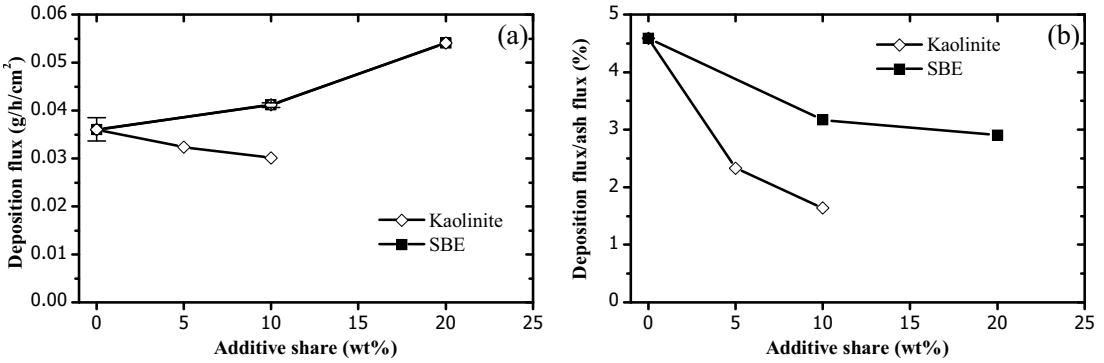

Figure 5.9 (a) Deposition flux (g/h/cm^2) during the EFR experiments with kaolinite and SBE addition, the error bars indicate the deviations of two repetition experiments (b) deposition flux/ash flux (%) during the EFR experiments with kaolinite and SBE addition.

The deposition flux is divided by the calculated ash flux towards the probe in order to calculate the relative deposit flux. The parameter, deposition flux/ash flux (%), is used to evaluate the deposition propensity of the fly ash. As shown in Figure 5.9b, the addition of SBE and kaolinite both reduce the ash deposition propensity considerably. With the addition of 5 wt% and 10 wt% kaolinite, the ash deposition propensity is decreased by about 49% and 64%, respectively. It is known that the main ash deposition mechanisms are inertial impaction, thermophoresis and condensation [244]. In the present work, the deposits formed by inertial impaction would dominate the deposit mass. Therefore, the decreased ash deposition propensity during kaolinite addition indicates that deposits formed by inertial impaction of fly ash particles will be reduced. This is most likely due to the smaller alkali chloride concentrations in the flue gas, caused by the injection of kaolinite particles. With depleted alkali chloride condensation, the stickiness of the

fly ash particles and deposits would be reduced significantly, thus lowering the ash deposition propensity. A similar explanation may be applied for the decreased ash deposition propensity during SBE addition. However, the observed ash deposition propensity during SBE addition is generally larger than that of kaolinite addition. This is partly because of the kaolinite particles may react with gaseous alkali chlorides more effectively than the SBE particles, as discussed previously. In addition, the reaction between kaolinite and alkali chlorides may form alkali-aluminosilicates with high melting temperature, whereas the reaction between SBE and alkali chlorides may result in alkali silicates with a lower melting temperature.

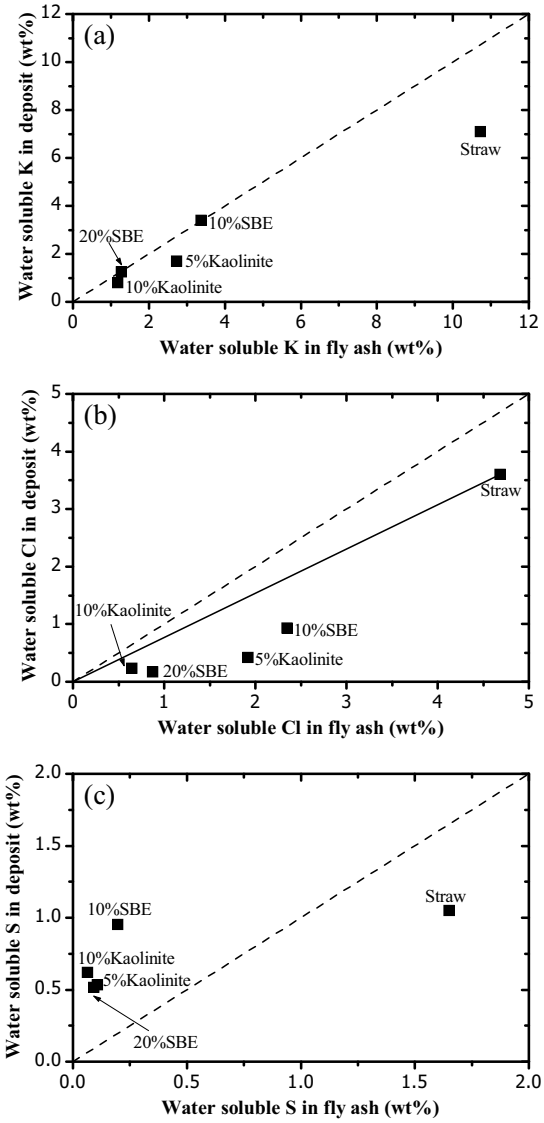

Figure 5.10. (a) Content of water soluble K in deposit and fly ash, (b) content of water soluble Cl in deposit and fly ash, (c) content of water soluble S in deposit and fly ash, the error bars indicate the deposit composition deviations of two repetition experiments on pure straw combustion.

The content of water soluble K, S and Cl in the collected deposits is analyzed and compared with that of the fly ash. It can be seen in Figure 5.10a that the water soluble K content in the deposits is reduced considerably with the addition of kaolinite/SBE, which is likely a result of both the dilution effect of kaolinite/SBE ash and the chemical effects discussed previously. During straw dust-firing, the water soluble K content in the deposits is found to be lower than that of the fly ash. This may be explained by the deposition mechanisms of the water soluble K species. During straw combustion, the majority of the water soluble K species found in fly ash, such as KCl and K_2SO_4, will be present as vapor or small nucleates in the flue gas. Therefore, the predominant deposition mechanisms for these species will be thermophoresis and condensation. However, the contribution of these mechanisms to the mass growth of deposit is minor, and decreases quickly with time due to the decrease of temperature gradient between flue gas and deposit surface.[332] Therefore, the deposition propensity of the water soluble K species is presumably lower than that of the larger Si rich fly ash particles for which the inertial impaction is the main deposition mechanism. This could be an explanation to the lower concentration of water soluble K in the deposit as compared to the fly ash. With the addition of SBE and kaolinite, it seems that the content of water soluble K in deposits becomes closer to that of fly ash. This may be due to the fact that the addition of SBE and kaolinite increases the concentration of large fly ash particles, which may promote the condensation of the water soluble K species on the large fly ash particles. In this way, the difference between the water soluble K content in fly ash and deposition becomes smaller. The effect is particularly pronounced with SBE addition, as shown in Figure 5.10a.

Figure 5.10b shows the water soluble Cl content in the fly ash and deposit collected from different experiments. Since the water soluble Cl content in the fly ash is found to be almost identical as the total Cl content, the results shown in Figure 5.10b can be read as the total Cl contents in fly ash and deposit. It is seen that the Cl content in the deposit is decreased significantly with the addition of kaolinite or SBE, which is related both to the dilution effect of the ash by the additives as well as the chemical reactions between gaseous alkali chlorides and the additives. With the addition of 10 wt% SBE and 20 wt% SBE, the Cl content in the deposit is decreased by approximately 74% and 95%, respectively. This implies that the corrosion potential of the deposits will be significantly reduced [140,261]. Compared to 10 wt% SBE addition, 5 wt% kaolinite addition seems to reduce the Cl content in the deposits more effectively. However, the reduction efficiency of 20 wt% SBE addition seems to be slightly higher than that of 10 wt% kaolinite addition.

The Cl content in the deposits is generally found to be lower than that of the fly ash. This is partly linked to the deposition mechanism of alkali chlorides, which has been explained previously. However, another reason is that a condensed phase sulphation takes place after the deposition of the alkali chlorides. This reaction, which has been found to be significant at temperatures above 750 ^{o}C, releases the deposited Cl as gaseous HCl [204]. Compared to pure straw combustion, the difference between the Cl contents of the deposits and the fly ash seems to become larger during the addition of kaolinite/SBE. This presumably because that the extent of the condensed phase sulphation reaction is higher when straw is mixed with additives. The measured SO_2 concentration in pure straw combustion is 23 ppmv (6% O_2, dry). However, with the addition of 10 wt% and 20 wt% SBE, the SO_2 concentration in the flue gas becomes 54 ppmv and 83 ppmv, respectively. The increased SO_2 concentration during SBE addition is linked to the larger S content in SBE. In addition, the relatively large Si content in SBE may inhibit the

gaseous sulphation reaction and thereby reduce the formation of sulphates, as illustrated in Figure 5.7a.

The influence of additives on the water soluble S content in the deposit is illustrated in Figure 5.10c. In general, the water soluble S content is decreased with the addition of additives, although the reducing effect is not as significant as that of water soluble K and Cl. This is partially due to the presence of condensed phase sulphation reaction, which is clearly demonstrated by the higher water soluble S content in the deposit than that of fly ash. However, for pure straw combustion, the water soluble S content in the fly ash seems to be larger than that in deposits. This may be explained by two reasons. Firstly, as discussed previously, the main deposition mechanisms for water soluble S species are likely to be condensation and thermophoresis, which will conceivably result in a reduced deposition propensity of the S species. Secondly, the extent of the sulphation reaction is probably quite limited during pure straw combustion, due to the low SO_2 concentration in the flue gas.

The results shown in Figure 5.9 and Figure 5.10 indicate that the addition of SBE can effectively decrease the Cl content in deposits, both through dilution and chemical reactions. Therefore, the corrosion potential of superheaters will be greatly decreased with the addition of SBE. Another advantage regarding corrosion is that the addition of SBE increases the SO_2 concentration in the flue gas, which can promote gas phase sulphation. However, the ash deposition rate on superheaters may be slightly increased with SBE addition. Although the ash deposition propensity is reduced by SBE addition, the fly ash concentration in the flue gas is significantly increased. In addition, the melting temperature of the fly ash from SBE addition may be lower than that from kaolinite addition. Therefore, it is important to characterize the melting behavior of the fly ash in order to assess the influence on deposit sintering and slagging formation. However, this is outside the scope of the present work.

5.4 Conclusion

Straw dust-firing experiment was carried out in an entrained flow reactor. For the straw used in the present work, the Cl was almost totally partitioned to fly ash, with negligible Cl present in bottom ash or in the flue gas. The morphology and composition of the fly ash from straw dust-firing indicated that the large fly ash particles (>~2.5 μm) were primarily molten or partial-molten spherical particles rich in K, Si and Ca, supplemented by some Si-rich flake-shaped particles. The finer fly ash particles (<~2.5 μm) were predominantly formed from nucleation followed by condensation and coagulation of the vaporized K, Cl, S and P species. Approximately 70% of the K in fly ash was found to be water soluble, and KCl was estimated to contribute to more than 40% of the water soluble K. The results indicated a high deposition and corrosion potential of the fly ash from straw dust-firing.

The influence of two additives (spent bleaching earth (SBE) and kaolinite) on the ash chemistry and deposit formation during straw dust-firing was investigated and compared. It was shown that the SBE could react with the gaseous alkali released from straw combustion, resulting in reduced Cl retention in fly ash, increased SO_2 emission, and decreased formation of water soluble alkalis. For the addition of 10 wt% and 20 wt% SBE, the alkali chloride formation in straw dust-firing was estimated to be reduced by about 39% and 67%, respectively, based on the obtained Cl retention results. With similar molar ratio of K/(Al+Si) in the fuel mixture, the reducing effect of

kaolinite on alkali chloride formation was only slightly more pronounced than that of SBE. The Cl content in the deposits was decreased significantly with the addition of SBE, both due to a dilution effect and chemical reactions. With the addition of 10 wt% and 20 wt% SBE, the Cl content in deposit was decreased by about 74% and 95%, respectively, indicating that the corrosion potential of the superheaters could be greatly reduced with the addition of SBE. Compared to pure straw combustion, the ash deposition propensity was reduced by SBE addition. However, the ash deposition rate was increased, primarily due to the significantly larger fly ash concentration in flue gas.

Based on the present work, it is suggested that SBE is a promising additive for straw dust-firing. Besides the identified effect on ash chemistry and deposition behavior, the SBE is characterized by high heating value, cheap price, negligible trace element concentration, and small particle size, which are favorable both from a technical and an economical point of view.

Acknowledgement

The work is part of the CHEC (Combustion and Harmful Emission Control) Research Center. The present work is sponsored by The Technical University of Denmark (DTU), ENERGINET.DK, BiofuelsGS-2 (Nordic Graduate School in Biofuel Science and Technolog-2), and The Danish Strategic Research Council (GREEN). We thank Aarhus Karlshamn AB for provide the spent bleaching earth. DONG Energy Power A/S is acknowledged for the fuel/ash analysis at Enstedværket Laboratory. DTU CEN is thanked for the helps in SEM-EDS analysis.

6 Release and Transformation of Inorganic Elements in the Combustion of a Residual Bran

Abstract

The release and transformation of inorganic elements during grate-firing of bran was studied via experiments in a laboratory-scale reactor, analyses of the fly ash from a grate-fired plant, and equilibrium modelling. It was found that K, P, S, and to a lesser extent Cl and Na were released to the gas phase during bran combustion. Laboratory-scale experiments showed that S was almost fully vaporized during pyrolysis below 700 ^{o}C. 60–70% of the K and P in bran were released during combustion, in a temperature range of 900–1100 ^{o}C. The release of K and P was attributed to the vaporization of KPO_3 generated from thermal decomposition of inositol phosphates, which were considered as a major source of P and K in the bran. The influence of additives such as $CaCO_3$, $Ca(OH)_2$, and kaolinite on the release was also investigated. Ca-based additives generally increased the molar ratio of the released K/P, whereas kaolinite showed an opposite effect. Thermodynamic modelling indicated that the fly ash chemistry is sensitive to the molar ratio of the released K/P. When the molar ratio of the released K/P was below 1, KPO_3 and P_4O_{10} (g) were the main stable K and P species at temperatures higher than 500 ^{o}C. Below 500 ^{o}C, the KPO_3 and P_4O_{10} (g) may be converted to H_3PO_4 (l), which may cause severe deposit build-up in the economizers of a grate-fired boiler. By increasing the molar ratio of the released K/P to above 2, the equilibrium distribution of the K and P species was significantly changed and the formation of H_3PO_4 (l) was not predicted by thermodynamic modelling.

6.1 Introduction

Utilization of biomass and biomass-derived waste materials in heat and power production plants is an important approach to reduce fossil fuel consumption and thereby the CO_2 level in the atmosphere. Seed-originated biofuels constitute a special type of biofuels which is usually characterized by a significantly higher P content than other biofuels [26,115-117,324,333,334]. Typical examples are grain from wheat, oat or other biomass [115,116,334], bran from wheat or rice [335], and rapeseed meal/cake which is a residue from rapeseed methyl ester (biodiesel) production [117-119,333]. In northern European countries, utilization of P-rich biofuels in grate-fired or fluidized bed combustion systems has gained interest in recent years [116-119,230,324,333]. The main driving force is the target of achieving a 20% renewable energy share in the EU by the year of 2020 [313], and the potential economical benefits from the possible low price of these biofuels [324,333].

Combustion of high-P biofuels may induce ash related problems in boilers, such as bed agglomeration [117], slagging [115,117], fouling [117], corrosion [324], fine particle emission [116], and deactivation of the SCR units [217,336]. These problems are linked to the high P and K content in these biofuels [115-117,324,333]. During combustion, part of the P and K is released and involve in complicated gas-gas and/or gas-solid reactions with other ash forming elements such as S, Cl, Ca, Mg, Si and Al. These transformations may generate K-phosphates with low melting temperature (such as KPO_3) and lead to bed agglomeration, slagging, and fouling problems [115,117]. On the other hand, some phosphorus compounds (such as Ca-phosphates) may mitigate ash deposition and corrosion in boilers, by forming ash species with high melting temperature and by converting the alkali chlorides to alkali-calcium phosphates and HCl(g) [169]. In order to better understand and minimize the ash related problems occurring during combustion of P-rich biofuels, a systematic study on the ash release and transformation mechanisms related to these fuels was conducted.

The aim of the present chapter was to characterize the release and transformation of inorganic elements during grate-firing of a residual bran from bio-ethanol production. This was achieved by multiple approaches. The association of P and other inorganic elements in bran was assessed through a literature review and SEM-EDS (scanning electron microscopy and electron dispersive X-rays spectroscopy) analysis. The release of inorganic elements was studied by conducting experiments in a horizontal tube reactor and by comparing with full-scale data obtained from a grate-fired plant. In addition to pure bran combustion, the effect of different additives such as $CaCO_3$, $Ca(OH)_2$, kaolinite and $MgCO_3$ were also investigated. In order to interpret the observed release behavior, the bran ash and a typical phosphorus compound, which might appear in ash, were characterized by an STA (simultaneous thermal analyzer) and by high-temperature oven experiments. The transformation of the vaporized inorganic elements at different release conditions was investigated by thermodynamic modeling.

6.2 Experimental

6.2.1 Fuel Characterization

Table 6.1 Chemical composition of the bran

Properties	Bran	Properties	Bran
Moisture (wt%)	8.22	P (wt% dry)	1.1
Ash (wt% dry)	5.3	Si (wt% dry)	0.13
C (wt% dry)	45	Mg (wt% dry)	0.38
H (wt% dry)	6.3	Ca (wt% dry)	0.092
O (wt% dry)	42.75	Al (wt% dry)	0.008
N (wt% dry)	2.65	Fe (wt% dry)	0.021
S (wt% dry)	0.19	Ti (wt% dry)	-
Cl (wt% dry)	0.071	Mn (wt% dry)	-
K (wt% dry)	1.3	Na (wt% dry)	0.005

Residual bran from bio-ethanol production is used as the fuel in a grate-fired plant in a European country. The chemical composition of the bran was analyzed by ICP-OES (inductively coupled

plasma-optical emission spectroscopy). As shown in Table 6.1, K, P and Mg are the dominant inorganic elements. The P content is significantly higher than of other biofuels such as straw [99] and wood [117], but is comparable with that of P-rich biofuels such as rapeseed cake [117] and oat grain [116]. The molar ratio of K/P in the bran is 0.94, which is within the range (~0.8–1.0) reported for other P-rich biofuels [115-117,119]. Other important inorganic elements in the bran are S, Si, Ca and Cl. The N content in the bran is about 2.2 wt%, which is much larger than that of other biofuels such as straw [99] and wood [117], probably due to the high protein content in the seed of biomass [337]. The particle size distribution of the bran was characterized by a laser diffraction method (Malvern Mastersizer 2000 particle size analyzer), showing that the d_{50} (meaning that 50 vol% of the particle are below this size) of the bran is about 230 μm.

6.2.2 Additives

Additives were used in the experiments in order to study their influence on the release of inorganic elements during bran combustion. The applied additives were $CaCO_3$, $Ca(OH)_2$, kaolinite, and $MgCO_3$. The $CaCO_3$ had a purity above 97% and particle size below 125 μm. The $Ca(OH)_2$ and $MgCO_3$ were powdery pure compounds. The d_{50} of the $Ca(OH)_2$ particles was about 3 μm and all of the particles were below 60 μm. The kaolinite was a powdery pure compound, with measured d_{50} about 8 μm.

6.2.3 Laboratory-Scale Release Experiments

Experiments were carried out in a horizontal tube reactor. The release was quantified by a mass balance calculation based on weight measurement and chemical analysis of the raw fuel and residual ash from the experiment. The details regarding the experimental setup and mass balance calculation can be found elsewhere [128,170]. A schematic drawing of the reactor is shown in Figure 6.1

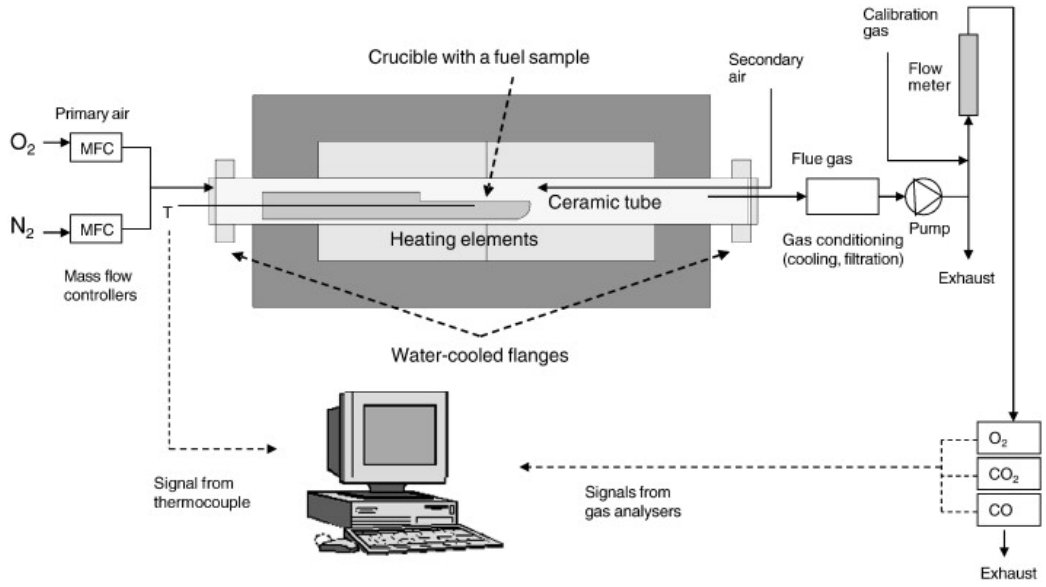

Figure 6.1 Schematic drawing of the horizontal tube reactor [172] .

During the experiment, the tube reactor was preheated to a desired temperature. A platinum/alumina boat with 5–10 g sample was then inserted in the reactor. A primary gas (5 Nl/min, 100% N_2) was added to create a pyrolysing condition for the sample, and downstream a secondary gas (5 Nl/min, 20% O_2) was injected to combust the volatiles released during pyrolysis. This pyrolysing condition was created in order to simulate the combustion in a grate-fired system, where the devolatilization and char oxidation may primarily take place in different zones. In addition, it can also minimize the temperature overshoot that may be caused by volatile oxidation. After placing the sample at pyrolysing condition for 60 min, 1% of O_2 was introduced to primary gas, and the O_2 content in primary gas was increased stepwise to 20% in order to minimize the temperature overshoot during char combustion [170]. The maximum temperature overshoot was measured to be 50 ^oC during the experiments, by inserting a thermalcouple into the fuel bed. After a total experimental period of 200 min, the boat was removed from the reactor and cooled down to room temperature in a N_2 environment. The weight of the residual ash was measured and the chemical composition was analyzed by ICP-OES. For the experiments carried out at pyrolysing condition, the primary gas was maintained as N_2 for a total experimental duration of 180 min. The combustion/pyrolysis experiments at different conditions were repeated several times, and the reproducibility was found to be satisfactory by comparing the quantity of residual ash/char.

Table 6.2 Experimental matrix of the release experiments in the horizontal tube reactor

Experiment number	Sample	Experiment condition	Temperature (^oC)	Molar ratio in the fuel				
				K/P	Ca/P	Mg/P	K/Si	K/(Cl+2S)
1	Bran	Pyrolysis	300	0.94	0.06	0.45	7.18	2.4
2	Bran	Pyrolysis	500	0.94	0.06	0.45	7.18	2.4
3	Bran	Pyrolysis	700	0.94	0.06	0.45	7.18	2.4
4	Bran	Pyrolysis	900	0.94	0.06	0.45	7.18	2.4
5	Bran	Combustion	500	0.94	0.06	0.45	7.18	2.4
6	Bran	Combustion	700	0.94	0.06	0.45	7.18	2.4
7*	Bran	Combustion	900	0.94	0.06	0.45	7.18	2.4
8	Bran	Combustion	1100	0.94	0.06	0.45	7.18	2.4
9	Bran+2wt%$CaCO_3$	Combustion	1100	0.94	0.69	0.45	7.18	2.4
10	Bran+5wt%$CaCO_3$	Combustion	1100	0.94	1.68	0.45	7.18	2.4
11	Bran+3.75wt%$Ca(OH)_2$	Combustion	1100	0.94	1.67	0.45	7.18	2.4
12	Bran+5wt% kaolinite	Combustion	1100	0.99	0.07	0.46	0.69	2.53
13	Bran+3.18wt%$MgCO_3$	Combustion	1100	0.94	0.06	1.56	7.18	2.4

* Chemical analysis has not been performed as the residue ash cannot be totally removed from the boat.

The experimental matrix is shown in Table 6.2. The combustion and pyrolysis experiments of pure bran were carried out at temperatures from 300 ^oC to 1100 ^oC. The effect of different additives ($CaCO_3$, $Ca(OH)_2$, kaolinite and $MgCO_3$) on the release of inorganic elements during bran combustion was studied at 1100 ^oC. During the additive experiments, the bran was well-mixed with the additive in a mortar. The properties of the bran and additives were described previously. For comparison, some molar ratios of the inorganic elements in the fuel mixture were calculated and listed in Table 6.2.

6.2.4 Full-Scale Tests

The bran used in the present work was obtained from a full-scale plant, where it was combusted on a grate. The hot flue gas from the boiler chamber subsequently passed through the superheaters and economizers to produce heat and power. Downstream of the economizers, baghouse filters were installed to remove the fly ash particles from flue gas. In order to reduce the emissions of SO_2 and HCl, $NaHCO_3$ particles were injected before the baghouse filters.

The plant was initially operated with pure bran. However, after successful operation of a few months, the baghouse filters were found to be blocked by "sintered" fly ash, which could not be removed by pressurized air and hindered the continuous operation of the plant. In addition, severe ash deposition was observed in the economizers of the plant, with flue gas temperate of ~380–180 ^oC. In order to minimize these problems, the plant was operated with the addition of 5–8 wt% $CaCO_3$. It appeared that the baghouse filter problem was mitigated by addition of $CaCO_3$ and by changing the operational condition of the filter, whereas the ash deposition problem in the economizers still appeared occasionally.

A large number of fly ash samples were collected from the plant and the composition of these were analyzed by SEM-EDS. The fly ash samples were collected during an operation period of more than a year, both with and without $CaCO_3$ addition. It should be noted that the composition of the bran used on the grate-fired plant varied over time, and often deviated from that shown in Table 6.1. In addition, the $CaCO_3$ applied in the plant was also different from that used in laboratory experiment. Due to these factors, the full-scale results can only be compared with the results from laboratory-scale experiments qualitatively.

6.2.5 Characterization of the ash/compound thermal behavior

A simultaneous thermal analyzer (STA, Netzsch 449 F1) was applied to study the thermal behavior of KH_2PO_4, which is considered to be a P and K containing compound that may be formed during bran combustion. The STA was operated at 5% O_2 in N_2. During the test, approximately 5 mg of the KH_2PO_4 was placed in a Pt-Rh crucible, and the crucible was heated from 25 ^oC to 1400 ^oC at a rate of 10 ^oC/min. Both the TG (thermogravimetric) and DSC (differential scanning calorimetry) curves were obtained from the STA analysis. The TG curve shows the continuous sample mass loss during heat-up, whereas the DSC curve gives a continuous measurement of the heat flow in the sample as a function of temperature.

A mixture of $CaCO_3$ and bran ash produced in the horizontal tube reactor at 700 ^oC was also tested in the STA. The Ca/P molar ratio in the mixture was controlled to be 1.68, similar to the condition of Exp. 10 and 11 in Table 6.2. The STA was operated at 5% O_2. During the test, the mixture was heated from 25 ^oC to 1100 ^oC at a rate of 10 ^oC/min, and then kept at 1100 ^oC for 6 h. In order to study the possible interactions between the bran ash and $CaCO_3$, the experimental weight loss of the mixture was compared with the weight loss calculated from the pure components tested at the same conditions,

Furthermore, a high temperature oven was applied to study the reactions between KH_2PO_4 and $Ca(OH)_2$. During the test, KH_2PO_4 and $Ca(OH)_2$ were mixed in a molar ratio of 1:1, and the mixture was heated from room temperature to 1500 ^oC at a rate of 10 ^oC/min. In order to identify the possible reactions between KH_2PO_4 and $Ca(OH)_2$, the obtained mass loss of the mixture was compared with that estimated from the pure compounds.

6.3 Results and discussions

6.3.1 Release of inorganic elements in bran combustion

6.3.1.1 *Association of inorganic elements in high-phosphorus biofuels*

In order to evaluate the association of inorganic elements in biofuels, a widely used approach is the chemical fractionation method, which was originally developed for coal[124] and further modified for biomass[127]. In the chemical fractionation method, the fuel is leached subsequently in different solutions (water, 1 M ammonium acetate, and 1 M hydrochloric acid), and the ash forming elements in the solutions as well as in the residue are analyzed in order to quantify the associations of these elements [127,131]. This method has been applied to study the association of inorganic elements in a rapeseed cake [117], which is a typical high-P biofuel. It revealed that approximately 70% of the P in the rapeseed cake was water/ammonium acetate soluble, whereas the remaining P was HCl soluble. For K, the water/ammonium acetate soluble comprised more than 90 % of the total K in the fuel. Similar tendencies were also seen for Cl, Na and Mg, indicating that the majority of P, K, Cl, Na and Mg in the rapeseed cake may exist as water soluble and/or organically bounded elements. For S, a certain fraction (~30%) was found to be present in the solid residue. This fraction of S might be covalently bonded to the organic structure of the fuel, and might be released to gas phase during combustion [117,118]. The majority of Ca in the rapeseed cake was ammonium acetate/HCl soluble, implying that the Ca might be associated with carboxylic groups or exist as calcium oxalate (CaC_2O_4) [117].

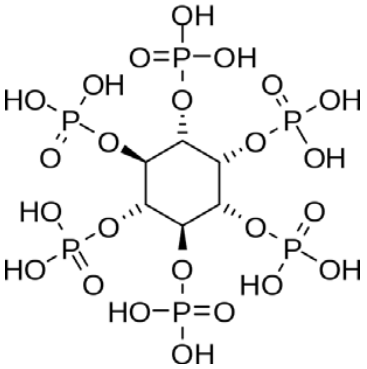

Figure 6.2 Chemical structure of phytic acid (also known as inositol hexakiphosphate or Ins P6).

Apart from the chemical fractionation method, the association of P in seed-originated biomass such as rapeseed meal, grains and bran has been investigated extensively in biological studies [337-342]. These studies generally suggest that the majority of P in seed-originated biomass is present as phytic acid (see the chemical structure in Figure 6.2) or phytate if the phytic acid is combined with inorganic elements such as K, Mg and Ca. It was reported that phytic acid/phytate represented approximately 75±10% of the total P in a seed, and the contribution could be greater than 90% in a mature seed [342]. An investigation carried out on a buckwheat bran showed that 60-92% of the total P in the bran was present as phytic acid/phytate [337]. For a rapeseed meal, it was reported that about 69% of the total P in the biomass was present as

inositol phosphates, and the phytic acid/phytate comprised of 64% of the inositol phosphates [338]. Phytic acid is a strong chelating agent which can form complexes with mineral cations such as K, Mg, Ca and Zn [337,343], and the formed phytate is the major storage of P, K and Mg in seeds [337]. Minerals that are associated as phytate are normally rather stable and poorly soluble at the pH of gastrointestinal tract [340]. The thermal stabilities of some solid state complexes of phytic acid with Mn, Co, Ni, Cu, Zn and Sn were investigated in a thermogravimetric analyzer (TGA) [343]. When the complexes were heated in air to 900 ^{o}C, the main thermal decomposition steps were found to be the loss of moisture, the decomposition of the aliphatic ring, and the loss of C_6H_6 due to combustion. The P in the complexes was not released during the thermal decomposition up to 900 ^{o}C, due to the formation of stable phosphates [343].

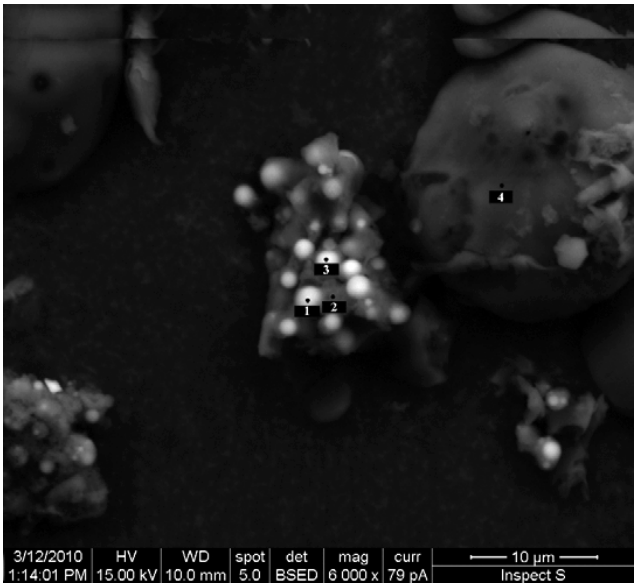

Spectrum	C (%)	Mg (%)	P (%)	S (%)	K (%)	O (%)
1	25.4	4.0	3.9		1.6	65.2
2	31.5	0.8	0.9	0.1	0.5	66.3
3	27.9	2.8	2.6		1.1	65.6
4	33.3				0.1	66.6

Figure 6.3 Back scatter electron image of bran, with spot analysis compositions (molar percentage).

For the residue bran used in the present work, SEM-EDS analysis has been performed on the fuel to evaluate the association of inorganic elements. A typical result is shown in Figure 6.3, together with spot-analysis compositions. The result is considered to be representative for a number of SEM-EDS analyses performed. It is seen that some spherical particles with heavier elements (illustrated by the brighter color) are present in the bran. The size of these spherical particles is around 1-3 µm, and EDS analysis of the particles (see Spectrum 1 and 3 in Figure 6.3) implies that the P, Mg and K content in these particles is significantly higher than that in other parts of bran. The results are generally consistent with the observations in literature [341,344], where the phytate in wheat bran or other mature grains was found to be concentrated in the

electron-dense parts of the protein storage vacuoles called phytate globoids, which had a size up to 5 µm. The P, Mg and K content in the globoids was reported to be 5-7 times higher than that in the whole bran, suggesting that the globoids are a major source of P, Mg and K in bran [344].

According to the literature results and the SEM-EDS analysis, it is conceivably that the majority of P, Mg and K in the bran used in this work are present as phytic acid/phytate or other inositol phosphate, which are concentrated in globoids. When bran is combusted at high temperature, the P in phytic acid/phytate may be transformed to phosphorus oxides/phosphates, thus the vaporization of P, Mg and K in combustion may to a large extent depend on the vapor pressure of the phosphorus oxide/phosphates. A detailed analysis of the associations of P and other inorganic elements in bran can be performed through similar approaches as used extensively in biological studies [337-342]. However, it is outside the scope of this work.

6.3.1.2 Release in laboratory-scale experiments

Figure 6.4a shows the release of P, K, Mg and S during bran pyrolysis at different temperatures. It can be seen that the release of P, K and Mg is negligible up to 900 °C, implying that these elements in bran are not associated with the volatiles released during pyrolysis. This also indicates that the inorganically associated or char bounded P, K and Mg are rather stable up to 900 °C. A similar study on wheat straw showed that the release of K was approximately 20% at a pyrolysis temperature of 900 °C and a pyrolysis duration of 120 min [167]. The release of K during straw pyrolysis was attributed to the vaporization of KCl present in the pores of char matrix, and the process was considered to be affected by pyrolysis duration [167]. In our experiments, pyrolysis duration at 900 °C was 180 min, and vaporization of K was still not observed. This suggests that the presence and vaporization of KCl during bran combustion are negligible, in agreement with the low Cl content of the bran. Compared to P, K and Mg, the behavior of S is quite different. More than 95% of the S is released to gas phase during bran pyrolysis at 500 °C. A similar phenomenon has been seen during straw pyrolysis at 500 °C, although the percentage of the released S was smaller (~40%) [167]. The significant release of S below 500 °C suggests that the majority of S in bran is organically-associated and is released together the volatiles.

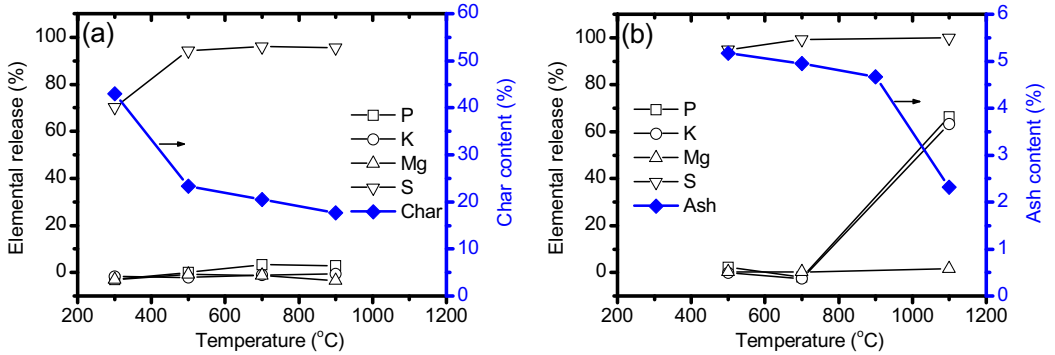

Figure 6.4 (a) the release of P, K, Mg and S, and the char content of bran at different temperature during pyrolysis, (b) the release of P, K, Mg and S, and the ash content of bran at different temperature during combustion.

Figure 6.4b depicts the release of P, K, Mg and S during bran combustion at 500, 700 and 1100 ^{o}C. The results of the experiment at 900 ^{o}C are not shown, because the residual ash from this experiment is molten and cannot be fully removed from the boat. From Figure 6.4b, it can be seen that the release of P, K and Mg is negligible at combustion temperatures of 500 ^{o}C and 700 ^{o}C, whereas the release of S is almost complete, in agreement with the pyrolysis results. The data suggest that during char combustion, organically associated P, K and Mg in the bran are likely transformed to stable inorganic compounds which are not vaporized at 700 ^{o}C. For the experiment at 900 ^{o}C, although the release of P, K and Mg is not quantified, the ash amount from the experiment indicates that the vaporization of inorganic elements is not significantly greater than that of 700 ^{o}C.

When the combustion temperature is increased from 900 ^{o}C to 1100 ^{o}C, a significant decrease in residual ash content is observed (see Figure 6.4b), implying that a large fraction of the inorganic elements is released in this temperature range. This is consistent with the significant release of K and P obtained at 1100 ^{o}C, which is about 63% and 66%, respectively. The release of Mg is still negligible at 1100 ^{o}C, whereas the release of S is almost 100%. The results suggest that the major ash forming elements that are vaporized during bran combustion is K, P and S. In addition, it should be mentioned that the Na and Cl content in the residual ash from the 1100 ^{o}C experiment is below the detection limit of ICP-OES (i.e. Na <0.02 wt% and Cl <0.05 wt%). This indicates that the majority (>90%) of the Na and Cl in the bran are released to gas phase at 1100 ^{o}C. In addition to the elements shown in Figure 6.4, the release of other inorganic elements, such as Si and Ca, is generally found to be negligible during bran combustion. The reliability of the experiments can be reflected by the results of Mg, which should be a non-volatile element at the given experimental conditions. As shown in Figure 6.4, the maximum deviation of Mg release from the base line (0%) is about 3%, which indicates a good reliability of the experiments.

The release of K, Mg, and P during bran pyrolysis may be explained by the association of these elements. The majority of K, Mg, and P in bran may be present as phytate/phytic acid or other inositol phosphates, as discussed in previous section. During bran pyrolysis, the structure of the inositol phosphates may not decompose and the vaporization of K and P may not occur. On the other hand, the decomposition of inositol phosphates may have happened at pyrolysis temperature of 900 ^{o}C, but the temperature is not high enough to vaporize of the K and P species. Thus the release of K and P is negligible at pyrolysis temperature of 900 ^{o}C.

During bran combustion, it is likely that the K, Mg and P present as phytate/phytic acid (or other inositol phosphates) are converted to K-phosphate, Mg-phosphate, K-Mg-phosphate or phosphorus oxide. According to the structure of phytic acid shown in Figure 6.2, a major K-phosphate product from the combustion of inositol phosphates is conceivably KPO_3. The thermal behavior of KPO_3 at high temperature has been evaluated in a STA instrument by heating a pure KH_2PO_4 sample from 25 ^{o}C to 1400 ^{o}C. KH_2PO_4 decomposes to KPO_3 at temperatures below 400 ^{o}C [345,346]. This transformation is confirmed by the STA results presented in Figure 6.5, showing that the mass loss of KH_2PO_4 is about 13.7 wt% at 400 ^{o}C. When the KPO_3 formed is heated further, a DSC peak appears at around 800 ^{o}C, accompanied by a negligible mass loss. This DSC peak suggests that an endothermic process (melting) occurs at around 800 ^{o}C, in agreement with the melting point of KPO_3 (807 ^{o}C) reported in literature [347]. It should be noted that the KPO_3 formed in the STA experiment is probably present in a polymer form, as suggested in literature [345,346]. Thus the observed melting temperature is related to the chain length of the polymer, which is not determined in the present work. According to the TG curve,

the vaporization of KPO_3 starts at around 1000 °C and is almost completed at around 1300 °C. Although the vaporization degree of the KPO_3 seems to be not significant at 1100 °C, one should be aware that the STA is operated at a heating rate of 10 °C/min, thus it may be difficult to achieve equilibrium in such a heating rate. With a longer holding time at 1100 °C, the KPO_3 may be fully vaporized.

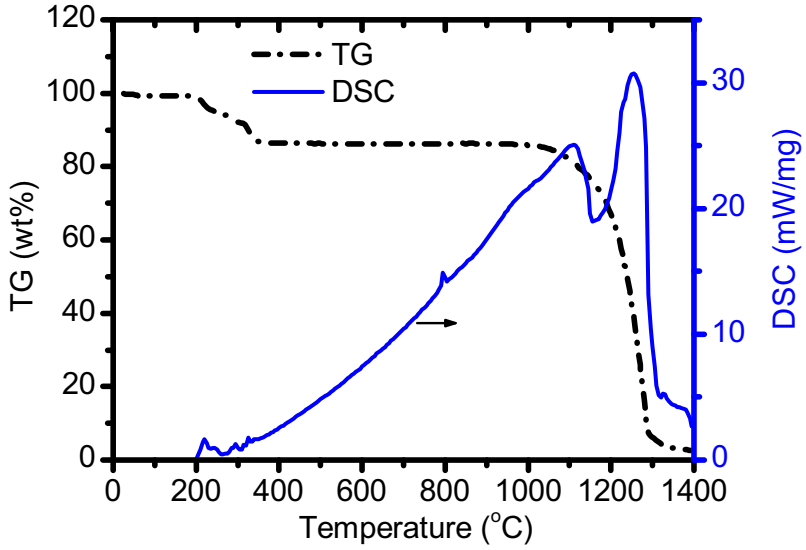

Figure 6.5 STA (Simultaneous Thermal Analysis) measurement of pure KH_2PO_4 at 5% O_2 condition and heating rate of 10 °C/min.

According to the results shown above, the primary release mechanism of P and K during bran combustion is proposed in Figure 6.6. During combustion, the inosital phosphates in bran may be converted to KPO_3. At temperatures around 800 °C, the KPO_3 may be melted. When the temperature is increased to a range of 900–1100 °C, vaporization of KPO_3 may happen, which may release P and K to gas phase. This proposed mechanism is supported by several experimental observations. Firstly, the residual ash from bran combustion is melted in a temperature range of 700–900 °C, which is consistent with the melting temperature of KPO_3. However, the initial melting temperature of the residue ash may not determined by the melting point of pure KPO_3, but rather by the closest eutectic or peritectic point in the K_2O-MgO(CaO)-P_2O_5 system [115]. Secondly, the release of K and P during bran combustion happens at a temperature range of 900–1100 °C, which is also in agreement with the observed vaporization behavior of KPO_3. Moreover, during bran combustion at 1100 °C, the molar ratio of the released K/P is about 0.9, which further supports that KPO_3 is likely a major K and P species vaporized. However, the molar ratio of the released K/P also indicates that a small fraction of P may be released in other forms. Since the release of Na is found to be significant (~90%) in the temperature range of 900–1100 °C, it is likely that Na-phosphate is formed and released during bran combustion. The release of P as oxides or phosphoric acids is less likely to happen, since the majority of phosphorus oxides or phosphoric acids have high vapor pressures at 700 °C [320], which contrasts with the negligible P release observed during bran combustion at 700 °C. For the retention of P and K in residual ash at 1100 °C, it is probably related to the formation of Mg-K or

Ca-K phosphates, which can have melting points higher than 1100 °C [347]. For K, K-silicates or K-aluminosilicates may also be a source of the K found in residual ash at 1100 °C.

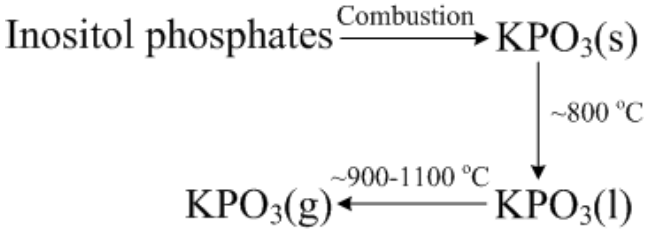

Figure 6.6 Proposed primary release mechanism of P and K during bran combustion.

It should noted that the mechanism of K and P release proposed above requires further confirmation through analyzing the properties of the residual ash from bran combustion (such as XRD, SEM-EDS or chemical fractionation analysis) as well as sampling the released K and P species and performing XRD or wet-chemical analysis. These investigations are beyond the scope of this work and are subjected to future work.

6.3.1.3 Release in full-scale grate-fired plant

In order to compare the release results obtained from the laboratory-scale experiments with those of full-scale plant, the typical morphology and composition of the fly ash particles collected in the baghouse filter of the grate-fired plant was investigated by SEM-EDS and presented in Figure 6.7. Since the fly ash from a grate-fired system is dominated by vaporized inorganic species [237,306], the composition can provide an estimation of the release of inorganic elements during bran combustion. From Figure 6.7, it can be seen that the fly ash primarily consists of P, K, Na and S. The presence of Cl is observed in some particles, but in smaller amounts compared to other inorganic elements. The P and K in the filter ash are probably a result of the vaporization of P and K during bran combustion. However, the majority of Na in the collected fly ash probably originates from the $NaHCO_3$ particles injected in front of the baghouse filters, as the Na content in bran is usually quite low. In addition, since the purpose of $NaHCO_3$ injection is to reduce the SO_2 and HCl emission from the plant, it naturally causes an increase of the S and Cl content in fly ash. In addition to SEM-EDS analysis, XRD analysis on the fly ash shows that the major crystalline phases are KH_2PO_4 and $K_3Na(SO_4)_2$.

Besides the typical fly ash composition, the bulk composition of a number of fly ash samples collected from the plant was analyzed by SEM-EDS. It generally found that the molar ratio of K/P in fly ash was in a range of 0.9–1.2, when the plant was operated with pure bran. This is comparable with the molar ratio of the released K/P (~0.9) obtained in laboratory-scale experiment at 1100 °C. The molar ratio of the released K/S in the laboratory-scale experiment at 1100 °C is around 3.5, which is also in agreement with the range (~3-4.5) found in the fly ash from the grate-fired plant. This suggests that the results obtained from the laboratory-scale experiment at 1100 °C are representative, as least qualitatively, for the release of inorganic elements in the grate-fired plant.

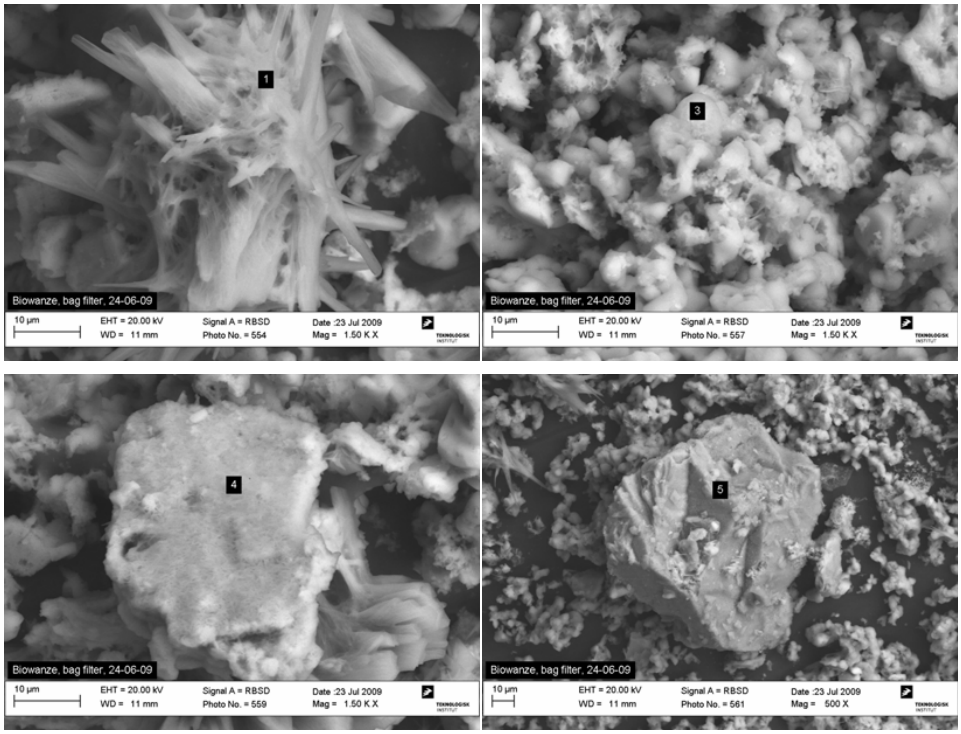

Spot	C (%)	O (%)	P (%)	K (%)	Na	S (%)	Cl (%)
1	9.71	47.23	21.8	8.48	11.99		
3		62.83	16.98	15.9	3.17		
4	2.28	56	5.5	13.93	11.55	8.68	2.05
5	8.92	54.93	5.75	4.42	17.66	7.97	0.34

Figure 6.7 Typical morphology of the fly ash collected during pure bran combustion in the grate-fired plant, with the spot compositions (molar percentage).

6.3.2 Effect of additives on the release of inorganic elements

6.3.2.1 Effect of additives during laboratory-experiments

In order to reduce the release of P species during combustion, a widely used method is to inject Ca-based additives[116,324], which will react with the gaseous P and form Ca-phosphates with a high melting temperature. In this work, the presence of such reactions has been examined by mixing KH_2PO_4 and $Ca(OH)_2$ at a molar ratio of 1:1, and then heating the mixture to 1500 ^oC at a rate of 10 ^oC/min in a high temperature oven. If no reaction takes place between KH_2PO_4 and $Ca(OH)_2$, the expected mass loss of the mixture is about 73.3 wt% at 1500 ^oC, meaning that KH_2PO_4 is fully vaporized and CaO is the only residual product. However, the mass loss obtained in the experiment was 16.2 wt%. This leads to the hypothesis that $KCaPO_4$ is formed during the heating of the mixture, and the vaporization of $KCaPO_4$ is negligible at 1500 ^oC. The hypothesis is supported by the fact that the theoretical mass loss of the $KCaPO_4$ formation reaction (17.1 wt%) is close to the measured mass loss (16.2 wt%). The result confirms that Ca-based additives can have a positive effect on the retention of phosphorous species during

combustion. Two plausible global mechanisms, depending on whether reaction or thermal decomposition occurs first, are proposed below:

$$KH_2PO_4 + Ca(OH)_2 \longleftrightarrow KCaPO_4 + 2H_2O \quad \text{(R6.1)}$$

$$KPO_3 + CaO \longleftrightarrow KCaPO_4 \quad \text{(R6.2)}$$

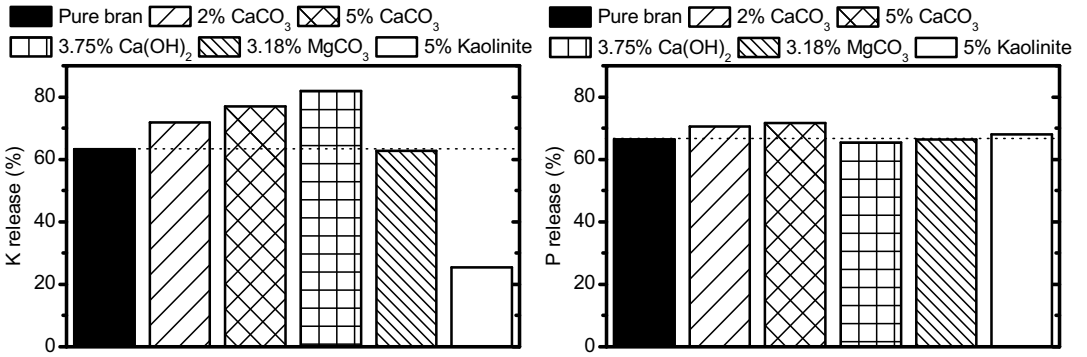

Figure 6.8 Influence of different additives on the release of K and P from bran combustion at 1100 °C, the percentage of additives is on weight basis.

In the release experiments, selected additives ($CaCO_3$, $Ca(OH)_2$, $MgCO_3$ or kaolinite) were mixed with bran, and the experiments listed in Table 6.2 were carried out. The combustion temperature for the additive experiments was chosen as 1100 °C, since the release of inorganic elements was found to be insignificant at other temperatures listed in Table 6.2. The effect of different additives on the release of K and P during bran combustion is shown in Figure 6.8. It can be seen that with the addition of Ca-based compounds ($CaCO_3$ and $Ca(OH)_2$), the K release is increased by about 8–19%. A possible explanation for this is that the Ca-based compounds may react with the K-silicates or K-aluminosilicates in the bran, and release part of the mineral-bound K to gas phase. The competition between the K and Ca for the reactive silicates or aluminosilicates has been observed previously [99,169]. However, the presence of silicates or aluminosilicates may be limited in the bran ash, due to the small content of Al and Si. Therefore the increased release of K during Ca addition may be related to the interactions between the K, Ca and P species, since an increased Ca/P molar ratio in the mixture seems to be favored by the vaporization of K. [169] The interpretations above may explain the observed increased release of K with increasing share of $CaCO_3$ (see Figure 6.8). For different calcium compounds, it seems that when the same molar ratio of Ca/K is applied, $Ca(OH)_2$ has a more significant effect on the release of K than the $CaCO_3$. This may be linked to the particle size of the $Ca(OH)_2$ and $CaCO_3$ used in the experiments, since the $Ca(OH)_2$ particles are much smaller compared to $CaCO_3$. Different from Ca-based additives, the addition of $MgCO_3$ shows a negligible effect on the release of K. However, the addition of kaolinite reduces the K release significantly, by about 75%. A primary reason for this is that the kaolinite reacts with gaseous K, resulting in formation of K-aluminosilicates. The reactions between kaolinite and gaseous alkali species are well-identified [99,107,176,178,182,187]. In the experiment with bran, it is suggested that a similar reaction may occur between kaolinite and the gaseous KPO_3, with a plausible global mechanism of:

$$2KPO_3(g) + Al_2O_3 \cdot 2SiO_2(metakaolin) \longleftrightarrow K_2O \cdot Al_2O_3 \cdot 2SiO_2 + 0.5P_4O_{10}(g) \quad \text{(R6.3)}$$

P_4O_{10} (g) is proposed as a product in the reaction above since it may be a thermodynamically favorable P species at high temperatures. However, the P_4O_{10}(g) may also react with other vaporized inorganic species, which will be discussed in detail in Section 3.3. It should be noticed that the mechanism above is proposed based on experimental observations. Further experiments and/or theoretical studies are needed in order to confirm the mechanism, which is beyond the scope of this work and is subjected to future work.

Compared to K, the influence of additives on the release of P is generally not significant. With the addition of Ca-based compounds, almost no reduction in the P release is observed. These results seem to be contrast with the performed test on the mixture of pure KH_2PO_4 and $Ca(OH)_2$, showing that the release of P is negligible when the mixture is heated from room temperature to 1500 ^oC. The discrepancy may be explained by the high combustion temperature and the short contacting time between the gaseous P and Ca compounds in the experiments. According to the experimental procedures, char oxidation takes place at 1100 ^oC during the additive experiments. At this temperature, the KPO_3 formed from char combustion may be vaporized directly. However, when heating the mixture of KH_2PO_4 and $Ca(OH)_2$ from room temperature to 1500 ^oC at 10 ^oC/min, there will be a certain period that the KPO_3 is in molten phase. This molten phase together with a relatively long residence time may greatly promote the reaction between KPO_3 and Ca-additives. Besides, solid-solid reactions may happen between KH_2PO_4/KPO_3 and $Ca(OH)_2$ during the heating. However, such reactions may be inhibited during the additive experiments, since the majority of P may remain as inositol phosphates before char oxidation. When the gaseous P is released from bran during char oxidation, the contact time between gaseous P and Ca-additives would be rather short in the reactor, as the fuel/ash bed is thin (a few millimeters) in the experiment. Therefore, the extent of reactions between gaseous P and Ca-additives is limited.

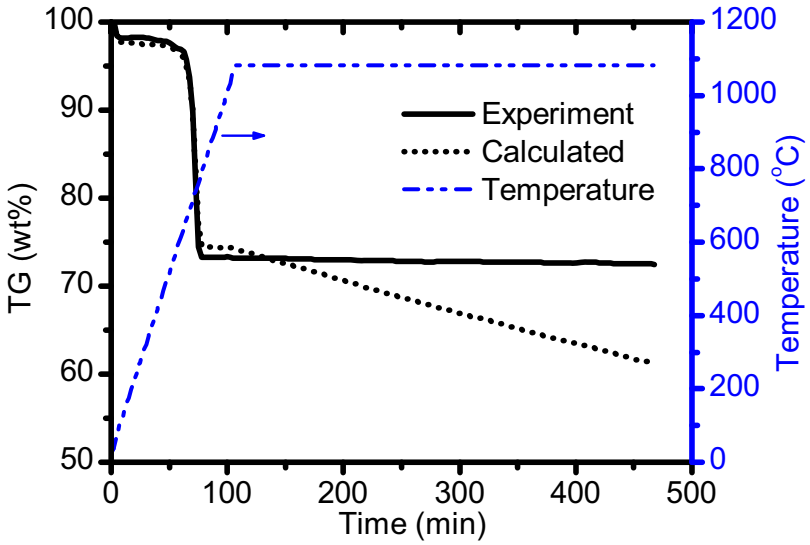

Figure 6.9 STA measurement of a mixture of bran ash from 700 ^oC and $CaCO_3$ (mass ratio 1:1.05, Ca/P molar ratio=1.68), at 5% O_2 condition; the sample was heated from 25 ^oC to 1100 ^oC at a heating rate of 10 ^oC/min and then held at 1100 ^oC for 6 h.

In order to evaluate the reactions between the bran ash and $CaCO_3$ at temperatures lower than 1100 ^oC, a mixture of bran ash produced at 700 ^oC and $CaCO_3$ was tested in the STA. As shown in Figure 6.9, when the mixture was heated from 25 ^oC to 1100 ^oC and maintained at 1100 ^oC for 6 h, the experimental mass loss was much lower than that predicted from the pure components tested at the same conditions, by assuming an additive behavior of the mixed $CaCO_3$ and bran ash. This suggests that reactions between $CaCO_3$/CaO and bran ash have taken place and inhibited the vaporization of K and P species. A plausible mechanism for this reaction is given in (R6.2). The results support the hypothesis that the presence of molten phase P species over a relatively long residence time may be important for the reactions between the P species and Ca additives.

Compared to Ca additives, the reaction between gaseous K and kaolinite is found to be quite significant in the experiment with kaolinite addition. This implies that the reaction rate between the gaseous P and Ca-additives is likely to be much slower than that of kaolinite (or metakaolin at the experimental temperature) and gaseous K. Besides the Ca-additives, the addition of $MgCO_3$ or kaolinite also shows a negligible effect on the release of P.

Table 6.3 Molar ratio of the released inorganic species in different experiments combusted at 1100 oC.

Experiment number	Sample	Molar ratio of the released inorganic species		
		K/P	K/Cl*	K/2S
9	Bran	0.89	10.54	1.78
10	Bran+2wt%$CaCO_3$	0.96	11.96	2.03
11	Bran+5wt%$CaCO_3$	1.01	12.84	2.18
12	Bran+3.75wt%$Ca(OH)_2$	1.18	13.66	2.35
13	Bran+5wt% kaolinite	0.37	4.48	0.76
14	Bran+3.18wt%$MgCO_3$	0.89	10.46	1.76

* The Cl release is assumed to be 100%, as the Cl content in the residue ash is below the detection limit

The results from the additive experiments indicate that the Ca-based additives can promote the release of K via reaction with mineral-bound K, whereas the effect on P release may to a large extent depend on the experimental conditions. Still, this will lead to an increase of the molar ratio of the released K/P. As shown in Table 6.3, the molar ratio of K/P released during Ca-addition is in the range of 0.96–1.18, which is larger than that of pure bran combustion (0.89). Besides the Ca-based additives, it can be seen that the addition of kaolinite significantly reduces the molar ratio of the released K/P to 0.37.

6.3.2.2 Effect of $CaCO_3$ addition in full-scale plant

In order to evaluate the effect of $CaCO_3$ addition on the release of K and P in the grate-fired plant, the molar ratios of K/P in the fly ash collected with and without $CaCO_3$ addition (5–8 wt%) are presented in Figure 6.10. It can be seen that the molar ratio of K/P in the fly ash from $CaCO_3$ addition is normally above 1.5, and can even exceed 4. This is significantly higher than the ratio (0.9~1.2) found in the fly ash of pure bran combustion. The increased K/P molar ratio in the fly ash from $CaCO_3$ addition is presumably caused both by an increased K release and/or a decreased P release. From Figure 6.10, it can be seen that the K/P molar ratio in the fly ash may

vary significantly during the addition of $CaCO_3$. This may be related to the variations in bran properties, $CaCO_3$ qualities, and the mixing between the $CaCO_3$ and bran.

Compared to laboratory-scale experiments, the effect of $CaCO_3$ addition seems to be more significant in the full-scale plant. This is probably due to that the bran combustion may start at a temperature lower than 1100 ^oC in the grate-fired plant. Therefore, the presence of molten K-phosphates may be possible over a relatively long residence time, which may promote the reaction between the Ca-additive and phosphates. In addition, the fuel/ash bed in the grate-fired plant is much thicker than that in the laboratory-scale experiment, which is a favorable condition for the reaction between gaseous phosphates and the Ca-additive.

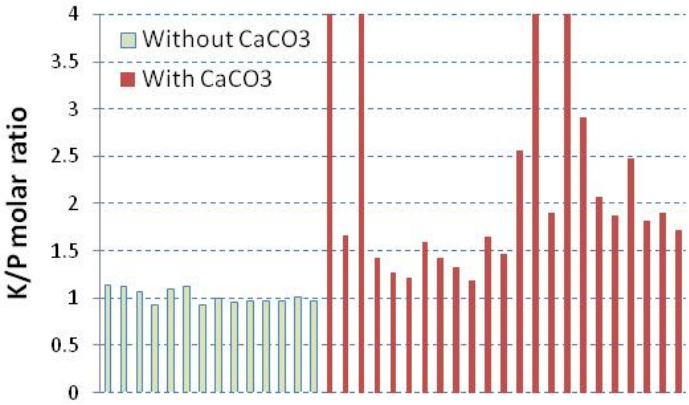

Figure 6.10 The K/P molar ratio in the fly ash collected from the grate-fired plant without $CaCO_3$ and with $CaCO_3$ addition (the maximum value shown in the figure is 4).

6.3.3 Transformation of vaporized inorganic elements in bran combustion

From previous sections, it was confirmed that the major inorganic elements released during bran combustion are K, P, S and Cl (the Na is neglected here due to the relatively low content). In a grate-fired system, once these elements are released from fuel bed, the interactions between these and other ash forming elements (such as Si and Ca) will be negligible, since the fly ash from a grate-fired system is dominated by flame-volatile inorganic species [237]. Although the vaporized inorganic elements during bran combustion may be primarily K, P, S and Cl, the interactions among these elements as well as with other organic elements such as C, O and H are still rather complicated.[217,320,321,336,348] According to the experiments carried out in a SCR reactor [320], polyphosphoric acid could be formed in a short residence time (~a few seconds) when H_3PO_4 aqueous solution was sprayed to the high temperature reactor (>850 ^oC) and subsequently cooled to a temperature below 500 ^oC. When the H_3PO_4 solution was replaced by a K_3PO_4 solution, more complicated transformations of the P and K species occurred and conceivably led to the formation of K and P compounds such as KH_2PO_4, K_2HPO_4, KOH and H_3PO_4 [321]. For a mixture of KCl, $Ca(OH)_2$, H_3PO_4, and H_2SO_4 [348], the composition of the fine particles formed during flue gas cooling showed that no Cl was present in the particles, suggesting that the Cl was mainly present in gas phase as HCl. All of the other inorganic elements were found in fine particles, and the formation of polyphosphoric acid was considered to be possible [348]. A recent experiment conducted in a circulating fluidized bed (CFB) boiler

showed that the injection of $(NH_4)_2HPO_4$ before the convective part of the boiler could significantly reduce the KCl concentration in flue gas [325]. This clearly identified that K-phosphates would be more stable (or thermodynamically favorable) than the KCl at high temperature, which was in-line with the fine particle results obtained in [348]. The main P products formed during the injection of $(NH_4)_2HPO_4$ was considered to be KPO_3 and K_3PO_4 [325].

In order to study the transformation of inorganic elements during bran combustion, equilibrium calculations have been performed in a temperature range from 25–1100 ^oC. The calculations were carried out on a simplified combustion system containing C, N, O, H, S, Cl, P and K. The elements Si, Ca, Mg, Al, Fe, Ti and Mn were neglected in the calculation, as these elements generally have low volatility in a grate-fired system. Na was also excluded in the thermodynamic calculation due to the small Na content in the bran as shown in Table 6.1.

The calculations were performed by using the commercial software HSC, version 6.1. The detailed database used in the calculation is listed as Supporting Information. The compounds with thermodynamic data not fully available for the studied temperature range (25–1100 ^oC) are specified. It is shown that for a large number of P compounds such as H_3PO_4, KH_2PO_4, K_2HPO_4, KPO_3, K_3PO_4, $K_4P_2O_7$ and $P_4O_{10}(g)$, thermodynamic data are only available for temperatures up to 800 ^oC. It indicates that in the temperature range of ~800–1100 ^oC, the thermodynamic data of these compounds are extrapolated from that of lower temperatures. To some extent this will influence the results obtained in the high temperature range, suggesting that the results below 800 ^oC are relatively more reliable. In addition, it should be noted that the thermodynamic data of some P compounds, such as polyphosphoric acids, are not available in the HSC database. This will also limit the reliability of the equilibrium calculations.

Besides the uncertainties of the database, equilibrium modeling itself also has a lot of limitations, which has been discussed throughout [282,349]. This approach generally ignores the physical constraints such as mixing and reaction time, and chemical kinetic limitations of a combustion system. Thus the results predicted by equilibrium modeling may not represent a real combustion system. However, it will still provide valuable information regarding the possible reaction pathways and the qualitative influence of different parameters on a combustion system [282,349]. This suggests that the results obtained from equilibrium modeling should be preferably treated qualitatively, rather than quantitatively. The limitations of the thermodynamic database and the modeling approach need to be considered in interpreting and applying the results.

The input data of the equilibrium calculations were based on the bran composition shown in Table 6.1. Since the K/P molar ratio in the fly ash from the grate-fired plant can vary significantly during operation (see Figure 6.10), the calculations were performed at different K/P molar ratio conditions. In order to simulate the conditions in the plant, the moisture content of the bran was assumed to be 10 wt% and the excess air ratio used in the simulation was 1.2. The S and Cl in the bran were assumed to be totally released to the flue gas. For P and K, three different conditions were applied in the simulations: in Condition A, it was assumed 70% of the K and P in the bran were released to the flue gas; in Condition B, the release of K was 30% and the release of P was 70%; in Condition C, the release of K was 70% and the release of P was 30%. The main objective to perform calculations at these three conditions was to evaluate the influence of K and P release on ash transformations in flue gas.

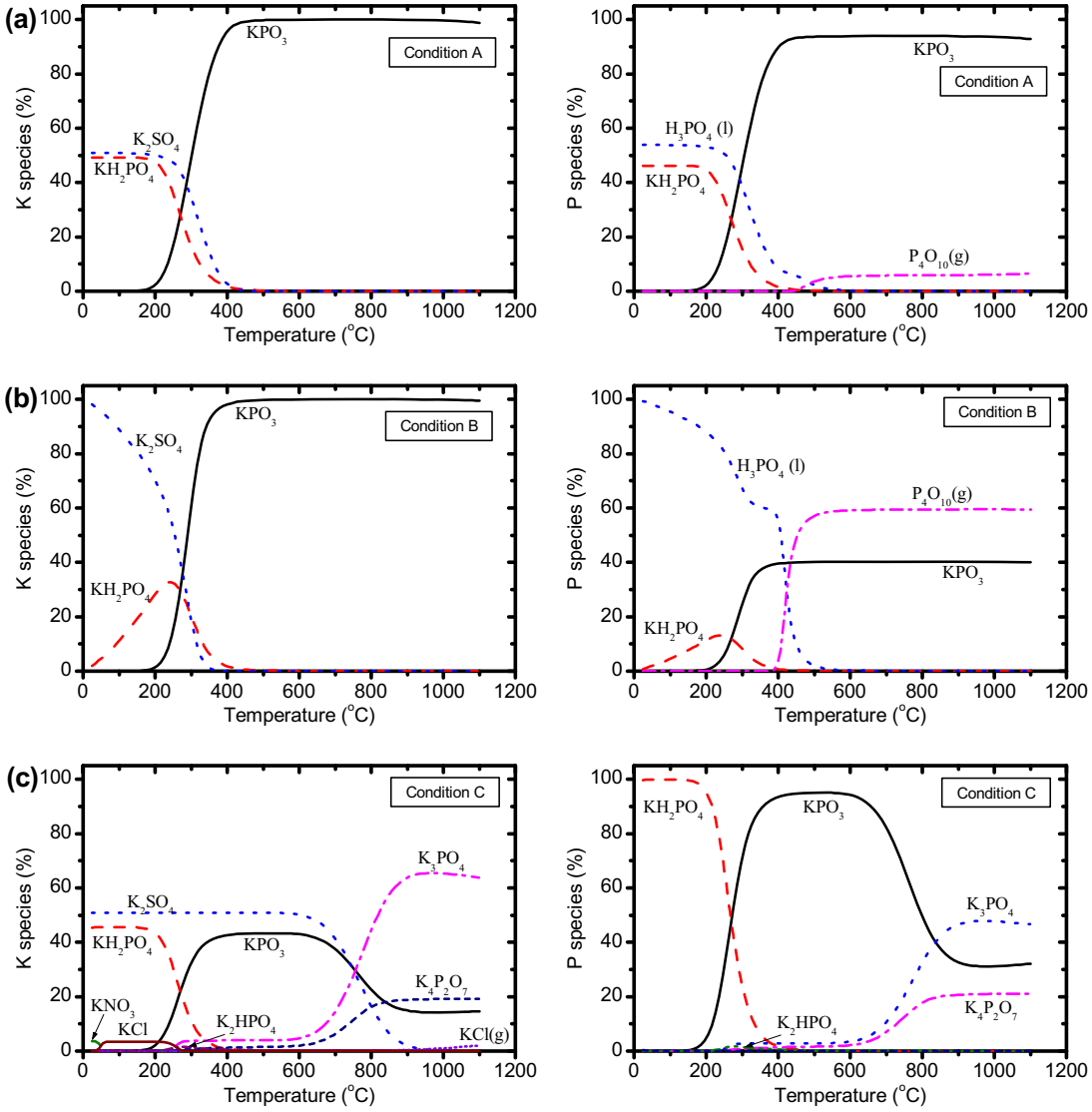

Figure 6.11 Equilibrium compositions of the K and P species at: (a) Condition A (assume 70% K and 70% P release, with K/P molar ratio=0.94 and K/2S molar ratio=1.96); (b) Condition B (assume 30% K and 70% P release, with K/P molar ratio of 0.40 and K/2S molar ratio of 0.84); (c) Condition C (assume 70% K and 30% P release, with K/P molar ratio of 2.19 and K/2S molar ratio of 1.96).

Figure 6.11a shows the equilibrium compositions of the K and P species obtained at Condition A, in which it is assumed that 70% of the K and P in the bran are released to flue gas. The results are representative for pure bran combustion condition. It can be seen that the KPO_3 is the only stable K-species at temperatures higher than 400 ^{o}C. When the temperature is decreased from 400 ^{o}C, KH_2PO_4 and K_2SO_4 gradually become the major stable K-species. Similar tendencies are also seen in the distribution of P-species. At temperatures higher than 500 ^{o}C, the major P-

species is KPO_3, followed by about 6% P_4O_{10} (g). The presence of P_4O_{10} (g) is related to the K/P molar ratio used in this simulation, which is below 1. When the temperature is decreased from 500 °C to 450 °C, the majority of the P_4O_{10} (g) is converted to H_3PO_4 (l). The plausible global mechanism for this conversion is:

$$P_4O_{10}(g) + 6H_2O(g) \longleftrightarrow 4H_3PO_4(l) \quad \text{(R6.4)}$$

At temperatures lower than 400 °C, the KPO_3 starts to convert to H_3PO_4 and/or KH_2PO_4, with plausible global mechanisms of:

$$2KPO_3 + SO_2(g) + 0.5O_2(g) + 3H_2O(g) \longleftrightarrow K_2SO_4 + 2H_3PO_4(l) \quad \text{(R6.5)}$$

$$KPO_3 + H_2O(g) \longleftrightarrow KH_2PO_4 \quad \text{(R6.6)}$$

Thermodynamic calculations in Figure 6.11a predicted the presence of liquid phase H_3PO_4 (l) at temperatures below 500 °C. Experimentally, it was found that the presence of polyphosphoric acid at temperatures lower than 500 °C was possible, in a form of submicron liquid particles [320]. However, in the thermodynamic calculations of this work, the formation of polyphosphoric acids was neglected, due to the absence of thermodynamic data for these compounds.

When the bran is mixed with kaolinite or silicates, the release of K to the gas phase may be inhibited. In order to simulate such a situation, thermodynamic calculations were performed by assuming the release of K is 30% and the release of P remains 70% (Condition B). The equilibrium composition of K and P species obtained under this condition is shown in Figure 6.11b. It can be seen that the dominant K species above 400 °C is still KPO_3. In the temperature range of 400–200 °C, the KPO_3 is progressively converted to K_2SO_4 and KH_2PO_4. At temperatures below 200 °C, K_2SO_4 becomes the major stable compound. The distribution of P-species in Condition B is quite different from that in Condition A. In Figure 6.11b, it is seen that the major P species above 500 °C is P_4O_{10} (g), followed by about 40% KPO_3. Due to the large fraction of P_4O_{10} (g), the formation of H_3PO_4 from P_4O_{10} (g) is significant in the temperature range of 400–500 °C. Below 400 °C, the KPO_3 starts to convert to H_3PO_4 and KH_2PO_4. The KH_2PO_4 may be further converted to H_3PO_4, at temperature lower than 250 °C, with a plausible global mechanism of:

$$2KH_2PO_4 + SO_2(g) + 0.5O_2(g) + H_2O(g) \longleftrightarrow K_2SO_4 + 2H_3PO_4(l) \quad \text{(R6.7)}$$

As mentioned above, Ca-based additives can inhibit the release of P and promote the release of K during bran combustion. Therefore the molar ratio of the released K/P can be increased by adding Ca. In order to simulate such a situation, thermodynamic calculations have been conducted according to Condition C, which assumed that the release of K is 70% and the release of P is 30% in bran combustion. The simulation results are shown in Figure 6.11c. It can be seen that the distribution of K-species is rather complicated at this condition. At a temperature higher than 800 °C, the main stable K-species are K_3PO_4, $K_4P_2O_7$ and KPO_3, followed by a small amount of KCl (g). In the temperature range of 400–800 °C, the dominant K-species become K_2SO_4 and KPO_3, which are presumably a result of the following plausible global mechanisms:

$$K_3PO_4 + SO_2(g) + 0.5O_2(g) \longleftrightarrow K_2SO_4 + KPO_3 \quad \text{(R6.8)}$$

$$K_4P_2O_7 + SO_2(g) + 0.5O_2(g) \longleftrightarrow K_2SO_4 + 2KPO_3 \quad \text{(R6.9)}$$

One should be aware that the mechanisms above (also other mechanisms involving sulphation reactions) may be significantly limited by the oxidation of SO_2 to SO_3. Thus the actual conversion may be orders of magnitude lower than that predicted from equilibrium calculations. More fundamental experiments are needed in order to validate these mechanisms in practical conditions, which is outside the scope of this work.

When the temperature is decreased from 400 °C to 200 °C, a transition from KPO_3 to KH_2PO_4 is observed. At temperature lower than 200 °C, the presence of a small amount of KCl and KNO_3 is predicted. For P-species, it is seen that the major P-species above 800 °C are K_3PO_4, KPO_3 and $K_4P_2O_7$. With decreasing temperature, transition from K_3PO_4 and $K_4P_2O_7$ to KPO_3 happen between 800 °C and 600 °C. When the temperature becomes lower than 400 °C, a transformation from KPO_3 to KH_2PO_4 occurs. Below 200 °C, the P-species is dominant by KH_2PO_4. Compared with the distribution of P-species in Figure 6.11a and Figure 6.11b, it is found that the presence of H_3PO_4 (l) is negligible in Figure 6.11c, indicating that the formation of H_3PO_4 may be prevented by a large K/P molar ratio in flue gas.

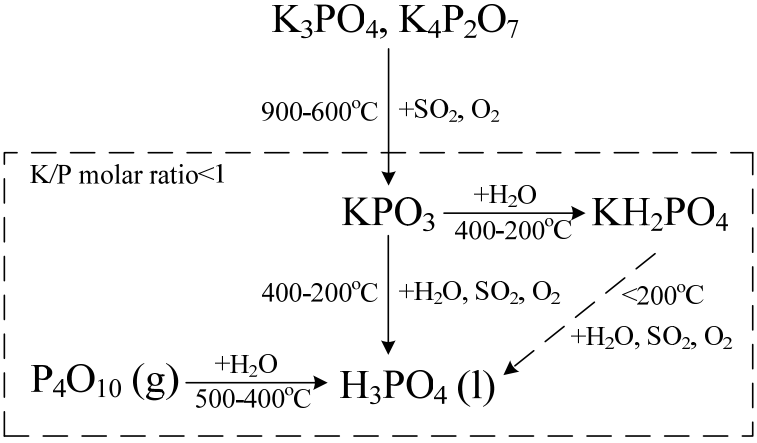

Figure 6.12 Proposed reaction pathways of the phosphorous containing species, based on equilibrium calculations.

According to the thermodynamic calculations, the possible reaction pathways of the P containing species in the flue gas are proposed, as shown in Figure 6.12. It is seen that when the molar ratio of the released K/P is below 1, KPO_3 and P_4O_{10} (g) are the dominant stable K and P species at temperatures above 500 °C. During flue gas cooling, the P_4O_{10} (g) can be converted to H_3PO_4 (l) in a temperature range of 500–400 °C, whereas the KPO_3 can be transformed to either KH_2PO_4 or H_3PO_4 (l), in a temperature range of 400–200 °C. Although such pathways seems to be thermodynamically feasible, the conversion of KPO_3 to H_3PO_4 (l) may be kinetically limited, due to the relatively low temperature and low concentration of SO_2 in flue gas. The conversion of P_4O_{10} (g) to H_3PO_4 may more likely happen, as the concentration of H_2O will be much higher than that of SO_2. The experimental results in literature also support that this may be a feasible pathway for the formation of H_3PO_4 (l), or polyphosphoric acids which are not considered in the thermodynamic calculations.[320] Below 200 °C, thermodynamic calculation predicts a

conversion of KH2PO4 to H3PO4 (l), when the K/2S molar ratio is 0.84 (see Figure 6.11b). However, such conversion is not predicted when the K/2S molar ratio is 1.96 (see Figure 6.11c).

When the molar ratio of the released K/P is high (e.g. >2), the stable P species at temperatures above 600 ^{o}C will be KPO_3, K_3PO_4 and $K_4P_2O_7$. According to thermodynamic calculations, the K_3PO_4 and $K_4P_2O_7$ may be converted to KPO_3 and K_2SO_4 in a temperature range of 900–600 ^{o}C, through reacting with SO_2 and H_2O. The formed KPO_3 will be primarily converted to KH_2PO_4 in a temperature range of 400–200 ^{o}C. The formation of H_3PO_4 (l) is not likely to happen under this condition, unless extra SO_2 is available for reacting with KPO_3.

One should be aware the reaction pathways proposed in Figure 6.12 is based on the equilibrium calculation results. Therefore, it has been naturally influenced by the limitations of equilibrium modeling, which have been discussed previously. In order to minimize these limitations, more reliable thermodynamic data regarding P species need to be developed, which is outside the scope of the present work. In addition, it is also favored to develop detailed kinetic models for the P related species.

6.3.4 Practical implications

The results from the present work have some practical implications for a grate-fired plant utilizing bran or similar P-rich fuel. In order to reduce the K and P release during bran combustion, addition of Ca-based additives such as $CaCO_3$ and $Ca(OH)_2$ is a feasible solution, as it may both reduce the K and P release through a plausible mechanism proposed in (R6.2). On the other hand, the Ca-based additives can also react with K-phosphates or K-silicates/K-aluminosilicates in bran and thereby release the K to gas phase. A combination of the mechanisms mentioned above will increase the molar ratio of K/P released to gas phase, which is confirmed by the full-scale data shown in Figure 6.10. The effect of Ca addition seems to be sensitive to the injection method. The effect would be more pronounced when the Ca additive is premixed with bran before combustion. This is likely related to the presence of molten phase phosphate over a relatively long residence time, which may promote the reaction between Ca additive and phosphate. The reaction rate between gaseous P and Ca additives is probably quite low, at least much lower than that of kaolinite and gaseous alkali species. Therefore, injection of Ca additive directly to the flue gas may not significantly reduce the vaporized K and P species. Besides Ca based additives, addition of kaolinite can greatly reduce the release of K via a plausible mechanism proposed in (R6.3), whereas the effect on P release is insignificant. It therefore will cause a significant decrease of the molar ratio of K/P released to gas phase.

The formation of fine particles during bran combustion may primarily be related to the quantity of K and P released on the grate. However, for other ash related problems, such as deposits formation and corrosion, the fly ash chemistry in the flue gas also plays a significant role. Thermodynamic calculations indicate that the distribution of P species in the flue gas is quite sensitive to the molar ratio of the released K/P. As seen in Figure 6.11a and Figure 6.11b, KPO_3 and P_4O_{10} (g) are the main inorganic species present in the flue gas at temperatures above 500 ^{o}C, when the molar ratio of the released K/P is below 1. Since the melting temperature of KPO_3 is approximately 800 ^{o}C (see Figure 6.5) and the P_4O_{10} (g) is present in the gas phase at temperatures above 500 ^{o}C, it is likely that the deposit built-up in the superheaters may not be significant if the flue gas temperature in the convective part of the boiler is below 800 ^{o}C, as the formed deposits may be in a powdery and non-sticky form which can be easily removed by soot-

blowing. This hypothesis is supported by the observations in the grate-fired plant, and the tests performed in a fluidized bed boiler [325]. However, when the flue gas temperature becomes lower than 500 ^{o}C, part of the KPO_3 and P_4O_{10} (g) may be converted to H_3PO_4 (l). The presence of liquid phase H_3PO_4 (l) may increase the deposit built-up in the economizers of the grate-fired boiler, which is normally operated at a flue gas temperature of 200–400 ^{o}C. In order to minimize the deposit built-up in the economizers, a possible solution is to increase the molar ratio of K/P and K/S in the flue gas. As shown in Figure 6.11c, the presence of H_3PO_4 (l) becomes negligible, when the molar ratio of K/P and K/2S is about 2.19 and 1.96, respectively. In addition, at this condition, the stable main P species at temperatures above 800 ^{o}C becomes K_3PO_4, $K_4P_2O_7$ and KPO_3. Both K_3PO_4 and $K_4P_2O_7$ have higher melting temperature than that of KPO_3 [347], which may be more favorable with respect to deposit built-up. Therefore, in order to minimize deposit built-up in the convective part and economizer of the boiler, a higher molar ratio of K/P in the flue gas may be desirable. One should be aware that if both the molar ratio of K/P and the Cl content in the flue gas are significantly high, it will lead to the formation of KCl, which will cause severe ash deposition and corrosion problems. However, in P-rich fuels, the Cl content is normally quite low, and the formation of KCl will probably not be important during combustion of these fuels.

6.4 Conclusion

In the present work, the release and transformation of inorganic elements during combustion of a residual bran from bio-ethanol production were characterized. Through a literature review and SEM-EDS analysis of the bran, it was suggested that a large fraction of the P, K and Mg in the seed-originated biofuels may be present as phytic acid/phytate or other inositol phosphates. By performing experiments in a horizontal tube reactor, the main inorganic elements released during bran combustion were found to be K, P and S, supplemented by Cl and Na. The S in bran was almost totally vaporized during bran pyrolysis at temperatures below 700 ^{o}C. About 60-70% of the K and P in bran were released in a temperature range of 900–1100 ^{o}C during bran combustion. The release of K and P was presumably related to the vaporization of the KPO_3 generated from thermal decomposition of inosital phosphate. The release results obtained in the laboratory experiments were in agreement with the observations from a grate-fired plant using similar fuel. On the other hand, the release mechanism we proposed requires confirmation through further investigations, such as XRD analysis on the residue ash obtained at different temperatures, as well as through sampling and characterization of the released K and P species.

The effect of additives such as $CaCO_3$, $Ca(OH)_2$, and kaolinite on the release of inorganic elements during bran combustion was studied in a horizontal tube reactor. The addition of Ca-based additives promoted the vaporization of K, whereas the influence on P release was insignificant. For the addition of kaolinite, the release of K was significantly inhibited, while the release of P was almost unaffected. By comparing the laboratory results with that of full-scale plant, it revealed that the effect of Ca-based additive was more pronounced in the full-scale plant, as the addition of Ca-based additive greatly increased the molar ratio of K/P in flue gas. The discrepancies between the experimental and full-scale implied that the presence of molten phase phosphate over a relatively long residence time may be important for the reaction between Ca-based additive and phosphate.

Thermodynamic calculations based on a simplified system indicated that the molar ratio of the released K/P could greatly influence the fly ash chemistry. With a molar ratio of K/P lower than 1, KPO_3 and P_4O_{10} (g) were the major stable K and P species at temperature higher than 500 ^oC. Below 500 ^oC, part of the KPO_3 and P_4O_{10} (g) were converted to H_3PO_4 (l), which might cause severe ash deposition in the economizers of the grate-fired boiler. However, by increasing the molar ratio of the released K/P, the ash chemistry could be changed significantly and the formation of H_3PO_4 (l) might not be thermodynamically favorable. Based on thermodynamic calculations, the transformation mechanisms of the K and P species in the flue gas have been proposed. However, it should be noted that the results/mechanisms derived from the thermodynamic calculations are restricted by the reliability of the thermodynamic data as well as a number of factors which have not been considered in the calculations, such as the reaction rate, residence time and mixing. Thus, the mechanisms proposed require further validation through fundamental experiments or theoretical studies, which is beyond the scope of this work.

Practical implications of the present work were discussed. It was suggested that Ca-based additives could be used to reduce the release of P and to some extent increase the release of K during grate-firing of bran, whereas kaolinite could be applied to inhibit the release of K. The effect of Ca addition might be more pronounced if it was premixed with fuel before combustion. The molar ratio of K/P in flue gas could be increased by Ca-based additives, which is a favorable condition for minimizing deposit built-up in the convective part and economizer of the boiler.

Acknowledgment

The present work is sponsored by Babcock & Wilcox Vølund A/S (BWV). The work is part of the CHEC (Combustion and Harmful Emission Control) Research Centre at the Technical University of Denmark (DTU). DTU-CEN and Danish Technological Institute and Enstedværket Laboratory at DONG Energy Power A/S are acknowledged for the helps on fuel and ash analysis.

6.5 Appendix

Database used in thermodynamic calculation with HSC 6.1

N2(g)	C2N(g)	ClO3(g)	K2(g)	NO(g)	P4O6(g)	*H3PO4
C(g)	C2N2(g)	Cl2O(g)	KCN(g)	NO2(g)	P4O7(g)	H2SO4
C2(g)	C4N(g)	ClOCl(g)	K2(CN)2(	NO3(g)	P4O8(g)	H2SO4(l
C3(g)	C4N2(g)	ClOClO(g	K2CO3(g	N2O(g)	P4O9(g)	K2CO3
C4(g)	C5N(g)	ClOO(g)	KCl(g)	N2O2(g)	P4O10(g	*KH2P
C5(g)	CNCl(g)	H(g)	K2Cl2(g)	N2O3(g)	POCl3(g	*K2HP
C60(g)	CNN(g)	H2(g)	KH(g)	N2O4(g)	PS(g)	KNO2
CCN(g)	CN4O8(g)	HCCN(g)	KNO2(g)	N2O5(g)	P4S3(g)	KNO3
CCl(g)	C2NO(g)	HCN(g)	KNO3(g)	NOCl(g)	S(g)	K2O(l)
CCl2(g)	C3N2O(OPDNg)	HCO(g)	KO(g)	NO2Cl(	S2(g)	KO2
CCl3(g)	CO(g)	HCOOH(g	K2O(g)	NS(g)	S3(g)	K2O
CCl4(g)	CO2(g)	HCOOH(	K2O2(g)	O(g)	S4(g)	K2O2
C2Cl(g)	C2O(g)	HCOOH(	KOH(g)	O2(g)	S5(g)	KOH
C2Cl2(g)	C3O2(g)	HCl(g)	K2(OH)2	O3(g)	S6(g)	*KPO3
C2Cl3(g)	COCl(g)	HClCO(g)	K2O2H2(	OClO(g)	S7(g)	*K3PO4
C2Cl4(g)	COCl2(g)	HN3(g)	KS(g)	OH(g)	S8(g)	*K4P2O
C2Cl5(g)	C12OCl8(12346789OCD	HNCO(g)	K2S(g)	P(g)	SCl(g)	*K2SO3
C2Cl6(g)	C12O2Cl8(OCDBDg)	HNO(g)	K2SO4(g	P2(g)	SCl2(g)	K2SO4
C4Cl6(13HCB	COOH(g)	HNO2(g)	N(g)	P3(g)	S2Cl(g)	NH4NO
C6Cl6(g)	COS(g)	HNO2(Cg	N2(g)	P4(g)	S2Cl2(g)	*P2O5
C12Cl10(DCB	CP(g)	HNO2(Tg)	N3(g)	PCl(g)	SN(g)	P2O5(l)
C2Cl4O(TCCg)	CP2(g)	HNO3(g)	NCN(g)	PCl2(g)	SO(g)	*P4O10
CH(g)	C2P(g)	HO2(g)	NCO(g)	PCl3(g)	SO2(g)	CS2(l)
CH2(g)	C2P2(g)	H2O(g)	NH(g)	PCl5(g)	SO3(g)	K2S
CH3(g)	CS(g)	H2O2(g)	NH2(g)	PH(g)	S2O(g)	KCN
CH4(g)	CS2(g)	HOCN(g)	NH3(g)	PH2(g)	SOCl2(g	P3N5
C2H(g)	Cl(g)	HOCl(g)	N2H2(g)	PH3(g)	SO2Cl2(	C
C2H2(g)	Cl2(g)	HPO(g)	N2H2(Bg	PN(g)	SPCl3(g	C(D)
C2H3(g)	Cl3(g)	HS(g)	N2H2(Cg	PO(g)	KCl	K
C2H4(g)	Cl4(g)	H2S(g)	N2H2(tg)	PO2(g)	NH4ClO	P
C2H5(g)	ClClO(g)	H2S2(g)	N2H4(g)	P2O3(g)	HCOOH	P(R)
C2H6(g)	ClClO2(g)	H2SO4(g)	N3H(g)	P2O4(g)	*H2O	S
CN(g)	ClO(g)	HSO3Cl(g	NH2NO2	P2O5(g)	*H2O(l)	S(l)
CN2(g)	ClO2(g)	K(g)	NH2OH(	P3O6(g)	H2O2(l)	

* Species with thermodynamic data not fully available in the temperature range of 25-1100 ^{o}C.

7 Conclusions and Suggestions for Future Work

7.1 Conclusions

This thesis is concerned with the alternative methods of utilizing waste-derived fuels in power production, with an emphasis on the following subjects: 1) co-combustion of coal and solid recovered fuel (SRF) under pulverized fuel combustion conditions; 2) dust-firing of straw and the use of a waste-derived additive; 3) combustion of a biomass residue rich in phosphorus.

7.1.1 Conclusions on co-combustion of coal and SRF

Co-combustion of a bituminous coal and SRF was carried out in an entrained flow reactor (EFR), at conditions of different SRF share and different additives (such as PVC, NaCl, kaolinite and ammonium sulphate) simulating a significant variation of the SRF/coal properties. The results showed that when coal was co-fired with up to 25 wt% SRF, the burnout, and the emissions of SO_2 and NO were decreased with increasing share of SRF. The decreased burnout was primarily related to the relatively large particle size of the SRF and its aggregation tendency during the injection. The lower SO_2 emission in co-combustion was mostly due to the relatively small S content and the large Ca content in the SRF, which could result in a decreased SO_2 formation and an enhanced sulphur capture by ash. The reduced NO emission was attributed to the relatively small N content and the large volatile content of the SRF. Most of the additives did not significantly influence the burnout and the emissions of SO_2 and NO, except for the ammonium sulphate which greatly increased the SO_2 emission and decreased the NO emission. Chemical analyses of the fly ash revealed that above 99 wt% of the K and Na in the fly ash was present in water insoluble form (such as alkali aluminosilicates) when coal was co-fired with up to 25 wt% SRF. The Cl content in the fly ash was extremely low (<0.07 wt%), indicating that the majority of the Cl in the SRF was released to gas phase when co-firing with coal, presumably due to the large amount of aluminosilicates in the coal. On the other hand, when PVC or NaCl was added to the mixture of coal and SRF, a significant increase of the Cl content in the fly ash was observed, suggesting the importance of controlling the Cl and alkali content in the SRF. The vaporization degree of Na and K appeared to be correlated in the experiments, indicating an interaction between the vaporization of Na and K during pulverized fuel combustion. The deposit formation on a probe simulating superheater tubes decreased with an increasing share of SRF during co-combustion, and the resulting deposits had considerably small Cl content (<0.01 wt%), implying a very low corrosion potential when coal is co-fired with up to 25 wt% SRF. However, with the addition of PVC or NaCl, significant increase of the Cl content in the deposits was observed which might lead to severe corrosion.

The content of trace elements in the SRF is usually significantly larger than that of coals. The partitioning of As, Cd, Cr, Pb, Sb and Zn during co-combustion of coal and SRF was studied through the EFR experiments. They showed that the content of As, Cd, Pb, Sb and Zn in the fly ash almost increased linearly with their content in the fuel ash when coal was co-fired with the SRF. On the other hand, this linear tendency was influenced to some extent with the addition of PVC, NaCl, kaolinite or ammonium sulphate, presumably due to the effect of chemical reactions. Volatility analyses indicated that As, Cd, Pb, Sb and Zn were highly volatile during combustion, whereas the volatility of Cr was relatively low. Compared to dedicated coal combustion, the volatility of Cd, Pb and Zn was slightly increased in co-combustion of coal and SRF, whereas the volatility of Cr and Sb was reduced. The addition of PVC or NaCl enhanced the volatility of Cd, Pb and Zn significantly, while the addition of ammonium sulphate generally reduced the volatility of the trace elements. The addition of kaolinite reduced the volatility of Pb, whereas the effect on other trace elements was insignificant. The results generally implied that co-combustion of coal and SRF in a coal-fired power plant may increase the trace element content in the fly ash considerably, primarily due to the significantly larger trace element content in the SRF compared to coal, but also related to the fuel interactions in co-combustion. In order to minimize the trace element emission during co-firing coal and SRF, besides reducing the trace element content in SRF, utilizing a coal with high S and aluminosilicates content and a SRF with low Cl content would be preferable.

Full-scale tests on co-combustion of coal and SRF were carried out in a pulverized coal-fired power plant, and the formation of fine particles was investigated by using a low-pressure cascade impactor. Compared to the dedicated coal combustion, co-combustion of coal and SRF (up to 10% thermal share) generally increased the formation of ultrafine particles with a concentration peak around 0.1 μm, while the total concentration of $PM_{2.5}$ decreased. TEM (transmission electron microscopy) analyses indicated that the ultrafine particles with primarily particle size of 10–30 nm were predominantly comprised of aggregated particles originating from homogeneous nucleation, while the remaining submicron particles were mainly a mixture of the aggregates and the spherical particles originating from the melted minerals, with the contribution of the latter being more significant with increasing particle size. Composition analyses showed that the Ca, S and P were significantly enriched in the ultrafine particles. Compared to dedicated coal combustion, the content of Ca, P and K was generally larger in the fine particles generated from co-combustion, whereas the S content was slightly smaller. In the full-scale tests, the dust emission was found to be significantly increased during co-combustion of coal and SRF, which was conceivable related to a deficiency of the electrostatic precipitator (ESP).

7.1.2 Conclusions on straw dust-firing and the utilization of additives

Dust-firing of straw was carried out in the EFR, and the feasibility of utilizing spent bleaching earth (SBE) as an additive in straw dust-firing was investigated through comparison with kaolinite. About 70% of the K in the fly ash from straw-dust firing appeared to be water soluble, and KCl contributed with more than 40% of the water soluble K. With the addition of 10-20 wt% of SBE, the Cl retention in ash was reduced, the SO_2 emission in the flue gas was increased, and the formation of water soluble alkali species was decreased. Compared to kaolinite, the inhibiting effect of SBE on the formation of alkali chlorides was slightly smaller, when the molar ratio of K/(Al+Si) in the fuel mixture was similar. The addition of SBE significantly reduced the Cl content of the deposits collected on a probe, both due to a dilution effect and chemical

reactions. Compared to pure straw combustion, the deposition rate was slightly increased during SBE addition, despite of the decreased deposition propensity. The results generally suggested SBE could be an advantageous additive to be used in straw dust-firing.

7.1.3 Conclusions on combustion of a phosphorus-rich biomass residue

The release and transformation of inorganic elements during the combustion of a residual bran was studied via experiments and equilibrium modeling. The work revealed that the major inorganic elements released during bran combustion were K, P and S. The S was almost fully vaporized during pyrolysis at temperatures below 700 ^{o}C, whereas about 60–70 % of the K and P in the bran were released during combustion in a temperature range of 900–1100 ^{o}C. The release of K and P was presumably due to the vaporization of KPO_3 generated from the thermal decomposition of the inositol phosphates in the bran. Additives such $CaCO_3$, $Ca(OH)_2$ and kaolinite generally influenced the release of K and P. The Ca-based additives mostly increased the molar ratio of the released K/P, whereas kaolinite showed an opposite effect. Thermodynamic modelling indicated that the fly ash chemistry was sensitive to the molar ratio of the released K/P. When the molar ratio of the released K/P was below 1, KPO_3 and P_4O_{10} (g) were the main stable K and P species at temperatures higher than 500 ^{o}C. Below 500 ^{o}C, the KPO_3 and P_4O_{10} (g) may be converted to H_3PO_4 (l), which may cause severe deposit-build up in the economizers of a grate-fired boiler. By increasing the molar ratio of the released K/P to above 2, the equilibrium distribution of the K and P species was changed significantly and the formation of H_3PO_4 (l) was not predicted by thermodynamic modelling.

7.2 Suggestions for future work

7.2.1 Future work on co-combustion of coal and SRF

Based on the results from the present thesis, the major technical issues which may hamper co-combustion of coal and SRF in a pulverized coal-fired power plant are probably the burnout and the problems related to the formation of fine particles, such as the dust/trace element emissions and the influence on the performance of the SCR unit.

Investigation on the burnout of the SRF particles in a pulverized coal-fired power plant is rather complicated due to the significantly different combustion/aerodynamic characteristics of the SRF compared to pulverized coal as well as the highly heterogeneous nature of the SRF. The SRF used in the full-scale pulverized coal-fired plants is usually in a fluffy form with a typical particle size of around 1 cm. These fluffy SRF particles may be comprised of different materials such as paper, wood, and plastics. Thus the combustion and aerodynamic behavior of different SRF particles/materials should be investigated at conditions similar to a pulverized coal-fired power plant. This requires a considerable retrofitting of the entrained flow reactor used in this work or the design of a new reactor at suspension-firing conditions. On the other hand, the fundamental aspects of SRF combustion, such as the pyrolysis and char reactivity of the SRF, also need to be investigated throughout. We have carried out some preliminary studies on the pyrolysis and co-pyrolysis of coal and different waste materials in a TGA. However, the results were not comprehensive enough and also deviated significantly from the practical conditions. Therefore, these results are not included in this thesis, but will be the subject of future studies. The fundamental aspects of SRF combustion described above may be implemented in CFD codes and allow a possibility to optimize the co-combustion through modeling.

A significant increase of the dust and trace element emissions has been observed in full-scale co-combustion of coal and SRF. This was presumably related to a reduced collection efficiency of the ESP, which may be induced by a decreased SO_3 formation. This explanation requires further confirmation through some fundamental tests, and the possibility of decreasing the dust emission by modifying the ESP operation needs to be investigated. The association and vaporization of trace elements during SRF combustion should be better characterized through further characterization, and the interactions between the vaporized trace elements and coal can be investigated through experiments and/or thermodynamic modeling. Another interesting aspect which needs further exploration is the generally high volatility of Ca during pulverized coal combustion. This phenomenon has been observed in the full-scale tests and entrained flow experiments of this thesis, as well as in a number of full-scale tests in literature. However, the interpretations provided in this thesis were qualitative, and need to be confirmed by further experiments.

7.2.2 Future work on straw dust-firing and the utilization of additives

In the present thesis, it was revealed that the addition of SBE could considerably inhibit the formation of KCl during straw dust-firing, thus having the potential to minimize the corrosion and ash deposition problems in straw combustion. In addition, the SBE has a relatively low price, a high heating value and a small particle size, which are all favorable conditions to be used as an additive in straw dust-firing. However, more investigations and characterizations are required in order to use the SBE under practical conditions. The sintering behavior of the deposits formed during SBE addition should be investigated, possibly through a long-term sintering test of the fly ash/deposits. This is mainly because of the relatively large Si content in the SBE, which may result in the formation of K-silicates with relatively low melting temperature. In addition, the pretreatment and dosage of SBE should be optimized based on the practical straw dust-firing conditions, and the effect of SBE addition on the formation of fine particles during straw-dust firing should be investigated by performing LPI measurements. A fundamental aspect of straw dust-firing which has not been well-explored is the release of the inorganic elements under suspension-firing conditions. This can be studied either through experiments or modeling, and will provide more insights into the selection of proper additives.

7.2.3 Future work on combustion of a phosphorus-rich biomass residue

In general, the combustion of phosphorus-rich biomass, particularly the behavior of ash, has not been well-understood. The work in the present thesis has shed some light on the association, release and transformation of P-related species during the combustion of a typical phosphorus-rich biomass. Although the proposed mechanisms require further validations both through experiments and more reliable modeling approach, the present results indicate that the P-rich biomass may have a significant potential to be used in co-combustion or biomass dust-firing. According to the present work, it seems that the formation of K_3PO_4 or KPO_3 are generally more thermodynamically favorable than that of KCl, and a high K/P molar ratio in the flue gas may favor the formation of K_3PO_4, which has a higher melting temperature than that of KPO_3. Therefore, with a well-controlled K, P and Cl ratio in the flue gas, the formation of KCl may be inhibited through a mechanism which is similar to sulphation. Besides, the formation of KPO_3 or K_3PO_4 may be thermodynamically favorable at high combustion temperature. This may be an advantage compared to the sulphation reaction, since the sulphation reactions are usually

thermodynamically restricted at high temperature. In addition, the formed KPO_3 or K_3PO_4 may have lower corrosion potential compared to K_2SO_4. In addition, the KPO_3 and K_3PO_4 may be quite suitable for use as fertilizers since both K and P are important elements to the growth of plants. In summary, the behavior of P species during combustion is an area which has not been well-explored. A lot of fundamental issues need to be addressed for this area with significant application potential.

References

[1] Leckner B. Co-combustion: A summary of technology. Thermal Science 2007;11:5-40.
[2] Sami M, Annamalai K, Wooldridge M. Co-firing of coal and biomass fuel blends. Prog Energy Combust Sci 2001;27:171-214.
[3] Baxter L Biomass-Coal Cofiring: an Overview of Technical Issues. In: Grammelis P, editor. Solid Biofuels for Energy. : Springer, 2011:43-73.
[4] Baxter L. Biomass-coal co-combustion: opportunity for affordable renewable energy. Fuel 2005;84:1295-302.
[5] Nussbaumer T. Combustion and co-combustion of biomass: fundamentals, technologies, and primary measures for emission reduction. Energy Fuels 2003;17:1510-21.
[6] Hupa M. Interaction of fuels in co-firing in FBC. Fuel 2005;84:1312-9.
[7] Tillman DA. Biomass cofiring: the technology, the experience, the combustion consequences. Biomass Bioenergy 2000;19:365-84.
[8] Sondreal EA, Benson SA, Hurley JP, et al. Review of advances in combustion technology and biomass cofiring. Fuel Process Technol 2001;71:7-38.
[9] Spliethoff H, Hein KRG. Effect of co-combustion of biomass on emissions in pulverized fuel furnaces. Fuel Process Technol 1998;54:189-205.
[10] Niksa S, Liu G, Hurt RH. Coal conversion submodels for design applications at elevated pressures. Part I. devolatilization and char oxidation. Prog Energy Combust Sci 2003;29:425-77.
[11] Solomon PR, Serio MA, Suuberg EM. Coal pyrolysis: Experiments, kinetic rates and mechanisms. Prog Energy Combust Sci 1992;18:133-220.
[12] Glarborg P, Jensen AD, Johnsson JE. Fuel nitrogen conversion in solid fuel fired systems. Prog Energy Combust Sci 2003;29:89-113.
[13] Solomon P, Fletcher T, Pugmire R. Progress in coal pyrolysis. Fuel 1993;72:587-97.
[14] Fletcher TH, Kerstein AR, Pugmire RJ, Solum MS, Grant DM. Chemical percolation model for devolatilization. 3. Direct use of carbon-13 NMR data to predict effects of coal type. Energy Fuels 1992;6:414-31.
[15] Chen JC, Niksa S. Coal devolatilization during rapid transient heating. 1. Primary devolatilization. Energy Fuels 1992;6:254-64.
[16] Serio MA, Hamblen DG, Markham JR, Solomon PR. Kinetics of volatile product evolution in coal pyrolysis: experiment and theory. Energy Fuels 1987;1:138-52.
[17] Suuberg EM, Peters WA, Howard JB. Proc Combust Inst 1979;17:117-30.
[18] Xu WC, Tomita A. Effect of coal type on the flash pyrolysis of various coals. Fuel 1987;66:627-31.
[19] Griffin TP, Howard JB, Peters WA. Pressure and temperature effects in bituminous coal pyrolysis: experimental observations and a transient lumped-parameter model. Fuel 1994;73:591-601.
[20] Xu WC, Tomita A. Effect of temperature on the flash pyrolysis of various coals. Fuel 1987;66:632-6.

[21] Chen JC, Castagnoli C, Niksa S. Coal devolatilization during rapid transient heating. 2. Secondary pyrolysis. Energy Fuels 1992;6:264-71.
[22] Zhang H, Fletcher TH. Nitrogen transformations during secondary coal pyrolysis. Energy Fuels 2001;15:1512-22.
[23] Xu WC, Tomita A. The effects of temperature and residence time on the secondary reactions of volatiles from coal pyrolysis. Fuel Process Technol 1989;21:25-37.
[24] Serio MA, Peters WA, Howard JB. Kinetics of vapor-phase secondary reactions of prompt coal pyrolysis tars. Ind Eng Chem Res 1987;26:1831-8.
[25] Doolan KR, Mackie JC, Tyler RJ. Coal flash pyrolysis: secondary cracking of tar vapours in the range 870-2000 K. Fuel 1987;66:572-8.
[26] Jenkins BM, Baxter LL, Miles Jr TR, Miles TR. Combustion properties of biomass. Fuel Process Technol 1998;54:17-46.
[27] Mohan D, Pittman Jr CU, Steele PH. Pyrolysis of wood/biomass for bio-oil: a critical review. Energy Fuels 2006;20:848-89.
[28] Di Blasi C. Combustion and gasification rates of lignocellulosic chars. Prog Energy Combust Sci 2009;35:121-40.
[29] Grammelis P, Basinas P, Malliopoulou A, Sakellaropoulos G. Pyrolysis kinetics and combustion characteristics of waste recovered fuels. Fuel 2009;88:195-205.
[30] Sørum L, Grønli MG, Hustad JE. Pyrolysis characteristics and kinetics of municipal solid wastes. Fuel 2001;80:1217-27.
[31] Heikkinen JM, Hordijk JC, De Jong W, Spliethoff H. Thermogravimetry as a tool to classify waste components to be used for energy generation. J Anal Appl Pyrolysis 2004;71:883-900.
[32] Zevenhoven R, Axelsen EP, Hupa M. Pyrolysis of waste-derived fuel mixtures containing PVC. Fuel 2002;81:507-10.
[33] De Jong W, Di Nola G, Venneker B, Spliethoff H, Wójtowicz M. TG-FTIR pyrolysis of coal and secondary biomass fuels: determination of pyrolysis kinetic parameters for main species and NOx precursors. Fuel 2007;86:2367-76.
[34] Vuthaluru HB. Investigations into the pyrolytic behaviour of coal/biomass blends using thermogravimetric analysis. Bioresour Technol 2004;92:187-95.
[35] Collot AG, Zhuo Y, Dugwell DR, Kandiyoti R. Co-pyrolysis and co-gasification of coal and biomass in bench-scale fixed-bed and fluidised bed reactors. Fuel 1999;78:667-79.
[36] Park DK, Kim SD, Lee SH, Lee JG. Co-pyrolysis characteristics of sawdust and coal blend in TGA and a fixed bed reactor. Bioresour Technol 2010;101:6151-6.
[37] Cordero T, Rodriguez-Mirasol J, Pastrana J, Rodriguez JJ. Improved solid fuels from co-pyrolysis of a high-sulphur content coal and different lignocellulosic wastes. Fuel 2004;83:1585-90.
[38] Ulloa CA, Gordon AL, Garcia XA. Thermogravimetric study of interactions in the pyrolysis of blends of coal with radiata pine sawdust. Fuel Process Technol 2009;90:583-90.
[39] Jones JM, Kubacki M, Kubica K, Ross AB, Williams A. Devolatilisation characteristics of coal and biomass blends. J Anal Appl Pyrolysis 2005;74:502-11.
[40] Haykiri-Acma H, Yaman S. Interaction between biomass and different rank coals during co-pyrolysis. Renewable Energy 2010;35:288-92.
[41] Moghtaderi B, Meesri C, Wall TF. Pyrolytic characteristics of blended coal and woody biomass. Fuel 2004;83:745-50.
[42] Zhang L, Xu S, Zhao W, Liu S. Co-pyrolysis of biomass and coal in a free fall reactor. Fuel 2007;86:353-9.

[43] Idris SS, Rahman NA, Ismail K, Alias AB, Rashid ZA, Aris MJ. Investigation on thermochemical behaviour of low rank Malaysian coal, oil palm biomass and their blends during pyrolysis via thermogravimetric analysis (TGA). Bioresour Technol 2010;101:4584-92.
[44] Biagini E, Lippi F, Petarca L, Tognotti L. Devolatilization rate of biomasses and coal-biomass blends: an experimental investigation. Fuel 2002;81:1041-50.
[45] Vamvuka D, Troulinos S, Kastanaki E. The effect of mineral matter on the physical and chemical activation of low rank coal and biomass materials. Fuel 2006;85:1763-71.
[46] Raveendran K, Ganesh A, Khilar KC. Influence of mineral matter on biomass pyrolysis characteristics. Fuel 1995;74:1812-22.
[47] Jensen A, Dam-Johansen K, Wójtowicz MA, Serio MA. TG-FTIR study of the influence of potassium chloride on wheat straw pyrolysis. Energy Fuels 1998;12:929-38.
[48] Skodras G, Grammelis P, Basinas P. Pyrolysis and combustion behaviour of coal-MBM blends. Bioresour Technol 2007;98:1-8.
[49] Cai J, Wang Y, Zhou L, Huang Q. Thermogravimetric analysis and kinetics of coal/plastic blends during co-pyrolysis in nitrogen atmosphere. Fuel Process Technol 2008;89:21-7.
[50] Sharma S, Ghoshal AK. Study of kinetics of co-pyrolysis of coal and waste LDPE blends under argon atmosphere. Fuel 2010;89:3943-51.
[51] Sharypov VI, Beregovtsova NG, Kuznetsov BN, et al. Influence of reaction parameters on brown coal-polyolefinic plastic co-pyrolysis behavior. J Anal Appl Pyrolysis 2007;78:257-64.
[52] Matsuzawa Y, Ayabe M, Nishino J. Acceleration of cellulose co-pyrolysis with polymer. Polym Degrad Stab 2001;71:435-44.
[53] Du X, Annamalai K. The transient ignition of isolated coal particle. Combust Flame 1994;97:339-54.
[54] Essenhigh RH, Misra MK, Shaw DW. Ignition of coal particles: a review. Combust Flame 1989;77:3-30.
[55] Sun CL, Zhang MY. Ignition of Coal Particles at High Pressure in a Thermogravimetric Analyzer. Combust Flame 1998;115:267-74.
[56] Katalambula H, Hayashi J, Chiba T, Kitano K, Ikeda K. Dependence of single coal particle ignition mechanism on the surrounding volatile matter cloud. Energy Fuels 1997;11:1033-9.
[57] Du X, Gopalakrishnan C, Annamalai K. Ignition and combustion of coal particle streams. Fuel 1995;74:487-94.
[58] Zhao Y, Kim HY, Yoon SS. Transient group combustion of the pulverized coal particles in spherical cloud. Fuel 2007;86:1102-11.
[59] Wendt C, Eigenbrod C, Moriue O, Rath HJ. A model for devolatilization and ignition of an axisymmetric coal particle. Proc Combust Inst 2002;29:449-57.
[60] Pedersen LS, Nielsen HP, Kiil S, et al. Full-scale co-firing of straw and coal. Fuel 1996;75:1584-90.
[61] Hansen PFB, Andersen KH, Wieck-Hansen K, et al. Co-firing straw and coal in a 150-MWe utility boiler: in situ measurements. Fuel Process Technol 1998;54:207-25.
[62] Andersen KH, Frandsen FJ, Hansen PFB, et al. Deposit formation in a 150 MWe utility PF-boiler during co-combustion of coal and straw. Energy Fuels 2000;14:765-80.
[63] Ballester J, Barroso J, Cerecedo LM, Ichaso R. Comparative study of semi-industrial-scale flames of pulverized coals and biomass. Combust Flame 2005;141:204-15.
[64] Damstedt B, Pederson JM, Hansen D, et al. Biomass cofiring impacts on flame structure and emissions. Proc Combust Inst 2007;31:2813-20.

[65] Yin C, Kær SK, Rosendahl L, Hvid SL. Co-firing straw with coal in a swirl-stabilized dual-feed burner: Modelling and experimental validation. Bioresour Technol 2010;101:4169-78.
[66] Lu H, Robert W, Peirce G, Ripa B, Baxter LL. Comprehensive study of Biomass particle combustion. Energy Fuels 2008;22:2826-39.
[67] Abbas T, Costen P, Kandamby NH, Lockwood FC, Ou JJ. The influence of burner injection mode on pulverized coal and biomass co-fired flames. Combust Flame 1994;99:617-25.
[68] Lu G, Yan Y, Cornwell S, Whitehouse M, Riley G. Impact of co-firing coal and biomass on flame characteristics and stability. Fuel 2008;87:1133-40.
[69] Gani A, Morishita K, Nishikawa K, Naruse I. Characteristics of co-combustion of low-rank coal with biomass. Energy Fuels 2005;19:1652-9.
[70] Arias B, Pevida C, Rubiera F, Pis JJ. Effect of biomass blending on coal ignition and burnout during oxy-fuel combustion. Fuel 2008;87:2753-9.
[71] Hurt RH. Structure, properties, and reactivity of solid fuels. Proc Combust Inst 1998;27:2887-904.
[72] Pedersen KH, Jensen AD, Skjøth-Rasmussen MS, Dam-Johansen K. A review of the interference of carbon containing fly ash with air entrainment in concrete. Prog Energy Combust Sci 2008;34:135-54.
[73] Lang T, Hurt RH. Char combustion reactivities for a suite of diverse solid fuels and char-forming organic model compounds. Proc Combust Inst 2002;29:423-31.
[74] Campbell PA, Mitchell RE, Ma L. Characterization of coal char and biomass char reactivities to oxygen. Proc Combust Inst 2002;29:519-26.
[75] Zolin A, Jensen A, Dam-Johansen K. Kinetic analysis of char thermal deactivation. Proc Combust Inst 2000;28:2181-8.
[76] Zolin A, Jensen AD, Jensen PA, Dam-Johansen K. Experimental study of char thermal deactivation. Fuel 2002;81:1065-75.
[77] Kastanaki E, Vamvuka D. A comparative reactivity and kinetic study on the combustion of coal-biomass char blends. Fuel 2006;85:1186-93.
[78] Zolin A, Jensen A, Jensen PA, Frandsen F, Dam-Johansen K. The influence of inorganic materials on the thermal deactivation of fuel chars. Energy Fuels 2001;15:1110-22.
[79] Wieck-Hansen K, Overgaard P, Larsen OH. Cofiring coal and straw in a 150 MWe power boiler experiences. Biomass Bioenergy 2000;19:395-409.
[80] Kostamo JA. Co-firing of sawdust in a coal fired utility boiler. IFRF Combustion Journal 2000.
[81] Kruczek H, RĄCzka P, Tatarek A. The effect of biomass on pollutant emission and burnout in co-combustion with coal. Combust Sci Technol 2006;178:1511-39.
[82] Munir S, Nimmo W, Gibbs BM. The effect of air staged, co-combustion of pulverised coal and biomass blends on NOx emissions and combustion efficiency. Fuel 2011;90:126-35.
[83] Smart JP, Patel R, Riley GS. Oxy-fuel combustion of coal and biomass, the effect on radiative and convective heat transfer and burnout. Combust Flame 2010;157:2230-40.
[84] Gera D, Mathur MP, Freeman MC, Robinson A. Effect of large aspect ratio of biomass particles on carbon burnout in a utility boiler. Energy Fuels 2002;16:1523-32.
[85] Boylan DM. Southern company tests of wood/coal cofiring in pulverized coal units. Biomass Bioenergy 1996;10:139-47.
[86] Lang T, Jensen AD, Jensen PA. Retention of organic elements during solid fuel pyrolysis with emphasis on the peculiar behavior of nitrogen. Energy Fuels 2005;19:1631-43.

[87] Tian FJ, Yu J, McKenzie LJ, Hayashi J, Li CZ. Conversion of fuel-N into HCN and NH3 during the pyrolysis and gasification in steam: a comparative study of coal and biomass. Energy Fuels 2007;21:517-21.
[88] Di Nola G, de Jong W, Spliethoff H. TG-FTIR characterization of coal and biomass single fuels and blends under slow heating rate conditions: Partitioning of the fuel-bound nitrogen. Fuel Process Technol 2010;91:103-15.
[89] Di Nola G, de Jong W, Spliethoff H. The fate of main gaseous and nitrogen species during fast heating rate devolatilization of coal and secondary fuels using a heated wire mesh reactor. Fuel Process Technol 2009;90:388-95.
[90] Li CZ, Tan LL. Formation of NOx and SOx precursors during the pyrolysis of coal and biomass. Part III. Further discussion on the formation of HCN and NH3 during pyrolysis. Fuel 2000;79:1899-906.
[91] Pedersen LS, Morgan DJ, Van de Kamp WL, Christensen J, Jespersen P, Dam-Johansen K. Effects on SOx and NOx emissions by co-firing straw and pulverized coal. Energy Fuels 1997;11:439-46.
[92] Annamalai K, Thien B, Sweeten J. Co-firing of coal and cattle feedlot biomass (FB) fuels. Part II. Performance results from 30 kWt (100,000) BTU/h laboratory scale boiler burner. Fuel 2003;82:1183-93.
[93] Robinson AL, Junker H, Buckley SG, Sclippa G, Baxter LL. Interactions between coal and biomass when cofiring. Proc Combust Inst 1998;27:1351-9.
[94] Vilas E, Skifter U, Jensen AD, López C, Maier J, Glarborg P. Experimental and modeling study of biomass reburning. Energy Fuels 2004;18:1442-50.
[95] Harding NS, Adams BR. Biomass as a reburning fuel: a specialized cofiring application. Biomass Bioenergy 2000;19:429-45.
[96] Wei X, Lopez C, von Puttkamer T, Schnell U, Unterberger S, Hein KRG. Assessment of Chlorine− Alkali− Mineral Interactions during Co-Combustion of Coal and Straw. Energy Fuels 2002;16:1095-108.
[97] Cao Y, Zhou HC, Jiang W, Chen CW, Pan WP. Studies of the Fate of Sulfur Trioxide in Coal-Fired Utility Boilers Based on Modified Selected Condensation Methods. Environ Sci Technol 2010;44:3429-34.
[98] Leckner B, Karlsson M. Gaseous emissions from circulating fluidized bed combustion of wood. Biomass Bioenergy 1993;4:379-89.
[99] Zheng Y, Jensen PA, Jensen AD, Sander B, Junker H. Ash transformation during co-firing coal and straw. Fuel 2007;86:1008-20.
[100] Robinson AL, Junker H, Baxter LL. Pilot-scale investigation of the influence of coal-biomass cofiring on ash deposition. Energy Fuels 2002;16:343-55.
[101] Kupka T, Mancini M, Irmer M, Weber R. Investigation of ash deposit formation during co-firing of coal with sewage sludge, saw-dust and refuse derived fuel. Fuel 2008;87:2824-37.
[102] Ferrer E, Aho M, Silvennoinen J, Nurminen RV. Fluidized bed combustion of refuse-derived fuel in presence of protective coal ash. Fuel Process Technol 2005;87:33-44.
[103] Fernandez A, Wendt JOL, Wolski N, Hein KRG, Wang S, Witten ML. Inhalation health effects of fine particles from the co-combustion of coal and refuse derived fuel. Chemosphere 2003;51:1129-37.
[104] Wei X, Wang Y, Liu D, Sheng H, Tian W, Xiao Y. Release of Sulfur and Chlorine during Cofiring RDF and Coal in an Internally Circulating Fluidized Bed. Energy Fuels 2009;23:1390-7.

[105] Vassilev SV, Baxter D, Andersen LK, Vassileva CG. An overview of the chemical composition of biomass. Fuel 2010;89:913-33.
[106] Vainikka P, Enestam S, Silvennoinen J, et al. Bromine as an ash forming element in a fluidised bed boiler combusting solid recovered fuel. Fuel 2011;90:1101-12.
[107] Zheng Y, Jensen PA, Jensen AD. A kinetic study of gaseous potassium capture by coal minerals in a high temperature fixed-bed reactor. Fuel 2008;87:3304-12.
[108] Cenni R, Frandsen F, Gerhardt T, Spliethoff H, Hein KRG. Study on trace metal partitioning in pulverized combustion of bituminous coal and dry sewage sludge. Waste Manage 1998;18:433-44.
[109] Seames WS, Fernandez A, Wendt JOL. A study of fine particulate emissions from combustion of treated pulverized municipal sewage sludge. Environ Sci Technol 2002;36:2772-6.
[110] Yao H, Mkilaha ISN, Naruse I. Screening of sorbents and capture of lead and cadmium compounds during sewage sludge combustion. Fuel 2004;83:1001-7.
[111] Werther J, Ogada T. Sewage sludge combustion. Prog Energy Combust Sci 1999;25:55-116.
[112] Sweeten JM, Annamalai K, Thien B, McDonald LA. Co-firing of coal and cattle feedlot biomass (FB) fuels. Part I. Feedlot biomass (cattle manure) fuel quality and characteristics* 1. Fuel 2003;82:1167-82.
[113] Tortosa Masiá AA, Buhre BJP, Gupta RP, Wall TF. Characterising ash of biomass and waste. Fuel Process Technol 2007;88:1071-81.
[114] Sable SP, De Jong W, Meij R, Spliethoff H. Effect of secondary fuels and combustor temperature on mercury speciation in pulverized fuel CO-combustion: Part 1. Energy Fuels 2007;21:1883-90.
[115] Lindström E, Sandström M, Boström D, Öhman M. Slagging characteristics during combustion of cereal grains rich in phosphorus. Energy Fuels 2007;21:710-7.
[116] Bäfver LS, Rönnbäck M, Leckner B, Claesson F, Tullin C. Particle emission from combustion of oat grain and its potential reduction by addition of limestone or kaolin. Fuel Process Technol 2009;90:353-9.
[117] Piotrowska P, Zevenhoven M, Davidsson K, et al. Fate of Alkali Metals and Phosphorus of Rapeseed Cake in Circulating Fluidized Bed Boiler Part 1: Cocombustion with Wood. Energy Fuels 2010;24:333-45.
[118] Piotrowska P, Zevenhoven M, Davidsson K, et al. Fate of Alkali Metals and Phosphorus of Rapeseed Cake in Circulating Fluidized Bed Boiler Part 2: Cocombustion with Coal. Energy Fuels 2010;24:4193-205.
[119] Eriksson G, Hedman H, Boström D, Pettersson E, Backman R, Öhman M. Combustion Characterization of Rapeseed Meal and Possible Combustion Applications. Energy Fuels 2009;23:3930-9.
[120] Davidson RM, Clarke LB. Trace elements in coal. : IEA Coal Research, 1996.
[121] Lighty JS, Veranth JM, Sarofim AF. Combustion aerosols: factors governing their size and composition and implications to human health. J Air Waste Manage Assoc 2000;50:1565-618.
[122] Gupta RP, Wall TF, Kajigaya I, Miyamae S, Tsumita Y. Computer-controlled scanning electron microscopy of minerals in coal--Implications for ash deposition. Prog Energy Combust Sci 1998;24:523-43.
[123] Huggins FE. Overview of analytical methods for inorganic constituents in coal. Int J Coal Geol 2002;50:169-214.

[124] Benson SA, Holm PL. Comparison of inorganic constituents in three low-rank coals. Ind Eng Chem Prod Res Dev 1985;24:145-9.
[125] Miller RN, Given PH. The association of major, minor and trace inorganic elements with lignites. I. Experimental approach and study of a North Dakota lignite. Geochim Cosmochim Acta 1986;50:2033-43.
[126] Baxter LL, Miles TR, Miles Jr TR, et al. The behavior of inorganic material in biomass-fired power boilers: field and laboratory experiences. Fuel Process Technol 1998;54:47-78.
[127] Zevenhoven-Onderwater M, Blomquist JP, Skrifvars BJ, Backman R, Hupa M. The prediction of behaviour of ashes from five different solid fuels in fluidised bed combustion. Fuel 2000;79:1353-61.
[128] Frandsen FJ, van Lith SC, Korbee R, et al. Quantification of the release of inorganic elements from biofuels. Fuel Process Technol 2007;88:1118-28.
[129] Werkelin J, Skrifvars BJ, Zevenhoven M, Holmbom B, Hupa M. Chemical forms of ash-forming elements in woody biomass fuels. Fuel 2010;89:481-93.
[130] Miles TR, Miles Jr. TR, Baxter LL, Bryers RW, Jenkin BM, Oden LL. Alkali deposits found in biomass power plants: a preliminary investigation of their extent and nature: Vol I, SAND96-8225, Vol. 2 and NREL/TP-433-8142. 1996.
[131] Pettersson A, Zevenhoven M, Steenari BM, Åmand LE. Application of chemical fractionation methods for characterisation of biofuels, waste derived fuels and CFB co-combustion fly ashes. Fuel 2008;87:3183-93.
[132] Zevenhoven-Onderwater M, Öhman M, Skrifvars BJ, Backman R, Nordin A, Hupa M. Bed agglomeration characteristics of wood-derived fuels in FBC. Energy Fuels 2006;20:818-24.
[133] Aho M, Gil A, Taipale R, Vainikka P, Vesala H. A pilot-scale fireside deposit study of co-firing Cynara with two coals in a fluidised bed. Fuel 2008;87:58-69.
[134] Aho M, Ferrer E. Importance of coal ash composition in protecting the boiler against chlorine deposition during combustion of chlorine-rich biomass. Fuel 2005;84:201-12.
[135] Baxter LL. Ash Deposit Formation and Deposit Properties. A Comprehensive Summary of Research Conducted at Sandia's Combustion Research Facility. Ash Deposit Formation and Deposit Properties.A Comprehensive Summary of Research Conducted at Sandia's Combustion Research FacilitySandia National Labs., Albuquerque, NM (US); Sandia National Labs., Livermore, CA (US), 2000.
[136] Westberg HM, Bystrom M, Leckner B. Distribution of potassium, chlorine, and sulfur between solid and vapor phases during combustion of wood chips and coal. Energy Fuels 2003;17:18-28.
[137] Huggins FE, Seidu LBA, Shah N, et al. Elemental modes of occurrence in an Illinois# 6 coal and fractions prepared by physical separation techniques at a coal preparation plant. Int J Coal Geol 2009;78:65-76.
[138] Zhang L, Ninomiya Y, Yamashita T. Occurrence of inorganic elements in condensed volatile matter emitted from coal pyrolysis and their contributions to the formation of ultrafine particulates during coal combustion. Energy Fuels 2006;20:1482-9.
[139] Wall TF. Mineral matter transformations and ash deposition in pulverised coal combustion. Proc Combust Inst 1992;24:1119-26.
[140] Tillman DA, Duong D, Miller B. Chlorine in solid fuels fired in pulverized fuel boilers - sources, forms, reactions and consequences: a literature review. Energy Fuels 2009;23:3379-91.
[141] van lith SC. Release of inorganic elements during wood-firing on a grate. PhD thesis, Department of Chemical Engineering, Technical University of Denmark, 2005.

[142] Knudsen JN. Volatilization of inorganic matter during combustion of annual biomass. PhD thesis. Department of Chemical Engineering, Technical University of Denmark, 2004.
[143] Calkins WH. The chemical forms of sulfur in coal: a review. Fuel 1994;73:475-84.
[144] Knudsen JN, Jensen PA, Lin W, Frandsen FJ, Dam-Johansen K. Sulfur transformations during thermal conversion of herbaceous biomass. Energy Fuels 2004;18:810-9.
[145] Senior CL, Helble JJ, Sarofim AF. Emissions of mercury, trace elements, and fine particles from stationary combustion sources. Fuel Process Technol 2000;65:263-88.
[146] Linak WP, Wendt JOL. Toxic metal emissions from incineration: mechanisms and control. Prog Energy Combust Sci 1993;19:145-85.
[147] Buhre BJP, Hinkley JT, Gupta RP, Wall TF, Nelson PF. Submicron ash formation from coal combustion. Fuel 2005;84:1206-14.
[148] Linak WP, Wendt JOL. Trace metal transformation mechanisms during coal combustion. Fuel Process Technol 1994;39:173-98.
[149] Xu M, Yu D, Yao H, Liu X, Qiao Y. Coal combustion-generated aerosols: Formation and properties. Proc Combust Inst 2011;33:1681-97.
[150] Frandsen FJ, Visser R, Jokiniemi J, Wigley F, Sarofim AF. A humble note on gaps in the understanding of release fly ash and combustion aerosol formation in boilers. Proceedings of the Impacts of Fuel Quality on Power Generation and the Environment, 2010, Lapland, Finland.
[151] Linak WP, Miller CA, Seames WS, et al. On trimodal particle size distributions in fly ash from pulverized-coal combustion. Proc Combust Inst 2002;29:441-7.
[152] Quann RJ, Sarofim AF. Vaporization of refractory oxides during pulverized coal combustion. Proc Combust Inst 1982;19:1429-40.
[153] Neville M, Sarofim AF. The fate of sodium during pulverized coal combustion. Fuel 1985;64:384-90.
[154] Quann RJ, Neville M, Janghorbani M, Mims CA, Sarofim AF. Mineral matter and trace-element vaporization in a laboratory-pulverized coal combustion system. Environ Sci Technol 1982;16:776-81.
[155] Helble JJ, Sarofim AF. Factors determining the primary particle size of flame-generated inorganic aerosols. J Colloid Interface Sci 1989;128:348-62.
[156] Lee CM, Davis KA, Heap MP, Eddings E, Sarofim A. Modeling the vaporization of ash constituents in a coal-fired boiler. Proc Combust Inst 2000;28:2375-82.
[157] Eddings EG, Sarofim AF, Lee CM, Davis KA, Valentine JR. Trends in predicting and controlling ash vaporization in coal-fired utility boilers. Fuel Process Technol 2001;71:39-51.
[158] Flagan RC, Taylor DD. Laboratory studies of submicron particles from coal combustion. Proc Combust Inst 1981;18:1227-37.
[159] Senior CL, Flagan RC. Ash vaporization and condensation during combustion of a suspended coal particle. Aerosol Sci Tech 1982;1:371-83.
[160] Senior CL, Flagan RC. Synthetic chars for the study of ash vaporization. Proc Combust Inst 1984;20:921-9.
[161] McNallan MJ, Yurek GJ, Elliott JF. The formation of inorganic particulates by homogeneous nucleation in gases produced by the combustion of coal. Combust Flame 1981;42:45-60.
[162] Srinivasachar S, Helble JJ, Ham DO, Domazetis G. A kinetic description of vapor phase alkali transformations in combustion systems. Prog Energy Combust Sci 1990;16:303-9.
[163] Lindner ER, Wall TF. Sodium ash reactions during combustion of pulverised coal. Proc Combust Inst 1991;23:1313-21.

[164] Zhang L, Wang Q, Sato A, Ninomiya Y, Yamashitas T. Interactions among Inherent Minerals during Coal Combustion and Their Impacts on the Emission of PM10. 2. Emission of Submicrometer-Sized Particles. Energy Fuels 2007;21:766-77.
[165] Korbee R, Shah KV, Cieplik MK, Betrand CI, Vuthaluru HB, van de Kamp WL. First Line Ash Transformations of Coal and Biomass Fuels during PF Combustion. Energy Fuels 2010;24:897-909.
[166] Shah KV, Cieplik MK, Betrand CI, Van de Kamp WL, Vuthaluru HB. Correlating the effects of ash elements and their association in the fuel matrix with the ash release during pulverized fuel combustion. Fuel Process Technol 2010;91:531-45.
[167] Knudsen JN, Jensen PA, Dam-Johansen K. Transformation and release to the gas phase of Cl, K, and S during combustion of annual biomass. Energy Fuels 2004;18:1385-99.
[168] van Lith SC, Jensen PA, Frandsen FJ, Glarborg P. Release to the Gas Phase of Inorganic Elements during Wood Combustion. Part 2: Influence of Fuel Composition. Energy Fuels 2008;22:1598-609.
[169] Novaković A, van Lith SC, Frandsen FJ, Jensen PA, Holgersen LB. Release of Potassium from the Systems K− Ca− Si and K− Ca− P. Energy Fuels 2009;23:3423-8.
[170] van Lith SC, Alonso-Ramírez V, Jensen PA, Frandsen FJ, Glarborg P. Release to the gas phase of inorganic elements during wood combustion. Part 1: development and evaluation of quantification methods. Energy Fuels 2006;20:964-78.
[171] Pedersen AJ, Frandsen FJ, Riber C, et al. A Full-scale Study on the Partitioning of Trace Elements in Municipal Solid Waste Incineration—Effects of Firing Different Waste Types. Energy Fuels 2009;23:3475-89.
[172] Pedersen AJ, Van Lith SC, Frandsen FJ, Steinsen SD, Holgersen LB. Release to the gas phase of metals, S and Cl during combustion of dedicated waste fractions. Fuel Process Technol 2010;91:1062-72.
[173] Jensen PA, Frandsen FJ, Dam-Johansen K, Sander B. Experimental investigation of the transformation and release to gas phase of potassium and chlorine during straw pyrolysis. Energy Fuels 2000;14:1280-5.
[174] Dayton DC, Jenkins BM, Turn SQ, et al. Release of inorganic constituents from leached biomass during thermal conversion. Energy Fuels 1999;13:860-70.
[175] Björkman E, Strömberg B. Release of Chlorine from Biomass at Pyrolysis and Gasification Conditions1. Energy Fuels 1997;11:1026-32.
[176] Wendt JOL, Lee SJ. High-temperature sorbents for Hg, Cd, Pb, and other trace metals: Mechanisms and applications. Fuel 2010;89:894-903.
[177] Gale TK, Wendt JOL. High-temperature interactions between multiple-metals and kaolinite. Combust Flame 2002;131:299-307.
[178] Gallagher NB, Peterson TW, Wendt JOL. Sodium Partitioning in a Pulverized Coal Combustion Environment. Proc Combust Inst 1996;26:3197-204.
[179] Mwabe PO, Wendt JOL. Mechanisms governing trace sodium capture by kaolinite in a downflow combustor. Proc Combust Inst 1996;26:2447-53.
[180] Gale TK, Wendt JOL. Mechanisms and Models Describing Sodium and Lead Scavenging by a Kaolinite Aerosol at High Temperatures. Aerosol Sci Tech 2003;37:865-76.
[181] Takuwa T, Naruse I. Detailed kinetic and control of alkali metal compounds during coal combustion. Fuel Process Technol 2007;88:1029-34.
[182] Uberoi M, Punjak WA, Shadman F. The kinetics and mechanism of alkali removal from flue gases by solid sorbents. Prog Energy Combust Sci 1990;16:205-11.

[183] Punjak WA, Uberoi M, Shadman F. High-temperature adsorption of alkali vapors on solid sorbents. AICHE J 1989;35:1186-94.
[184] Punjak WA, Shadman F. Aluminosilicate sorbents for control of alkali vapors during coal combustion and gasification. Energy Fuels 1988;2:702-8.
[185] Gale TK, Wendt JOL. In-furnace capture of cadmium and other semi-volatile metals by sorbents. Proc Combust Inst 2005;30:2999-3007.
[186] Tran KQ, Iisa K, Steenari BM, Lindqvist O. A kinetic study of gaseous alkali capture by kaolin in the fixed bed reactor equipped with an alkali detector. Fuel 2005;84:169-75.
[187] Steenari BM, Lindqvist O. High-temperature reactions of straw ash and the anti-sintering additives kaolin and dolomite. Biomass Bioenergy 1998;14:67-76.
[188] Kyi S, Chadwick BL. Screening of potential mineral additives for use as fouling preventatives in Victorian brown coal combustion. Fuel 1999;78:845-55.
[189] Dou B, Shen W, Gao J, Sha X. Adsorption of alkali metal vapor from high-temperature coal-derived gas by solid sorbents. Fuel Process Technol 2003;82:51-60.
[190] Wu B, Jaanu KK, Shadman F. Multi-functional sorbents for the removal of sulfur and metallic contaminants from high-temperature gases. Environ Sci Technol 1995;29:1660-5.
[191] Iisa K, Lu Y, Salmenoja K. Sulfation of potassium chloride at combustion conditions. Energy Fuels 1999;13:1184-90.
[192] Glarborg P, Marshall P. Mechanism and modeling of the formation of gaseous alkali sulfates. Combust Flame 2005;141:22-39.
[193] Glarborg P. Hidden interactions--Trace species governing combustion and emissions. Proc Combust Inst 2007;31:77-98.
[194] Hindiyarti L, Frandsen F, Livbjerg H, Glarborg P, Marshall P. An exploratory study of alkali sulfate aerosol formation during biomass combustion. Fuel 2008;87:1591-600.
[195] Steinberg M, Schofield K. The controlling chemistry in flame generated surface deposition of Na2SO4 and the effects of chlorine. Proc Combust Inst 1996;26:1835-43.
[196] Wolf KJ, Smeda A, Müller M, Hilpert K. Investigations on the influence of additives for SO2 reduction during high alkaline biomass combustion. Energy Fuels 2005;19:820-4.
[197] Aho M, Vainikka P, Taipale R, Yrjas P. Effective new chemicals to prevent corrosion due to chlorine in power plant superheaters. Fuel 2008;87:647-54.
[198] Davidsson KO, Åmand LE, Steenari BM, Elled AL, Eskilsson D, Leckner B. Countermeasures against alkali-related problems during combustion of biomass in a circulating fluidized bed boiler. Chemical Engineering Science 2008;63:5314-29.
[199] Kassman H, Bäfver L, Åmand LE. The importance of SO2 and SO3 for sulphation of gaseous KCl-An experimental investigation in a biomass fired CFB boiler. Combust Flame 2010;157:1649-57.
[200] Steinberg M, Schofield K. The chemistry of sodium with sulfur in flames. Prog Energy Combust Sci 1990;16:311-7.
[201] Schofield K, Steinberg M. Sodium/sulfur chemical behavior in fuel-rich and-lean flames. J Phys Chem 1992;96:715-26.
[202] Steinberg M, Schofield K. The controlling chemistry of surface deposition from sodium and potassium seeded flames free of sulfur or chlorine impurities. Combust Flame 2002;129:453-70.
[203] Boonsongsup L, Iisa K, Frederick Jr WJ. Kinetics of the sulfation of NaCl at combustion conditions. Ind Eng Chem Res 1997;36:4212-6.

[204] Matsuda H, Ozawa S, Naruse K, Ito K, Kojima Y, Yanase T. Kinetics of HCl emission from inorganic chlorides in simulated municipal wastes incineration conditions. Chem Eng Sci 2005;60:545-52.
[205] Jensen JR, Nielsen LB, Schultz-Møller C, Wedel S, Livbjerg H. The nucleation of aerosols in flue gases with a high content of alkali-A laboratory study. Aerosol Sci Tech 2000;33:490-509.
[206] Christensen KA, Livbjerg H. A plug flow model for chemical reactions and aerosol nucleation and growth in an alkali-containing flue gas. Aerosol Sci Tech 2000;33:470-89.
[207] Christensen KA, Stenholm M, Livbjerg H. The formation of submicron aerosol particles, HCl and SO2 in straw-fired boilers. J Aerosol Sci 1998;29:421-44.
[208] Jimenez S, Ballester J. Effect of co-firing on the properties of submicron aerosols from biomass combustion. Proc Combust Inst 2005;30:2965-72.
[209] Jimenez S, Ballester J. Influence of operating conditions and the role of sulfur in the formation of aerosols from biomass combustion. Combust Flame 2005;140:346-58.
[210] Nielsen HP, Baxter LL, Sclippab G, Morey C, Frandsen FJ, Dam-Johansen K. Deposition of potassium salts on heat transfer surfaces in straw-fired boilers: a pilot-scale study. Fuel 2000;79:131-9.
[211] Frandsen FJ. Utilizing biomass and waste for power production—a decade of contributing to the understanding, interpretation and analysis of deposits and corrosion products. Fuel 2005;84:1277-94.
[212] Broström M, Kassman H, Helgesson A, et al. Sulfation of corrosive alkali chlorides by ammonium sulfate in a biomass fired CFB boiler. Fuel Process Technol 2007;88:1171-7.
[213] McElroy MW, Carr RC, Ensor DS, Markowski GR. Size distribution of fine particles from coal combustion. Science 1982;215:13.
[214] Kauppinen EI, Pakkanen TA. Coal combustion aerosols: a field study. Environ Sci Technol 1990;24:1811-8.
[215] Yi H, Hao J, Duan L, Tang X, Ning P, Li X. Fine particle and trace element emissions from an anthracite coal-fired power plant equipped with a bag-house in China. Fuel 2008;87:2050-7.
[216] Zheng Y, Jensen AD, Johnsson JE. Deactivation of V2O5-WO3-TiO2 SCR catalyst at a biomass-fired combined heat and power plant. Appl Catal B-Environ 2005;60:253-64.
[217] Beck J, Brandenstein J, Unterberger S, Hein KRG. Effects of sewage sludge and meat and bone meal co-combustion on SCR catalysts. Applied Catalysis B: Environmental 2004;49:15-25.
[218] Zhang L, Ninomiya Y, Yamashita T. Formation of submicron particulate matter (PM1) during coal combustion and influence of reaction temperature. Fuel 2006;85:1446-57.
[219] Senior CL, Bool LE, Srinivasachar S, Pease BR, Porle K. Pilot scale study of trace element vaporization and condensation during combustion of a pulverized sub-bituminous coal. Fuel Process Technol 2000;63:149-65.
[220] Senior CL, BoolIII LE, Morency JR. Laboratory study of trace element vaporization from combustion of pulverized coal. Fuel Process Technol 2000;63:109-24.
[221] Linak WP, Yoo JI, Wasson SJ, et al. Ultrafine ash aerosols from coal combustion: Characterization and health effects. Proc Combust Inst 2007;31:1929-37.
[222] Yu D, Xu M, Yao H, Liu X, Zhou K. A new method for identifying the modes of particulate matter from pulverized coal combustion. Powder Technol 2007.
[223] Yu D, Xu M, Yao H, et al. Use of elemental size distributions in identifying particle formation modes. Proc Combust Inst 2007;31:1921-8.

[224] Seames WS. An initial study of the fine fragmentation fly ash particle mode generated during pulverized coal combustion. Fuel Process Technol 2003;81:109-25.
[225] Nielsen MT, Livbjerg H, Fogh CL, et al. Formation and emission of fine particles from two coal-fired power plants. Combust Sci Technol 2002;174:79-113.
[226] Nielsen LB, Livbjerg H. Aerosol measurement at MKS1: supplementary measurements 3a, 8a, and 9a. Department of Chemical Engineering, Technical University of Denmark, 1997.
[227] Nielsen LB, Pedersen C, Røkke M, Livbjerg H. Aerosol measurements at MKS1 - final report. Department of Chemical Engineering, Technical University of Denmark, 1996.
[228] Markowski GR, Filby R. Trace element concentration as a function of particle size in fly ash from a pulverized coal utility boiler. Environ Sci Technol 1985;19:796-804.
[229] Skrifvars BJ, Laurén T, Hupa M, Korbee R, Ljung P. Ash behaviour in a pulverized wood fired boiler--a case study. Fuel 2004;83:1371-9.
[230] Tissari J, Sippula O, Kouki J, Vuorio K, Jokiniemi J. Fine particle and gas emissions from the combustion of agricultural fuels fired in a 20 kW burner. Energy Fuels 2008;22:2033-42.
[231] Jimenez S, Ballester J. Particulate matter formation and emission in the combustion of different pulverized biomass fuels. Combustion Sci Technol 2006;178:655-83.
[232] Wolski N, Maier J, Hein KRG. Fine particle formation from co-combustion of sewage sludge and bituminous coal. Fuel Process Technol 2004;85:673-86.
[233] Sarofim AF, Howard JB, Padia AS. The physical transformation of the mineral matter in pulverized coal under simulated combustion conditions. Combustion Sci Technol 1977;16:187-204.
[234] Damle AS, Ensor DS, Ranade MB. Coal combustion aerosol formation mechanisms: a review. Aerosol Sci Tech 1982;1:119-33.
[235] Nielsen LB. Combustion aerosols from potassium-containing fuels, PhD Thesis. Department of Chemical Engineering, Technical University of Denmark, 1998.
[236] Jimenez S. Submicron particle formation in biomass combustion, PhD Thesis. LITEC/Fluid Mechanics Group, University of Zaragoza, Spain, 2004.
[237] Zeuthen JH, Jensen PA, Jensen JP, Livbjerg H. Aerosol formation during the combustion of straw with addition of sorbents. Energy Fuels 2007;21:699-709.
[238] Kauppinen EI, Lind TM, Valmari T, et al. The structure of submicron ash from combustion of pulverized South African and Colombian coals. Applications of Advanced Technology to Ash-Related Problems in Boilers 1996:471.
[239] Yan L, Gupta RP, Wall TF. A mathematical model of ash formation during pulverized coal combustion. Fuel 2002;81:337-44.
[240] Helble JJ, Sarofim AF. Influence of char fragmentation on ash particle size distributions. Combust Flame 1989;76:183-96.
[241] Christensen KA, Livbjerg H. A field study of submicron particles from the combustion of straw. Aerosol Sci Tech 1996;25:185-99.
[242] Zeuthen JH. The formation of aerosol particles during combustion of biomass and waste, PhD Thesis. Department of Chemical Engineering, Technical University of Denmark, 2007.
[243] Bryers RW. Fireside slagging, fouling, and high-temperature corrosion of heat-transfer surface due to impurities in steam-raising fuels. Prog Energy Combust Sci 1996;22:29-120.
[244] Baxter LL. Ash deposition during biomass and coal combustion: a mechanistic approach. Biomass Bioenergy 1993;4:85-102.
[245] Nielsen HP. Deposition and high-temperature corrosion in biomass-fired boilers, PhD Thesis. Department of Chemical Engineering, Technical University of Denmark, 1998.

[246] Kupka T, Zając K, Weber R. Effect of Fuel Type and Deposition Surface Temperature on the Growth and Structure of an Ash Deposit Collected during Co-firing of Coal with Sewage Sludge and Sawdust. Energy Fuels 2009;23:3429-36.
[247] Zbogar A, Frandsen F, Jensen PA, Glarborg P. Shedding of ash deposits. Prog Energy Combust Sci 2009;35:31-56.
[248] Heinzel T, Siegle V, Spliethoff H, Hein KRG. Investigation of slagging in pulverized fuel co-combustion of biomass and coal at a pilot-scale test facility. Fuel Process Technol 1998;54:109-25.
[249] Theis M, Skrifvars BJ, Hupa M, Tran H. Fouling tendency of ash resulting from burning mixtures of biofuels. Part 1: Deposition rates. Fuel 2006;85:1125-30.
[250] Theis M, Skrifvars BJ, Zevenhoven M, Hupa M, Tran H. Fouling tendency of ash resulting from burning mixtures of biofuels. Part 2: Deposit chemistry. Fuel 2006;85:1992-2001.
[251] Wigley F, Williamson J, Malmgren A, Riley G. Ash deposition at higher levels of coal replacement by biomass. Fuel Process Technol 2007;88:1148-54.
[252] Fryda L, Sobrino C, Cieplik M, Van de Kamp WL. Study on ash deposition under oxyfuel combustion of coal/biomass blends. Fuel 2010;89:1889-902.
[253] Hansen LA, Frandsen FJ, Dam-Johansen K, Sorensen HS, Skrifvars BJ. Characterization of ashes and deposits from high-temperature coal− straw co-firing. Energy Fuels 1999;13:803-16.
[254] Lokare SS, Dunaway JD, Moulton D, Rogers D, Dale R, Baxter LL. Investigation of ash deposition rates for a suite of biomass fuels and fuel blends. Energy Fuels 2006;20:1008-14.
[255] Bartolomé C, Gil A, Ramos I. Ash deposition behavior of cynara-coal blends in a PF pilot furnace. Fuel Process Technol 2010;91:1576-84.
[256] Abreu P, Casaca C, Costa M. Ash deposition during the co-firing of bituminous coal with pine sawdust and olive stones in a laboratory furnace. Fuel 2010;89:4040-8.
[257] Arvelakis S, Frandsen FJ. Rheology of fly ashes from coal and biomass co-combustion. Fuel 2010;89:3132-40.
[258] Arvelakis S, Frandsen FJ. Melting Behavior of Ashes from the Co-combustion of Coal and Straw. Energy Fuels 2007;21:3004-9.
[259] Theis M, Skrifvars BJ, Zevenhoven M, Hupa M, Tran H. Fouling tendency of ash resulting from burning mixtures of biofuels. Part 3. Influence of probe surface temperature. Fuel 2006;85:2002-11.
[260] Weber R, Kupka T, Zając K. Jet flames of a refuse derived fuel. Combust Flame 2009;156:922-7.
[261] Nielsen HP, Frandsen FJ, Dam-Johansen K, Baxter LL. The implications of chlorine-associated corrosion on the operation of biomass-fired boilers. Prog Energy Combust Sci 2000;26:283-98.
[262] Harb JN, Smith EE. Fireside corrosion in pc-fired boilers. Prog Energy Combust Sci 1990;16:169-90.
[263] Montgomery M, Larsen OH. Field test corrosion experiments in Denmark with biomass fuels. Part 2: Co-firing of straw and coal. Materials and Corrosion 2002;53:185-94.
[264] Montgomery M, Vilhelmsen T, Jensen SA. Potential high temperature corrosion problems due to co-firing of biomass and fossil fuels. Materials and Corrosion 2008;59:783-93.
[265] Cenni R, Janisch B, Spliethoff H, Hein KRG. Legislative and environmental issues on the use of ash from coal and municipal sewage sludge co-firing as construction material. Waste Manage 2001;21:17-31.

[266] European Committee for Standardization (CEN). EN 197-1: Cement-part 1: composition, specifications and conformity criteria for common cements. 2000.
[267] European Committee for Standardization (CEN). EN 450-1:2005+A1: Fly ash for concrete-part 1: definition, specifications and conformity criteria. 2007.
[268] Wang S, Miller A, Llamazos E, Fonseca F, Baxter L. Biomass fly ash in concrete: Mixture proportioning and mechanical properties. Fuel 2008;87:365-71.
[269] Dunnu G, Maier J, Hilber T, Scheffknecht G. Characterisation of large solid recovered fuel particles for direct co-firing in large PF power plants. Fuel 2009;88:2403-8.
[270] Wolski N, Maier J, Hein KRG. Trace metal partitioning from co-combustion of RDF and bituminous coal. IFRF Combustion Journal 2002;200203.
[271] Izquierdo M, Moreno N, Font O, et al. Influence of the co-firing on the leaching of trace pollutants from coal fly ash. Fuel 2008;87:1958-66.
[272] Hilber T, Maier J, Scheffknecht G, et al. Advantages and Possibilities of Solid Recovered Fuel Cocombustion in the European Energy Sector. J Air Waste Manage Assoc 2007;57:1178.
[273] Hilber T, Thorwarth H, Stack-Lara V, Schneider M, Maier J, Scheffknecht G. Fate of mercury and chlorine during SRF co-combustion. Fuel 2007;86:1935-46.
[274] Su S, Pohl JH, Holcombe D, Hart JA. Techniques to determine ignition, flame stability and burnout of blended coals in pf power station boilers. Prog Energy Combust Sci 2001;27:75-98.
[275] Fan M, Brown RC. Comparison of the loss-on-ignition and thermogravimetric analysis techniques in measuring unburned carbon in coal fly ash. Energy Fuels 2001;15:1414-7.
[276] McGhee B, Norton F, Snape CE, Hall PJ. The copyrolysis of poly (vinylchloride) with cellulose derived materials as a model for municipal waste derived chars. Fuel 1995;74:28-31.
[277] House JE, Kemper KA. Proton affinities of sulfate and bisulfate ions. J Therm Anal Calorim 1987;32:1855-8.
[278] Wu H, Pedersen AJ, Glarborg P, Frandsen FJ, Dam-Johansen K, Sander B. Formation of fine particles in co-combustion of coal and solid recovered fuel in a pulverized coal-fired power station. Proc Combust Inst 2011;33:2845-52.
[279] Saeed L, Tohka A, Haapala M, Zevenhoven RK. Pyrolysis and combustion of PVC, PVC-wood and PVC-coal mixtures in a two-stage fluidized bed process. Fuel Process Technol 2004;85:1565-83.
[280] Dunnu G, Hilber T, Schnell U. Advanced size measurements and aerodynamic classification of solid recovered fuel particles. Energy Fuels 2006;20:1685-90.
[281] Agraniotis M, Nikolopoulos N, Nikolopoulos A, Grammelis P, Kakaras E. Numerical investigation of Solid Recovered Fuels' co-firing with brown coal in large scale boilers-Evaluation of different co-combustion modes. Fuel 2010;89:3693-709.
[282] Frandsen F, Dam-Johansen K, Rasmussen P. Trace elements from combustion and gasification of coal--An equilibrium approach. Prog Energy Combust Sci 1994;20:115-38.
[283] Cenni R. Heavy metals behavior in co-combustion of coal and sewage sludge. Universität Stuttgart: VDI Verlag Düsseldorf, 2001.
[284] Smith RD. The trace element chemistry of coal during combustion and the emissions from coal-fired plants. Prog Energy Combust Sci 1980;6:53-119.
[285] Swaine DJ, Goodarzi F. Environmental aspects of trace elements in coal. : Kluwer Academic Pub, 1995.
[286] Wu H, Glarborg P, Frandsen FJ, Dam-Johansen K, Jensen PA, Sander B. Co-combustion of pulverized coal and solid recovered fuel in an entrained flow reactor – General combustion and ash behaviour. Fuel 2011;90:1980-91.

[287] Norton GA, Malaby KL, DeKalb EL. Chemical characterization of ash produced during combustion of refuse-derived fuel with coal. Environ Sci Technol 1988;22:1279-83.
[288] Querol X, Juan R, Lopez-Soler A, Fernandez-Turiel JÈL, Ruiz CR. Mobility of trace elements from coal and combustion wastes. Fuel 1996;75:821-38.
[289] Huggins FE, Huffman G. Modes of occurrence of trace elements in coal from XAFS spectroscopy. International Journal of Coal Geology 1996;32:31-53.
[290] Vassilev SV, Braekman-Danheux C. Characterization of refuse-derived char from municipal solid waste: 2. Occurrence, abundance and source of trace elements. Fuel Process Technol 1999;59:135-61.
[291] Miller B, Dugwell DR, Kandiyoti R. The influence of injected HCl and SO2 on the behavior of trace elements during wood-bark combustion. Energy Fuels 2003;17:1382-91.
[292] Bool LE, Helble JJ. A laboratory study of the partitioning of trace elements during pulverized coal combustion. Energy Fuels 1995;9:880-7.
[293] Galbreath KC, Toman DL, Zygarlicke CJ, Pavlish JH. Trace element partitioning and transformations during combustion of bituminous and subbituminous US coals in a 7-kW combustion system. Energy Fuels 2000;14:1265-79.
[294] Querol X, Fernández-Turiel JL, Lopez-Soler A. Trace elements in coal and their behaviour during combustion in a large power station. Fuel 1995;74:331-43.
[295] Martinez-Tarazona MR, Spears DA. The fate of trace elements and bulk minerals in pulverized coal combustion in a power station. Fuel Process Technol 1996;47:79-92.
[296] Sørum L, Frandsen FJ, Hustad JE. On the fate of heavy metals in municipal solid waste combustion. Part II. From furnace to filter. Fuel 2004;83:1703-10.
[297] Contreras ML, Arostegui JM, Armesto L. Arsenic interactions during co-combustion processes based on thermodynamic equilibrium calculations. Fuel 2009;88:539-46.
[298] Diaz-Somoano M, Unterberger S, Hein KRG. Prediction of trace element volatility during co-combustion processes. Fuel 2006;85:1087-93.
[299] George A, Larrion M, Dugwell D, Fennell PS, Kandiyoti R. Co-firing of Single, Binary, and Ternary Fuel Blends: Comparing Synergies within Trace Element Partitioning Arrived at by Thermodynamic Equilibrium Modeling and Experimental Measurements. Energy Fuels 2010;24:2918-23.
[300] Sloss LL, Smith IM. PM10 and PM2. 5: an international perspective. Fuel Process Technol 2000;65:127-41.
[301] Meij R, te Winkel H. The emissions of heavy metals and persistent organic pollutants from modern coal-fired power stations. Atmos Environ 2007;41:9262-72.
[302] Chen Y, Shah N, Huggins FE, Huffman GP. Transmission electron microscopy investigation of ultrafine coal fly ash particles. Environ Sci Technol 2005;39:1144-51.
[303] Zhuo JK, Li SQ, Yao Q, Song Q. The progressive formation of submicron particulate matter in a quasi one-dimensional pulverized coal combustor. Proc Combust Inst 2009;32:2059-66.
[304] Zeng T, Helble JJ, Bool LE, Sarofim AF. Iron transformations during combustion of Pittsburgh no. 8 coal. Fuel 2009;88:566-72.
[305] Liu X, Xu M, Yao H, et al. Effect of combustion parameters on the emission and chemical composition of particulate matter during coal combustion. Energy Fuels 2007;21:157-62.
[306] Zeuthen JH, Pedersen AJ, Hansen J, et al. Combustion aerosols from municipal waste incineration-Effect of fuel feedstock and plant operation. Combust Sci Technol 2007;179:2171-98.

[307] McLennan AR, Bryant GW, Stanmore BR, Wall TF. Ash formation mechanisms during pf combustion in reducing conditions. Energy Fuels 2000;14:150-9.
[308] Kauppinen EI. Aerosol formation in coal combustion processes. J Aerosol Sci 1991;22.
[309] Lipsky E, Stanier CO, Pandis SN, Robinson AL. Effects of sampling conditions on the size distribution of fine particulate matter emitted from a pilot-scale pulverized-coal combustor. Energy Fuels 2002;16:302-10.
[310] Pallarés J, Arauzo I, Williams A. Integration of CFD codes and advanced combustion models for quantitative burnout determination. Fuel 2007;86:2283-90.
[311] Tognotti L, Longwell JP, Sarofim AF. The products of the high temperature oxidation of a single char particle in an electrodynamic balance. Proc Combust Inst 1990;23:1207-13.
[312] Bayless DJ, Jewmaidang J, Tanneer S, Birru R. Kinetics of low-temperature homogeneous SO3 formation for use in flue gas conditioning for improved electrostatic precipitator performance. Proc Combust Inst 2000;28:2499-505.
[313] Communication from the Commission to the European Parliament, the Council, the European Economic and Social Committee and the Committee of the Regions, 20 20 by 2020 Europe's climate change opportunity. Brussels, Belgium: Commission of the European Communities, 2008.
[314] Sander B. Bioenergy for electricity and heat - experiences from biomass-fired CHP plants in Denmark. : DONG Energy, 2007.
[315] A visionary Danish energy policy 2025. : Danish Energy Authority, 2007.
[316] Davidsson KO, Åmand LE, Elled AL, Leckner B. Effect of cofiring coal and biofuel with sewage sludge on alkali problems in a circulating fluidized bed boiler. Energy Fuels 2007;21:3180-8.
[317] Hansen LA, Nielsen HP, Frandsen FJ, Dam-Johansen K, Hørlyck S, Karlsson A. Influence of deposit formation on corrosion at a straw-fired boiler. Fuel Process Technol 2000;64:189-209.
[318] Michelsen HP, Frandsen F, Dam-Johansen K, Larsen OH. Deposition and high temperature corrosion in a 10 MW straw fired boiler. Fuel Process Technol 1998;54:95-108.
[319] Zheng Y, Jensen AD, Johnsson JE. Laboratory investigation of selective catalytic reduction catalysts: Deactivation by potassium compounds and catalyst regeneration. Ind Eng Chem Res 2004;43:941-7.
[320] Castellino F, Rasmussen SB, Jensen AD, Johnsson JE, Fehrmann R. Deactivation of vanadia-based commercial SCR catalysts by polyphosphoric acids. Appl Catal : B 2008;83:110-22.
[321] Castellino F, Jensen AD, Johnsson JE, Fehrmann R. Influence of reaction products of K-getter fuel additives on commercial vanadia-based SCR catalysts:: Part I. Potassium phosphate. Appl Catal : B 2009;86:196-205.
[322] Aho M, Silvennoinen J. Preventing chlorine deposition on heat transfer surfaces with aluminium–silicon rich biomass residue and additive. Fuel 2004;83:1299-305.
[323] Tobiasen L, Skytte R, Pedersen LS, Pedersen ST, Lindberg MA. Deposit characteristic after injection of additives to a Danish straw-fired suspension boiler. Fuel Process Technol 2007;88:1108-17.
[324] Boström D, Grimm A, Boman C, Björnbom E, Öhman M. Influence of Kaolin and Calcite Additives on Ash Transformations in Small-Scale Combustion of Oat. Energy Fuels 2009;23:5184-90.

[325] Almark M, Edvardsson E, Berg M. Reduction of alkali chlorides in flue gas and chlorine in deposits by phosphate addition. Proceedings of the Impacts of Fuel Quality on Power Generation and the Environment, 2010, Lapland, Finland.
[326] Tsai WT, Chen HP, Hsieh MF, Sun HF, Chien SF. Regeneration of spent bleaching earth by pyrolysis in a rotary furnace. J Anal Appl Pyrolysis 2002;63:157-70.
[327] Tobiasen L, Knudsen J. Alternative additives. : DONG Energy (PSO FU 6532), 2007.
[328] Yin C, Rosendahl LA, Kær SK. Grate-firing of biomass for heat and power production. Prog Energy Combust Sci 2008;34:725-54.
[329] Wei X, Schnell U, Hein KRG. Behaviour of gaseous chlorine and alkali metals during biomass thermal utilisation. Fuel 2005;84:841-8.
[330] Lin W, Dam-Johansen K, Frandsen F. Agglomeration in bio-fuel fired fluidized bed combustors. Chem Eng J 2003;96:171-85.
[331] Vuthaluru HB, Vleeskens JM, Wall TF. Reducing fouling from brown coals by sodium-binding additives. Fuel Process Technol 1998;55:161-73.
[332] Zhou H, Jensen PA, Frandsen FJ. Dynamic mechanistic model of superheater deposit growth and shedding in a biomass fired grate boiler. Fuel 2007;86:1519-33.
[333] Boström D, Eriksson G, Boman C, Öhman M. Ash Transformations in Fluidized-bed Combustion of Rapeseed Meal. Energy Fuels 2009;23:2700-6.
[334] Capablo J, Jensen PA, Pedersen KH, et al. Ash Properties of Alternative Biomass. Energy Fuels 2009;23:1965-76.
[335] Eeckhout W, De Paepe M. Total phosphorus, phytate-phosphorus and phytase activity in plant feedstuffs. Anim Feed Sci Technol 1994;47:19-29.
[336] Beck J, Müller R, Brandenstein J, et al. The behaviour of phosphorus in flue gases from coal and secondary fuel co-combustion. Fuel 2005;84:1911-9.
[337] Steadman KJ, Burgoon MS, Lewis BA, Edwardson SE, Obendorf RL. Minerals, phytic acid, tannin and rutin in buckwheat seed milling fractions. J Sci Food Agric 2001;81:1094-100.
[338] Pontoppidan K, Pettersson D, Sandberg AS. The type of thermal feed treatment influences the inositol phosphate composition. Anim Feed Sci Technol 2007;132:137-47.
[339] Ravindran V, Ravindran G, Sivalogan S. Total and phytate phosphorus contents of various foods and feedstuffs of plant origin. Food Chem 1994;50:133-6.
[340] Ekholm P, Virkki L, Ylinen M, Johansson L. The effect of phytic acid and some natural chelating agents on the solubility of mineral elements in oat bran. Food Chem 2003;80:165-70.
[341] Ockenden I, Dorsch JA, Reid MM, et al. Characterization of the storage of phosphorus, inositol phosphate and cations in grain tissues of four barley (Hordeum vulgare L.) low phytic acid genotypes. Plant Science 2004;167:1131-42.
[342] Raboy V. myo-Inositol-1, 2, 3, 4, 5, 6-hexakisphosphate. Phytochemistry 2003;64:1033-43.
[343] Vasca E, Materazzi S, Caruso T, Milano O, Fontanella C, Manfredi C. Complex formation between phytic acid and divalent metal ions: A solution equilibria and solid state investigation. Anal Bioanal Chem 2002;374:173-8.
[344] Bohn L, Josefsen L, Meyer AS, Rasmussen SK. Quantitative analysis of phytate globoids isolated from wheat bran and characterization of their sequential dephosphorylation by wheat phytase. J Agric Food Chem 2007;55:7547-52.
[345] Brown ME, Glasser L, Larson J. High temperature thermal properties of KH2PO4: Phase transitions and decompositions. Thermochimica Acta 1979;30:233-46.
[346] Park JH, Lee KS, Choi BC. High-temperature transformation in KH2PO4 and RbH2PO4 crystals. J Phys : Condens Matter 2001;13:9411-9.

[347] Lide DR. CRC Handbook of Chemistry and Physics, (Internet Version, 2009). 2009.
[348] Castellino F, Jensen AD, Johnsson JE, Fehrmann R. Influence of reaction products of K-getter fuel additives on commercial vanadia-based SCR catalysts:: Part II. Simultaneous addition of KCl, Ca (OH) 2, H3PO4 and H2SO4 in a hot flue gas at a SCR pilot-scale setup. Appl Catal : B 2009;86:206-15.
[349] Becidan M, Sørum L, Frandsen F, Pedersen AJ. Corrosion in waste-fired boilers: a thermodynamic study. Fuel 2009;88:595-604.

Centre on Combustion and Harmful Emission Control (CHEC)
Department of Chemical and
Biochemical Engineering
Technical University of Denmark
Søltofts Plads, Building 229
DK-2800 Kgs. Lyngby
Denmark

Phone: +45 4525 2957
Fax: +45 4525 2258
Web: www.chec.kt.dtu.dk

ISBN : 978-87-92481-55-9